Evaluatie van een alkalische brandstofcel als micro-warmtekrachtkoppeling (micro-WKK) voor gebouwtoepassingen door middel van simulatie

Model Based Evaluation of an Alkaline Fuel Cell System as Micro-Cogeneration for Building Applications

Ivan Verhaert

Promotor: prof. dr. ir. M. De Paepe
Proefschrift ingediend tot het behalen van de graad van
Doctor in de Ingenieurswetenschappen: Werktuigkunde-Elektrotechniek

Vakgroep Mechanica van Stroming, Warmte en Verbranding
Voorzitter: prof. dr. ir. J. Vierendeels
Faculteit Ingenieurswetenschappen en Architectuur
Academiejaar 2012 - 2013

UNIVERSITEIT GENT

ISBN 978-90-8578-573-6
NUR 961
Wettelijk depot: D/2013/10.500/6

Universiteit Gent
Faculteit Ingenieurswetenschappen en Architectuur
Vakgroep Mechanica van Stroming, Warmte en Verbranding

Promotor: Prof. dr. ir. Michel De Paepe

Universiteit Gent
Faculteit Ingenieurswetenschappen en Architectuur

Vakgroep Mechanica van Stroming, Warmte en Verbranding
Sint-Pietersnieuwstraat 41, B-9000 Gent, België

Tel.: +32-9-264.32.88
Fax.: +32-9-264.35.75

Dit werk kwam tot stand in het kader van een samenwerking tussen VITO, Thomas More Kempen en Universiteit Gent.

Department of Flow, Heat and Combustion Mechanics

Proefschrift tot het behalen van de graad van
Doctor in de Ingenieurswetenschappen:
Werktuigkunde - Elektrotechniek
Academiejaar 2012-2013

VITO
Vlaams instituut voor technologisch onderzoek
Unit Energietechnologie

Assessor: ir. Grietus Mulder

VITO

Unit Energietechnologie
Boeretang 200, B-2400 Mol, België

Tel.: +32-14-33.58.59
E-mail.: grietus.mulder@vito.be

Dit werk kwam tot stand in het kader van een samenwerking tussen Thomas More Kempen, Universiteit Gent en VITO.

Proefschrift tot het behalen van de graad van
Doctor in de Ingenieurswetenschappen:
Werktuigkunde - Elektrotechniek
Academiejaar 2012-2013

Thomas More Kempen vzw
Groep Wetenschap & Technologie
Onderzoeksgroep Kenniscentrum Energie

Doctorandus : ir. Ivan Verhaert

Cordinator onderzoeksgroep: dr. Griet Janssen

Thomas More Kempen
KULeuven, campus Geel

Kenniscentrum Energie (KCE)
Kleinhoefstraat 4, B-2440 Geel, België

Tel.: +32-14-56.23.10
Fax.: +32-14-58.48.59
http: www.kenniscentrumenergie.be

Dit werk kwam tot stand in het kader van een samenwerking tussen Universiteit Gent, VITO en Thomas More Kempen.

Proefschrift tot het behalen van de graad van
Doctor in de Ingenieurswetenschappen:
Werktuigkunde - Elektrotechniek
Academiejaar 2012-2013

Dankwoord

Een doctoraat is een proces van lange adem: een opleiding als onderzoeker, een introductie in de wetenschappelijke wereld. Ik wil hierbij mijn promotor en mijn begeleider bij het VITO uitdrukkelijk bedanken. Michel en Grietus, ik heb de kans gehad om met veel mensen samen te werken en van hen bij te leren, maar jullie hebben mij gedurende het hele traject gecoacht en feedback gegeven, zodat ik dit doctoraat tot een goed eind kon brengen.
Dit doctoraat was er niet gekomen zonder de bereidheid om een samenwerkingsverband te sluiten tussen de drie onderzoeksinstellingen. Daarom wil ik ook zeker de directie en (ex)-collega's danken bij zowel VITO, Thomas More Kempen en UGent die mij hierin altijd gesteund hebben en op moeilijke momenten me de motivatie gaven om door te zetten.

Daarnaast wil ik ook de mensen rond mij bedanken. Een doctoraat is immers officieel een individueel traject, maar het heeft ook een impact op de personen rond je. Ik wil hierbij mijn ouders en schoonouders bedanken om er te zijn wanneer het nodig was en om mijn drie prinsessen bij te staan op het thuisfront.
Mijn drie prinsessen die ik allerminst mag vergeten in dit dankwoord.
Lou & Oona, mijn twee grootste verwezenlijkingen tijdens dit doctoraat, bedankt om mijn idealisme warm te houden, om me te vergeven dat papa moest werken en om jullie oprechte interesse in al mijn papiertjes.
Sophie, mijn steun en baken als ik met mijn gedachten weer ver weg zit en al de rest vergeet. Bedankt om me met de voeten op aarde te houden en om zo goed te zorgen voor alles wat me dierbaar is. Ik zou nog een boek kunnen schrijven over de zaken waarvoor ik je allemaal moet danken, maar ik ga hiervoor een ander medium gebruiken.

Tenslotte ook u lezer bedankt. U maakt het alleszins voor mij de moeite waard. Ik hoop van harte dat dit boek, op welke manier ook, u kan inspireren in uw eigen bezigheden.

Gent, januari 2013
Ivan Verhaert

Table of Contents

List of Figures

List of Tables

Nomenclature

A	effective area of the fuel cell	m^2
c_j	coefficient j for the electrochemical model	$*$
D	Diffusion constant	m^2/s
E_{Nernst}	thermodynamic potential	V
F	molar flow rate	$kmol/hr$
Far	constant of Faraday	C/mol
G	Gibbs free energy	$GJ/kmol$
h	total enthalpy	$GJ/kmol$
H	total enthalpy	J/kg
hA	overall conductance	W/K
I	load current	A
$\dot{M}_i$	Mass flow rate of i	kg/s
N_i	molar flux	$mol/m^2 \cdot s$
Nu	Nusselt number	–
p	pressure	Pa
p_I	(partial) pressure of flow I	bar
P	power	W
Q	heat	W
R	universal gas constant	$J/mol.K$
Re	Reynolds number	–
T	temperature	$^\circ C$
U	voltage	V
v	velocity	m/s
V	volume	l
y_i	molar fraction of species i	–
z	1-dimensional coordinate of location in the diffusion layer	m
$(a.u.)$	arbitrary unit	$a.u.$

Greek symbols

α	transfers coefficient	–
$\alpha_{partial}$	partial efficiency	$\%$
Δ	difference	-
ϵ	effectiveness	-
η	efficiency	-
η	overvoltage	V
ϕ	flow rate	l/s

Subscripts

$A,B,...$	identification of flow
an	anode
c	cold
cat	cathode
e	electrical
el	electrolyte
FCB	fuel cell body
h	hot
ref	reference
$surr$	surroundings
w	water/water vapour

Acronyms

AC	Alternating Current
AFC	Alkaline Fuel Cell
AGC	Anode Gas Chamber
AGDF	Anode Gas Diffusion Layer
CFD	Computational Fluid Dynamics
CGC	Cathode Gas Chamber
CGDF	Cathode Gas Diffusion Layer
CHP	Combined Heat and Power or cogeneration
COP	Coefficient of Performance
DC	Direct Current
DHW	Domestic hot water
EIS	Electrochemical Impedance Spectroscopy
EPBD	Energy Performance of Buildings Directive
FCB	Fuel Cell Body
GDF	Gas Diffusion Layer
HHV	Higher Heating Value
HVAC	Heating, Ventilation, Air Conditioning
IEA	International Energy Agency
KPI	Key Performance Indicator
LHV	Lower Heating Value
MCFC	Molten Carbonate Fuel Cell
NG	Natural Gas
PAFC	Phosphoric Acid Fuel Cell
PEMFC	Proton Exchange Membrane Fuel Cell
PI	Proportional - Integral
RH	Relative Humidity
RPES	Relative Primary Energy Savings
RT	Return Temperature
SOFC	Solid Oxide Fuel Cell
WKK	Warmtekrachtkoppeling

Nederlandse samenvatting
–Summary in Dutch–

De laatste decennia nam ons energiegebruik enorm toe. Dit heeft voor welvaart en vooruitgang gezorgd. Onze voornaamste energiebronnen, zoals fossiele en nucleaire energie zijn echter niet onuitputtelijk en hun gebruik heeft daarenboven een negatieve impact op het milieu. Om onze welvaart en economie te vrijwaren, is het daarom noodzakelijk om efficiënter met onze grondstoffen om te springen.

Gebouwen hebben een groot aandeel - in Europa ongeveer 40% - in het totale primaire energiegebruik. Bovendien is hier nog een groot besparingspotentieel (ca. 30%) aanwezig. Dit heeft zich vertaald in de Europese gebouwenrichtlijn. Hierbij is het vooral belangrijk op te merken dat de richtlijn niet alleen aandacht heeft voor de isolatiegraad van het gebouw, maar ook voor de energetische prestatie van de installaties eigen aan het gebouw die zorgen voor verwarming, verlichting, ...

Omdat warmtekrachtkoppeling (WKK) op een efficiënte manier brandstof omzet in nuttige energievormen, groeit de interesse om deze technologie ook in gebouwen te introduceren. Nochtans is dit geen evidentie. Oorspronkelijk was WKK immers enkel succesvol vanuit technisch-economisch perspectief wanneer er een grote en continue warmtevraag aanwezig was.
Onder druk van een wijzigend energielandschap, met meer aandacht voor decentrale energieconversie wordt WKK echter ook interessant op plaatsen met een relatief kleine warmtevraag.
Deze kleine WKK-systemen, micro-WKKs, zijn inzetbaar in gebouwen, waar ze instaan voor de basislast van de warmtevraag en ze ondertussen het netto elektriciteitsverbruik verminderen. In gebouwen is de energievraag vooral warmtegedreven, en in mindere mate elektriciteitsgedreven. Dit vertaalt zich in de eisen die gesteld worden aan de micro-WKK.
Het energiegebruikspatroon in gebouwen heeft echter de laatste decennia een evolutie ondergaan van een meer warmtevraag gedreven energievraag naar een meer elektriciteitsvraag gedreven energievraag. Dit komt enerzijds door de betere isolatiegraad, maar anderzijds ook door de toenemende elektrificatie in onze gebouwen. De eisen voor micro-WKK veranderen dus van een hoge warmtekrachtverhouding naar een lage warmtekrachtverhouding en dit voor alsmaar kleinere systemen.

In tegenstelling tot de andere micro-WKK technologieën hebben brandstofcellen deze eigenschappen wel, omwille van hun modulaire opbouw. Brandstofcellen zetten immers brandstof rechtstreeks om in elektriciteit.
Er zijn diverse types brandstofcellen die in aanmerking komen om te integreren in micro-WKK-systemen, met name PEMFC, SOFC en AFC. Zowel voor PEMFC als voor SOFC komen de eerste systemen momenteel op de markt. In deze studie is de integratie, sturing en toepasbaarheid van de alkalische brandstofcelstack (AFC) in een micro-WKK systeem geëvalueerd door middel van simulatie op basis van gevalideerde modellen.

Aangezien het de bedoeling is om de stack thermisch en elektrisch in een systeem te integreren, is het nodig dat het model van de alkalische brandstofcelstack zowel het thermische als elektrische gedrag van de stack kan voorspellen. Een bijkomend probleem bovendien bij het gebruik van brandstofcellen is dat er water gevormd wordt. Dit water moet afgevoerd worden om te voorkomen dat het gaskanalen gaat verstoppen of het alkalische mengsel zal verdunnen. Dit leidt immers niet alleen tot rendementsverlies, maar ook tot mogelijk falen van het systeem.
Een literatuurstudie van de bestaande modellen leert dat de meeste modellen van de AFC-stack enkel tot doel hebben de elektrische prestatie van de cel te karakteriseren, om de cel zelf te verbeteren. Om die reden is een model ontwikkeld dat zowel de thermische huishouding als de waterhuishouding van de stack voorspelt op basis van de ingaande stromen, inclusief haar impact op de elektrische prestatie.
Hierbij is een benadering gebruikt op basis van controlevolumes gelinkt aan de verschillende lagen in de brandstofcel, die geschaald zijn naar stackniveau. Voor elk van die lagen is een massa en energiebalans opgesteld om debieten en temperaturen te voorspellen. Om de waterhuishouding te voorspellen is aangenomen dat waar het water gevormd wordt, water zich in gesatureerde toestand bevindt en deels door diffusie, beschreven door de diffusievergelijkingen, wordt afgevoerd in de gasstromen en deels in het elektrolyt oplost.
Aangezien verscheidene massastromen doorheen de stack stromen, is de stack in feite ook een warmtewisselaar, waarbij een correctie op de overdrachtscoëfficiënt is aangebracht op basis van de stroomsnelheden. De resultaten van het model zijn vergeleken met experimenten uitgevoerd op een bestaand AFC-systeem als micro-WKK, waarmee de bruikbaarheid van het model is bewezen.

Met dit model is de invloed onderzocht van diverse systeem- en regelstrategie afhankelijke factoren op de energetische prestatie en op de waterhuishouding. De energetische prestatie is benaderd vanuit het standpunt van primaire energiebesparing.
Het blijkt dat vanaf een minimale belasting de stack steeds een primaire energiebesparing realiseert. Het optimale werkingspunt is afhankelijk van zowel de elektrolyt temperatuur als de belasting.

Deze stelling geldt eveneens voor de waterhuishouding, waarbij een voldoende hoge temperatuur van het elektrolyt noodzakelijk is om het water als waterdamp via het luchtkanaal te verwijderen.
Bij te hoge temperaturen is er echter een risico op overmatige verdamping van water uit het elektrolyt, tenzij hete vochtige lucht wordt aangevoerd aan de luchtkanalen. Dit verhoogt bovendien de energetische prestatie door een verlaging van de warmteverliezen en vormt dus mogelijk een interessant uitgangspunt voor systeemintegratie.
Uit de analyse blijkt verder dat het terugdringen van deze warmteverliezen door isolatie of hogere omgevingstemperaturen op welke manier ook het meest doeltreffend is om de prestatie als micro-WKK te verbeteren.

Op basis van deze inzichten zijn naast het referentiesysteem waarmee de validatie is gebeurd, verbeterde systeemconfiguraties vooropgesteld en vertaald naar een systeemmodel.
Met behulp van deze modellen zijn de diverse systemen vergeleken met elkaar en is de impact op het totale rendement van de diverse systeemcomponenten onderzocht.
Een systeemconfiguratie waarbij de warmte uit de afvoerlucht gerecupereerd wordt door middel van een binnenopstelling of een warmteterugwinningsunit verhoogt de energetische prestatie van de WKK.
Verder blijkt dat voor de meeste componenten, zoals de pompen en ventilatoren, er geen hoge eisen gesteld moeten worden met betrekking tot systeemrendement. Enkel de inverter en de purgeereffeciëntie hebben een noemenswaardige impact op het totale rendement.
Er is hierbij tevens een regelstrategie opgesteld die de waterhuishouding op systeemniveau onder controle houdt.

Naast deze analyse is het model ook gebruikt om na te gaan hoe de stacks best met elkaar kunnen geconnecteerd worden. De voornaamste aandachtspunten hierbij zijn het vermijden van de vorming van waterdruppels in de gaskanalen en het verhogen van de prestatie. In beide gevallen biedt het parallel aansluiten van de electrolytstroom op de stacks een licht voordeel.
Met oog op gebouwintegratie is vervolgens de vergelijking gemaakt met andere WKKs wat betreft deellastgedrag. Hierbij is de beginstelling bevestigd die aanleiding gaf tot de keuze voor brandstofcellen als micro-WKK .

Tenslotte is ook gekeken naar de gebouwintegratie van dergelijk systeem en de implementatie van een passende regelstrategie. In eerste instantie is gekozen voor een eenvoudige strategie, opdat het systeem niet zou falen, omwille van de gevoelige waterhuishouding.
De resultaten tonen aan dat er besparingspotentieel aanwezig is, maar dat enkele randvoorwaarden vervuld moeten zijn. Het is namelijk noodzakelijk dat het systeem enkel bedreven wordt in het energetisch gunstige werkingsgebied, bij

voldoende hoge belasting. De hierdoor groeiende risico's wat betreft stabiliteit van de waterhuishouding, moeten hierbij opgevangen kunnen worden door een verbeterde regelstrategie.
Omwille van de complexiteit van het systeem, is het aangewezen dat een voldoende grote buffer wordt voorzien opdat gebouw en WKK zoveel mogelijk kunnen ontkoppeld worden van elkaar. Dit geeft meer vrijheid aan de optimalisering van de regelstrategie.

Vanuit financieel oogpunt is de casus sterk afhankelijk van de randvoorwaarden. Binnen de huidige context, is terugleveren aan het net immers ongunstig, ondanks de complementariteit met bvb. zonnepanelen. Daarom is het belangrijk een casus te vinden waarbij de elektriciteitsvraag veel hoger is dan de warmtevraag, in overeenstemming met de warmtekrachtverhouding van de brandstofcelgebaseerde micro-WKK.
Voor woningen is het echter niet te verwachten dat deze verhouding bereikt wordt, zelfs niet voor passiefhuizen. Passiefkantoren echter zijn in deze een toepassingsdomein waar de technologie wel tot zijn recht kan komen.
Gezien de evolutie in de gebouwde omgeving en de mogelijkheid om op een duurzame manier waterstofgas te genereren, stelt de auteur dat verdere ontwikkeling van de brandstofcel voor deze stationaire toepassing verdedigbaar is. Het blijft immers noodzakelijk dat de verhouding van de prijs tot levensduur van de brandstofcel verder blijft dalen opdat deze toestellen succesvol op de markt gebracht kunnen worden. Het veranderende energielandschap biedt daarbij op termijn nog bijkomende mogelijkheden om ook in andere casi interessant te zijn vanuit economisch standpunt. Dit zijn zaken waaraan in mogelijke vervolgstudies verder invulling gegeven kan worden.

English summary

The last decades energy use increased enormously. This has led to prosperity and progress. Our main energy sources, such as fossil and nuclear energy, however, are finite. Besides this their conversion has a negative impact on the environment. Increasing energy efficiency is therefore necessary to safeguard our prosperity and economy. Focus should therefore be on those sectors, responsible for the largest share in primary energy use.
Studies show that in Europe, buildings are responsible for 40% of total primary energy consumption, with a savings potential of about 30%. As defined in the European building directive, these savings can potentially be found in an improved insulation level of the buildings as well as in more efficient (energy) systems within these buildings (such as heating, lighting, etc.).

Because of its efficient use of primary energy, cogeneration (CHP) is an interesting technology for heating purposes. From a techno-economic point of view, originally CHP systems are interesting in applications with a continuous and high heat demand.
The changing energy market and evolution towards decentralised electricity production, changed these size limitations for CHP in favour of smaller CHP-units. These small systems or micro-CHPS, can also be used for heating purposes in buildings and in the mean time reduce the net electricity consumption.
The energy use pattern in buildings changed in the last decades. The energy demand in buildings is shifting from a more heat driven demand towards a more electricity driven energy demand.
This is due to a better insulation rate, next to a growing electrification in our buildings. This changes the conditions for a micro-CHP-unit to higher power-to-heat ratios and smaller sizes for successful implementation.
Unlike the other micro-CHP technologies fuel cells have these properties, due to their modular structure. There are different types of fuel cells which are eligible, such as PEM, SOFC and AFC. Regarding PEM and SOFC, the first systems are gradually entering the market.
In this study the integration, steering and feasibility of an alkaline fuel cell stack in a micro-CHP system is evaluated. The evaluation is based on simulation with the use of validated models.

Since it is intended to integrate the stack thermally and electrically into a system, the stack model should be able to predict thermal and electrical behaviour

of the stack. An additional problem with the use of fuel cells is the formation of reaction water. This water must be drained to prevent clogging in the gas channels or dilution of the electrolyte. Not only because of possible efficiency loss, but also because it can cause system failure.

A review of the literature on existing models shows that most models of the AFC stack aim to characterize the electrical performance of the cell, to obtain improvements at cellular level. For this reason, a model is developed predicting both thermal household and water management, including their impact on electrical performance, based on the inlet flows.
The model uses a control volume approach, with each control volume linked to a different layer in the fuel cell. This composition of the fuel cell is scaled to stack level. For each of the layers a mass and energy balance is solved to calculate flow rates and temperatures.
In order to understand the water management, it is assumed that during reaction the water is formed in a saturated state. It is removed from the reaction area, partly as vapour by diffusion into the gas flows, described by the diffusion equations, and partly as liquid in the electrolyte.
Since several mass flows pass through the stack, the stack is in fact also a heat exchanger, for which a correction to the transfer coefficient is made based on flow velocity.
The results of the model are compared with experiments performed on an existing AFC based micro-CHP system, which proves the usability of the model is proven.

Consequently the model is used to investigate the influence on energy performance and water management of various system and control parameters.The energetic performance is based on primary energy savings.
It turns out that a minimal load from the stack is necessary to realize primary energy savings. The optimum operating point depends on both the electrolyte temperature and on electric load.
This is also true for the water management. With a sufficiently high electrolyte temperature, the water is removed as water vapour within the air flow. However, when temperatures are too high, this increases the risk of excessive evaporation of water from the electrolyte, unless hot humid air is introduced at the air inlet.
This also increases the energetic performance through reduction of the heat losses. This offers an interesting perspective for new system set-ups.
In general, the analysis shows that reducing heat losses by insulation or higher ambient temperatures is the most effective way to improve stack performance as a CHP.

Based on these insights and in addition to the reference system used for the validation, enhanced system configurations are developed and compared to one another.
Next to that, a control strategy to control the water balance at system level is elaborated.

A system configuration which recycles the heat from the exhaust air through a heat recovery unit or within a container set-up increases the energetic performance of the CHP. As for system components it is shown that most of them, like pumps and fans have a relatively low impact on performance. Only the inverter and purge efficiency show a large influence.

In addition to this analysis the system model is used to determine how the stacks can be optimally connected with each other. The analysis is mainly based on the prevention of water droplets in the gas channels and improving performance. It is shown that a parallel connection of the electrolyte flow through the stack shows a minimal positive result.

Within the perspective of building integration, a comparison is made with other CHP installations regarding part load behaviour. It is shown that the original assumption about the interesting behaviour of a fuel cell based CHP-system is valid.

Finally, building integration is evaluated including the implementation of an adequate control strategy. Initially a very simple strategy is used, with the only goal to prevent system failure, due to its sensitive water balance.
The results show that there is a savings potential present, when an number of boundary conditions are fulfilled.
It is necessary that the system is only operated at high load. Next, it is appropriate a sufficiently large buffer is provided to disconnect CHP and heat load from each other as much as possible, because of system complexity.

From a financial point of view, the case is strongly dependent on meeting the boundary conditions. Within the current context, delivering electricity back to the grid is not favourable, despite the complementarity of CHPs with e.g. solar panels.
For this reason, it is important to find a case where the electricity demand is much higher than the heat demand, in accordance with the heat-to-power ratio of the fuel cell based micro-CHP.
In residential buildings, it is not expected that this ratio is reached, not even in passive houses, but passive offices promise to be a location where this technology potentially has some advantages over other systems. Given the evolution within this sector and with the ability to generate hydrogen gas in a sustainable manner, the author poses that further development of fuel cell systems for this stationary application is valuable.
However, it is still critical that the price-to-lifetime ratio continues to drop, in order to successfully introduce these devices on the market. From an economic point of view, the changing energy landscape possibly offers additional interesting opportunities in the long-term in other cases. These remarks and this perspective can be used as a starting point for future research surveys.

1 Introduction

1.1 Energy use in the world

The last decades global energy use has increased exponentially, supporting economic growth and human development. To meet these high and increasing energy demands, both fossil, nuclear and renewable energy resources are mined.

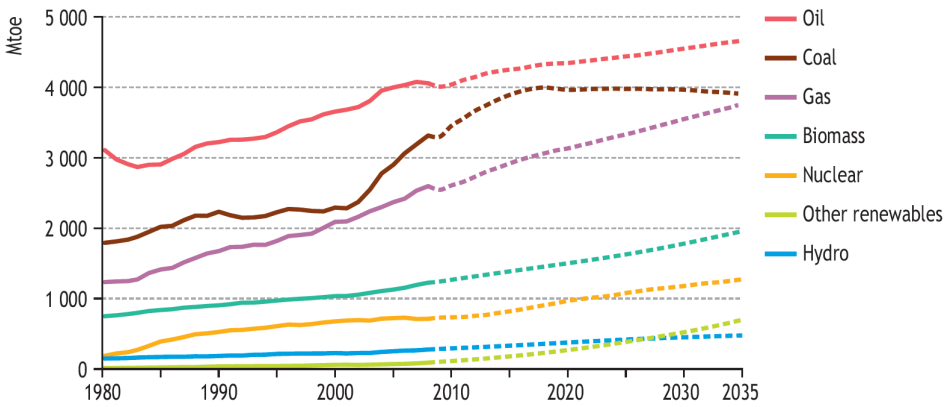

Figure 1.1: World primary energy demand by fuel in the New Policies Scenario, reported by the International Energy Agency (IEA)in 2010 [1]

Environmental, economical and energy concerns

Figure 1.1 shows that fossil fuels (such as coal, natural gas and oil) still dominate this energy mix [2]. These fossil fuel and also nuclear(fission) resources are finite, resulting in increasing energy prices.
Next to energy shortage and high energy prices, the domination of fossil fuels in the energy mix causes also environmental concerns. The conversion of fossil fuels into useful forms of energy, like heat and electricity, contributes to global warming by adding greenhouse gases to the atmosphere. Global warming changes climate and weather patterns. Possible consequences are flooding, severe weather conditions (hurricanes, droughts,...), spread of diseases, etc.

Drive towards energy efficiency

Aware of the economical, environmental and energy concerns, a sustainable energy supply has to be established. At the end of 2008 the European Union translated these concerns into a series of climate and energy targets to be met by 2020. These 20-20-20 targets are [3]:

- A reduction of EU greenhouse gas emissions of at least 20% compared to 1990 levels;
- 20% of EU energy use has to come from renewable resources;
- 20% reduction in primary energy use compared with projected levels, to be achieved by improving energy efficiency.

To reach these targets and implement such a sustainable energy supply, the first step to be taken is to reduce energy demand.

Sectoral differences and saving potential

In order to minimize energy demand, extra attention has to be given to those sectors, which have the largest savings potential. According to the International Energy Agency (IEA) [1], the main energy-using sectors are:

- Manufacturing: metal products and equipment, food and beverages, chemicals, paper, pulp and printing, ...
- Transport: passenger and freight transport (light-duty vehicles, trucks, buses, trains, planes, ships)
- Households: space heating and cooling, lighting, cooking, water heating, appliances and equipment, ...

- Services: trade, finance, health, education, commercial services, food and lodging, ...

Figure 1.2 shows that the energy use and its related CO_2-emissions grew in all sectors of the economy between 1970 and today and will keep on rising in every possible scenario presented by the IEA [1, 4]. With households and services, a

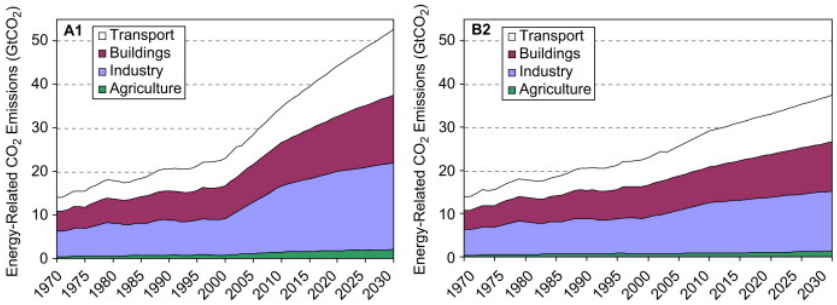

Figure 1.2: Global primary energy by end-use sector [4].

large amount of the global energy use can be addressed to buildings [4, 5] (See Figure 1.2). In the European Union, buildings are responsible for approximately 40% of the total energy use [6]. Next to the size of their share, the energy savings potential in residential and commercial buildings is estimated at 27% and 30%, respectively [7]. This makes buildings one of the key sectors to address in order to obtain EU's Action Plan for Energy Efficiency [7] and has led to the European Building Directive (EPBD) [8].

1.2 Energy in buildings

As illustrated in Figure1.3 and Figure1.4 the energy use within buildings can be addressed to following end-uses:

- Space conditioning (HVAC)
- Domestic hot water production (DHW)
- Food preparation
- Lighting
- Appliances: office equipment, electronics and all other electric equipment

Both for residential (See Figure1.3) and service buildings (See Figure1.4), space conditioning has the largest impact on the total energy use within buildings [10].

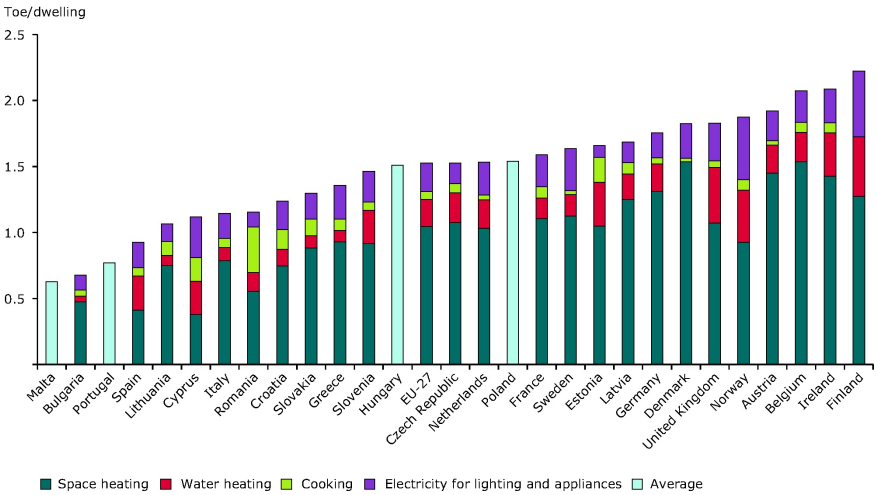

Figure 1.3: Average energy utilisation by end uses per dwelling for the European countries, reported by the European Environmental Agency (EEA) [9].

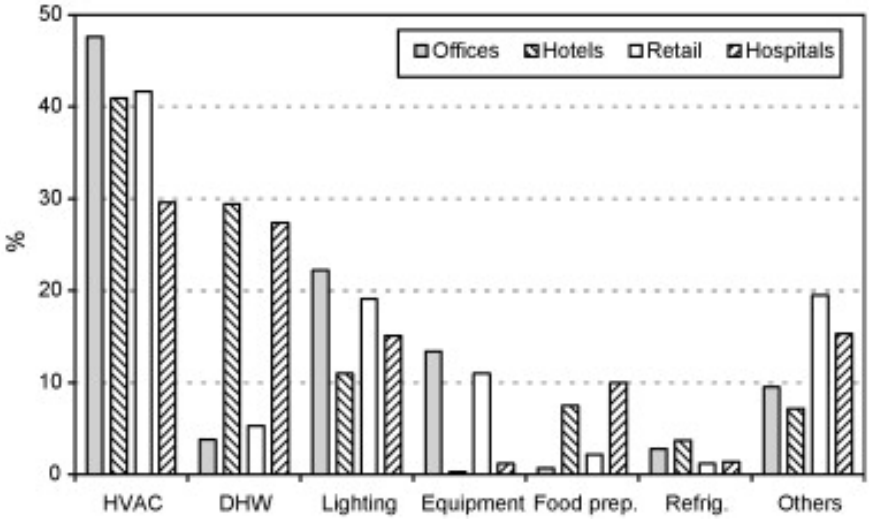

Figure 1.4: Energy utilisation by end use for different building types [10] .

It represents 30% (for hospitals) to almost 70% of the energy use within buildings. A large amount of this can be addressed to space heating, more particularly for the older building stock.
Including domestic hot water production (DHW), the older building stock has a relatively large heat demand compared to its electricity use. Reducing heat demand and implementing efficient energy systems for heat production will therefore have a large impact on the energy use in buildings.

Changing energy demand

Thanks to an improved rate of insulation and efficiency gains, enforced by the EPBD [8], the (thermal) energy needed for the same level of thermal comfort is declining. However, due to the rebound effect of an improved insulation rate [11] and change in user behaviour, the level of this thermal comfort is still increasing [10].
As a result, in most cases the heat demand declines, however at a slower rate as could be expected based on the efficiency gains. Therefore, an efficient (and small) heating system for domestic hot water production and space heating remains significant to reduce energy use in buildings.

Besides, in modern offices and even in residential buildings the energy demand for space conditioning is shifting from heating purposes to ventilation and air conditioning. Due to these higher demands for cooling and ventilation, but also due to an increasing number of electric appliances [12–14], the electricity demand in buildings is rising or at least staying the same, despite efficiency gains in lighting and appliances.
Because of all this, the energy profile in buildings is changing [15]: compared to the older buildings, the future building stock will have a lower heat demand and a similar or even higher electricity use.
This evolution is illustrated for commercial buildings by Figure 1.5 as the use of fossil fuels within buildings can be largely addressed to heating purposes. Figure 1.5 is the result of an elaboration of statistical data, reported by the U.S department of Energy [16] and shows the specific energy use by source, relative to floor area, which has increased over the years. It can be seen that energy demand is shifting to a lower heat-to-electricity ratio.
Nevertheless a heat demand will still be present and is still significant, as even passive houses require heat for domestic hot water production.

Improving energy systems in buildings

With the implementation of the EPBD [8], not only the building, but also the included energy systems are taken into account to evaluate energy performance

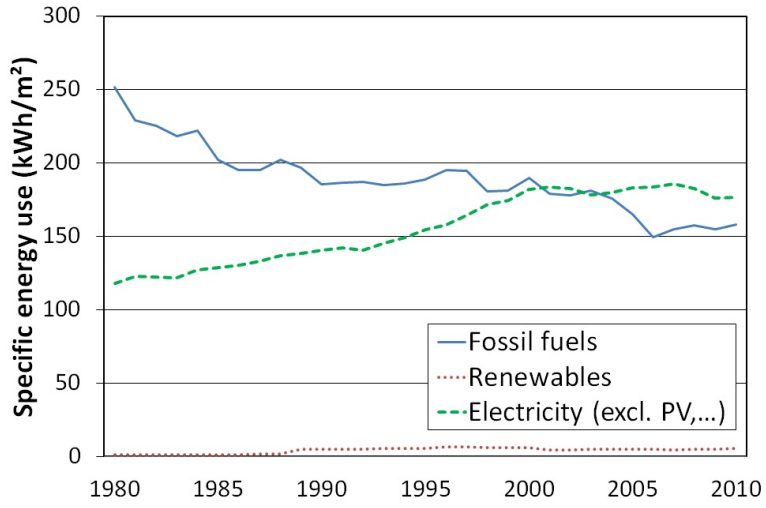

Figure 1.5: Evolution of the specific energy ($\frac{kWh}{m^2}$)in commercial buildings based on statistical data from the U.S. Department of energy [16].

of buildings. As CHP is an efficient way to convert fuel into useful energy and complimentary to other distributed (renewable) energy production, also micro-cogeneration (micro-CHP) for building applications is getting more attention [17–20].

1.3 Micro-CHP in buildings

1.3.1 Cogeneration

Combined heat and power (CHP) or cogeneration is an efficient way to utilize (fossil) energy resources. In Figure 1.6 the primary energy savings potential of cogeneration is illustrated. As heat and power are produced together the overall losses can be lower, if CHP is applied in the right way. Next to that, CHP proofs to be complementary to other and renewable distributed energy systems [21]. For this reason specific goals for CHP are set within the 20-20-20 targets [3, 22] of the European Union.

Sizing a CHP-unit

As transportation of thermal energy does not have a similar efficiency as it has for electrical energy, heat demand is most critical to size a CHP [23–25]. For a

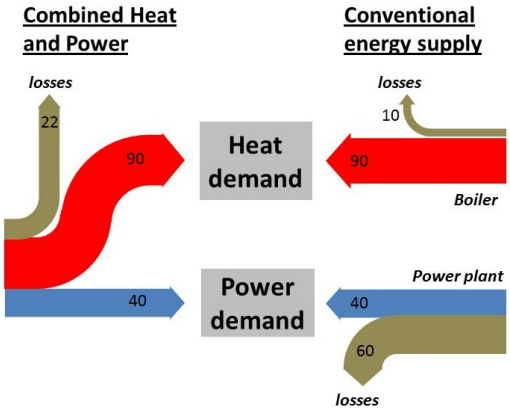

Figure 1.6: Comparison of a combined heat and power supply to a conventional (separate) energy supply as an indication for the savings potential.

successful implementation of a CHP unit, the unit has to have sufficient operating hours. Therefore, sites with a large and stable heat demand, in relation to the thermal power output of the CHP offer the highest economical feasibility and saving potential.

Size of a CHP-unit

As efficiency gains and installation costs are size dependent, originally only large industrial applications were installed. Due to increasing energy prices, technical improvements and cost reduction smaller CHP-units entered the market. Today units for residential purposes are commercially available.

Definition for micro-CHP

As several interpretations can be given to micro-CHP, a definition is given in Ref. [26] by the Flemish parliament, defining micro-CHP as a CHP-unit with an electrical power output of less than $50kW_e$. Other definitions exist, but within the objective of this book this definition will be used to categorize CHP-units as micro-CHP or not.

1.3.2 Available technologies for micro-CHP

Depending on size, several technologies are available. An overview of suitable technologies is given in Figure1.7. The most mature technologies are combustion based technologies, like micro-turbines, internal combustion engines [27] and Stirling engines [27, 28]. An illustration of these technologies is provided in

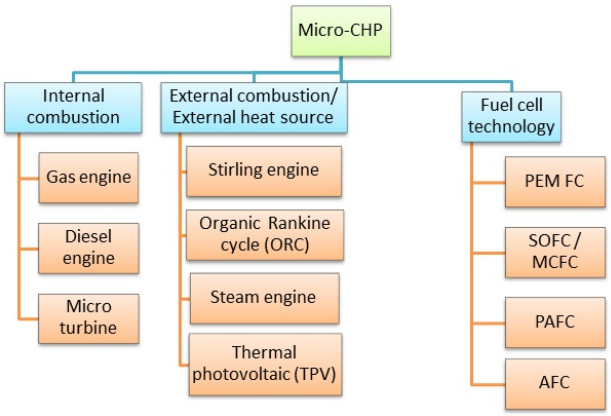

Figure 1.7: Overview of technologies suitable for micro-CHP

Figure1.8. More technical data can be found in Section 6.4, in which a comparison between these technologies is elaborated.
The efficiency of all these heat driven systems is limited by Carnot efficiency, due to the second law of thermodynamics. Temperature limitations due to size and used materials, and the presence of many moving parts and their friction losses result in a relatively low power-to-heat ratio for these CHP-units. This ratio even declines at part load (See also chapter 6).
This makes them suitable for buildings with a relatively high heat demand. For the existing building stock they can be an alternative solution to boiler driven heating systems. However, as discussed in Section 1.2, the energy profile within buildings is changing. To meet these future demands in buildings, those technologies are preferred, which promise higher power-to-heat ratios even at small scale.
In this prospect, fuel cell based micro-CHPs are a promising alternative technology in buildings with a relatively low heat demand. Fuel cells have the potential for high electrical efficiencies, compared to other technologies [32–34]. Contrary to other types of CHP-technologies, their electrical efficiency is independent of size. Moreover the electrical efficiency even increases at part load (See also Section 6.4). Therefore, fuel cell technology and the most significant types within the application domain as a micro-CHP will be discussed in the following section.

1.4 Fuel cell systems as a micro-CHP

Compared to conventional CHP-systems, fuel cells have the potential for high electrical efficiencies.

(a) micro-turbine

(b) Gas engine

(c) Stirling

Figure 1.8: Examples of commercially available micro-CHP technologies: a) a 15kW Capstone micro-turbine [29] b) a small gas engine from Honda Ecowill [30] c) a Whispergen Stirling engine [31]

1.4.1 Basic principle

Energy conversion

In Figure 1.9 the energy conversion for both technologies are illustrated, to understand this difference. Within a fuel cell, the chemical energy of a fuel (mostly hydrogen) is directly converted into electricity. Combustion based technologies convert the chemical energy first into heat, which drives afterwards a heat engine, producing mechanical energy. Next, an alternator converts the mechanical energy into electricity (See Figure 1.9(a)). As each energy conversion occurs with losses, this will affect the overall efficiency.
The theoretical energetic efficiency of a heat engine is limited by the Carnot factor, while the direct energy conversion of chemical energy into electricity is limited by the change in Gibbs free energy (ΔG).
Gibbs free energy represents the work potential of a reaction, as this is the net energy which is put into a system in order to create one [36]. As enthalpy change (ΔH) represents the total energy delivered by the fuel, the maximum thermodynamic efficiency is given by Eq. (1.1).

$$\eta = \frac{\Delta G}{\Delta H} \tag{1.1}$$

$$\Delta G = \Delta H - T \cdot \Delta S \tag{1.2}$$

Enthalpy can be interpreted as the total energy put into a system in order to create one [36]. Compared to Gibbs free energy, this also includes the heat transfer from the surroundings into the system.
Both efficiencies are temperature dependent as shown in Figure 1.9(b). It is shown that for low temperatures fuel cells have a higher theoretical efficiency.

Reaction

Despite the different ways to convert the chemical energy of a fuel into electricity, the chemical reactants are the same, if the same fuel is used. For hydrogen, which is the most conventional fuel for a fuel cell,the basic reaction is represented by following equation.

$$H_2 + \frac{1}{2} \cdot O_2 \longrightarrow H_2O \tag{1.3}$$

At the atomic scale bonds are broken and formed, respectively absorbing and releasing energy by the transfer of electrons. Normally, the net energy difference is released as heat, which can be converted into electricity by a heat engine and alternator. Within fuel cells the transfer of electrons is guided through an external electric circuit, by spatially separating the hydrogen and oxygen reactants [36] as illustrated in Figure 1.10 for a proton exchange membrane fuel cell (PEMFC) . At

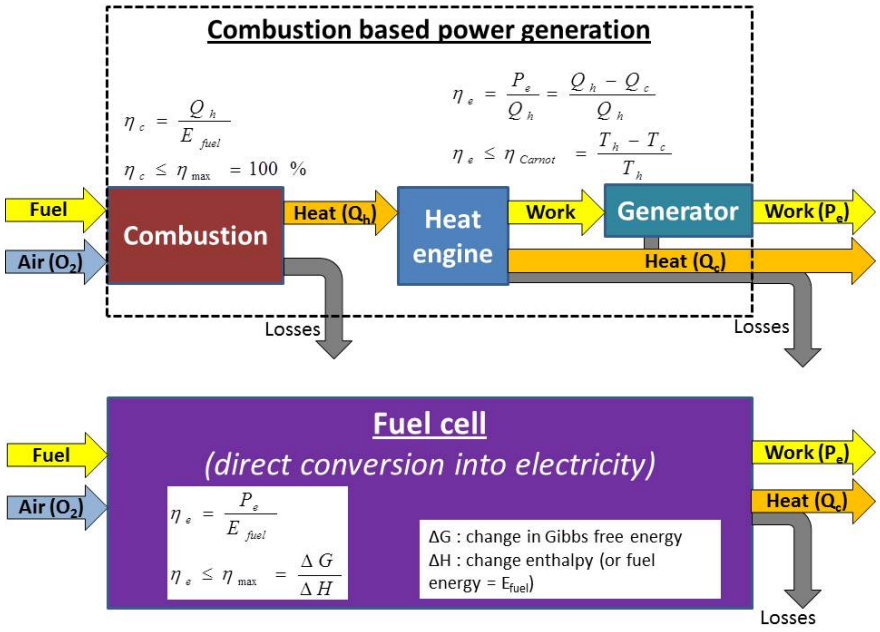

(a) Energy conversion

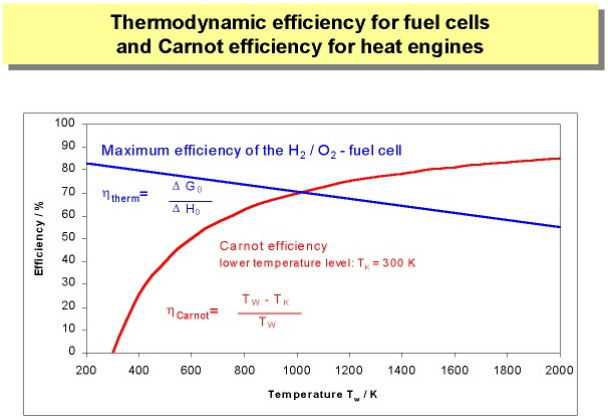

(b) Theoretical efficiencies

Figure 1.9: Comparison of the energy conversion between fuel cell based systems and heat-driven systems: a) different steps in energy conversion b) comparison of maximum theoretical efficiencies [35] .

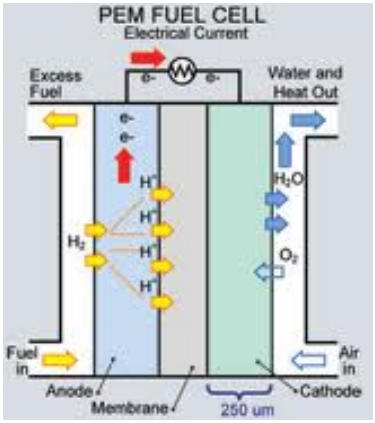

Figure 1.10: Working principle of a proton exchange membrane fuel cell (PEMFC) [37].

the electrode at the hydrogen side, the anode, hydrogen is split into protons and electrons.

$$H_2 \longrightarrow 2H^+ + 2e^- \tag{1.4}$$

The protons diffuse through a membrane (PEM) to the other side of the fuel cell, the cathode. The electrons are guided through an external circuit to the cathode. At the cathode they react with the oxygen into water (vapour), which is the result of the overall reaction.

$$\frac{1}{2} \cdot O_2 + 2H^+ + 2e^- \longrightarrow H_2O \tag{1.5}$$

The difference in Gibbs free energy is translated into an electric potential over the anode and the cathode the Nernst potential, E_{Nernst}. This potential and the voltage losses can be illustrated in a polarization curve (See Figure 1.11). Ideally the fuel cell would have a fixed potential, the Nernst potential, E_N, as shown in Figure 1.11. To start, an amount of activation energy is needed, comparable to the spark in an engine. This results in the activation losses, causing a voltage drop as soon as some current is drawn out of the fuel cell.
Because ideal conduction does not exist, there will also be some resistance losses both for the electrons leaving the fuel cell as for the ions transferred between the electrodes.
As the reaction takes place on a catalyst (mostly platinum) on the electrodes, the reaction area is limited. Consequently, the diffusion of the gasses to this reaction area will limit the maximum reaction rate. This results in concentration (or diffusion) losses at higher current densities, limiting the maximum current and power, which can be obtained from a fuel cell.

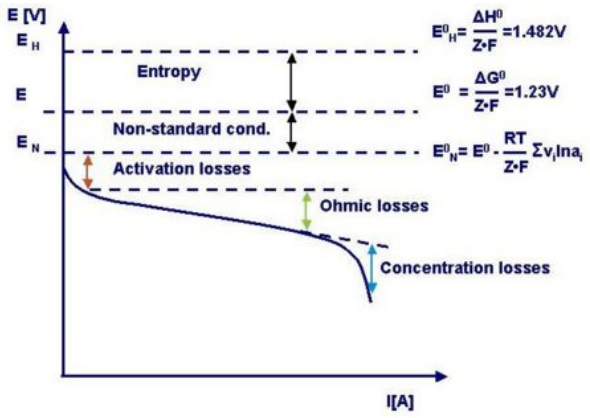

Figure 1.11: Polarization curve: characterisation methode and illustration of fuel cell performance (Source: [38]).

The influence parameters on these losses are discussed more in detail for the alkaline fuel cell model in chapter 2 with the elaboration of the model and more in general in Refs. [36, 39]. Important to emphasise here, is the fact that these losses are also temperature dependent and decline with rising temperature. Therefore, temperature is an important parameter to increase electric voltage of the fuel cell.
Theoretically the potential over the fuel cell is about $1.23V$, in practical case this is about $0.7V$. Fuel cell research and developments focus on improving this efficiency and increasing lifetime, as it is noticed performance degrades over time [40].

1.4.2 From cell to system

To use the fuel cell within real applications, $1V$ is too low. Therefore, several fuel cells are serially stacked together into a fuel cell stack (See Figure 1.12(a)).
As the stack generates DC electricity, an inverter is needed to put the electricity on the grid. Next to an inverter, also piping, blowers, pumps and units to purify the air inlet and to monitor and manage the removal of water (vapour) and the hydrogen pressure are needed within a fuel cell system.(See Figure 1.12(b))
The application of fuel cell technology as micro-CHP refocused the research and development efforts on fuel cells [41]. Next to stack performance and lifetime, the ability of heat recovery in the system design became an important research topic for possible improvements [41, 42].

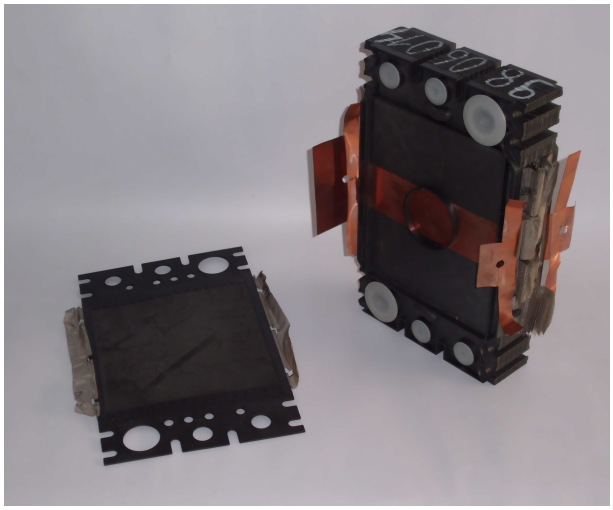

(a) Single cell and stack

(b) Complete fuel cell system

Figure 1.12: Illustration of the integration of a) cell into a stack and b) stack into a complete system for an AFC of $5.5kW_e$

1.4.3 Fuel cell economics

Next to these technical improvements, also reducing installation cost is critical for the economical feasibility of fuel cell projects [43, 44]. This cost reduction can be found on the level of the fuel cell in the use of cheaper (non-noble) materials or in a more cost effective system design, with less (expensive) components.

1.4.4 Hydrogen and Fuel cell technologies

An overview of the different fuel cell technologies and their working conditions is presented in Figure 1.13.

Hydrogen

As can be seen in Figure 1.13 most fuel cells work with hydrogen as a fuel. As for the high temperature fuel cells, like solid oxide fuel cells (SOFC) and molten carbonate fuel cells (MCFC), hydrogen can be produced by internal reforming, which makes these types suitable to run on natural gas. For the other types, hydrogen has to be produced by electrolysis or reforming. With a sustainable energy source for this process, this energy carrier can contribute to a reduction of greenhouse gases and the issue of energy storage within a sustainable energy supply [45]. New types of fuel cells, like microbiological fuel cells, which only exist as a prototype, are renewable by nature.

Fuel cell types

The more conventional fuel cells, listed in Figure 1.13, are already used in practical applications. Table 1.1 presents an overview of this, including some details about their performance. As can partially be deducted out of Table 1.1, four prominent fuel cell technologies are suitable as micro-CHP for building applications, namely solid oxide fuel cells (SOFC), proton exchange membrane fuel cells (PEMFC), phosphoric acid fuel cells (PAFC) and alkaline fuel cells (AFC) [42, 46].
Molten carbonate fuel cells are only used in large CHP-units and are possibly useful to integrate in larger power plants [47].
The fuel cell types suitable within micro-CHPs are briefly discussed.

SOFC

Solid oxide fuel cell (SOFC) technology is the most mature technology, with reported lifetimes of more than $10,000$ – $26,000h$ [48, 49] and a degradation rate of about 1% for $1,000h$ [48–50]. Next to this advantage, it can run on natural gas [32, 51] by internal reforming. Other types of fuel cells run on hydrogen and are poisoned by CO (PEMFC) or CO_2 (AFC), which limits reforming within a

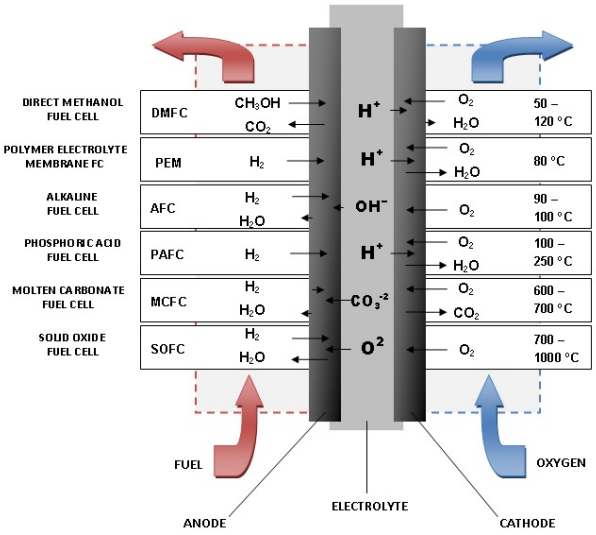

Figure 1.13: Overview of different fuel cell types and their working conditions: fuel, temperature and ion transport.

Type	Electrolyte	Cell efficiency	Nominal power (systems)	Applications
AFC	KOH (NaOH)	45 – 60%	1 – 100kW_e	Aerospace, Military, back-up power, CHP
PEMFC	Membrane	30 – 60%	1 – 250kW_e	Mobile applications, back-up power, CHP
PAFC	Liquid H_3PO_4	35 – 40%	< 250kW_e	CHP
MCFC	Li_2CO_3 and K_2CO_3	45 – 60%	< 1MW	CHP
SOFC		45 – 65%	1 – 300kW_e	CHP

Table 1.1: Overview of different fuel cell types with their main characteristics, besides those mentioned in Figure 1.13

system set-up. Within buildings SOFC show to be already competitive with fuel oil and electrical heating systems. Their viability could be increased by improving utilization of waste heat [52].

PEMFC

Next to SOFC, also micro-CHP systems based on proton exchange membrane fuel cells (PEMFC)are developing rapidly [51, 53–55]. Lifetimes of $5\,000$ – $26\,000h$ and degradation rates of 1 – $20mV/1000h$ are reported (See Refs. in [56]). The energetic-exergetic comparison in [57] shows that PEMFC based systems use their fuel energy input more efficiently than SOFC based systems for building application. This was expected, since building applications do not require the high temperature of the SOFC system.

PAFC

The earliest fuel cell successes and commercial breakthrough were achieved with the phosphoric acid fuel cell (PAFC). Already in the nineties lifetimes of more than $10\,000h$ and degradation rates of about $2mV/1000h$ were reported. Despite the original interest of a number of companies in this technology, the activities in PAFC are almost vanished. An important drawback for the PAFC is the use of the liquid electrolyte, namely concentrated phosphoric acid. Because the PAFC is operated at a high temperature, some acid loss cannot be avoided during operation. With the emerging interest in PEM technology, almost all activities in PAFC were shelved [39].

AFC

Like PEMFCs, alkaline fuel cells (AFC) work at relatively low temperature, in the range of $50°C$ to $90°C$. In [46, 58, 59] it is shown that within the domain of (micro-)CHPs for building applications, also an AFC-based system offers possibilities.

1.5 Alkaline fuel cells

Alkaline fuel cells (AFCs) are often forgotten since the surge of interest in PEMFC and SOFC [60]. The major reasons for this decline in interest is the known CO_2-intolerance of the liquid electrolyte, where the CO_2 leads to the formation of carbonates, degrading the fuel cell and limiting lifetime [61]. In strong alkaline environments, like sodium hydroxide (NaOH) this is even more pronounced as the solubility of carbonate is much lower here. Therefore, alkaline fuel cells (AFCs) normally use a mobilized or immobilized aqueous solution (30 – $45wt\%$)

of potassium hydroxide (KOH) as an electrolyte [36].
Reported lifetime is about $4\,000h$ [39, 62]. Next to this, the non-solid liquid electrolyte is experienced as a drawback for the AFC-system, since it is (even for KOH-solutions) corrosive and limits orientation of the stack [39].
Recently, research and development efforts of alkaline membrane fuel cells are rising [63, 64], hoping to combine the advantages of both PEMFC and AFC. Despite a diminished interest in the last decade in alkaline fuel cells, compared to PEMFC, the electrical efficiencies presented in [59, 65] are still competitive to PEMFC and SOFC used for micro-CHP [52, 66] and certainly to other CHP-technologies [20, 27, 28]. Recent studies even show that efficiency improvements are still possible by using different preparation methods for the development of electrodes [67].
Next to a high efficiency, the AFC also has some other interesting prospects such as cheaper construction, as it can be manufactured at less cost by non-noble materials [60, 68–70]. The perceived disadvantage of carbon dioxide intolerance was found to be a minor problem. Next to several cost-effective solutions for carbon dioxide removal [42], in recent publications also a carbon dioxide tolerance of the AFC was found [60, 71]. This led to renewed interest in AFC technology [42, 68].
As discussed earlier, next to lifetime improvements and handling degradation, the biggest advancements and reduction in total environmental impact are to be expected in reducing catalyst loading and optimising the overall system [42]. To optimise the overall system of an AFC-based micro-CHP for buildings it is necessary to understand the complete thermodynamic behaviour of the fuel cell.

1.6 Objective and motivation of this PhD

As research and development efforts used to focus on electrical performance of the stack, it is expected most improvement potential is to be found in increasing thermal efficiency of the system. Besides this, also an effective and stable water management is a necessary boundary condition to each system design. Also in this area, system efficiency and applied control strategy show some improvement potential.
However, before new system set-ups and control strategies can be evaluated, it is necessary to understand how electric performance, thermal behaviour and water household of the alkaline fuel cell stack can be influenced.
With a thorough insight in the behaviour of the alkaline fuel cell new set-ups and control strategies can be explored, allowing to evaluate the potential of an AFC-based micro-CHP within buildings.

Objectives and work plan

In this Ph.D. following objectives and corresponding work plan were posed in order to improve system design and control strategy for an alkaline fuel cell system as a micro-CHP within building applications.

- First and main objective is to develop a validated model of an alkaline fuel cell stack. This model has to be able to predict electric performance, thermal behaviour and water household, based on conditions of operation. The results to fulfil this objective are described in chapters 2 and 3, whereas the model development and model validation are elaborated.
- Secondly to coordinate system improvements, a thorough analysis of the fuel cell stack behaviour is necessary. The focus of this analysis is not how to optimize the stack, but at which conditions it works best. (See chapter 4).
- Subsequently, these recommendations need to be translated into several system models, each containing all necessary sub models and an adjusted control strategy (See chapter 5).
- Next, an evaluation and comparison between these different system designs need to be made to specify the sensitivity to a careful selection of auxiliary components and to illustrate the improvement potential (See chapter 6).
- Finally, it is necessary to illustrate the potential of the AFC-based micro-CHP. This can be done by comparing the part load behaviour to other technologies or by elaborating a case study (See chapters 6, 7 and 8).

With this work plan, the author aims to explore the potential of an AFC-based micro-CHP system for building applications in order to focus future system improvements and developments.

2

Model development of an alkaline fuel cell stack

A model does not only have to be pretty, but is subordinate to the goal for which it is made for. For this reason, a detailed study of the electrochemical reactions is beyond the scope of this model. Such a model could be useful in order to improve materials or cell configuration or to understand transient electric behaviour of the different cells.
However, the goal of this research is to understand and study stack behaviour regarding system integration within stationary applications like micro-CHP. Therefore, an alkaline fuel cell model is developed predicting thermal behaviour and water removal of the stack, including their influence on performance under different operation modi.

2.1 General operation

An overview of the general operation of an AFC system is given in [59]. As shown in Figure 2.1 an AFC operates by introducing hydrogen at the anode and oxygen/air at the cathode.

- At the hydrogen inlet a gas mixture of water vapour and hydrogen enters the gas chamber of the fuel cell. The hydrogen diffuses out of the gas chamber into the working area of the anode.

- At the oxygen inlet CO_2-free air or pure oxygen arrives in the gas chamber. The oxygen diffuses into the working area of the cathode to take part in the reaction.

Both electrodes, anode and cathode, are separated by a circulating electrolyte, a 6M potassium hydroxide solution (Figure 2.1). At the anode hydrogen reacts with

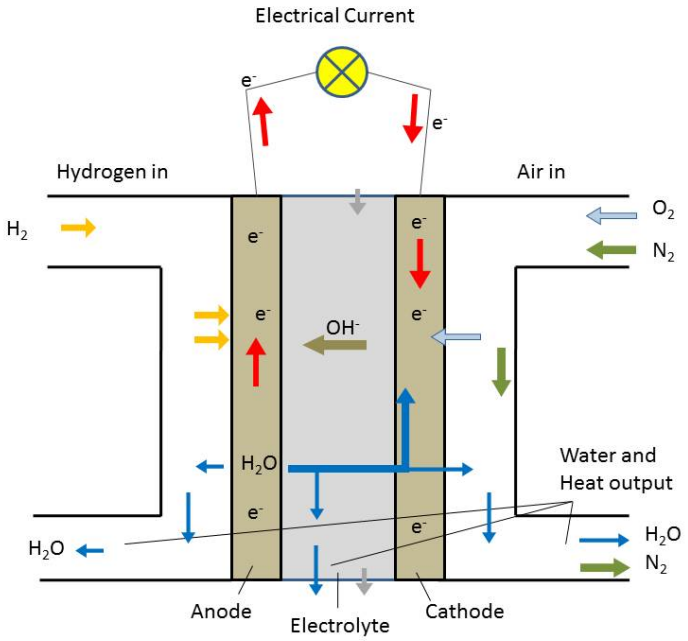

Figure 2.1: Working Principle of an Alkaline Fuel Cell

hydroxyl ions into water and free electrons, Eq. (2.1):

$$H_2 + 2(OH)^- \longrightarrow 2H_2O + 2e^- \tag{2.1}$$

Within the electrolyte, the water is transported from the anode to the cathode. An external electric circuit leads the electrons to the cathode. At the cathode oxygen reacts with water and electrons into hydroxyl ions, Eq. (2.2):

$$H_2O + \frac{1}{2}O_2 + 2e^- \longrightarrow 2(OH)^- \tag{2.2}$$

These ions flow from cathode to anode through the electrolyte, to sustain the total electrochemical reaction. Combining both reactions the overall reaction, Eq. (2.3),

shows that the end product is water, which can be removed in one or both gas streams or in the electrolyte, depending on the fuel cell configuration.

$$H_2 + \frac{1}{2}O_2 \longrightarrow H_2O \tag{2.3}$$

The overall reaction is exo-energetic. This energy has an electric part, which is transferred in the external electric circuit, and a thermal part, which results in a temperature rise inside the fuel cell. To maintain the overall fuel cell temperature, heat is removed by outlet mass flows or by losses to the surroundings.
Recuperation and utilization of this heat will enable the fuel cell to be operated as a CHP.

2.2 Literature review on AFC models

To understand AFC behaviour for integration into a CHP-unit, an alkaline fuel cell stack model has to be able to predict electric performance and thermal behaviour. Next to these, also a good understanding of the water household is necessary for a stable operation.
Originally, however, only the ability of electricity generation drove fuel cell research and the development of alkaline fuel cell models.

Focus on electric performance

In order to improve fuel cell performance, mathematical models were developed which were able to predict electrical power. In the early nineties Kimble and White proposed a model for a complete fuel cell, where they take into account the polarization and physical phenomena going on in the solid, liquid and gaseous phase of both anode, separator and cathode regions, assuming a macro homogeneous, three-phase porous electrode structure [72].
The model divides the fuel cell in five layers, a gas diffusion layer and reaction layer for both anode and cathode and a separator, containing the electrolyte.
In 1999 this model was the basis for the model of Jo and Yi. They made corrections to some invalid correlations and parameters e.g. in the open-circuit potential and the liquid diffusion parameters [73]. Both Kimble and White and Jo and Yi used immobilized or re-circulating electrolyte and removed water in the gas streams.
In 2006 Duerr et al. translated the model of Jo and Yi to a stack-model in a Matlab/Simulink surroundings and added dynamics to the electrical part of the model [74]. The stack is simulated as a large cell and the cell results and inputs are translated into stack results and inputs and vice versa. Few details were given on the calculation method and the estimation method of some physical parameters.
Recently, the first results were shown of a 3D-model of an AFC-stack, built by De

Schepper et al. [75]
All these models are meant to predict the polarization curve or electric response of the fuel cell. However, they do not make any predictions on thermal behaviour and they all make assumptions on the water household, with the water being removed in a predefined gas stream.
These models can be used to optimize electrical integration or to understand the electrochemical reactions within the fuel cell in more detail in order to improve its performance on level of the cell. However, they are not sufficient to meet the goal of our research, for which a good understanding and prediction of the thermal behaviour and water household is a necessity.

General thermodynamic behaviour

To understand the general thermodynamic behaviour a few stack models were built.
In 1998 Rowshanzamir et al. studied the mass balance and water management in the AFC [76] by only applying mass balances and diffusion laws (Stefan-Maxwell) for the gas diffusion layer. However, their model does not provide any prediction on fuel cell performance or on thermal behaviour.
In 2009 a first version of the model was presented predicting both electrical performance and thermal behaviour (See Appendix A or Ref. [77]). In Zhang et al. [78] part of this model was used and extended with incorporation of the influence of the electrolyte concentration on the electrochemical model.

Critical view on the water management

In all previous models the reaction water was assumed to be disposed into the gas streams as vapour, either into one or into both. This assumption was the consequence of the used alkaline fuel cell type, with or without circulating electrolyte, the desired working point and/or the scope of the model.
However, in general this assumption is not valid in real life, as water can also be removed in liquid phase in the electrolyte flow.
The fuel cell (system) in our research removes water by both exhaust gases and electrolyte flow. After the fuel cell, all these streams are collected in one reservoir, where eventually at nominal working point, the air flow is responsible for the disposal of water (vapour). At nominal operation all reaction water is removed by the air flow. However, in practice there is a net evaporation or production of liquid water in the electrolyte, resulting in an unstable state and eventually switching the system off into safety mode.

For an improved system design and control strategy it is necessary to understand this behaviour. Therefore, in this work, the possibility of water disposal into the

electrolyte, is included, in order to predict the water management within the stack allowing to generate intelligent control strategies in the future.

2.3 Steady state model

As the thermal behaviour and water household react rather slowly compared to changes in the electrical circuit, first the development of the steady state model is discussed, neglecting all dynamics. In Section 2.4 dynamics will be added to the model equations in order to describe the transient thermal behaviour of the stack.

2.3.1 General equation and model assumptions

Similar to Duerr et al. [74] a cell model is used to describe (sub)stack behaviour, since the cells within a (sub)stack are all parallel to each other and experience the same conditions.
The alkaline fuel cell model is divided into 5 sub volumes, each with their own physical and thermodynamic behaviour. For each control volume the mass and energy balance are posed. Next to this, the following assumptions were made:

- Dynamic pressure losses within the fuel cell are neglected. In this way the total pressure is assumed constant over the entire fuel cell. The same approach is used for a PEM fuel cell in [79], which is more critical than AFC to pressure drops, because it has no liquid electrolyte. This assumption is acceptable, since the actual pressure drop (about 15 – $60\ mbar$) is relatively low, compared to the absolute pressure ($1\ bar$).
  Based on the datasheet of the system used for validation (See chapter 3), the maximum possible pressure drop is only $60\ mbar$ in the electrolyte flow and $40\ mbar$ in the two gas flows. During the experiments, described in Chapter 3, the monitored pressure drops in the electrolyte flow, hydrogen flow and air flow did not exceed 40, 28 and $15\ mbar$.

- The temperature is assumed to be uniform in each control volume and is a weighted average of the in- and output flows. Next to that, all output flows have the same temperature, which is similar to the approach in [79].

- The partial pressures within the gas chambers are the mean (partial) pressures of the input and output flow in the direction of the gas channels.

- The heat losses from the gas chambers to the surroundings are neglected, because the heat transfer surface is relatively small. All heat losses to the surroundings are therefore modelled as heat losses of the fuel cell body to the surroundings.

The five parts that are considered in the control volume model, are the anode and cathode gas chambers (AGC and CGC), the anode and cathode gas diffusion layers (AGDF and CGDF) and the fuel cell body (FCB), where the reaction takes place (See Figure 2.2). The model is modularly built. In this way a more detailed model can be obtained by serially connecting several individual models. Table 2.1 gives an overview of the molar and energy flows shown in figure 2.2. Model specific elements are

- that the heat transfer between the reaction layer and the gas chambers is modelled as a convective heat transfer. In this equation the influence of flow velocity on the heat transfer coefficient is taken into account, according to the appropriate Nusselt - Reynolds relation.
- that the hydrogen and oxygen consumption and the water vapour removal of the fuel cell model is based upon diffusion laws. The diffusion is described by the Stefan-Maxwell equation, Eq.(2.4):

$$\frac{dy_i}{dz} = \frac{RT}{p} \cdot \sum_j \frac{y_i \cdot N_j - y_j \cdot N_i}{D_{ij}} \tag{2.4}$$

  In this equation, the z-coordinate represents the dimension in which the diffusion occurs.

- that the water vapour in the fuel cell body is assumed to be saturated. In this way a direct relation between cell temperature and partial pressure of water vapour can be posed, Eq.(2.5):

$$p = f(T) \tag{2.5}$$

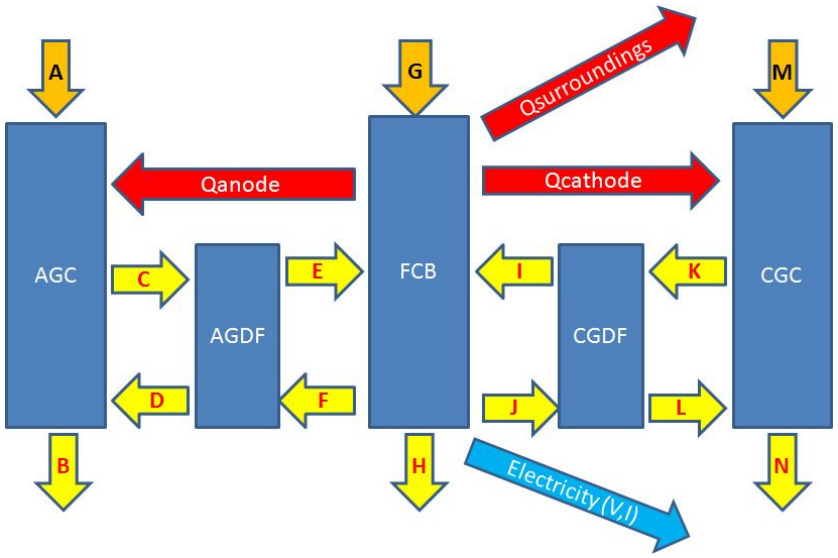

Figure 2.2: Lay-out of the alkaline fuel cell model (See Table 2.1 for a detailed description), which is representative for a complete (sub)stack.

Name	Description
AGC	Anode gas chamber, part of the hydrogen flow channel in contact with the fuel cell.
AGDF	Anode gas diffusion layer, boundary layer where gasses (hydrogen and water vapour) diffuse into and out of the fuel cell.
FCB	Fuel cell body, existing of both catalytic layers (with the electrodes) and of the separator layer (the electrolyte, in which the ion transport takes place.)
CGDF	Cathode gas diffusion layer, boundary layer where gasses (oxygen and water vapour) diffuse into and out of the fuel cell.
CGC	Cathode gas chamber, part of the air flow channel in contact with the fuel cell.
A	Input molar flow at the anode, containing hydrogen (and water vapour).
B	Output molar flow at the anode, containing water vapour (and hydrogen).
C	Molar flow of hydrogen, diffusing from AGC into FCB, at the boundary with AGC.
D	Molar flow of water vapour, diffusing from FCB into AGC, at the boundary with AGC.
E	Molar flow of hydrogen, diffusing from AGC into FCB, at the boundary with FCB.
F	Molar flow of water vapour, diffusing from FCB into AGC, at the boundary with FCB.
G	Input molar flow for FCB, containing electrolyte (water).
H	Output molar flow from FCB, containing electrolyte (water).
I	Molar flow of oxygen, diffusing from CGC into FCB, at the boundary with FCB.
J	Molar flow of water vapour, diffusing from FCB into CGC, at the boundary with FCB.
K	Molar flow of oxygen, diffusing from CGC into FCB, at the boundary with CGC.
L	Molar flow of water vapour, diffusing from FCB into CGC, at the boundary with CGC.
M	Input molar flow for CGC, containing (wet)air
N	Output molar flow from CGC, containing wet air
Q_{anode}	Energy flow: (convective) heat transfer from FCB to AGC.
$Q_{cathode}$	Energy flow: (convective) heat transfer from FCB to CGC.
$Q_{surroundings}$	Energy flow: heat losses to the surroundings.
Electricity	Energy flow: generated electricity.

Table 2.1: Description of the control volumes and the molar and energy flows in Figure 2.2

2.3.2 Model Variables

Each molar flow shown in Figure 2.2 is determined by 8 variables (See Table 2.2). Next to the molar flows five other variables are shown in Figure 2.2 and described in Table 2.2, the three heat fluxes and the electric power output, determined by voltage and current. The goal of the model is to predict the output flows (B, H and N), the generated electric power and the heat loss to the surroundings based upon the input flows (A, G and M). The other flows are intermediate stages which provide more understanding of the physical behaviour of the fuel cell. Based upon Figure 2.2 all variables within the model are defined. The model exists of 14 mass flows and 4 energy flows. Each mass flow is characterized by 8 variables which describe the state of the flow (See Table 2.2). The energy flows are heat or electricity. The electric power is characterised by current and voltage.

Variables	Symbol	Unit
Molar Flow	F	$kmol/h$
Temperature	T	$°C$
Pressure	p	bar
Enthalpy	h	$GJ/kmol$
Molar Fraction Hydrogen	y_{H_2}	
Molar Fraction Oxygen	y_{O_2}	
Molar Fraction Water(Vapour)	y_w	
Molar Fraction Nitrogen	y_{N_2}	

Table 2.2: List of variables in each mass (molar) stream

2.3.3 Model equations

For each control volume a mass and energy balance is solved. The energy balances are closed by heat fluxes between neighbouring control volumes or between a control volume and the surroundings. This heat flux is modelled as a convective heat flux. Next to heat and mass transfer between control volumes, also electric energy, generated in the fuel cell body is transferred to the surroundings. An electrochemical model is used to describe the electric behaviour of the fuel cell. Finally the gas diffusion equations are used to relate the gas flows to the partial pressure of water vapour, which is assumed to be saturated in the fuel cell body.

2.3.3.1 Variable reduction

Since the intermediate flows are defined as component specific flows and based upon the nature of the inlet flows a number of molar fractions can be predefined, which will reduce the number of equations in the following model description.

2.3.3.2 Anode gas chamber

As shown in Figure 2.2, the fuel (A), a mixture of hydrogen and water vapour, enters the gas chamber, where the hydrogen diffuses into the gas diffusion layer (B). A part of the water, formed during the reaction in the fuel cell body, diffuses as water vapour back into the hydrogen gas chamber (C). A mixture of unused fuel and water vapour leaves the gas chamber to a next stage (D). Translating this to the molar flow and fractions within the anode gas chamber the following equations can be posed.

Molar balance:

$$\begin{aligned} F_A + F_D &= F_B + F_C \\ F_A \cdot y_{H_2,A} &= F_B \cdot y_{H_2,B} + F_C \\ F_A \cdot y_{w,A} + F_D &= F_B \cdot y_{w,B} \end{aligned} \tag{2.6}$$

As boundary condition in the simulation the fuel entering the (first) gas chamber is pure hydrogen and there is no hydrogen leaving the (last) gas chamber as unused fuel, because it is an end-of-pipe system. This means the anode gas chamber of the complete stack is only connected with a hydrogen source and kept pressurized, without any circulation. More details on this are given in Chapter 3.

Energy balance:
Within the energy balance a heat transfer is defined from the fuel cell body to the gas chamber, since the gas and electrolyte flows in the channels are not insulated from each other.
At fixed flow rates, heat transfer can be calculated taking only temperature difference into account. However, like wind influences the cooling effect on a building, higher flow velocities will increase this heat transfer. This effect is also shown in the experimental results shown in Section 3.1.3.
For this reason, the heat transfer coefficient is modelled to be a function of the gas velocity in the gas chamber. This dependency finds its origin in the Nusselt - Reynolds correlation, which is discussed further in Section 3.1.3.

$$\begin{aligned} F_A \cdot h_A + F_D \cdot h_D + Q_{anode} &= F_B \cdot h_B + F_C \cdot h_C \\ Q_{anode} &= hA_{FCB,an} \cdot (T_{FCB} - T_{AGC}) \\ hA_{FCB,an} &= c_5 \cdot v_{gasstream}^{c_6} \end{aligned} \tag{2.7}$$

The calculation of the temperatures will be determined by the energy balance, since the calculation of the enthalpies is based upon temperature, molar fraction and pressure. See section 3.4.8 for more details on enthalpy calculation in Matlab. Next to these equations the assumptions offer extra relations, regarding pressure

and temperature, which can be translated in the following equations for the anode gas chamber.

Temperatures and pressures:

$$\begin{aligned} T_{AGC} &= \frac{F_A \cdot T_A + F_B \cdot T_B}{F_A + F_B} \\ T_B &= T_C \\ p_A &= p_B \\ p_C &= \frac{p_A \cdot (F_A \cdot y_{H_2,A}) + p_B \cdot (F_B \cdot y_{H_2,B})}{F_A + F_B} \\ p_D &= \frac{p_A \cdot (F_A \cdot y_{w,A}) + p_B \cdot (F_B \cdot y_{w,B})}{F_A + F_B} \end{aligned} \tag{2.8}$$

2.3.3.3 Cathode gas chamber

The entering air contains oxygen, nitrogen and water vapour. There is a large excess of air because air is used to remove water vapour from the cathode. While oxygen diffuses to the fuel cell body, water vapour diffuses into the gas stream. The same remarks regarding heat transfer in the energy balance which were made for the anode are valid for the cathode.

Molar balance:

$$\begin{aligned} F_L + F_M &= F_K + F_N \\ F_M \cdot y_{O_2,M} &= F_K + F_N \cdot y_{O_2,N} \\ F_L + F_M \cdot y_{w,M} &= F_N \cdot y_{w,N} \\ F_M \cdot y_{N_2,M} &= F_N \cdot y_{N_2,N} \end{aligned} \tag{2.9}$$

Energy balance:

$$\begin{aligned} F_L \cdot h_L + F_M \cdot h_M + Q_{cathode} &= F_K \cdot h_K + F_N \cdot h_N \\ Q_{cathode} &= hA_{FCB,cat} \cdot (T_{FCB} - T_{CGC}) \\ hA_{FCB,cat} &= c_5 \cdot v_{gasstream}^{c_6} \end{aligned} \tag{2.10}$$

Temperatures and pressures:

$$\begin{aligned} T_{CGC} &= \frac{F_M \cdot T_M + F_N \cdot T_N}{F_M + F_N} \\ T_K &= T_N \\ p_M &= p_N \\ p_K &= \frac{p_M \cdot (F_M \cdot y_{O_2,M}) + p_N \cdot (F_N \cdot y_{O_2,N})}{F_M + F_N} \\ p_L &= \frac{p_M \cdot (F_M \cdot y_{w,M}) + p_N \cdot (F_N \cdot y_{w,N})}{F_M + F_N} \end{aligned} \tag{2.11}$$

The cathode outlet temperature is one of the main parameters for which the model is validated.

2.3.3.4 Anode gas diffusion layer

Between gas chamber and active surface a layer can be defined in which the diffusion or migration of the gases towards the reaction zone takes place. Since molar fractions are fixed, the molar balance is very simple. The energy balance is built in the same way as for the gas chambers. Temperatures are calculated similar to the gas chambers.

Molar balance:

$$\begin{aligned} F_C &= F_E \\ F_D &= F_F \end{aligned} \tag{2.12}$$

Energy balance:

$$F_C \cdot h_C + F_F \cdot h_F = F_D \cdot h_D + F_E \cdot h_E \tag{2.13}$$

Temperature :

$$T_D = T_E \tag{2.14}$$

Diffusion equations and pressures:
In absence of a global pressure drop between the gas chamber and fuel cell body, the driving force behind this migration is the concentration difference of the gases between the gas chamber and the boundary of the fuel cell body. This concentration difference is captured in the partial pressure difference between fuel cell body and gas chamber. The pressure of the intermediate flows in the model are

in fact partial pressures. E.g. p_C is the partial pressure of hydrogen in the anode gas chamber and p_E will be the partial pressure of hydrogen at the boundary with the fuel cell body. The total pressure at each boundary is the sum of the pressure of the flows passing this boundary, since only water vapour and hydrogen are present at the anode side.

$$p_C + p_D = p_E + p_F \tag{2.15}$$

$$y_w + y_{H_2} = 1 \tag{2.16}$$

Taking this into account the Stefan-Maxwell equation (2.4) results in one independent differential equation, describing the diffusion and the lack of global pressure drop between the two boundaries (one of the assumptions, mentioned above).

$$\frac{dy_{H_2}}{dz} = \frac{RT}{P} \cdot \frac{y_{H_2} \cdot N_w - y_w \cdot N_{H_2}}{D_{Hw}}$$

with:

$$\begin{aligned} N_w &= -a_1 \cdot F_D \\ N_{H_2} &= a_1 \cdot F_C \\ a_1 &= \frac{1}{n_{stack} \cdot n_{parallel} \cdot A_{cell}} \end{aligned} \tag{2.17}$$

The resulting differential equation is a first order equation (Eq.2.18)

$$\frac{dy_{H_2}}{dz} = \frac{RT}{P} \cdot \frac{y_{H_2} \cdot (N_w + N_{H_2}) - N_{H_2}}{D_{Hw}} \tag{2.18}$$

Since the diffusion occurs between the two boundaries, each boundary can be represented by a z-coordinate. As boundary condition the molar fraction in the gas chamber is set equal to a weighted mean of input and output flow, which was also the case for the (partial) pressure. Therefore at the anode side the following conditions have to be fulfilled.

$$y_{H_2} \cdot p_{tot} = p_C \tag{2.19}$$

$$y_w \cdot p_{tot} = p_D \tag{2.20}$$

$$z = 0 \tag{2.21}$$

Since these partial pressures are a function of the molar flow, within the diffusion equations, an extra boundary condition is needed. This boundary condition is found at the side of the fuel cell body, which can be defined by the thickness of the gas diffusion layer, L_{GDF}. At this side, it is assumed that the partial pressure

of the water vapour is equal to the saturation pressure in the fuel cell body, as a result of the earlier mentioned model assumptions. This results in the following equations:

$$y_{H_2} \cdot p_{tot} = p_E \tag{2.22}$$

$$y_w \cdot p_{tot} = p_F \tag{2.23}$$

$$p_F = p_{saturation,FCB} \tag{2.24}$$

$$z = L_{GDF} \tag{2.25}$$

The saturated water vapour pressure is a property function of temperature and calculated based on the temperature in the fuel cell body (FCB), T_{FCB}. The calculation of physical properties is discussed in Section 2.3.4.

$$p_{saturation,FCB} = f\left(T_{FCB}\right) \tag{2.26}$$

2.3.3.5 Cathode gas diffusion layer

Similar to the anode gas chamber, at the cathode side a gas diffusion layer can be defined. Instead of diffusion of hydrogen and water vapour, at the cathode side there is a net diffusion of oxygen and water vapour.

Molar balance:

$$F_I = F_K \tag{2.27}$$
$$F_J = F_L$$

Energy balance:

$$F_K \cdot h_K + F_J \cdot h_J = F_I \cdot h_I + F_L \cdot h_L \tag{2.28}$$

Temperature :

$$T_I = T_L \tag{2.29}$$

Diffusion equations and pressures
Next to oxygen and water vapour also nitrogen exists in the cathode gas diffusion layer. Since nitrogen does not react in the fuel cell body there is no net nitrogen consumption of the fuel cell body and therefore no net transport of nitrogen over the diffusion layer. However the presence of nitrogen has an impact on the complexity of the formulation of the diffusion. The Stefan-Maxwell equation is used to formulate the diffusion equations.

$$\frac{dy_i}{dz} = \frac{RT}{p} \cdot \Sigma_j \frac{y_i \cdot N_j - y_j \cdot N_i}{D_{ij}} \tag{2.30}$$

which results in the following equations for oxygen, nitrogen and water vapour

$$\frac{dy_O}{dz} = \frac{RT}{p} \cdot \frac{y_O \cdot N_N - y_N \cdot N_O}{D_{ON}} + \frac{RT}{p} \cdot \frac{y_O \cdot N_w - y_w \cdot N_O}{D_{Ow}} \tag{2.31}$$

$$\frac{dy_N}{dz} = -\frac{RT}{p} \cdot \frac{y_O \cdot N_N - y_N \cdot N_O}{D_{ON}} - \frac{RT}{p} \cdot \frac{y_w \cdot N_N - y_N \cdot N_w}{D_{wN}} \tag{2.32}$$

$$\frac{dy_w}{dz} = \frac{RT}{p} \cdot \frac{y_w \cdot N_N - y_N \cdot N_w}{D_{wN}} - \frac{RT}{p} \cdot \frac{y_O \cdot N_w - y_w \cdot N_O}{D_{Ow}} \tag{2.33}$$

with

$$\begin{aligned} N_{O_2} &= -a_1 \cdot F_K = -a_1 \cdot F_I \\ N_w &= a_1 \cdot F_L = a_1 \cdot F_J \end{aligned} \tag{2.34}$$

Since no net nitrogen flow is assumed in the model, N_N can be set to zero. Next to that the sum of the molar fractions is always one.

$$N_N = 0 \tag{2.35}$$

$$y_N = 1 - y_O - y_w \tag{2.36}$$

$$\frac{dy_N}{dz} = -\frac{dy_O}{dz} - \frac{dy_w}{dz} \tag{2.37}$$

Combining and deriving these equations results in a differential equation of the second order for y_O. This results in the following differential equation:

$$\begin{aligned} &\left(\frac{p}{RT}\right)^2 \cdot \frac{d^2 y_O}{dz^2} \\ &- \left(\frac{p}{RT}\right) \cdot \left(\frac{N_O}{D_{ON}} + \frac{N_w}{D_{Ow}} + \frac{N_w}{D_{wN}} + \frac{N_O}{D_{Ow}}\right) \cdot \frac{dy_O}{dz} \\ &+ \left(\frac{N_O \cdot N_w}{D_{Ow} \cdot D_{wN}} + \frac{N_O \cdot N_w}{D_{Ow} \cdot D_{ON}} + \frac{N_w^2}{D_{Ow} \cdot D_{wN}} + \frac{N_O^2}{D_{Ow} \cdot D_{ON}}\right) \cdot y_O \\ &+ \frac{N_O \cdot N_w}{D_{wN}} \cdot \left(\frac{1}{D_{ON}} - \frac{1}{D_{Ow}}\right) = 0 \end{aligned} \tag{2.38}$$

This equation can be solved using similar boundary conditions as formulated for the anode diffusion.

At the side of the fuel cell body:

$$z = 0 \tag{2.39}$$

$$y_{w,FCB} = \frac{p_J}{p_{tot}} \tag{2.40}$$

$$p_J = p_{saturation,FCB} \tag{2.41}$$

At the side of the gas chamber:

$$z = L_{GDF} \tag{2.42}$$

$$y_{w,CGC} = \frac{p_L}{p_{tot}} \tag{2.43}$$

$$y_{O_2,CGC} = \frac{p_K}{p_{tot}} \tag{2.44}$$

2.3.3.6 Fuel cell body

Within the fuel cell body, the driving electrochemical reaction takes place. The mass and molar balances relate the hydrogen and oxygen consumption to the generation of water and electric current. The current is linked to the molar flows by Faraday's law.

Molar Balance:

$$\begin{aligned} F_G + \frac{I_{ref} \cdot n_{series}}{2Far} &= F_H + F_F + F_J \\ F_E &= \frac{I_{ref} \cdot n_{series}}{2Far} \\ F_I &= \frac{I_{ref} \cdot n_{series}}{4Far} \end{aligned} \tag{2.45}$$

Energy balance:
Within the fuel cell body the catalytic and separator layer are enclosed [72–74]. Although different layers exist in the fuel cell, in this model the properties of the electrolyte/separator are considered to define the thermodynamic behaviour of the fuel cell body. The mass flows between fuel cell body and gas chamber however will only consist of gas in accordance to the boundary conditions of the gas diffusion layers. This will affect the enthalpy of these streams and will limit the mass or molar flow, because the partial pressure cannot exceed the saturation pressure.

$$\begin{aligned} &F_G \cdot h_G + F_E \cdot h_E + F_I \cdot h_I = \\ &F_H \cdot h_H + F_F \cdot h_F + F_J \cdot h_J + Q_{FCB} + P_e \\ &Q_{FCB} = Q_{FCB,surr} + Q_{FCB,cat} + Q_{FCB,an} \\ &Q_{FCB,surr} = hA_{FCB,surr}.(T_{FCB} - T_{surr}) \\ &h_F = h_J \end{aligned} \tag{2.46}$$

The energy balance of the fuel cell body consists not only of incoming and outgoing mass streams and heat flows, but also of an electric power output. This output is more detailed in the electrochemical model.

Temperatures:
The temperature of the fuel cell body is characterized by the average electrolyte temperature in the steady state model, Eq. (2.47).

$$T_{FCB} = \frac{T_G + T_H}{2} \tag{2.47}$$

$$T_H = T_F \tag{2.48}$$

$$T_H = T_J \tag{2.49}$$

Later, in the dynamic model the fuel cell body is characterized by the stack temperature, Eq. (2.63).

2.3.3.7 Electrochemical model

The goal of the presented research is to find a model which can predict outlet temperatures, next to electrical output. Therefore the electrochemical model is based on a parameter approach of the polarization curve, which relates current to voltage and operating parameters and is able to show effects of composition, flow rate, temperature, $\cdots$ on the cell performance [56]. The electric power is a product of both current and voltage. Current can be determined using Faraday's law. The fuel cell voltage is defined by the Nernst potential, the activation overvoltage, the ohmic voltage and the diffusion or concentration losses (See also Figure 1.11).

$$P_e = U \cdot I \tag{2.50}$$

$$U = E_{Nernst} - \eta_{act} - \eta_{res} - \eta_{diff} \tag{2.51}$$

The Nernst potential is calculated from the Gibbs free energy of the electrochemical reaction.

$$E_{Nernst} = -\frac{\Delta G_0}{2F} + \frac{RT_{cell}}{2F}\left[ln\left(p_{H_2}\right) + \frac{1}{2}ln\left(p_{O_2}\right)\right] \tag{2.52}$$

The activation, ohmic and diffusion losses are calculated by the equations found in the literature [36, 80]. To calculate these losses following expressions Eqs. (2.53), (2.54) and (2.55) are used.

$$\eta_{act} = \frac{R \cdot T}{\alpha \cdot n \cdot F} ln\left(\frac{\frac{I_{cell}}{A}}{j_0}\right) \tag{2.53}$$

$$\eta_{res} = R_e \cdot I_{cell} \tag{2.54}$$

$$\eta_{diff} = \frac{R \cdot T}{\alpha \cdot n \cdot F} ln\left(\frac{j_L}{j_L - \frac{I_{cell}}{A}}\right) \tag{2.55}$$

The activation overvoltage, given by Eq. (2.53), is a function of the exchange current, j_0, which is temperature dependent given by Eq. (2.56).

$$j_0 = c_1 \cdot exp\left(\frac{-c_2}{T_{cell}}\right) \tag{2.56}$$

The ohmic resistance is a result of resistance due to resistance of electron collector and a term inversely related to conductivity of the electrolyte. This conductivity is related to the cell temperature. This relation results in a linear expression (Eq. (2.57))

$$R_e = c_3 - c_4 \cdot T_{cell} \tag{2.57}$$

2.3.3.8 Discussion on parameter estimation

Table 2.3 contains all semi-empiric parameters, which were used to tune the model. In this paragraph a brief discussion of every parameter is included to justify these values.

Parameter	Value	Unit
j_L	2000	A/m^2
α	0.1668	
c_1	174512	A/m^2
c_2	5485	K
c_3	0.0045	Ω
c_4	$5.9e-6$	Ω/K
c_5	$1.5e-3$	$N \cdot \sqrt{s}/K \cdot \sqrt{m}$
c_6	1.5	
hA_{sur}	51.2	W/K
L_{GDF}	0.2	cm

Table 2.3: List of the used semi-empiric parameters

Parameters in the electrochemical model

The first five values in Table 2.3, from j_L to c_4 refer to the electrochemical model. This semi-empiric model, described in 2.3.3.7, shows great similarity to the one used by Amphlett et al. [81] and later by Huisseune et al. [79] in their modelling work on PEM fuel cells. These general equations are useful for all types of fuel cells. The parameter values however will differ.

The first parameter is the limiting or maximum current density, j_L. From this current density, the diffusion losses become too high to allow a higher number of reactions. The value is based on stack construction (See Section 3.1.1), maximum current and active cell area ($A = 0.064\,m^2$). Ref. [36] shows for other fuel cell

types values of $20000\,A/m^2$. The relatively low value is due to the use of air instead of oxygen (reduction by a factor 5)and due to the low development rate in AFC technology.
The activation parameters are a best fit for the measured data, within an acceptable range. Those ranges went for α from 0.1 to 0.5 and for j_0 from $10^{-4}\,A/cm^2$ or $1\,A/m^2$ to $10^{-9}\,A/cm^2$ or $10^{-5}\,A/m^2$.
The resistive parameters are in the same order as those in [79, 81] for PEMFC.

Parameters describing heat and mass transfer within the fuel cell
During model development, the description of the internal heat and mass transfer is evolved. This evolution is illustrated in Table 2.4. In Table 2.4 the different model parameters describing the internal heat and mass transfer are presented.

The different heat transfers in the model are described by convective heat

Parameter	Base Model (presented at FUCE2008, See Appendix A)	Improved heat transfer [77]	Including mass transfer and water management [82]
hA_{an}	$3.2\,W/K$		
hA_{cat}	$6.4\,W/K$		
c_5		$3.375 \cdot 10^{-3}\,\frac{N\cdot\sqrt{s}}{K\cdot\sqrt{m}}$	$1.5 \cdot 10^{-3}\,\frac{N\cdot\sqrt{s}}{K\cdot\sqrt{m}}$
c_6		1.5	1.5
L_{GDF}			$0.2\,cm$

Table 2.4: Overview of the evolution of the semi-empiric parameters used in the model within the development process of the presented model.

transfer. In a first model approach the convective heat transfer coefficient was fixed, although it is function of amongst others, temperature and velocity. This led to the introduction of the internal convective heat transfer coefficients to anode and cathode, respectively hA_{an} and hA_{cat} and the external heat transfer coefficient to the surroundings, hA_{surr}.
For these convective values is again referred to Amphlett et al. [81] and Huisseune et al. [79]. Similar results are shown for a PEMFC stack of the same size. Both anode and cathode transfer coefficients are in a similar range. Compared to Amphlett et al. [81] and Huisseune et al. [79], the overall conductance, hA_{surr}, to the surroundings is higher (See Table 2.3). However, this is acceptable as here the system consists of 4 stacks, while in [79, 81] only one stack is considered which is more compact and has a smaller heat loss surface.

As discussed earlier in the base model the influence of, amongst others, temperature and flow velocity on these convective heat transfer coefficients is

neglected. Especially the last influence parameter, flow velocity, seemed too important to be neglected. In the model validation for the base model, elaborated in Chapter 3, it was shown that at high air flow rates (overflow) the model underestimates the air temperature (See Section 3.1.3). Therefore both convection coefficients are configured as a function of the gas flow rate, Eq. (2.58). This resulted in much better experimental validation (See Chapter 3).

$$hA_{gas} = c_5 \cdot v^{c_6} \tag{2.58}$$

The values for c_5 and c_6 were matched to the original model parameters, so the transfer coefficients remained in the same range as the ones in the base model.
Because the overall conductance to the surroundings does not depend on flow velocity, its value is not changed. Also the last model improvement will not affect hA_{surr}. Therefore it is not listed in Table 2.4.

As the final model only incorporates water management next to the used thermal management, most values remain the same. However, due to the extra layer at each side the parameters, regarding the heat transfer coefficient towards anode and cathode will be different. This difference is found in c_5. Its value is reduced, since part of the heat transfer from the electrolyte into the gas stream is already included in the energy balance of the diffusion layer.
Next to this difference a new parameter is introduced, namely L_{GDF}. To determine an acceptable range for L_{GDF} a comparison was made with Jo et al. [83]. In this paper values from 0.05 to $0.55\,mm$ were found to be representative for the thickness of the gas diffusion layer. These variations however had no significant influence on performance. Since the model, presented in this paper, has a gas diffusion layer, but no catalyst layer, the gas diffusion layer is chosen to be thicker to include the diffusion resistance of the catalyst layer.
The catalyst layer is 2 to 5 times thinner than the diffusion layer and the diffusion coefficients are 10 to 100 times larger for gas diffusion compared to diffusion through liquid [73]. Therefore, in this model a value between 0.05 and $1\,cm$ is acceptable.

2.3.4 Implementation of the model in Matlab

For the implementation of the model, Matlab is chosen. Originally the model was built in Aspen Custom Modeller (See Appendix A and [77]). The main advantage of this choice was the possibility to link all physical properties (enthalpy, Gibbs free energy, $\cdots$) to the libraries of the Aspen surroundings.
Aspen Custom Modeller however is not built to deal with complex mathematical problems, which are sensitive to small distortions. The diffusion equations led to an increased complexity and therefore Matlab is chosen, which is more appropriate

Gas	b $[GJ/kmol]$	c $[GJ/(kmol \cdot ^\circ C)]$
Hydrogen	$-7.22573286 \cdot 10^{-4}$	$2.89388143 \cdot 10^{-5}$
Nitrogen	$-7.28014 \cdot 10^{-4}$	$2.91195 \cdot 10^{-5}$
Oxygen	$-7.32343 \cdot 10^{-4}$	$2.92833 \cdot 10^{-5}$

Table 2.5: Constants for enthalpy calculation

for the scope of our work.
As a consequence the libraries of Aspen are not available any more to calculate all necessary physical properties. As a solution, the different thermodynamic properties of Aspen Custom Modeller are translated into constants or linear functions so they could be implemented in Matlab. For the properties of the gasses hydrogen, nitrogen and oxygen this is acceptable, since they are considered to be ideal. For enthalpy and Gibbs free energy calculations of water (vapour) a published Matlab function by Magnus Holmgren [84] is used. Table 2.5 presents an overview of the used constants in the linear expression (2.59) to calculate enthalpy.

$$h_{gas} = c_{gas} \cdot T(^\circ C) + b_{gas} \tag{2.59}$$

Also the diffusion constants in the Stefan-Maxwell equations need to be imported. In a first approach they were imported as a constant from the libraries of Aspen Custom Modeller. However, because the diffusion is a function of temperature, already mentioned by Jo et al. in [83], this correlation is included into the model, Eq. (2.60).

$$D(T) = D_0 \cdot T^{2.334} \tag{2.60}$$

2.3.5 Application boundaries of the model

In the previous sections a model is developed. The model is useful to predict thermal behaviour and water removal on the level of the (sub)stack. The objective of the model is not to get insight in the 3D-design of a cell into a stack, but to understand the behaviour of the stack in order to find a best configuration set-up to implement one or more (sub)stacks into a complete system. With the model the difference with serially or in parallel connected (sub)stacks for each flow (either electrolyte, air or hydrogen) can be examined. The difference with serially or in parallel connected cells within a stack cannot be examined with this model, as some phenomena like ionic short-circuit or dimensional aspects are not included in the model.

2.4 Dynamic model

To evaluate a possible control strategy for the stack regarding thermal and water management, dynamics have to be added to the model.

2.4.1 Overview of the dynamic behaviour of a stack

Within a stack several subsystems can be distinguished:

- electrical subsystem, meaning the stack as a component within an electric circuit.
- thermal management of the stack, the stack as a body exchanging heat with the surroundings and passing mass flows
- the hydraulic subsystem(s), the stack as a pipe or vessel in which liquids (the electrolyte) or gasses (fuel and air flow) can be stored or redirected.

Each of these subsystems has its own dynamics, which can be characterized by a transient response time or time frame in which transient behaviour between two steady states can be observed.
Next to the dynamics of these subsystems also the degradation and contamination of the stack is part of the long term dynamic behaviour of the stack. In the following subsection each effect will be discussed.

2.4.2 Electrical dynamics of the AFC-stack

In Duerr et al. [74] a dynamic electrochemical model is developed, allowing to study the electric behaviour of an alkaline fuel cell. The dynamics of the electric response are affected by the double layer capacitance of the electrodes. Duerr et al. [74] implemented this in their model and observed a response time of less than $0.5\,s$ to changes in current and/or voltage. The time step in our validation data (See Chapter 3) is $0.5\,s$ and the objective of this study is to focus on thermal and water management which react a lot slower. For this reason the transient electric behaviour, characterized by the double layer capacitance is not taken into account in this study.

2.4.3 Thermal dynamics of the AFC-stack

The dynamics of the thermal behaviour of the stack are characterized by the thermal capacity of the stack, C_{stack}. As the stack itself is made of solid materials,

Model Parameter	Value	Unit
$hA_{FCB,stack}$	6000	$\frac{W}{K}$
C_{stack}	100	$\frac{kJ}{K}$

Table 2.6: Dynamic model parameters

this capacity can be understood as the mass of the stack, m_{stack}, multiplied by the specific heat of the stack material, c_{stack}, Eq.(2.61).

$$C_{stack} = m_{stack} \cdot c_{stack} \tag{2.61}$$

Thermal capacity will therefore be an additional parameter in the model. To take this thermal inertia into account an additional heat flux from the working area to the stack material and vice versa has to be taken into account, Eq.(2.62). As the heat is produced within the fuel cell body and all heat fluxes are defined within this control volume, also this thermal capacity will be taken into account here. This leads to following modifications of Equations (2.46). Also cell temperature is now defined as stack temperature, which is not the same anymore as the average electrolyte temperature, $T_{el,mean}$. This temperature is used to calculate the heat transfer between the electrolyte and the mass of the stack (2.65).

$$Q_{FCB} = Q_{FCB,sur} + Q_{FCB,cat} + Q_{FCB,an} + Q_{FCB,stack} \tag{2.62}$$

$$T_{FCB} = T_{cell} = T_{stack} \tag{2.63}$$

$$T_{el,mean} = \frac{T_G + T_H}{2} \tag{2.64}$$

$$Q_{FCB,stack} = hA_{FCB,stack} \cdot (T_{el,mean} - T_{FCB}) \tag{2.65}$$

$$Q_{FCB,stack} = C_{stack} \cdot \frac{dT_{FCB}}{dt} \tag{2.66}$$

As can be seen in Eqs.(2.65) and (2.66), the additional heat transfer, $Q_{FCB,stack}$, is modelled as an extra heat loss or gain of the FCB control volume. The heat loss is characterized by a convective heat transfer coefficient, $hA_{FCB,stack}$, listed in Table 2.6.

As $hA_{FCB,stack}$ represents the total heat transfer coefficient between stack and electrolyte, this value has to be a result of the total contact surface (cell surface, $0.064\,m^2$, multiplied by number of cells, which is 384 for the sum of all stacks in the system used for validation) and convective heat transfer coefficient between liquid flow and contact surface ($230\frac{W}{m^2 \cdot K} - 455\frac{W}{m^2 \cdot K}$). Therefore, the total heat transfer coefficient is expected to be about $5650 - 11200\frac{W}{K}$).
The thermal capacity is the product of the mass of the stack and specific heat. The

stack consist mainly of steel ($500\frac{J}{kg.K}$), nickel ($440\frac{J}{kg.K}$) and propylene ($1850\frac{J}{kg.K}$). In mass percentages, steel and nickel will determine the behaviour of the stack (about 500 – $1000\frac{J}{kg.K}$). The total mass of the stack(s), based on product information is about 50 – $70kg$. The casing in which the stacks are held is estimated at another 10 – $100kg$. The capacity, C_{stack}, is expected to be within a range of 25 – $170\frac{kJ}{K}$. Therefore, a thermal capacity of $100\frac{kJ}{K}$ is acceptable.

2.4.4 Hydraulic subsystems and dynamics

As the stack has a certain volume and storage capacity in which fluids and gasses flow, also these dynamics can be taken into account in a complete dynamic description. However, the dynamics of the the hydraulic subsystem are not taken into account at the level of the stack, which will be argued here. At the level of the system these dynamics are more significant (See Chapter 5).
Each control volume has its own dynamics. We can distinguish the two gas diffusion layers, both gas chambers and the fuel cell body in which the electrolyte passes.

- As the gas diffusion layers are too small in actual size, the storage capacity in the diffusion layer which can cause possible transients is negligible. An immediate (faster than $1s$) response is assumed.
- The gas chamber has a certain volume, represented by the overall net section area (A) and the path length (L). Changes in flow rate or dynamic pressure will therefore have an impact on the static pressure in the gas chamber. However, as can be understood from following simplified calculations, Eq.(2.69), flow rate changes will affect the pressure with less than 1.5%. The simplifications, like constant density, even exaggerate this influence. For the control volume shown in Figure 2.3 the Bernoulli equation can be simplified to following expression.

$$p + \frac{\rho \cdot \Phi^2}{2 \cdot A^2} = Constant \tag{2.67}$$

$$\Delta p = \frac{\rho}{2 \cdot A^2} \cdot \left(\Phi_1^2 - \Phi_2^2\right) \tag{2.68}$$

$$\Delta p_{max} = \frac{\rho}{2 \cdot A^2} \cdot \Phi_{max}^2 \tag{2.69}$$

  Using the values enumerated in Table 2.7, it can be seen that these influences are negligible, as the present pressure is set at 1 bara.

- As the electrolyte is a liquid, a possible storage capacity can be introduced using the fuel cell body as a vessel or tank, meaning that the electrolyte

Parameter	Symbol	Value	Unit
Air density	ρ	1.2	$\frac{kg}{m^3}$
Total net section area	A	1.5	cm^2
Flow rate	Φ	22.41	$\frac{m^3}{h}$

Table 2.7: Numeric values used in Eq.(2.69)

level within this tank can be altered. However, for safety reasons it has to be ensured that the electrolyte channels are completely filled. Otherwise the oxygen and hydrogen gasses are not separated anymore. Therefore, within start-up of the system this filling time matters, but this is better simulated on a system level, as it has little effect on stack performance.

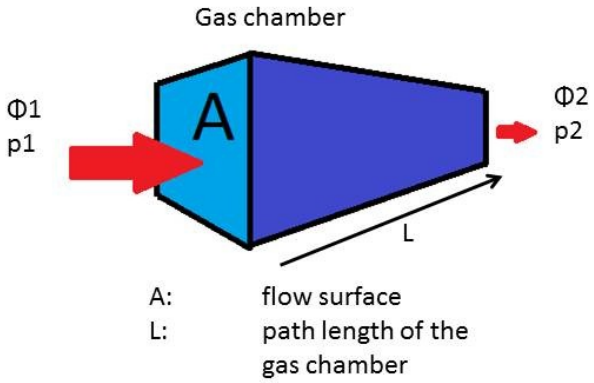

Figure 2.3: Simplified representation of a gas chamber, with indication of dimension and flow rates (Φ_i) and pressures (p_i) of the in- and output flow.

2.4.5 Translation into Simulink environment

As the steady state model was built in the Matlab surroundings, the dynamics of the model, which can be reduced to the thermal capacity of the stack, are implemented into an embedded version of the Matlab model. In this way the model can be used in Simulink, which allows further applications in a complete system configuration. Figure 2.4 gives an overview of the Simulink model. On the left side different input signals can be detected:

- Hydrogen flow rate
- Electrolyte temperature and flow rate

- Outdoor air characteristics: temperature, humidity and flow rate of the air flow
- Initial stack temperature

Some of these flows are normalised to fit into the model as it is built in this Chapter. The heart of the model is the embedded model, which has the heat to the stack as an output signal, Q_{FCB}, and the temperature of the stack as an input signal, T_{FCB}. By integrating (I) the output signal, Q_{FCB}, and multiplying it proportionally (P) with the inverse of the thermal capacity the temperature change of the stack is calculated. Hereby, the input signal, T_{FCB}, of the stack model is looped in a PI-algorithm.
Other out- and inputs are meant to speed up the calculation, like the re-initialisation of the embedded model. The computation time of the embedded model depends on the initial values for all variables inserted in the model. A logic initial value for all these variables are those of the previous time step. These values are stored in the memory block in the simulation. At t = 0, an initial set of values are stored based on the intermediate values for a valid working point.

2.4.6 Other dynamics and other possible model extensions

2.4.6.1 Degradation and contamination

An important dynamic character of the fuel cell is not taken into account in this model. Degradation (life time) of the stack is a very important parameter to evaluate the fuel cell performance over a longer period. The semi-empiric models, of which an example is given in Section 2.3.3.7 are often fitted using model identification (See also Appendix B). This characterization can be used for monitoring and control of the stack, using cell voltage monitoring as an indicator of the state of cell and stack [85] . Degradation or contamination, due to the formation of carbonate in the electrolyte, can often be seen as a change in one or more model parameters. The ohmic resistance, R_{cell}, and the diffusion current, j_L are expected to change in time because of degradation and contamination. However, since long-term measurements have not been possible, this is not taken into account.

2.4.6.2 Electrolyte concentration

Within the stack the electrolyte concentration will remain more or less the same as the net water production ($< 0.2\,kmol/h$) is negligible compared to the electrolyte flow rate ($20\,kmol/h$). However, within a complete system model, in which the electrolyte is temporarily stored this net water production can cause a dilution of the electrolyte. To examine this dynamic effect, the stack model has to be able

to work with different electrolyte concentrations. This is not implemented in the current model. Zhang et al. [78] have presented a model in which this influence is taken into account to define the optimal concentration, which is in the range of our model. The influence can be understood and also modelled as a change in ohmic resistance. Although the influence on performance is certainly present. It can be seen that for different concentrations within a small range around the optimum the influence is limited to less than 1%. It is expected that this range will not be trespassed since the net water production or evaporation has to be kept under control otherwise a big electrolyte tank would be required (See Chapter 5). However, this model improvement can be the topic for future research.

2.5 Closure

In order to evaluate the potential of an AFC-stack within CHP-applications by simulation, it is necessary to understand electrical and thermal performance. Besides those aspects, it was also necessary to understand the water removal in the stack at different working points. For this evaluation, a stack model has to meet following requirements:

- It has to be able to predict electrical performance, based on the condition of the input flows. Next to load, it is important the influence of temperature on electric power is taken into account in the model. Also the possible influence of the water household is to be discussed.
- Next to electric performance the model has to give a complete picture on the thermal behaviour by predicting temperatures of all output flows.
- Finally, the model should provide a prediction on the water removal, preferably without any preliminary assumptions and exclusion of one or more output flows.

After an evaluation of the existing models on alkaline fuel cells, it could be concluded no model meets all these requirements. Most existing models only meet one of these requirement and sometimes not even completely, as they were built for different purposes.

In this chapter the development of a stack model is presented, which meets these requirements.

The model uses a temperature and pressure dependent semi-empiric electrochemical model to predict electric performance. Compared to other models this allows a good prediction, but is not meant to be used to improve cell performance.

Different from other models, within this model a lot of attention is paid to thermal behaviour; assuming velocity dependent heat transfer coefficients for the gas channels and taking thermal inertia of the stack into account in the description of the dynamic behaviour of the stack.
Also a prediction on the water household is included without any preliminary assumptions, in which flow the water is removed. Also new here is the possibility of water removal in the electrolyte. The extra equations for this extra degree of freedom within the model can be found in the diffusion equations and the assumption of a saturated water pressure at the surface of the electrolyte.

Next to the model development and the explication of the possibilities and boundaries to use it to simulate different configurations, also possible improvements are suggested and how they can be incorporated.
An incorporation of the influence of the electrolyte concentration as performed within the Zhang model [78] can make the model even more complete to evaluate the effect of the water management on electric performance. In this model, it is not included as this could be neglected in the range of operation we want to study. Also the influence of degradation and contamination can be introduced by making some electrochemical model parameter time and/or contamination dependent.

Finally, to evaluate the quality of the model, the model validation is presented in the next chapter.

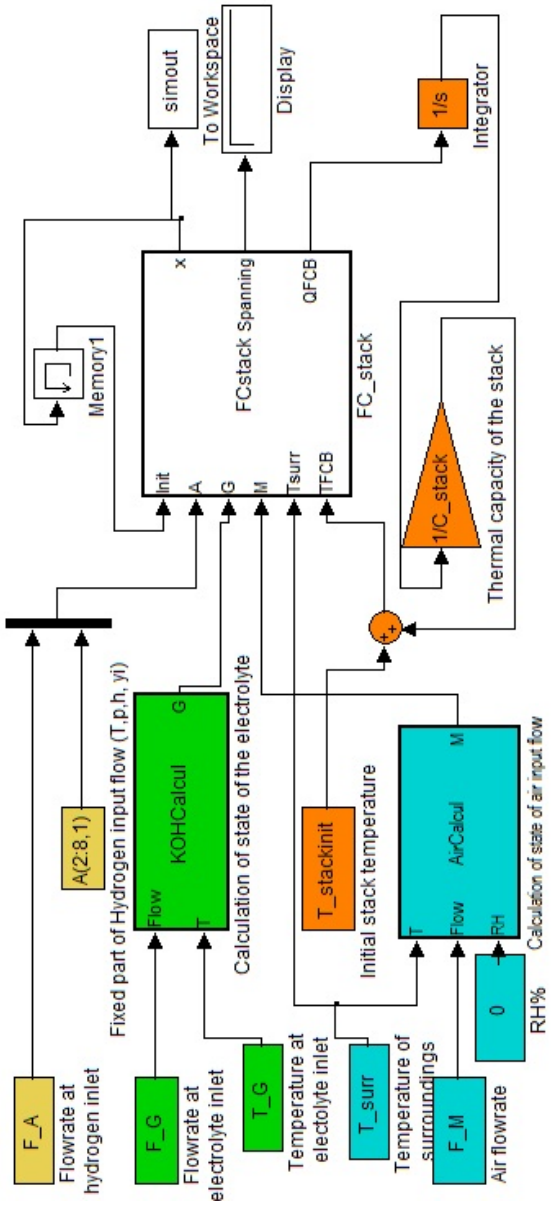

Figure 2.4: Overview of the implementation of the dynamic stack model into the Simulink environment

3 Model Validation

In this chapter the validation of the model is described. First the experimental work and collection of measurement data will be discussed. Afterwards the model results are compared with the experimental data.

3.1 Experimental work

The model is validated using experimental data which were generated with the AFC system described in detail in [58, 77] and shown in Figure 3.1. As the stack is already incorporated in a complete system set-up, this limits the experimental freedom to install measurement points and to enable operation within the complete working range of the stack. This section will provide the reader a clear overview of the experimental set-up and the data analysis which is performed to obtain useful data to validate the model.

3.1.1 Experimental set-up

Experimental tests for model validation were carried out at the VITO on the AFC-system of the KHLim. Figure 3.2 shows a schematic view of the experimental set-up. In Table 3.1 a summary and a brief description of the main operating parameters, marked on Figure 3.2 is given.
As shown in Figure 3.2, the system consists of 4 stacks. To operate these stacks, hydrogen and air flow have to be supplied, next to these flows also an electrolyte flow is present to enable separation between both gas streams. The system is

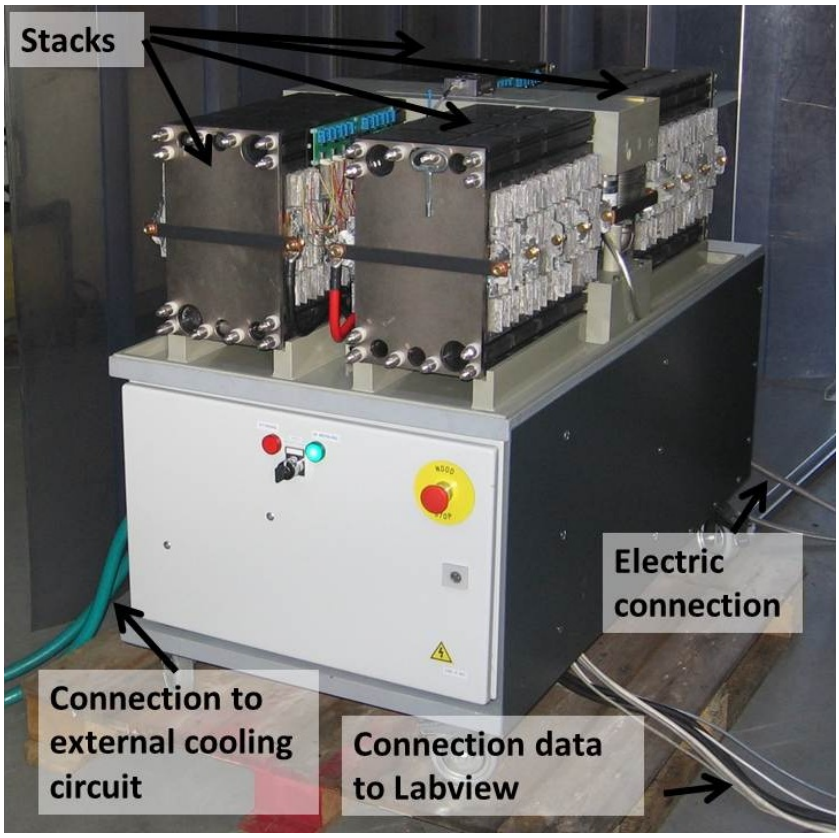

Figure 3.1: Picture of the AFC-system, in the lab environment of VITO.

completed with a connection to a monitoring unit and an external electric circuit.

Air/oxygen supply

First the air circuit is discussed. The stacks are supplied with ambient air at a measured temperature (measuring point a). The air flow is controlled by an electric fan with variable speed. This air flow rate is indirectly measured by the electric current absorbed by the fan drive (point b). Measurements show a linear correlation between this current and the air flow rate in the nominal working range. Subsequently, the air is guided through a CO_2-scrubber, where a slight temperature rise is expected. This final inlet temperature (point c) is not measured directly, but is estimated to be the rounded up value in point a.
The air is divided in parallel over the stacks. Within every stack the air is again

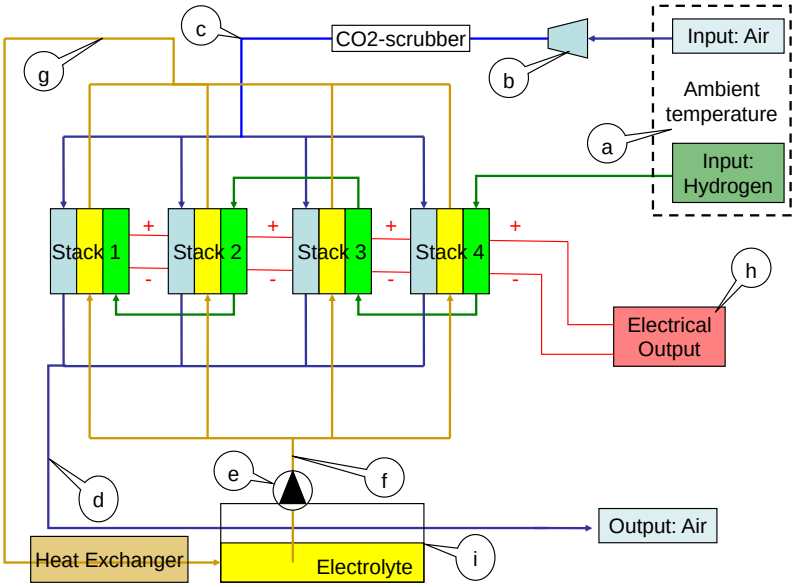

Figure 3.2: Experimental set-up of the AFC-system, in which the main operating parameters are marked and described in Table 3.1.

in parallel divided over the different cells. The outlet air temperature is measured (point d). The air overflow will be guided over the electrolyte tank. This will enable extra evaporation of water out of the electrolyte circuit. The hot and humidified air is removed to the surroundings.

KOH recirculation

Next to separation of the gas streams the electrolyte -potassium hydroxide (KOH) in the set-up- also ensures cooling of the stacks. A centrifugal pump pumps the electrolyte (point e) out of an electrolyte reservoir and enables the circulation of the electrolyte.
The electrolyte flow is indirectly measured (point e) in the same way as the air supply, by an empirically determined correlation between flow rate and current absorbed by the drive of the pump. Before the electrolyte enters the stacks, its temperature is measured (point f). Then the electrolyte is in parallel divided over the different stacks and cells. After the passage through the fuel cells, the temperature is measured (point g) and the electrolyte is cooled in an external heat exchanger.
As part of the water production in the stack can be removed in the electrolyte

Parameter	Description	Measuring method
a	Ambient temperature (input temperature for air and hydrogen supply)	Direct
b	Air flow	Indirect
c	Air temperature	Estimated
d	Output air temperature	Direct
e	Electrolyte flow	Indirect
f	Input electrolyte temperature	Direct
g	Output electrolyte temperature	Direct
h	Total voltage, Current, cell voltages	Direct
i	Level of the electrolyte in the tank	Direct

Table 3.1: List of operating parameters of the AFC-system, marked on Figure 3.2

circuit, the electrolyte level in the storage tank (measured in point i), will be an indication to monitor the effectiveness of the water management. The water management proves its effectiveness, if the electrolyte level does not vary much and is kept between a predefined upper and lower boundary. If these boundaries are exceeded, this means that for the upper boundary the electrolyte is being diluted and that electrolyte leakage is possible or it means that for the lower boundary there is a net evaporation out of the electrolyte, causing a re-concentration of the electrolyte and possible dry out of the system.
The measurement however is not that precise, because the water surface is not stable. This is caused by control of the KOH-pump which switches between different operation modi and also by the vapour transfer from or into the output air flow which passes over the electrolyte tank. Only an evaluation of the water level - with consideration of changes in electrolyte flow (point e) - over a long period of time will indicate when there is a net evaporation of water (electrolyte) or when there is a net formation of liquid water during this period of time.

Hydrogen supply

The hydrogen (99,98% purity) stored as pressurized gas on site, is delivered with an overpressure of about 28 $mbar$ to the system at ambient temperature (point a). It runs serially through the stacks. To prevent blockage by water droplets, the direction will be alternated (not shown in drawing).

Electrical connection

Finally, the electric current and cell voltages are measured by the cell voltage monitoring system (CVM) (point h) [85].
First, every cell is electrically in parallel connected with three neighbouring cells, to avoid an ionic short circuit [39]. These groups of four cells are than serially

connected in a stack (24 groups or 96 cells in each stack).
Finally, the (four)stacks are serially connected to each other. An external device will convert the DC-current to AC. To validate the model the average cell and total system values were used.

All the described measurements are logged with a time step of 0.5 seconds. Several steady state points were gathered by keeping the current constant and averaging the electrolyte temperature within an acceptable range. This range is discussed further in Section 3.1.2.
The electrolyte temperature is controlled by a cooler in the secondary circuit, which cools the electrolyte. Not every working point could be reached because the capacity of the cooler was limited. The combination of high currents and low temperature was therefore not possible. Secondly at low currents it wasn't possible to reach high temperatures as there was no external heater in the electrolyte circuit.
Despite these limitations, a large set of data with different working points could be obtained with the described set-up.

3.1.2 Data analysis

All gathered data - which were obtained during 1 week of experiments - were chronologically obtained and small fluctuations were inevitable. To reduce the amount of data to a workable set of working points, all data were stored and divided in several datasets. The boundary condition to every dataset is that current and temperature are at least 10 seconds within a certain range ($+-2.5°C$ and $2.5A$) without interruption. For each dataset, an average value and standard deviation is calculated for each parameter. It can be understood that for relatively small datasets this standard deviation will be rather high, compared to larger datasets.
If the standard deviations for the measured parameters are within the limitations as described in Table 3.2, the dataset is considered to be a valuable working point for model validation. This led to 50 valuable working points, containing information about electrolyte flow rate, inlet and outlet temperatures, about air flow rate and temperature, about cell current and voltage. These data are used to validate performance and thermal management in our steady state model. To validate the water management and dynamics of the model the data are used in chronological order.
For the water management some larger standard deviations are allowed, because otherwise the working point would only describe operation over a limited period of time. As the water management can only be monitored by measurement of the tank level, which has a slow response time, larger standard deviations are allowed to detect different semi-stable working periods (See Section 3.2.2).

Parameter	σ_{max}
Total Current	2 A
Total Voltage	2 V
Air Flow Rate	0.183 kmol/h
Air Outlet Temperature	$2°C$
Electrolyte Flow Rate	2.2 kmol/h
Electrolyte Temperature inlet	$4°C$
Electrolyte Temperature outlet	$4°C$

Table 3.2: List of all maximum standard deviations for each dataset, describing a steady state working point.

For the dynamics of the model, the data are used chronologically. Noise or small variations, which can be subscribed to a measurement error, are filtered out of the data to shorten simulation time, by using a running average. In Figure 3.3 a comparison is made between the original and filtered data for the main inlet variables, electrolyte input temperature and current. As can be seen in the Figure small changes in operation modus will not be considered in the dynamic simulation and will be accounted to noise on the measurement and/or limitations of the dynamic model.

3.1.3 Discussion on experimental results

Before starting the actual validation of the model and comparing the model results to the measurements, the measured results are discussed. It is shown that some results which were at first not logical can be explained by the insights gained within the model development.

Voltage and current: fuel cell performance

To examine the performance of the fuel cell system, all experimental data are shown in a current-voltage diagram (Figure 3.4). The horizontal axis shows the total current of the fuel cell system, which is a measure for the current density. The vertical axis shows the total voltage of the fuel cell system. As expected the voltage drops with rising current.

Fuel cell performance and the electrolyte temperature

To examine the influence of the electrolyte temperature the data were divided in three data sets. Each data set represents a number of operating points within a certain temperature range of the electrolyte input flow.

- The blue dots represent experimental data with an electrolyte temperature between $25°C$ and $40°C$.

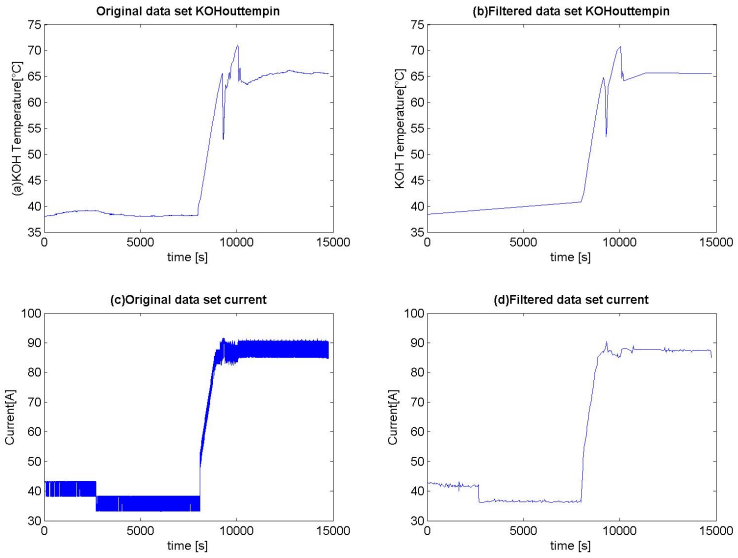

Figure 3.3: Comparison of measured values (a: electrolyte input temperature, c: current) and filtered input data (b: electrolyte input temperature, d: current), used for validation of the dynamic model.

- The red squares represent data at a temperature between $40°C$ and $60°C$.
- The green triangles represent the experiments at relatively high temperature from $60°C$ to $75°C$.

Comparing these three sets of data, it can be concluded the voltage increases with temperature (Figure 3.4).

Production of useful heat

The electrolyte flow is kept constant within an acceptable margin. The rise in temperature is therefore a good indication for the useful heat production. In Figure 3.5 the influence of temperature and electric load on useful heat production is illustrated. The vertical axis shows the temperature rise of the electrolyte, which is representative for the heat production. The horizontal axis shows the total electricity production (DC) of the fuel cell system. The operating points shown on the graph are divided in three groups, according to their temperature range. This is similar to the discussion on the polarisation curve.

At high temperature a linear relation between electricity generation and heat

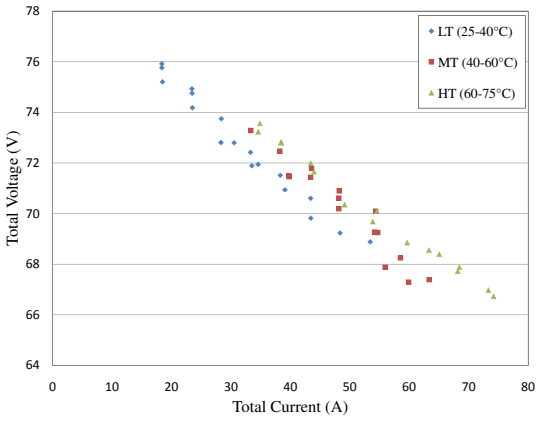

Figure 3.4: Polarization curve for different electrolyte temperature ranges (experimental)

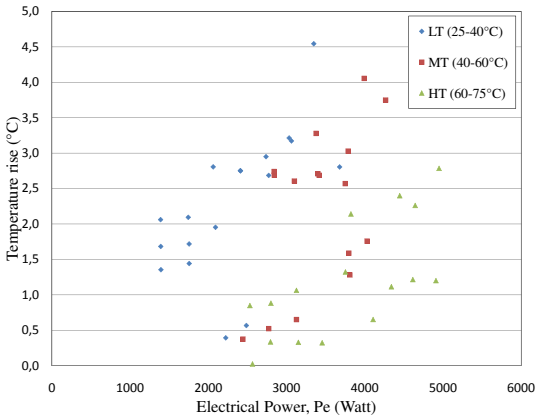

Figure 3.5: Useful heat (rise in electrolyte temperature) compared to power output

production is noticeable. At lower temperature this linear relation is not clear, although it would be expected. At lower temperature the small changes in ambient temperature are of a higher influence than at higher temperature. This is only part of the explanation. Analysing the results with the insights of the model, it is shown that the variety in air flow rate and the humidity of the air also has a large influence on the results (See Chapter 4).

Comparing high and low temperature the rise in temperature will be higher at low temperature. This is expected because less heat is lost in air flow and losses to the surroundings.

The air temperature and flow

The air flow rate fluctuates very much and the operating points themselves also show a relatively large standard deviation. The air flow rate is a control parameter in the water and thermal management and therefore could not be fixed; a certain fluctuation was inevitable.
Comparing air flow rate and total electric current at different electrolyte temperatures, a linear correlation is shown at temperatures below $60°C$, despite the large fluctuations (Figure 3.6).

At higher temperature this correlation also exists but the flow rate is increased

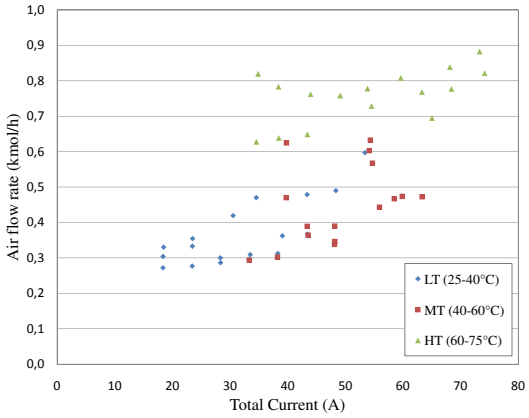

Figure 3.6: Air flow as a function of electric current at different temperatures

for better cooling and removal of the water vapour. Above and below $60°C$, the designed operating temperature, the applied control strategy for water management switches to a different air ratio.
As shown in Figure 3.7 the air temperature follows the electrolyte temperature. No influence of the different air flow rates for the high temperatures was noticed. Assuming a constant heat transfer coefficient and predefined water household, it would have been expected that at higher air rates, the output temperature would drop. This can be explained by the insights given by the model in the water removal and the velocity dependency of the convective heat transfer (See Chapter 2).
This last dependency is based on the definitions of the Reynold and Nusselt numbers, Eqs.(3.1) and (3.2), and the form of their correlation, Eq. (3.3).

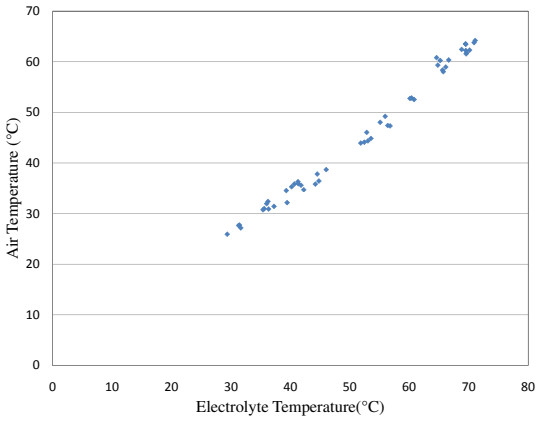

Figure 3.7: Relation between air and electrolyte temperature (experimental)

Following correlation is most found in the literature (e.g. See References in [86]).

$$Re \sim v \tag{3.1}$$

$$Nu \sim h_{convection} \tag{3.2}$$

$$Nu = a.Re^{b} \tag{3.3}$$

In the model this correlation can be found in Eqs. (2.7) and (2.10).

3.2 Model Validation

Current - which is directly proportional to the input hydrogen flow, because of the end-of-pipe operation - input air flow rate, input electrolyte flow rate and input electrolyte temperature are used as input parameters for model validation. The model is used to predict electrical performance, thermal behaviour and water removal.
The model will be validated on these three aspects, which can be characterized by voltage, output temperatures for both electrolyte and air and by output flow rate of the liquid electrolyte. The validation is performed in three stages.

- First the model is validated regarding the prediction on voltage and thermal behaviour, using a large selection of experimental data shown in Table 3.3. The selection of these working points is described in Section 3.1.2 and in ref. [77].
- Secondly the water management is validated by selecting a long period in which the fuel cell is relatively stable and the electrolyte level is monitored (See also [87]).

Identification number of working point	Current A	Electrolyte input flow kmol/hr	Electrolyte input temperature $^{\circ}C$	Air input flow kmol/hr
1	18.5 ± 0.9	22.1 ± 0.0	29.4 ± 1.8	0.3 ± 0.2
2	73.3 ± 1.8	19.8 ± 0.0	68.3 ± 1.9	0.9 ± 0.1
3	33.3 ± 0.2	21.8 ± 0.0	44.4 ± 1.9	0.3 ± 0.0
4	38.2 ± 0.2	22.2 ± 0.6	43.7 ± 1.8	0.3 ± 0.0
5	55.9 ± 2.2	20.0 ± 0.0	42.9 ± 2.2	0.4 ± 0.4
6	59.9 ± 2.8	19.5 ± 0.9	44.3 ± 1.6	0.5 ± 0.3
7	43.4 ± 1.9	21.3 ± 0.0	34.0 ± 1.9	0.4 ± 0.3
8	43.4 ± 1.6	20.4 ± 0.0	38.6 ± 1.7	0.5 ± 0.4
9	43.4 ± 0.8	21.8 ± 0.0	52.5 ± 3.4	0.4 ± 0.3
10	43.4 ± 1.1	21.5 ± 0.0	63.7 ± 2.9	0.6 ± 0.3

Table 3.3: Selection of measured operating point for model input

- Finally the dynamics of the model is validated by a comparison of the model output and the measurement data over a longer period of time. Here, most attention is paid to the transient thermal behaviour of the stack.

3.2.1 Validation on prediction of performance and thermal management

As described earlier in this chapter, all measured parameters are subject to uncertainties. Data analysis (See Section 3.1.2) led to a data set of 50 working points (See Appendix C). The measurements, which are used as input variables for the model, are illustrated by a representative selection of operating points. For the complete data set, including this selection is referred to Appendix C. The selection, shown in Table 3.3, is based on current and electrolyte temperature. These two are the most determining input variables, as can be deducted out of the model development in Chapter 2, and more specific in Section 2.3.3.7. Their importance is also illustrated in the discussion of the experimental results, whereas it was shown the observed correlations were all linked to both or either one of these two variables.
The first two operating points are representative for the range in which the data were obtained: the first one represents the lower bound and the second one the upper bound for both current and electrolyte temperature. The next four operating points are all measured at about the same average electrolyte temperature over a wide range of currents. The last four are all measured at the same average current, over a wide range of electrolyte temperatures.
The measured and modelled output parameters of these ten operating points are shown in Figures 3.8, 3.9 and 3.10. A complete data set with all 50 measured

and modelled operating points is listed in Appendix C. In each of these figures the experimental data are compared to the model, presented in Chapter 2. Next to experimental data the results are also compared with an earlier version of the model without any prediction on the water household (See also Appendix A and Ref. [77]).
As discussed in Section 2.3.3.8, the model has evolved during its development, with the inclusion of the water management in a final stage. The first model versions, which differences are shown in Table 2.4, focused on the prediction of the thermal behaviour. To proof the inclusion of the water management in the final model did not go to the expense of the prediction of thermal behaviour, the previous model [77] was used as a reference model and shown in the different graphs.

- The experimental output is represented by dots with error bars, which represent the uncertainty and standard deviations on the measurement, similar to the variation in the input value, shown in Table 3.3.
- The output of the model is represented by a floating bar. The line in the middle of this bar represents the modelled output of the mean input parameters listed in Table 3.3. To include the measurement error on the model input a corner analysis is executed; all possible combinations of extreme input values for each input parameter were used as input for the model, based upon the mean values and measurement errors, listed in Table 3.3. In the end, the maximum and minimum result were considered to be the upper and lower bound of the model output.
- The earlier model, with the focus on thermal behaviour, in [77] is represented with a circle. For this model the measurement error on the input parameters was not taken into account.

3.2.1.1 Electrical performance, voltage

In Figure 3.8 the prediction on electric performance is shown. The data are arranged by ascending current and electrolyte temperature, in case of similar currents (operating points 7 to 10). The model shows a better performance on prediction of the voltage, compared to the previous version of the model [77]. For two operating points no overlap is found between the experimental and the modelled voltage. This is however acceptable because in the complete set of 50 operating points these are indeed the only two points, where no overlap is found. In these points the new model has a smaller deviation than the previous model. Next to this, both for the experimental and for the modelled voltage, a similar influence of the current is shown in Figure 3.8. The same result is shown regarding the positive influence of the electrolyte temperature (operating point:

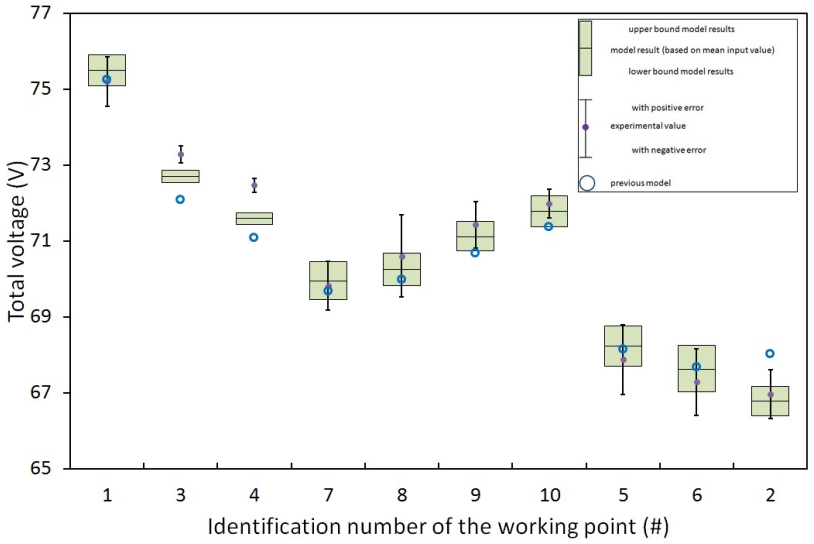

Figure 3.8: Model verification on electric performance (voltage) with the working points (See Table 3.3) arranged by ascending current and temperature in case of equal current (points 7 to 10). For every point the model prediction (floating bars) is compared to the experiments (dots) and the previous version of the model, described in [77] (circles).

7 to 10) on the electrical performance or total voltage. The model is therefore representative in predicting the voltage, including the effect of temperature and current on electrical performance.

3.2.1.2 Thermal behaviour, electrolyte temperature

In Figures 3.9 and 3.10 the thermal behaviour is shown. Figure 3.9 shows the prediction of the output electrolyte temperature. The model has comparable results to [77], in predicting the electrolyte temperature. This was expected as both model have the same governing equations, only a different heat and mass transfer between the electrolyte and the air flow.
For two operating points there is no overlap. In the complete data set three working points show no overlap. The deviation however is limited to a few degrees. The higher the electrolyte temperature, the higher the output electrolyte temperature. This is visible both in the experimental and in the modelled results. In the discussion on experimental results in [77] was already mentioned that the temperature rise in the electrolyte grows with higher current. This effect is visible

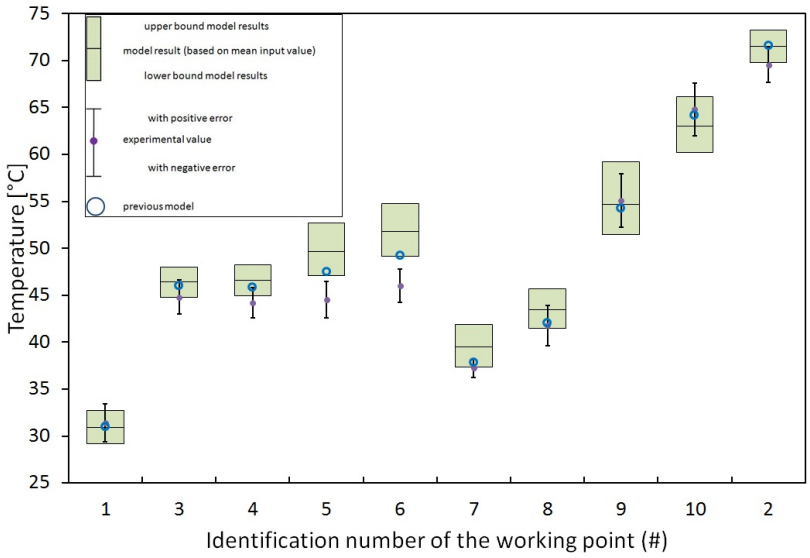

Figure 3.9: Model verification, output electrolyte temperature. Operating points 3 to 6 have all the same input electrolyte temperature and are arranged by ascending current. Operating points 7 to 10 have all the same current and are arranged by ascending input electrolyte temperature. Operating points 1 and 2 are the two most extreme values, considering current and input electrolyte temperature. For every point the model prediction (floating bars) is compared to the experiments (dots) and the previous version of the model, described in [77] (circles).

in the modelled output, but is not very clear in the shown experimental results (operating points 3 to 6).

3.2.1.3 Thermal behaviour, air temperature

Figure 3.10 shows the prediction of the output air temperature. For all 50 working points there is an overlap. Next to that, the relation with the electrolyte temperature is noticeable, both in the measurements and in the model. Therefore, the model is acceptable to predict thermal behaviour. Still the prediction of the air temperature is sensitive to the air flow, the parameter with the highest error range. As a result the modelled output shows a large difference between upper and lower boundary. The most remarkable result is the lower bound in working point 9. This represents an impossible situation, due to the high standard deviation in the measured air flow. The point however shows one of the limitations of the model, since it is assumed that the air flow is controlled to be at least sufficient to compensate the hydrogen input in Faraday's law. This assumption is not fulfilled in point 9, so the model

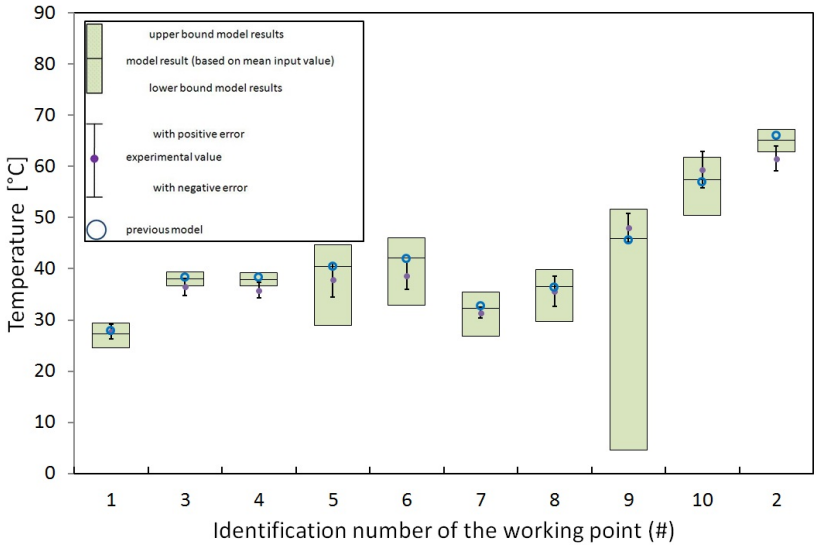

Figure 3.10: Model verification, output air temperature. Operating points 3 to 6 have all the same input electrolyte temperature and are arranged by ascending current. Operating points 7 to 10 have all the same current and are arranged by ascending input electrolyte temperature. Operating points 1 and 2 are the two most extreme values, considering current and input electrolyte temperature. For every point the model prediction (floating bars) is compared to the experiments (dots) and the previous version of the model, described in [77] (circles).

cannot be used with those input conditions.

3.2.2 Validation on the water management

3.2.2.1 Description of model validation

To validate the model regarding the water management, the level of the electrolyte in the KOH-tank is monitored in time over the duration of the experiments (Figure 3.11). In this time period it was possible to determine 6 periods in which the electrolyte level shows a clear and steady change and in which the variation on the inlet conditions was relatively stable (Table 3.4). These conditions were used as input data for our model to predict the water production in the electrolyte flow, which will result in a rise (or reduction) of the electrolyte level in the KOH-tank. If the model is representative to reflect the measurements, the modelled water production is directly proportional to the speed at which the measured electrolyte level rises. In Figure 3.12 the model results for the formation of liquid water in

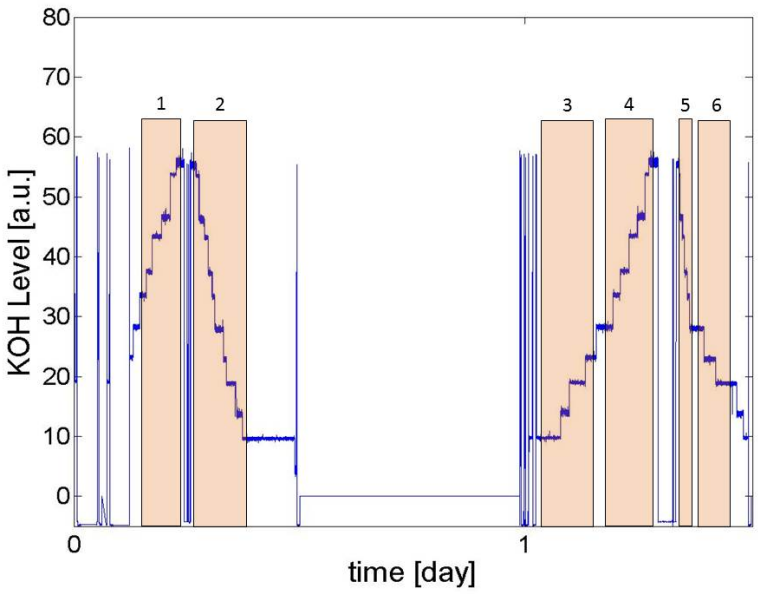

Figure 3.11: Measured fluctuation of the electrolyte level in the KOH-tank during two days of experiments. Six periods are selected in which the input parameters are relatively stable and marked on the figure. These 6 periods are described in Table 3.4

the electrolyte flow (Y-axis) are plotted as a function of the measured rise per unit of time of the electrolyte level in the KOH-tank (X-axis). These data sets are represented by the triangles, which are expected to be on a straight line through the origin. However, when the electrolyte level drops (periods 2, 5 and 6 in Table 3.4), the model overestimates the formation of liquid water in the electrolyte. At high currents (periods 2 and 6 in Table 3.4) the model predicts a rise in electrolyte level due to the high water production. The measurements show however a drop in electrolyte level. Table 3.4 shows that the positive effect of the current on the water formation is almost negligible compared to the negative effect of the air flow and electrolyte temperature. According to the measurements, air flow rate and temperature are the most determining parameters regarding rise or decrease of the electrolyte level. This could be due to the fact that the output air, which is not saturated, passes the tank. Assuming that this passage will result in an increased relative humidity ($RH\%$) of the output air, more water will be evaporated at higher air flow rate and higher temperature, resulting in a lower electrolyte level.

Period	Duration	Input conditions (mean +- standard deviation)				Evolution of
		Current	KOH flow	KOH temp.	Air flow	
	(s)	(A)	(kmol/hr)	(C)	(kmol/hr)	KOH Level
1	5 000	36.9 ± 2.8	21.5 ± 0.5	38.4 ± 0.3	0.31 ± 0.05	↗
2	12 500	82.2 ± 13.5	20.5 ± 1.5	63.5 ± 8.1	0.74 ± 0.23	↘↘
3	10 000	21.8 ± 2.4	24.2 ± 5.4	32.8 ± 3.4	0.32 ± 0.05	↗↗
4	6 500	31.5 ± 2.4	21,4 ± 0.7	35.6 ± 2.6	0.29 ± 0.04	↗↗
5	2 000	45.9 ± 17.3	19.8 ± 1.0	65.3 ± 2.6	0.78 ± 0.15	↘↘↘
6	5 000	79.9 ± 2.2	21.3 ± 0.9	64.0 ± 0.7	0.6 ± 0.19	↘

Table 3.4: Experimental data for validation of water management

3.2.2.2 Model extension for electrolyte tank

To verify this the evaporation in the electrolyte tank is modelled as a function of the following parameters:

- electrolyte temperature
- electrolyte flow
- air flow
- air temperature
- relative humidity of air
- percentage of evaporation: 0 means no evaporation - 100 means that the air is completely saturated

A complete description of the electrolyte tank model can be found in Chapter 5. With the evaporative effect of the KOH-tank added to the model validation it is shown that the model predictions on the production of liquid water are confirmed by the experimental results (See Figure 3.12). These are presented by the dots, which are aligned including the origin. This means that the model extension is sufficient and important to understand the results of the experimental set-up.

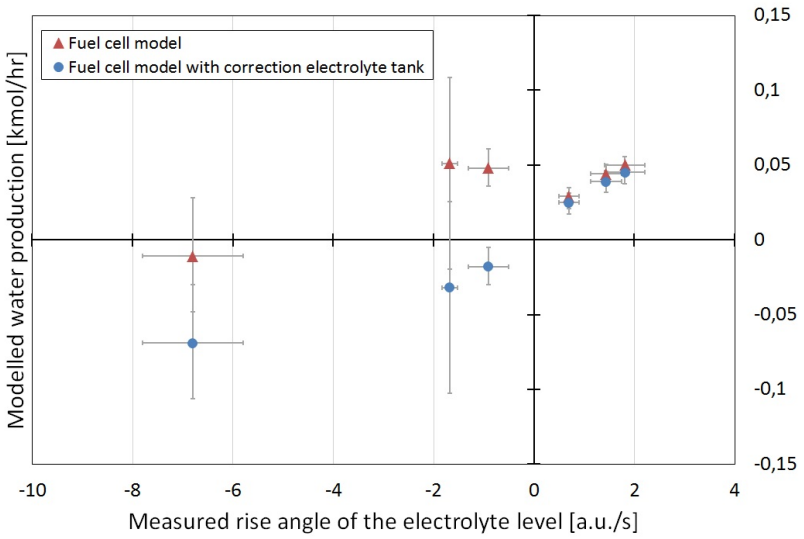

Figure 3.12: Prediction of liquid water production vs measured rise of electrolyte level. Both for the fuel cell model (triangle) as for the extended model with the electrolyte tank (dots) the model results are set as a function of the measurements.

3.2.3 Validation on the model dynamics

To validate the dynamics of the model, a filtered data set of chronologically obtained input measurements is used. The inlet variables are still the same as the ones, which are used for validation of the steady state model: current, air flow rate, electrolyte temperature and electrolyte flow rate. The output of the model is compared with the measurements over a period of time.

Figure 3.13 illustrates model results on predicting thermal behaviour of the stack (red lines) and compares it with the measurements (blue lines). A similar response for model and measurements can be noticed. As the filtered data differ a little from the measured inlet, the difference at the start is acceptable. In general it can be seen that the model overestimates the electrolyte temperature output in the studied period. This is partly due to the filtered inlet data input, which is a bit higher than the measurements, but can also be partly subscribed to the implementation of the stack as an extra layer between the electrolyte and the surroundings. However, since the general deviation is less than $2 - 3°C$, this is still acceptable.

Another parameter to evaluate the model dynamics is the response time to a sudden rise in inlet temperature, because this will also result in a change in outlet temperature. The response time of the model to this change is about 20 seconds faster than observed in the measurements (70 seconds for the model to response,

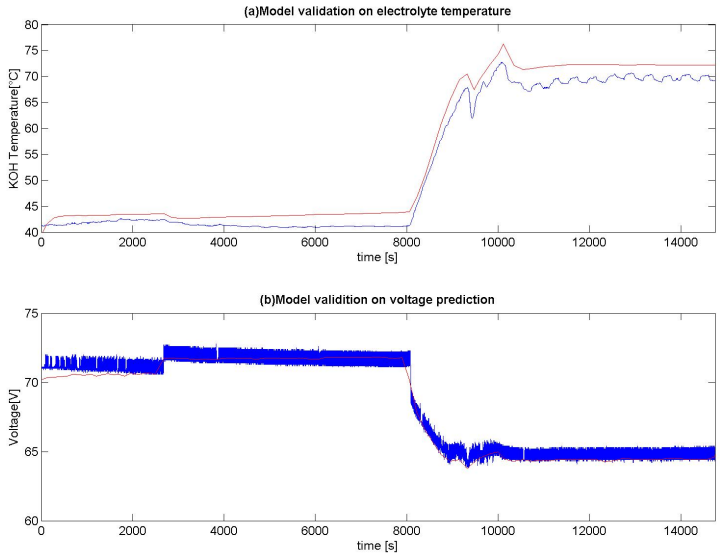

Figure 3.13: Comparison of measured output values, represented by a blue line and model output, represented by a red line.

compared to 90 seconds observed in the measurements). This is found acceptable, because this is also due to time the electrolyte needs to pass the stack, which is not incorporated in the model.
Next, the change in electrolyte temperature is compared. It is shown that for both model and the measurement this occurs at the same speed.
Finally, the electric response is evaluated. The electric response shows only a small distortion, because of the used data filter and the neglect of stack capacitance. Nevertheless, the model shows a good similarity with the measurements.
The dynamics in the model are validated, although improvements are still possible. Because of the scope of the model utilization, discussed in Section 2.4, this work is not elaborated.

3.3 Closure

Although the experimental work was bound to the limitations of the existing set-up, an analysis of the measured data made model validation possible. The steady state model developed in Chapter 2 is validated regarding predicting performance, thermal and water management. The dynamic model shows a

realistic transient thermal behaviour compared to the measurements. The model is not valid for fast electric transient behaviour in order to develop an appropriate DC control, as this is beyond the scope of the model and the experimental set-up. For this kind of fuel cell characterization, EIS measurements are more appropriate (See Appendix B).
Despite this limitation, it is shown that the model is valid for evaluation of stack behaviour with respect to water removal, thermal balance and their influence on electric performance.

4

Analysis of an alkaline fuel cell stack

In Chapter 2 a stack model is developed, which is validated in Chapter 3. In this chapter the stack model is used to gain insight in the water and thermal management in order to optimize system set-up and control strategy of an AFC-system as a micro-CHP.
Within the scope of the PhD, the applicability of an AFC stack within a micro-CHP is aimed. Therefore, an overview is given of the key performance indicators (KPI) regarding system integration within a micro-CHP. Afterwards a study is performed to optimize performance and control regarding these indicators.

4.1 Feasibility of an AFC-stack as a micro-CHP

Next to lifetime improvements and reducing degradation, the biggest advancements and reduction in total environmental impact are to be expected in reducing catalyst loading and optimising the overall system [42]. To optimise the overall system of an AFC-based micro-CHP for buildings it is necessary to understand and research the behaviour of the alkaline fuel cell from an engineering point of view.
For PEMFC a numerous amount of these studies have already been performed, examining performance, heat integration and water management [53, 66, 79, 88–90]. Although both PEMFC and AFC are low temperature fuel cells, these results cannot be copied or extrapolated, because the thermal and water management of an AFC stack shows some fundamental differences with the PEMFC. However,

the key performance indicators (KPI's) for a good stack integration are similar to PEMFC: electric performance, α_e, thermal performance, α_{th}, and a stable water management. On single stack level this means there is no net water production or evaporation in the electrolyte flow. For multi stacks, discussed in Chapter 5 and 6, also the occurrence of water droplets are taken into account for this KPI.
In the next sections in this chapter the influence of different parameters and configurations on these KPI's is elaborated at stack level. To facilitate this analysis, also an overview is given of the energy and water balance within the stack and a methodology based on primary energy savings is proposed to evaluate the CHP-potential of the stack.

4.1.1 Water and energy balance of the stack

4.1.1.1 Description of the water balance in the AFC-stack

In the investigated alkaline fuel cell, hydrogen and oxygen are separated by a circulating electrolyte. The electrolyte (KOH) is enclosed by two gas permeable membranes. Within the fuel cell, hydrogen and oxygen react into water (vapour), $\dot{m}_{w,reaction}$, which leaves the fuel cell as vapour in the hydrogen, $\dot{m}_{w,H_2}$, and/or air flow, $\dot{m}_{w,air}$, or as liquid in the electrolyte, $\dot{m}_{w,liq}$, where it dilutes the solution.

$$\dot{m}_{w,reaction} = \dot{m}_{w,H_2} + \dot{m}_{w,air} + \dot{m}_{w,liq} \tag{4.1}$$

To develop a more compact system design in order to reduce material cost, it is necessary to prevent the formation of liquid water, diluting the electrolyte and to prevent evaporation of water out of the electrolyte solution, as this would dry out the electrolyte, which is necessary to keep the gas chambers separated. Therefore, an unstable water management requires a larger buffer tank, resulting in higher material and installation costs.
Next to the ability to integrate the stack into a more compact design, an unstable water management will affect performance. In Ref. [78] it is found that dilution (or concentration in case of dry-out) will increase ohmic resistance within the electrochemical model.
To allow implementation of a smaller buffer tank and to keep an optimal electrolyte concentration [78], it is necessary to ensure that the water formed within the reaction, $\dot{m}_{w,reaction}$, evaporates and can be removed by the gas flows.
Next to removal of reaction water, it is also possible that the different flows exchange water (vapour) outside the reaction. This will result in one or two negative terms in Eq. (4.1). A negative term means that this flow contains less water (vapour) at the outlet than at the inlet.
In case of a negative production of liquid water in the electrolyte, $\dot{m}_{w,liq}$,this will result in (re)concentration of the electrolyte. The water is removed in the gas flows and the mass balance presented in Eq. 4.1 is still valid. In case a net removal of

water vapour out of the gas flows is observed, comparing water content of the input and output flow, there are two possibilities.

- A hot and wet input gas flow can cause an opposite diffusion of water vapour from the gas chamber into the electrolyte. This will result in a negative term for the water removed in the gas flow, $\dot{m}_{w,H_2}$ and/or $\dot{m}_{w,air}$, and a higher value for $\dot{m}_{w,liq}$.
- Another possibility is the formation of water droplets in the gas channels, due to saturation. In the mass balance (Eq.4.1) this mass flow is still included in the water removal by the gas flow. This means that the water removed in the air flow can be split into vapour, $\dot{m}_{w,air,vap}$, and droplets, $\dot{m}_{w,air,drop}$. For hydrogen a similar approach can be used.

$$\dot{m}_{w,air} = \dot{m}_{w,air,vap} + \dot{m}_{w,air,drop} \tag{4.2}$$

$$\dot{m}_{w,H_2} = \dot{m}_{w,H_2,vap} + \dot{m}_{w,H_2,drop} \tag{4.3}$$

In an end-of-pipe configuration for one of the gas flows, no gas leaves the stack, unless by purging or by the reaction itself. In this case all vapour in this gas flow will condensate due to cooling down of the stack. The result is the formation of water droplets. This has to be prevented, because water droplets can block gas channels, causing a reduction of active cells or active cell area.
To prevent the occurrence of water droplets in the gas channels, the stack geometry has to foresee a way to capture and remove these droplets and/or the stack need to be purged. In the investigated system, discussed in Chapter 3, the condensate in the hydrogen channels, which are end-of-pipe is removed mainly by purging.

4.1.1.2 Description of the energy balance in the AFC-stack

Next to water, heat and electricity are produced in the reaction. The generated electricity can be put on the grid using an inverter. The generated heat results in a temperature rise in the electrolyte flow and in the air flow (Also discussed in Section 3.1.3). A part of this heat however will be lost to the surroundings due to transmission losses and evacuation of water vapour to the surroundings.
In Figure 4.1 an overview is given of the different mass and energy flows in the perspective of a CHP-application. Regarding the mass flows, three input flows and two output flows are present. At the input side, hydrogen, oxygen and electrolyte can be specified, each at a certain temperature ($T1$ and $t1$). At the output side only air and electrolyte leave the fuel cell, since it is an end of pipe fuel cell. Both electrolyte and air can be diluted with water or water vapour, which is formed in the reaction. The output temperatures ($T2$ and $t2$) will differ from the input temperatures, due to the heat generated by the reaction. As for the energy flows, the electricity output represents the generated electric power, P_e.

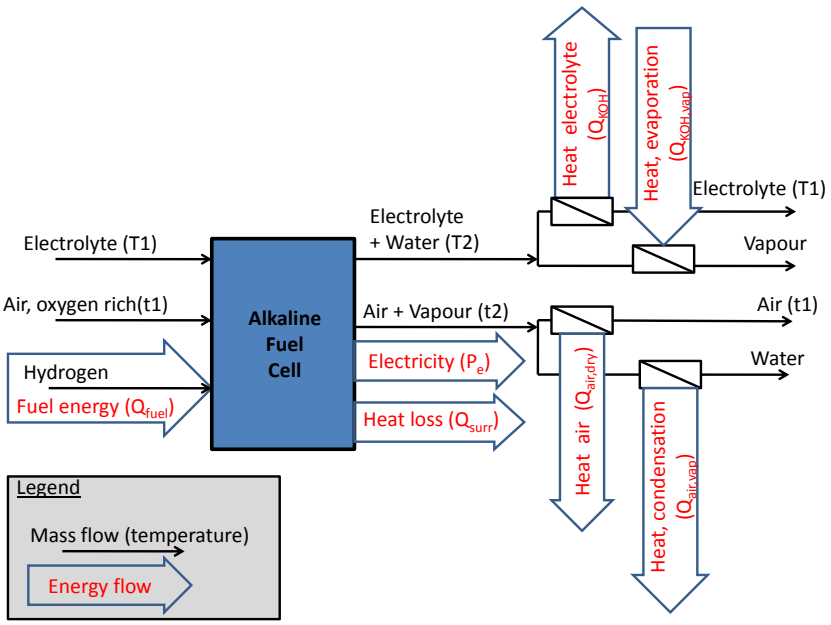

Figure 4.1: Overview of mass and energy flows of an AFC, with indication of the different energy flows.

To evaluate the CHP-application of the alkaline fuel cell, the potential to recover the generated heat is investigated. However, because not every heat flow is as useful for heat recovery, a more detailed description of the heat balance is needed. In Figure 4.1 five heat flows are specified:

- *Heat loss*, Q_{surr}, represents the heat lost to the surroundings due to transmission losses of the system, Eq.(4.4).

$$Q_{surr} = hA_{surr} \cdot (T_{KOH} - T_{surr}) \tag{4.4}$$

$$T_{KOH} = \frac{(T_1 + T_2)}{2} \tag{4.5}$$

- *Heat electrolyte*, Q_{KOH}, is the useful heat due to temperature change, $(T_2 - T_1)$, of the circulating electrolyte. This heat can easily be recovered, which is already the case in [59].

$$Q_{KOH} = \dot{m}_{KOH} \cdot c_w \cdot (T_2 - T_1) \tag{4.6}$$

- *Heat evaporation*, $Q_{KOH,vap}$, is the heat needed to evaporate the liquid water formed during the reaction.

- *Heat air*, $Q_{air,dry}$, is the sensible heat in the dry and oxygen-poor air flow, compared to the air input temperature.

$$Q_{air,dry} = \dot{m}_{air} \cdot c_{air} \cdot (t_2 - t_1) \tag{4.7}$$

- *Heat condensation*, $Q_{air,vap}$, is the extra heat which can be recovered if the water vapour in the air stream condenses.

$$Q_{air} = Q_{air,dry} + Q_{air,vap} \tag{4.8}$$

4.1.2 Stability of the water management

Each fuel cell based system configuration has to take care of the water management in order to prevent electrolyte dilution, dry-out, flooding or blockage of the gas channels by water droplets. In Section 4.1.1.1 a brief description of the water household in an AFC stack is given. To achieve a stable water management, following conditions have to be fulfilled:

- To prevent electrolyte dilution or concentration (dry-out) all water formed in the reaction has to be removed by the gas flows and net evaporation of the electrolyte has to be prevented. Therefore, a stable water management results in following equations.

$$\dot{m}_{liq} \approx 0 \tag{4.9}$$

$$\dot{m}_{reaction} \approx \dot{m}_{H_2} + \dot{m}_{air} \tag{4.10}$$

The net formation of liquid water, $\dot{m}_{w,liq}$, will be used for evaluation of the water management. A high absolute value will be an indicator for an unstable water management.

- As both blockage by water droplets caused by $\dot{m}_{w,H_2,drop}$ and purging to prevent $\dot{m}_{w,H_2,vap}$ from condensation will result in an overall efficiency loss, the presence of water in the end-of-pipe hydrogen flow, $\dot{m}_{w,H_2}$, has to be minimised. In this way the geometry of the stack is capable to dispose the water.
  The formation of water droplets within the hydrogen flow can be a problem if the hydrogen gas channels of different (sub)stacks are serially connected. Therefore, the removal of water vapour in the hydrogen gas channel is taken into account to evaluate the water management of different configuration set-ups in Chapter 6.

In the evaluation of the stack performance regarding water management, only the net production of liquid water is taken into account. In the system evaluation in Chapter 6 also the removal in the hydrogen gas flow will be of importance.

4.1.3 CHP-potential

To evaluate the CHP-potential of the fuel cell stack, the electrical and thermal efficiencies are defined. To interpret these efficiencies within a CHP-context it has to be clear that the system integration of the stack, will limit these efficiencies. A complete fuel cell system includes next to the fuel cell stack itself: fans, pumps, gas treatment, cooling, electric conversion, control, storage, etc. Also the actual deployment and control of the system will affect the efficiencies.
Therefore, first the boundary conditions for a system set-up and the deployment of an AFC as a micro-CHP are discussed. Secondly, to evaluate the electrical and thermal power output of the stack, a minimal set of system efficiencies needs to be introduced (See Table 4.1 in Section 4.1.3.2). As there will always be some system losses, these system efficiencies will have to be taken into account to evaluate the maximum realistic CHP-potential. The evaluation base for this potential is based on primary energy savings. This is briefly explained at the end of this subsection.

4.1.3.1 System integration and deployment of an AFC-based micro-CHP

Presently, micro-CHPs are used as a heater with additional electric power production. Since for small applications -like micro-CHP, there are no limits to put electricity on the grid, all produced electricity is seen as a useful energy output. The only limitation is a thermal load which uses the thermal power output of the micro-CHP. The dynamics of this load will determine the operation modus of the micro-CHP.

In building applications the heat demand is composed of hot water demand and space heating. The daily hot water demand is relatively constant over a year, while heat demand for space heating shows seasonal fluctuations. Due to an improved insulation rate, the share of space heating in the total heat demand is decreasing, reducing the seasonal fluctuations. The fluctuations on a day time basis, both for hot water demand and space heating, can be levelled out using a daily storage system.
This is also recommended to ensure a stable operation of the fuel cell system. In the present set-up (See Ref. [58]), which is used in the experimental work, a start-up time of almost 10 minutes has to be taken into account before nominal load can be achieved. This start-up time is a consequence of the present set-up and control strategy, but, since the system can be easily modulated into part load, an on-off control strategy is to be avoided. Within these boundaries of deployment and integration of the fuel cell as a micro-CHP, the energy efficiency in this working range can be evaluated at steady-state operation.
As for the electric performance it has to be taken into account that there will be conversion losses and losses due to parasitic load, depending on system configuration. As for the thermal performance also here the heat transfer, storage and distribution will reduce the actual thermal efficiency of the complete system, depending on set-up, control strategy and deployment. The focus of the study however is to maximize heat and power output of the stack itself, with an abstraction of these system losses (See Section 4.1.3.2) to evaluate the primary energy savings (See Section 4.2.4).
In a system evaluation also the energy source (natural gas, syn gas, pure hydrogen) will affect efficiency, at stack level pure hydrogen is withheld as a fuel source, allowing a generally applicable evaluation.

4.1.3.2 Efficiency

- The electrical efficiency, α_e, is defined as the ratio of the generated electric power to the fuel input, Q_{Fuel}, Eq.(4.11). The generated electric power (DC), $P_{e,DC}$, can be calculated from current and voltage, Eq.(4.12). To calculate the actual overall efficiency the conversion efficiency of the inverter, $\eta_{inverter}$, has to be taken into account, Eq.(4.13).

$$\alpha_e = \frac{P_{e,system}}{Q_{Fuel}} \tag{4.11}$$

$$P_{e,DC} = voltage \cdot current \tag{4.12}$$

$$P_{e,system} = \eta_{inverter} \cdot P_{e,DC} \tag{4.13}$$

- The thermal efficiency, α_{th}, is defined as the ratio of the useful heat output, Q_{TH}, to the fuel input, Q_{Fuel}, Eq.(4.14). The heat output due to

temperature change of the electrolyte, Q_{KOH}, can be used directly as a useful heat source, Eqs.(4.6) and (4.15). The thermal power output, Q_{TH}, can be improved by recovering the available heat in the output air flow, Q_{air}, reduced with possible losses due to water management, $Q_{KOH,vap}$, Eq.(4.16). Since the air flow is not a closed loop, unlike the electrolyte, the efficiency of the heat exchanger, $\epsilon_{air,HeX}$ has to be taken into account to calculate the net heat, $Q_{air,net}$, available for recovery, Eq.(4.17).
As can be seen in Eqs.(4.15) and (4.16), two different definitions of Q_{TH} are posed. The first one, $Q_{TH,nom}$, represents the nominal thermal output, which will be used to evaluate the influence of the operating parameters. The second one, $Q_{TH,max}$, represents the maximum heat available for recovery and gives an outlook on the improvement potential.

$$\alpha_{th} = \frac{Q_{TH}}{Q_{Fuel}} \tag{4.14}$$

$$Q_{TH,nom} = Q_{KOH} \tag{4.15}$$

$$Q_{TH,max} = Q_{KOH} - Q_{KOH,vap} + Q_{air,net} \tag{4.16}$$

$$Q_{air,net} = \epsilon_{air,HeX} \cdot Q_{air} \tag{4.17}$$

The fuel input (hydrogen) energy, Q_{Fuel}, is calculated as the fuel flow rate multiplied with its higher heating value (HHV), Eq.(4.18). Since it is an end-of-pipe system, the hydrogen flow rate, $\dot{m}_{H_2,system}$, is directly related to the cell current, I_{ref}, as a consequence of Faraday's law, Eq.(4.20). Part of the hydrogen however will be purged and lost to the surroundings, depending on the system control strategy, Eq. (4.19). As a result fuel input, $\dot{m}_{H_2,system}$, will be directly proportional to the current drawn from the fuel cell stack.

$$Q_{Fuel} = \dot{m}_{H_2,system} \cdot HHV_{Hydrogen} \tag{4.18}$$

$$\dot{m}_{H_2,AFC} = \eta_{purge} \cdot \dot{m}_{H_2,system} \tag{4.19}$$

$$\dot{m}_{H_2,AFC} = M_{H_2} \cdot \frac{I_{ref} \cdot n_{series}}{2 \cdot Far} \tag{4.20}$$

As can be seen in equations (4.18), (4.19), (4.20), (4.11) and (4.12), voltage is a good reference for electrical efficiency. The different system efficiencies, η_{purge}, $\eta_{inverter}$, and $\epsilon_{air,HeX}$, which are used to evaluate the CHP-potential, are listed in Table 4.1.
Efficiencies, $\eta_{inverter}$, and $\epsilon_{air,HeX}$ are based on average values of presently available technology. Purge efficiency, η_{purge}, is based on observations during the experiments, described in Chapter 3.

Efficiency	value[%]
η_{purge}	99
$\eta_{inverter}$	90
$\epsilon_{air,HeX}$	90

Table 4.1: Used system efficiencies to evaluate CHP-potential of the AFC.

4.1.4 Primary Energy

Reference efficiencies

To evaluate the different parameters the primary energy savings were calculated, compared to separate generation of electricity and heat. For heating, a boiler with 90% efficiency $(\eta_{t,ref})$ is considered, based on the higher heating value (HHV). Electricity is bought from the grid. The amount of primary energy needed to produce this electricity is strongly dependent on the used technology. In this way, in Belgium, two different values for $\eta_{el,ref}$ are interesting to compare with micro-CHP.

- To determine the quality of a cogeneration (CHP) unit, the CHP is compared with the best possible classic alternative: a combined cycle gas/steam turbine plant. A combined cycle plant has a typical efficiency between 53% and 56% (LHV). Considering transformation and transport losses, a realistic value of 50% (LHV) for the efficiency of separate electricity production $(\eta_{el,ref})$ is assumed [20].

- To calculate the actual primary energy savings an efficiency $(\eta_{el,ref})$ of 40% (LHV) is used which is representative for the average Belgian power plant. For fossil fuel plants the calculated average is 42% and for nuclear plants 37% [20].

The first values for $\eta_{el,ref}$ will be used to calculate possible financial support measures to promote CHP in Belgium. The second value will be used to calculate the primary energy use in buildings according to the European building directive. Because in this book all calculations are based on higher heating value (HHV), these efficiencies, best known in their definition at lower heating value (LHV), need to be converted. Since this conversion depends on the used energy source, it is assumed the plant is fuelled with natural gas, resulting in following values for $\eta_{el,ref}$ defined at HHV: 45% for a combined cycle plant and 36% for the average Belgian power plant.

Hydrogen conversion

Before primary energy calculations are started, it is also necessary to point out that hydrogen, which will be used as fuel source for the fuel cell system is no primary energy source. Hydrogen needs to produced first, which can be done in many ways: by electrolysis, by reforming, as a waste product (e.g. with the production of chlorine), ... Depending on this production method a different conversion factor needs to be taken into account.
Naturally, the most interesting option here is to assume a sustainable production of hydrogen, as a waste product or by electrolysis from renewable electricity. However, to allow a comparison with the chosen reference efficiencies, it is assumed the hydrogen to be produced by reforming of hydrocarbons, which is still accountable for the largest share in hydrogen production.
For this, a reforming efficiency, $\eta_{reforming}$, of 85% is taken into account to calculate the electric and thermal efficiencies of the fuel cell system based on primary energy utilization, $\alpha_{e,PE}$ and $\alpha_{th,PE}$. The difference with the efficiencies, defined in Section 4.1.3.2, α_e and α_{th} is illustrated by following equations.

$$\alpha_{e,PE} = \eta_{reforming} \cdot \alpha_e \tag{4.21}$$

$$\alpha_{th,PE} = \eta_{reforming} \cdot \alpha_{th} \tag{4.22}$$

Primary energy savings

Finally, Eq.(4.23) is used to calculate the relative primary energy savings (RPES) compared to a separate production of electricity and heat.

$$RPES = 1 - \frac{1}{\frac{\alpha_{th,PE}}{\eta_{t,ref}} + \frac{\alpha_{el,PE}}{\eta_{el,ref}}} \tag{4.23}$$

The relative primary energy savings are an important criterion to evaluate the performance of CHP systems [20].

4.2 Performance of an AFC-stack as a micro-CHP

A successful integration of an AFC-stack into a micro-CHP system depends on the feasibility to implement an inexpensive and efficient water management and on the possibility to achieve a high CHP performance.

The performance of a micro-CHP is characterized by return temperature and electric load. The return temperature limits the type of heat source that is available for recovery. The electric load gives an indication of the relative importance of friction and other kinds of losses. Translated to the operating parameters of a fuel

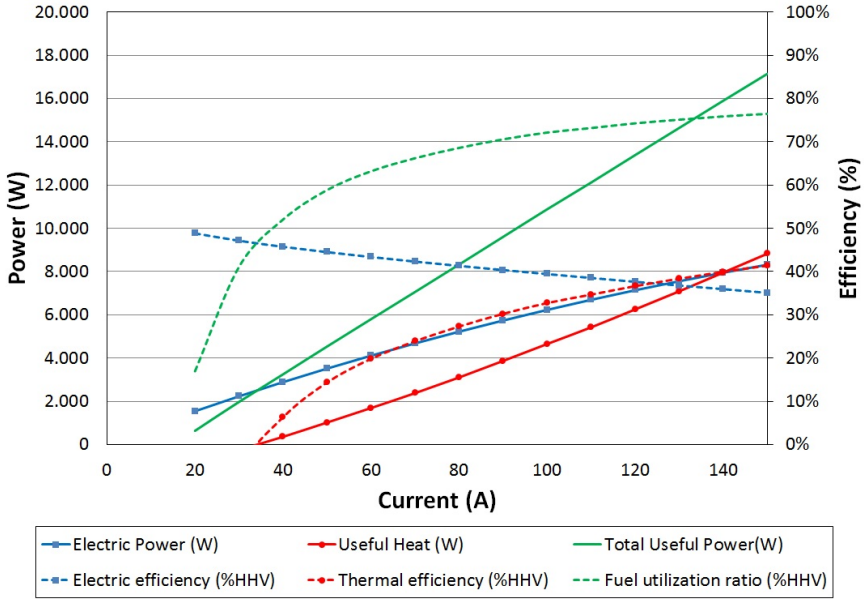

Figure 4.2: For an input electrolyte temperature of $60^{\circ}C$, the power curves and corresponding efficiency are presented as a function of current.

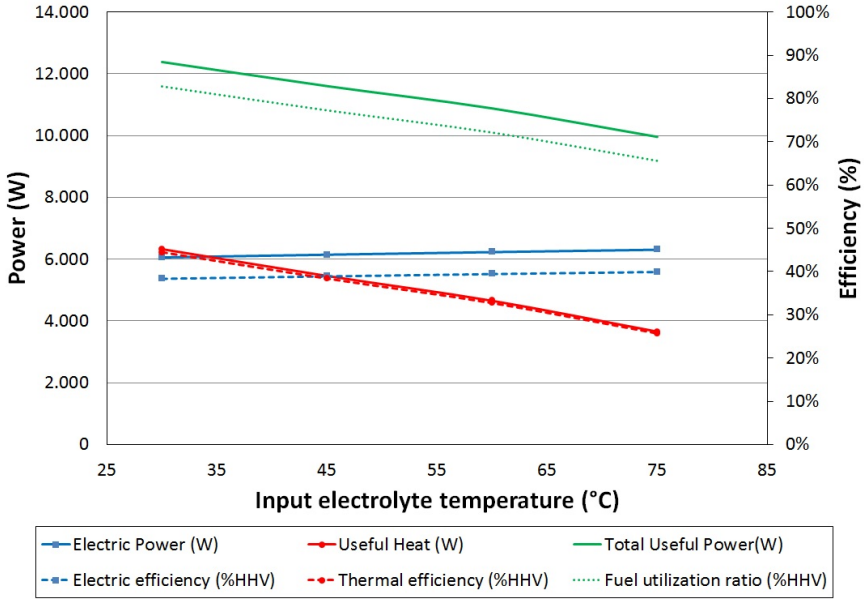

Figure 4.3: For a nominal current of 100A, the power curves and corresponding efficiency are presented as a function of input electrolyte temperature.

cell, the influence of current and input electrolyte temperature is examined.
In Figures 4.2 and 4.3, their influence is presented regarding electric and thermal performance and fuel utilization of the fuel cell stack. In Figures 4.4 and 4.5, their influence is presented regarding water management of the stack.

- The water management is represented by the net formation of liquid water, $\dot{m}_{liq}$ as discussed in Section 4.1.1.1.
- The electrical power output, $P_{e,system}$, and efficiency, α_{el}, are calculated with equations (4.13) and (4.11).
- The presented thermal performance is based on the basic heat output, Q_{KOH}, without considering heat recovery or water management.
- The total fuel utilization is represented by the total useful power output, Q_{tot}, and the fuel utilization ratio, η_{CHP}. Their definition is given by following equations:

$$Q_{tot} = P_{e,system} + Q_{KOH} \tag{4.24}$$

$$\eta_{CHP} = \frac{Q_{tot}}{Q_{Fuel}} \tag{4.25}$$

All other considered operating parameters (See Table 4.3) depend on system configuration and can give an indication of the improvement potential. This will be set out in Section 4.3.
First, water management will be discussed as this will be a boundary condition, limiting performance.

4.2.1 Water management

To evaluate the influence of the operation modus on water management in the stack, both current and electrolyte temperature at the input were set at different values. Their influence on the net water production, representative for the water management at single stack level is discussed in the following subsections.

4.2.1.1 The electrolyte temperature

It is shown that the electrolyte temperature has a large impact on the water management. In Figure 4.4 is shown that at low electrolyte temperature almost no water vapour diffuses and that the formed liquid water is proportional to the current, which is directly linked to the generated water, Eq. (2.45) (See also Figure 4.5). The impact of the electrolyte temperature on the evaporation is proportional to its impact on the saturation pressure.
At least a temperature of about $55°C$ has to be reached to avoid net rise of liquid

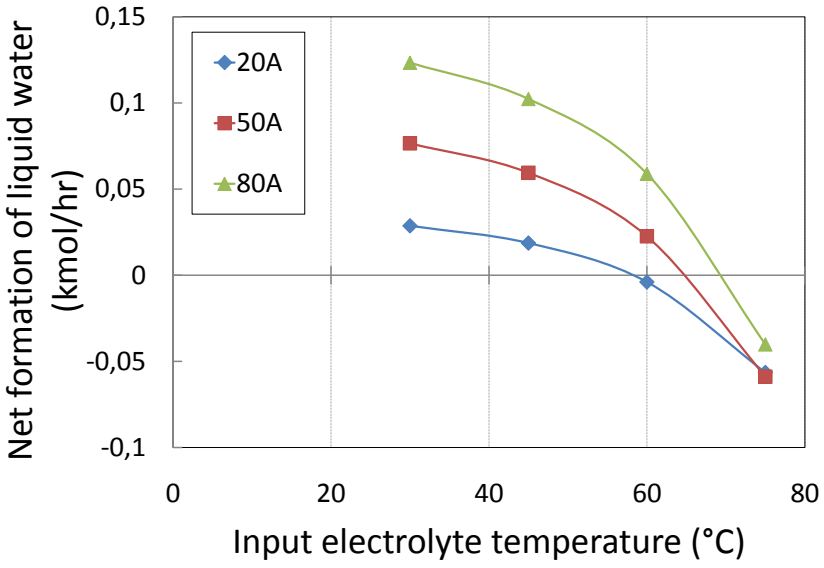

Figure 4.4: Sensitivity of liquid water production to electrolyte temperature at three different currents.

water in the electrolyte flow. At lower temperatures the saturation pressure drops rapidly. Because of this the driving force for the water vapour diffusion is strongly reduced. As a result liquid water builds up due to the formation of water, which is not transported out of the fuel cell by diffusion. For the same reason, but now in the opposite direction, there is a net evaporation at temperatures higher than $75°C$, at least for currents within nominal working range ($20A$ to $80A$). To avoid dry out of the fuel cell, $75°C$ is to be set as a maximum temperature when working with dry or cold air. This will limit the electric efficiency which is higher at higher temperature (See Chapter 3 and also Figure 4.6).

4.2.1.2 The electric current

At low temperature, current has no significant influence and all formed water will end up in the electrolyte flow. Figure 4.5 shows that for every input electrolyte temperature higher than the minimum value (about $55°C$, See Section 4.2.1.1) a current can be found at which all formed water is evaporated and diffuses into the gas streams. This is interesting regarding steady state working points.

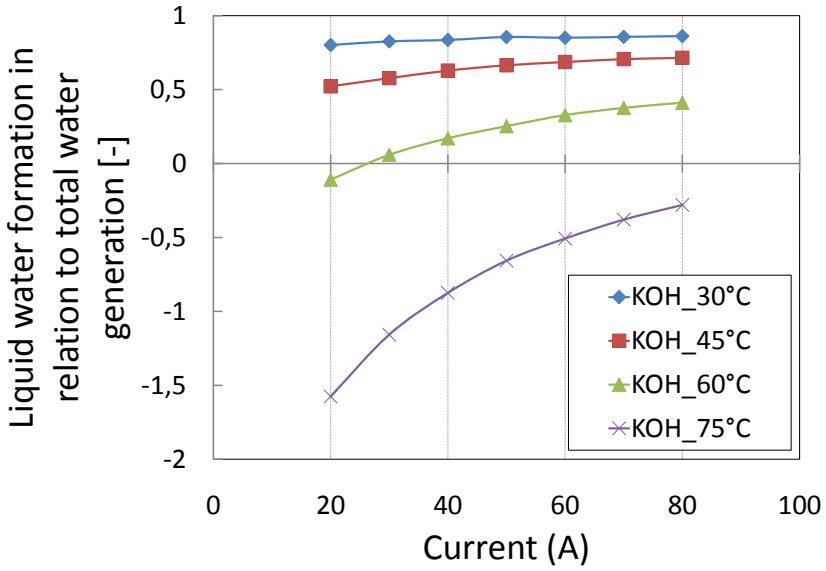

Figure 4.5: Sensitivity of liquid water production to total current at four different electrolyte temperatures.

4.2.2 Electrical performance

As can be seen in Figures 4.2 and 4.3 both electrolyte temperature and current influence the electrical efficiency and power output. As stated in Section 4.1.3.2 voltage is a good indicator of stack efficiency. In the polarization curve (See Figure 4.6), the positive effect of a rising electrolyte input temperature and the negative effect of a rising current on the stack voltage are shown together.

- At higher current the voltage will drop mainly due to resistance losses.
- At higher electrolyte temperatures the resistance losses and also the activation and diffusion losses are reduced, which results in a positive effect of the electrolyte temperature on the electric performance of the alkaline fuel cell. The power rises about 1% for every increase of input electrolyte temperature by $15°C$.

4.2.3 Thermal performance

To evaluate the CHP-potential of the fuel cell, next to electricity production the thermal performance is a decisive parameter. The influence of current and the

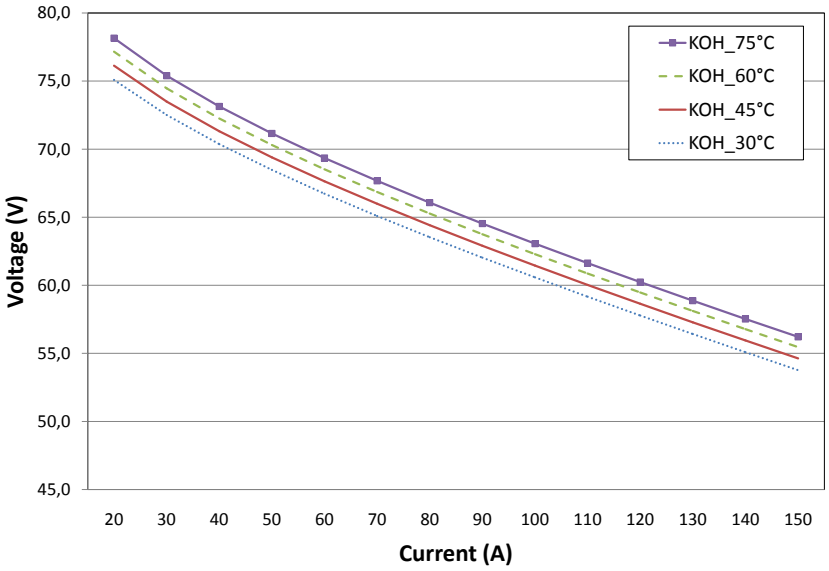

Figure 4.6: For different electrolyte temperatures, the polarization curve is shown, scaled to a complete fuel cell system.

influence of input electrolyte temperature are discussed for the different available heat flows shown in Figure 4.1. First, thermal performance is examined based on Eq.(4.14) and Eq.(4.15), which is representative for the basic heat output. Secondly, the different heat outputs are discussed, since they give an indication of the improvement potential, Eq.(4.16).

4.2.3.1 Basic heat output

As stated earlier in a first approach the heat output is reduced to Q_{KOH}, Eq.(4.6), since this heat is useful in every possible configuration. The other heat outputs can be used in several ways (See Section 4.2.3.2.).
The heat output is influenced by both electrolyte temperature and current. While electric efficiency drops at a higher current, more heat is produced and the thermal efficiency rises, since the heat losses to the surroundings, calculated in Eq.4.4, remain more or less constant (See Figure 4.2). A similar effect is presented for a PEMFC in [66].
Due to the heat losses to the surroundings, it is even possible the useful thermal power output and thermal efficiency turn into negative values, if these heat losses are higher than the heat produced in the reaction. This is the case at low currents, as can be seen in Figure 4.2. Therefore, in order to use the stack for heat production a minimal electric load is necessary.
In Figure 4.7 the available heat in the electrolyte is simulated for different currents as a function of electrolyte input temperature. As stated earlier, a high electrolyte temperature results in high transmission losses and is only acceptable at a sufficiently high current.

4.2.3.2 Improvement potential

In Figure 4.1 next to the basic heat output, represented by Q_{KOH}, also other heat flows are shown. These heat flows can be used to improve overall system performance, since different options (listed below) exist to integrate these heat flows in an improved system design. A better understanding of these heat flows will facilitate one or a combination of the following options for system improvement.

- The heat flows can be used to heat up an external circuit and maximize thermal performance.
- They can be used internally in the system for water management.
- They can be useful to influence operating parameters to maximize electric and basic thermal power output (See also Section 4.3.2).

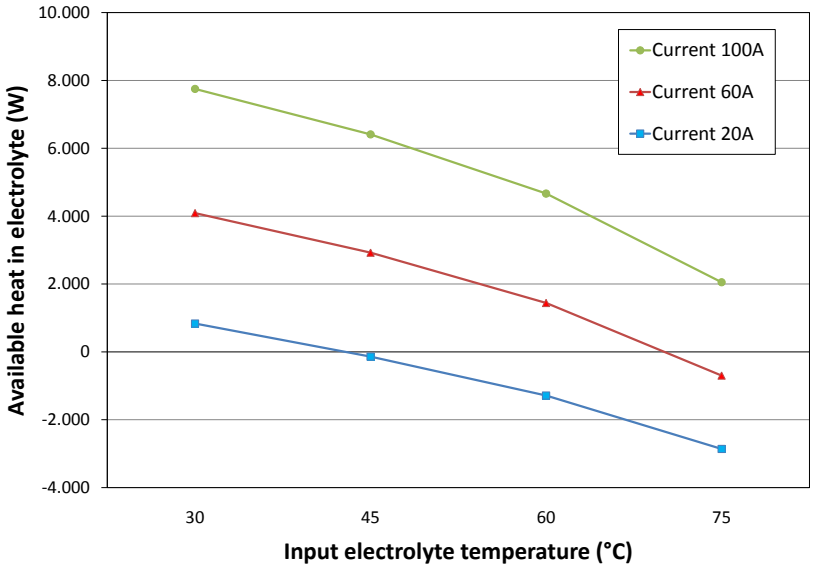

Figure 4.7: The heat available by cooling the electrolyte as a function of electrolyte temperature. This heat is defined in Figure 4.1 as Heat electrolyte, Q_{KOH}.

The effect of current and input electrolyte temperature on the other heat flows, indicated in Figure 4.1, is shown in Figures 4.8 and 4.9. As a high current and low input electrolyte temperature have a positive effect on the available heat in the electrolyte (See Section 4.2.3.1), they can have a negative effect on the water management. To maintain the water level in the electrolyte the input temperature has to be high enough otherwise the formed liquid water in the reaction will dilute the electrolyte (See discussion in Section 4.2.1).
The heat needed to evaporate the reaction water out of the electrolyte, $Q_{KOH,vap}$, is shown in Figure 4.8. At higher currents more heat will be needed, since more liquid water will be formed, despite the positive effect of current on electrolyte temperature. In the present set-up with a KOH-tank downstream (a detailed description can be found in Chapter 5 and in Refs. [59, 87]), this heat demand is partly compensated by the heat in the dry air, $Q_{air,dry}$, which passes over the tank. For high electrolyte temperatures this heat is sufficient to prevent dilution. At lower electrolyte temperatures there will be dilution in the present set-up. This is discussed in Chapter 6.
In Figure 4.9 the heat available in the output air flow, Q_{air}, is shown. Since the air flow is not a closed loop like the electrolyte, an efficiency of the heat exchanger, $\epsilon_{air,HeX}$, has to be included to obtain a realistic value for the heat output (See

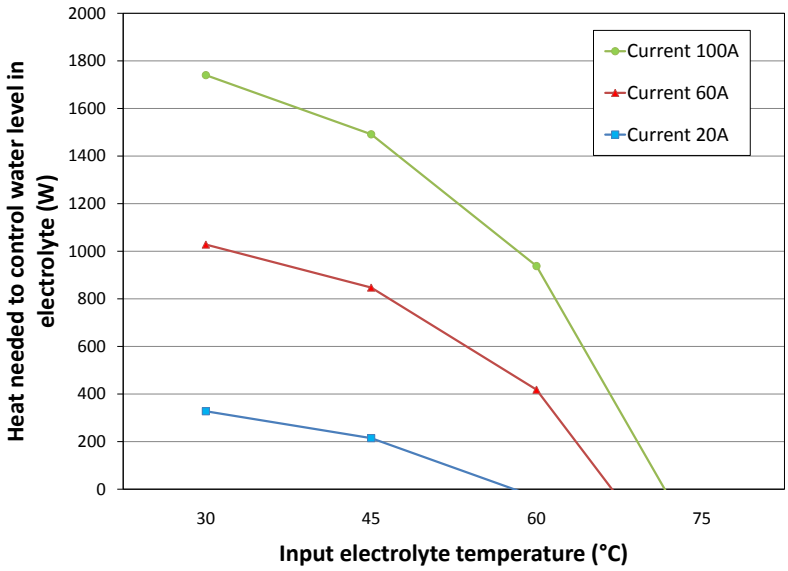

Figure 4.8: The necessary (evaporation) heat to maintain the water management in the electrolyte flow as a function of electrolyte temperature. This heat is defined in Figure 4.1 as Heat evaporation, $Q_{KOH,vap}$.

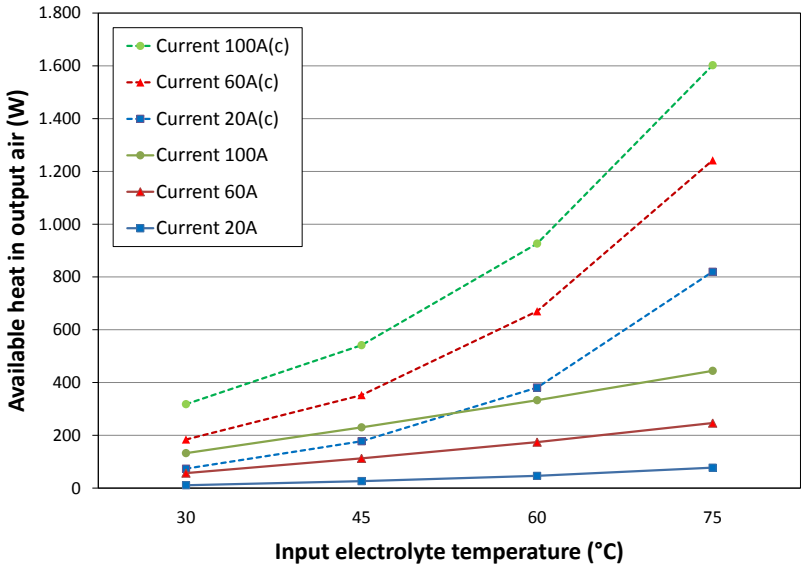

Figure 4.9: Available heat by cooling the output air with a heat exchanger efficiency, $\epsilon_{air,HeX}$ of 90%. Both possibilities, with ($Q_{air,dry} + Q_{air,vap}$) or without ($Q_{air,dry}$) condensation of the water vapour are shown. The available heat in the output air, including condensation is represented by (c). This heat can be used to improve system performance and illustrates the improvement potential.

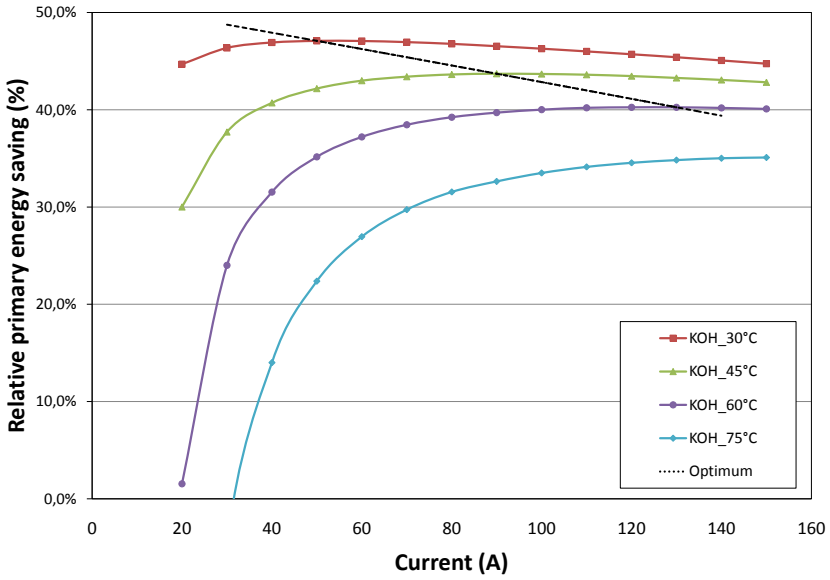

Figure 4.10: Relative primary energy savings, compared to a separate production of electricity and heat by an average Belgian power plant (40% at LHV) and an efficient boiler (90% at HHV).

Table 4.1). In the present set-up this heat is not recovered as a useful heat source, only part of it, to control water management. Figure 4.9 shows that heat recovery in the output air has a positive influence on the thermal power output of the fuel cell system, especially with condensation of the water vapour in the air stream. At higher electrolyte temperature and higher current the thermal power output will be increased even more significantly.
As can be seen from Figures 4.7 and 4.9, the thermal power output will be increased by approximately 80% at an electrolyte temperature of $75°C$ and a current of $100A$.

4.2.4 Primary energy savings

As discussed in Section 4.2.3.1 and shown in Figure 4.2, electrical efficiency decreases, while thermal efficiency increases with rising current. This positive effect on thermal performance will be larger at higher electrolyte temperatures. This will lead to a point of maximum fuel utilisation for every input electrolyte temperature. However, a maximum fuel utilisation does not imply that this is the optimal working point, since the primary energy needed for electricity or heat is

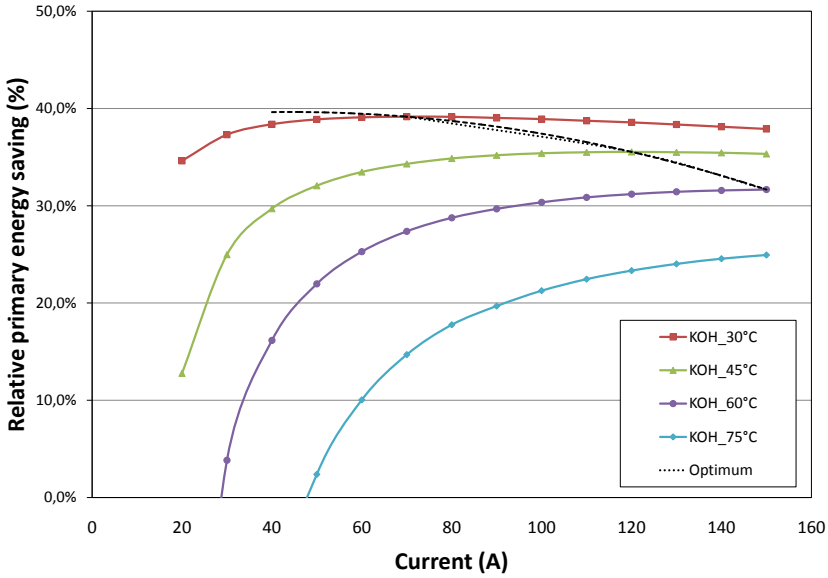

Figure 4.11: Relative primary energy savings, compared to a separate production of electricity and heat by a combined cycle plant (50% at LHV) and an efficient boiler (90% at HHV).

different in an alternative scenario with separate production (See Section 4.1.4). Because of this, the relative primary energy savings (Eq.4.23) are to be maximized to find the optimal current for every input electrolyte temperature.
In Figure 4.10 the relative primary energy savings, compared to average Belgian production efficiencies (See Section 4.1.4), are presented as a function of the current for different electrolyte temperatures. At low temperatures the ideal working point is found at lower currents. At low temperature the heat losses are negligible and the electrical efficiency will determine the optimal working point.
At higher electrolyte temperature the positive effect of the current on thermal performance is significantly higher than the losses in electrical efficiency. This results in a shift of the optimal current with increased electrolyte temperature. This shift also depends on the reference situation. Compared to an average Belgian production, the optimal current increases about $30A$ for every rise in electrolyte temperature with $15°C$. For qualitative cogeneration, with reference efficiencies of (50%) and (90%), the optimum is found at a higher current, compared to the results in Figure 4.10. As can be seen in Figure 4.11, the ideal current shifts up 40 – $50A$ for every rise with $15°C$.
Since at lower currents the savings drop rapidly and at higher current the savings drop only slowly, it is best to ensure that a sufficiently high current is drawn from the fuel cell (See Figures 4.10 and 4.11). The loss in relative primary energy savings at a current higher than the optimal current can be considered negligible.

4.3 Stack analysis for an optimal system integration

As discussed in Section 4.2 the operating parameters have a large influence on performance and water management. Next to these, control and other system dependent parameters can be adjusted to optimize performance. In this section an evaluation of stack performance and water management and its sensitivity to these parameters is elaborated. The results within this section will form the basis to improve system design and control strategy, discussed in chapters 5 and 6.

4.3.1 Analysis of the net liquid water production

With the validated model a sensitivity analysis is performed to gain insight in the effect of every input parameter on the net water production within the fuel cell. For the analysis the influence of seven parameters is examined by simulation (See Table 4.2). The cumulated influence of the first two parameters, current and electrolyte temperature with any other parameter is examined at every new condition, determined by the other five parameters. Table 4.2 presents an overview of the different inputs that are analysed below.

Parameter	base case	minimum	maximum	step size
Current	20A-80A	20A	80A	10A
Input electrolyte temperature	30 – 75°C	30°C	75°C	15°C
Input air temp	20°C	5°C	65°C	15°C
Input air RH%	0	0%	100%	50%
Input air flow (air ratio)	2.5	1	8	1.5
Input electrolyte flow	20.5 kmol/h	19	22	1.5 kmol/h
Temperature surroundings	20°C	−10°C	50°C	15°C

Table 4.2: Description of the sensitivity analysis

4.3.1.1 Influence of the electrolyte flow rate

To evaluate the influence of the electrolyte flow rate, it was set at different values. The electrolyte flow shows no significant influence on the water management.

4.3.1.2 Influence of the input air

To understand the influence of the air stream, three parameters were evaluated:

- the air ratio or the actual air flow in relation to the necessary air flow
- the relative humidity
- the air temperature

Figure 4.12 shows that a higher air ratio has a negative effect on the net formation of liquid water. The relative impact of an increased air ratio reduces if the ratio exceeds 2.5 to 4 (See Figure 4.12). Naturally, the impact of the air ratio on the evaporation of the electrolyte tank is directly related, as shown in the model extension for the electrolyte tank (See Section 3.2.2.2 and also Chapter 5).
The air ratio can be used as a control parameter for the water management within a small range within the stack itself (1 - 2.5). If the output air passes over the electrolyte tank, as in the used experimental set-up of the AFC-system, the air ratio can be a useful control parameter in a much wider range.
Next to the air ratio, the temperature and relative humidity will be of importance. Their effect however, is relatively low. If the input air is dry, the air temperature has only a very small positive effect on the diffusion, which results in a lower net liquid water formation.
The relative humidity only has a large impact at high input air temperature (See Figure 4.13). At lower temperature the water vapour content of saturated air is a lot lower and will have no significant influence on the water vapour content of the

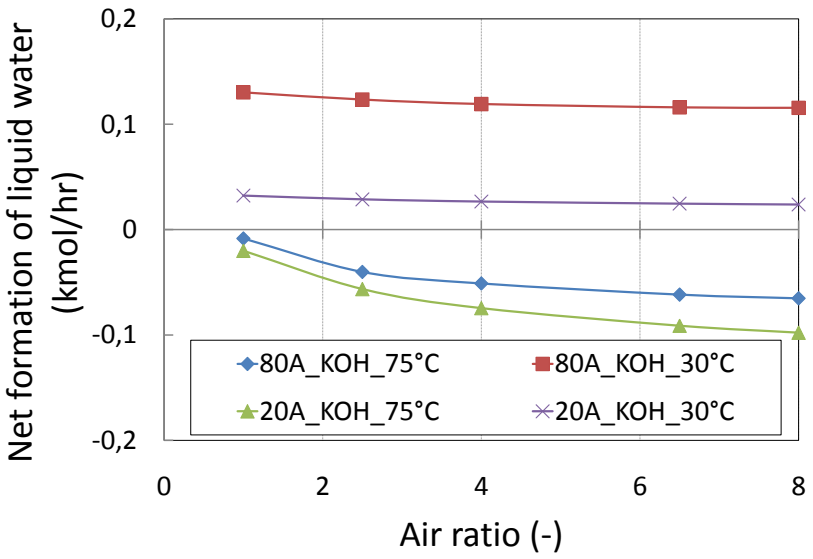

Figure 4.12: Sensitivity of liquid water production to air ratio.

heated output air stream.
As discussed earlier (See Section 4.1), to avoid dry out of the fuel cell a maximum temperature of the electrolyte has to be respected. However, this statement was posed using dry and cold air as inlet for the cathode. In Figure 4.13 it is shown that at higher electrolyte temperature it is still possible to maintain a water content in the electrolyte flow, if hot humidified air is used as input for the fuel cell. Because electrolyte temperature has a positive effect on the fuel cell performance (See Figure 4.6), this could increase the efficiency of the fuel cell.

4.3.2 Sensitivity study on the energy management

In Section 4.2.3.2, it is already mentioned that the heat flows in Figure 4.1 can be used to influence the operating parameters in order to increase the electric power output, P_e and/or the basic heat output, Q_{KOH}. Next to that, a reduction of the heat loss will also increase the useful energy output.
In this section a parameter study is performed on the different operating and system parameters, other than electrolyte temperature and current, to quantify possible savings. In reality a different set point for these operating parameters could be the result of a heat recovery on the different extra heat outputs, next to the basic heat output. For this reason, only this basic heat output, Q_{KOH} is included in the

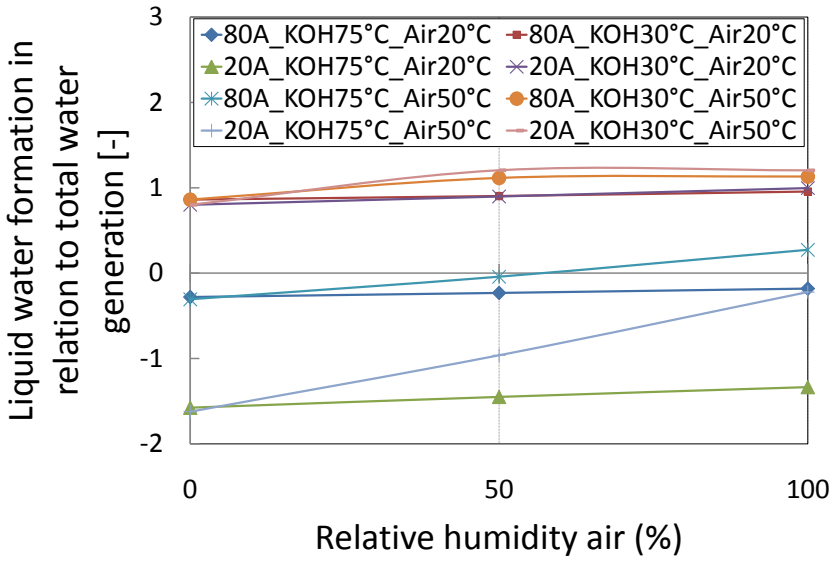

Figure 4.13: Sensitivity of liquid water production to relative humidity and air temperature. For 8 different combinations of currents (20A or 80A), electrolyte temperature ($30°C$ or $75°C$) and air temperature ($20°C$ or $50°C$) the net formation of liquid water is set as a function of the relative humidity of the input air.

evaluation of the thermal performance.

Other operating parameters

As discussed in Section 4.2 the efficiency of the fuel cell depends on the values of the two main operating parameters: electrolyte temperature and current. All other considered operating parameters (Table 4.3) influence indirectly the thermal and electrical efficiency, since they result in a temperature change of the electrolyte. Therefore, for all these parameters first the effect on electrolyte temperature is analysed and afterwards the effect on thermal and electrical efficiency.

4.3.2.1 Input air

The input air is one of the parameters which can be adapted to get a possible higher performance. Three input parameters characterize the input air flow.

- Air flow rate or air ratio, which represents the ratio of used flow rate to minimum air rate which keeps the reaction going.

Parameter	average value
Input air temp	$20°C$
Input air RH%	0
Input air flow (air ratio)	2.5
Input electrolyte flow	20.5 kmol/h
Temperature surroundings	$20°C$

Table 4.3: Standard values for the operating parameters, excluding input electrolyte temperature and current.

- Air temperature.
- Air humidity.

First the air ratio is altered with a step size of 1.5. In Table 4.4 it is shown that a higher air ratio has a negative effect on the output electrolyte temperature and on the electrical and thermal power. For every rise of the air ratio with 1.5, a temperature drop of the output electrolyte of more than $1°C$ is possible, resulting in a loss of thermal performance of more than 80%. At high input electrolyte temperatures, the temperature drop is most pronounced.
An increasing air flow rate will have the same effect as a forced cooling, because of the relatively low input air temperature of $20°C$ (See Table 4.3). At higher electrolyte temperatures the temperature difference with the input air will be larger resulting in more losses to the air flow. The cooling effect is especially negative regarding thermal efficiency. It was found that an air ratio higher than 2.5 has little effect on water management within the fuel cell, therefore a limitation on air ratio is recommended.
Secondly, the air temperature is changed. As expected, a higher air temperature results in a higher electrolyte output temperature (See Table 4.4). The effect is larger at high currents due to the same cooling effect mentioned earlier, because the air flow rate increases proportionally with current. In this case the cooling effect decreases since the air input temperature is higher, resulting in a higher output electrolyte temperature. The effect on electric power is negligible. The thermal power increases most at high temperature, since here the potential for improvement is the largest.
Finally, in addition to the temperature changes, the relative humidity is changed from dry air to complete saturation. As shown in Table 4.4 only for high air temperatures the effect is noticeable, because at high air temperatures the absolute humidity is higher. Since wet air has a higher energy density, the relative humidity has a positive effect on electrolyte temperature and thermal and electric power. At high electrolyte and air temperatures a high relative humidity increases the thermal power output significantly and balances the water management.

Therefore, at high temperatures the humidity of the input air flow is an important control parameter to improve efficiency and water management.

4.3.2.2 Electrolyte flow rate

The electrolyte flow rate has little effect on electrical or thermal performance of the fuel cell. At high electrolyte flow rates temperature changes are smaller, which ensures a more stable working state.

4.3.2.3 Ambient temperature

By altering the temperature of the surroundings the impact of several outdoor conditions can be investigated. Next to that it is possible to place the fuel cell stack in a room, conditioned at high temperature to reach higher efficiencies. To quantify the effect of the surroundings on the performance, the ambient temperature is altered from $5°C$ to $65°C$.
The temperature of the surroundings has a strong positive effect on output electrolyte temperature (about $1.5°C$ gain in electrolyte temperature for an increase of $10°C$ in temperature of the surroundings). This indicates that the transmission losses, Q_{surr}, to the surroundings are still high (See Eq.4.4). The effect on power output is shown in Figure 4.14.
A large gain in thermal efficiency is possible at higher temperature surroundings. Placing the fuel cell stack in a room or container with a high air temperature inside, could increase the thermal performance of the fuel cell.

System parameter

The analysis of the different set points for the studied operating parameters leads to following recommendations for an improved performance.

- A high ambient temperature, resulting in less transmission losses, Q_{surr} to the surroundings, Eq.(4.4).
- A low air ratio, resulting in low heat loss in the air overflow at the cathode.
- A high air temperature with high relative humidity, resulting in low heat loss in the air overflow.

As can be seen, all efficiency gains can be found in the limitation of heat losses. The largest potential can be found in reducing the transmission losses to the surroundings.
Another way to address this efficiency loss is by a higher rate of stack insulation. Compared to the others this parameter does not depend on control strategy but requires physical changes to the stack (or its direct environment).

Parameter	Step size	Working point	Output electrolyte temperature ΔT $^{\circ}C$	Electric Power ΔP W	$\frac{\Delta P}{P}$ %	Thermal Power ΔQ W	$\frac{\Delta Q}{Q}$ %
Air ratio	+1.5	$KOH 75^{\circ}C, 80A$	–1.1	-3.0	-0.06%	-485	-82%
		$KOH 30^{\circ}C, 80A$	-0.4	-1.0	-0.02%	-153	-3%
		$KOH 75^{\circ}C, 20A$	-0.9	-0.7	-0.02%	-379	-33%
		$KOH 30^{\circ}C, 20A$	-0.1	-0.1	0.00%	-49	-6%
Input air temperature	$+15^{\circ}C$	$KOH 75^{\circ}C, 80A$	0.2	0.6	0.01%	94	11%
		$KOH 30^{\circ}C, 80A$	0.2	0.5	0.01%	73	1%
		$KOH 75^{\circ}C, 20A$	0.1	0	0.00%	22	2%
		$KOH 30^{\circ}C, 20A$	0	0	0.00%	14	2%
Relative humidity of input air flow	+50%	$KOH 75^{\circ}C, 80A, Air 20^{\circ}C$	0.2	0.6	0.01%	95	13%
		$KOH 30^{\circ}C, 80A, Air 20^{\circ}C$	0.2	0.7	0.01%	104	2%
		$KOH 75^{\circ}C, 20A, Air 20^{\circ}C$	0.1	0.1	0.01%	61	-2%*
		$KOH 30^{\circ}C, 20A, Air 20^{\circ}C$	0.1	0.1	0.01%	55	7%
		$KOH 75^{\circ}C, 80A, Air 50^{\circ}C$	1.3	3.4	0.06%	547	57%
		$KOH 30^{\circ}C, 80A, Air 50^{\circ}C$	0.7	1.8	0.04%	297	5%
		$KOH 75^{\circ}C, 20A, Air 50^{\circ}C$	0.8	0.6	0.04%	349	-12%*
		$KOH 30^{\circ}C, 20A, Air 50^{\circ}C$	0.3	0.2	0.01%	113	13%

Table 4.4: Overview of the influence of the input air on output electrolyte temperature and electric and thermal power (the negative values here mean that there is not net heat production due to the high heat losses to the surroundings).*

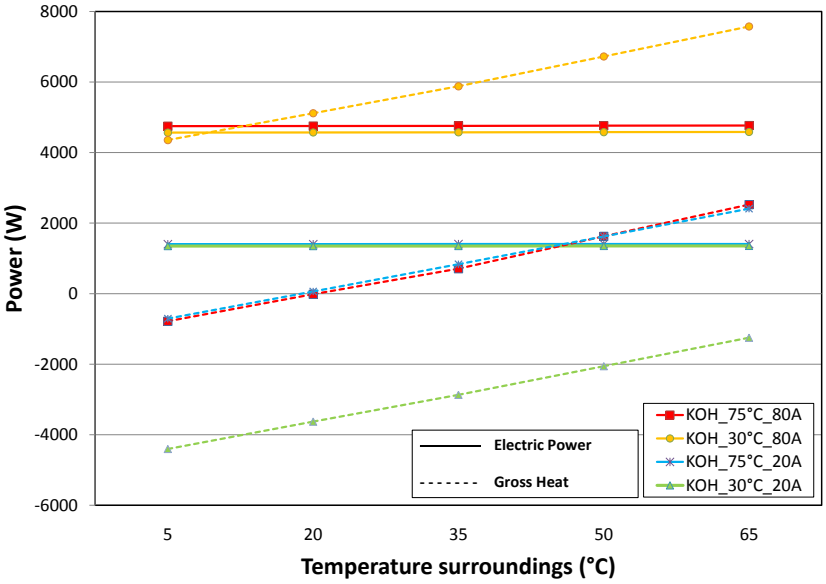

Figure 4.14: Influence of the ambient temperature on electrical and thermal power output.

4.3.2.4 Stack insulation thickness

Within system design, thickness of insulation could by an additional parameter to vary in order to optimize system integration. This will affect the system parameter hA_{surr}, which represents the overall conductance to the surroundings. For the used fuel cell this is set at $51.2 W/m^2K$, as discussed in Chapter 2.
The effect on electrolyte temperature is more pronounced at a high temperature difference between the electrolyte and the surroundings. For every temperature difference of $10°C$ the output electrolyte temperature will rise $1°C$ for a three times more insulated fuel cell system. The positive effect of insulation on electric power output is less than 0.3%. The influence of insulation on thermal power (shown in Figure 4.15) will result in higher relative primary energy savings (See Figure 4.16). As a result of an improved insulation, the ideal working point shifts towards lower currents. At higher average electrolyte temperatures the negative effect of the heat losses to the surroundings decreases with improved insulation.

4.3.3 Recommendations for system integration

Based on the analysis in this section, the following conclusions will be useful to take into account for an optimal design of a CHP-system based on alkaline fuel

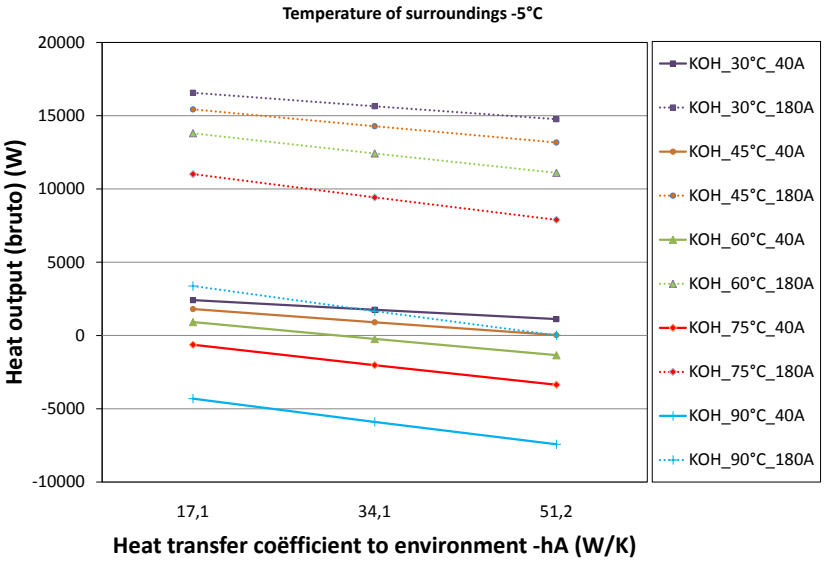

Figure 4.15: Influence of insulation on thermal power output.

cell technology.

Main results of the analysis

First a summary is given of the main results of the steady state analysis.

- To maintain the concentrations within the electrolyte, a minimum electrolyte temperature has to be reached (about $55°C$) to operate at low current.
- Higher currents will require higher input temperatures of the electrolyte to maintain the electrolyte concentration.
- The electrolyte temperature at a given current can be increased without dry out using hot humidified air.
- An air ratio higher than 2.5 is no more effective as a control parameter to maintain electrolyte concentration within the fuel cell.
- A higher electrolyte temperature has a positive effect on electrical power and efficiency, but results in a lower thermal efficiency. The size of this negative effect however depends on the heat recovery and total system integration and can be limited by a good design.

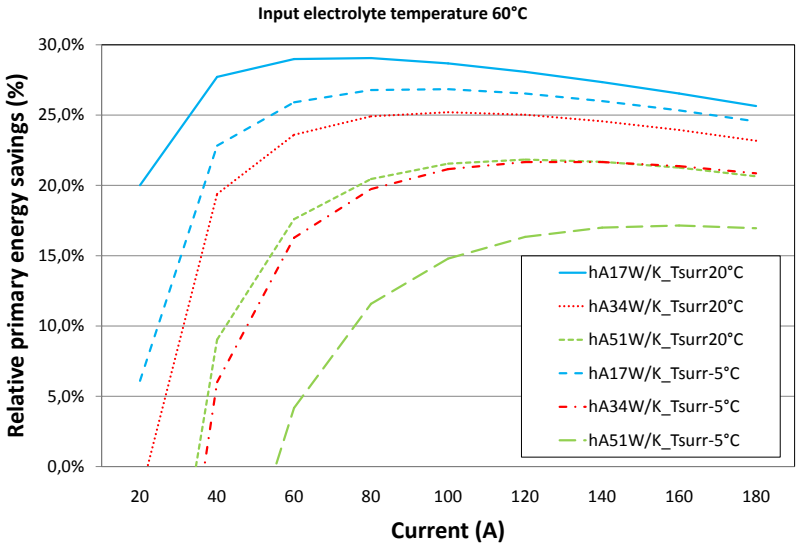

Figure 4.16: Relative primary energy savings compared to an average Belgian power plant as a function of current for different temperatures of the surroundings and different insulation levels.

- The current or load factor has an opposite effect on both efficiencies. At partial load or low currents the electrical efficiency rises, while the thermal efficiency drops.
- For an optimal use of the fuel cell as a micro-CHP it is shown that for every electrolyte temperature an optimal load or current drawn from the fuel cell can be found, based on primary energy savings.
- By increasing electrolyte temperature, the optimal working point (highest primary energy savings) shifts to higher currents to decrease the relative importance of the rising heat losses.
- A current higher than optimum however does not affect efficiency much, but a too small load can result in a significantly higher primary energy use.
- High air temperatures and wet air result in higher electrolyte output temperatures and higher thermal and electric powers. The combination of wet and hot input air is particularly interesting, because it results in a significant efficiency improvement and it allows an effective water management.

- A high air ratio has a negative effect on the thermal efficiency and should be set at a minimum.
- The electrolyte flow rate has no significant effect on performance only on temperature stability within the fuel cell.
- Reducing the heat losses to the surroundings proves to have the largest positive impact on the efficiency. This can be achieved by increasing the temperature of the surroundings or by insulating the fuel cell. Any improvement here will shift the optimum to a lower current.

System design

In every system an extra reservoir or vaporiser has to be foreseen to gain flexibility on the water management. High performance is possible at high electrolyte temperature, if high and wet air is used and if heat loss is limited.This will inmprove performance the most. Therefore, following system set-up in which the hot output air heats up the inlet air is an interesting possibility. If partial humidification is possible by mixing wet and fresh air, this would allow increasing temperature without dry-out of the fuel cell.
Indoor placement is also interesting in order to reduce heat loss to the surroundings, although other consequences as hydrogen leakage and the possible safety issues have to be taken into account.
With respect to control of the fuel cell, the recommendations regarding control parameters can be taken into account, but before implementing this it is also necessary to analyse stack dynamics and the response time of these possible actions.

4.4 Dynamic response

As the results of the analysis on the steady state model can be used to optimize system set-up and to define nominal operating conditions, this section documents the dynamic response of the stack to changes in operation. This analysis is useful to define future control strategies.

4.4.1 Description of the inlet variations

In order to get insight in the dynamic behaviour, four inlet variables were switched to a different value:

- The hydrogen flow rate is initially set at $0.072\,\frac{kmol}{h}$, which corresponds to a DC current of about $40\,A$. After running steady state for a while a load

switch is simulated, resulting in a hydrogen flow rate of $0.179\ \frac{kmol}{h}$, which corresponds to a DC current of about $100\ A$, representing nominal load.

- The electrolyte inlet temperature is initially set at $45°C$. After running steady state for a while a temperature switch is simulated, resulting in an inlet temperature of $60°C$.

- The air flow rate is initially set at $0.360\ \frac{kmol}{h}$, which corresponds to an air ratio of 2.5, compared to a hydrogen flow rate of $0.072\ \frac{kmol}{h}$. After running steady state for a while the flow rate is increased to $0.900\ \frac{kmol}{h}$. This could be achieved by a step regulated fan.

- The air inlet temperature is initially set at $20°C$, which corresponds to the ambient temperature in the simulation. After running steady state for a while a temperature switch is simulated, resulting in an inlet temperature of $50°C$. A sudden temperature switch could be the result of the start of an external pre heater of the air flow.

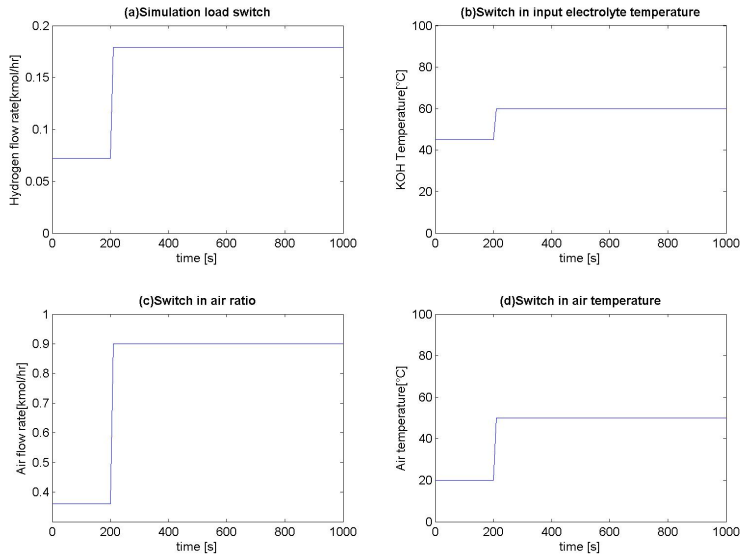

Figure 4.17: Overview of the different switches of the inlet variables, used to characterize dynamic behaviour.

In Figure 4.17 an overview is given of the inlet variables and how their values are changed in the simulation. In the simulations only one inlet variable is varied as illustrated in Figure 4.17. The other inlet variables are kept constant at the initial inlet state. Only when the hydrogen flow rate is altered, also the air flow rate is altered simultaneously. In this way the air ratio is kept constant.
For all simulations, the inlet value switch is initiated after 200 seconds. This waiting time is taken into account to ensure that no transient behaviour still occurs due to initialization of the model.
The step is no immediate step, as the inlet value is changed proportionally during 10 seconds to the new value. Therefore the new value is achieved after 210 seconds of simulation time. Once the new value is achieved, this is kept constant until the end of the simulation. The simulation ends after 1000 seconds.

4.4.2 Simulation results

In this section the influence of the value switch of the different (combinations of) inlet variables which are simulated is discussed. This analysis is based on the step response of the main output variables:

- Electric voltage
- Electrolyte output temperature
- Water management, based on net formation of liquid water in the electrolyte.
- Output air temperature

For each inlet variable, which is varied, their dynamic response is illustrated.

4.4.2.1 Dynamic behaviour to a load switch

As the hydrogen flow is dead-end in the the stack, a load switch from $40A$ to $100A$ total DC current, shown in Figure 4.17(a), can be simulated by changing hydrogen and air flow rate simultaneously. Figure 4.18 shows the dynamic step response of the outlet variables to these changes.
As shown in Figure 4.18 a response time of about $500s$ needs to considered, before a new steady state operation is obtained. The transient behaviour is most pronounced in the outlet electrolyte temperature, because here the thermal inertia of the stack influences directly the results.
The air temperature follows this evolution, but shows initially a quick response. It is possible this is due to the integration of the steady state Matlab-model into the dynamic Simulink model. However, with this in mind, air temperature follows the temperature evolution in the electrolyte.
Regarding net water production, initially there is an increase is noticed, due to the

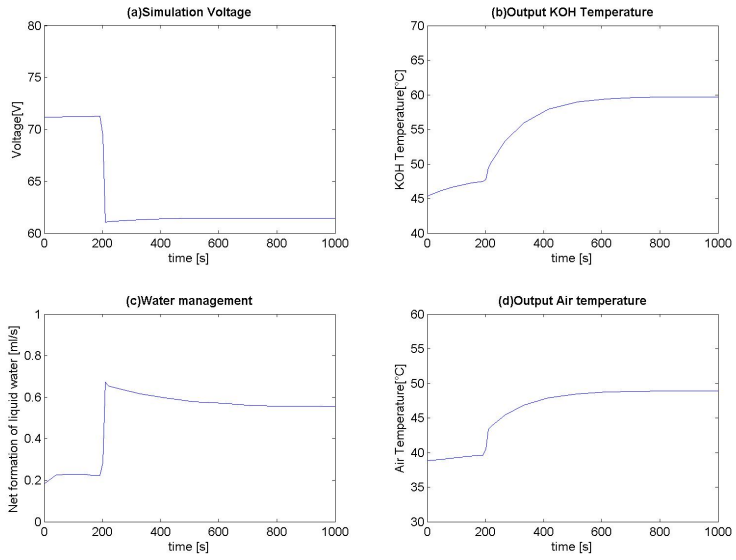

Figure 4.18: Overview of the dynamic response to a load switch (See Figure 4.17(a)), based on the main outlet variables.

increased current. With a slowly increasing electrolyte temperature, this net water production drops again.
A similar observation is accountable for the simulated voltage. The voltage shows an immediate response to the switch in current, after which it slowly increases a bit, due to the changing electrolyte and stack temperature.

4.4.2.2 Dynamic behaviour to a temperature switch in the electrolyte

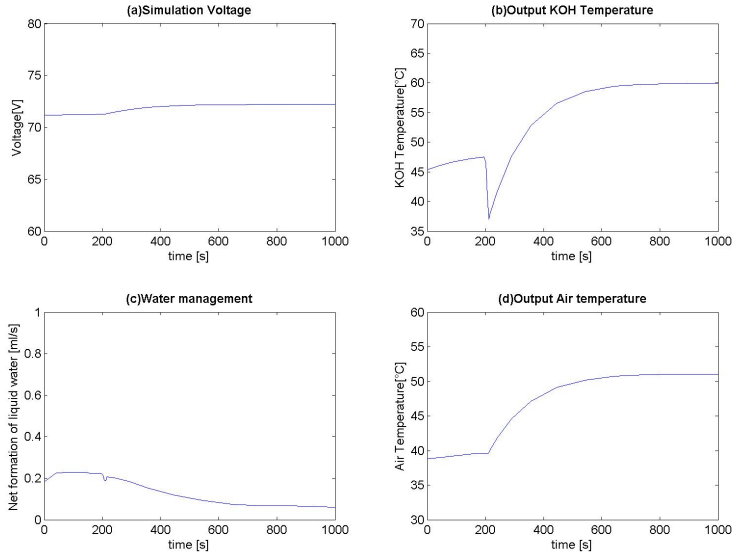

Figure 4.19: Overview of the dynamic response to an electrolyte temperature switch (See Figure 4.17(b)), based on the main outlet variables.

A possible way to control thermal and water management of the stack is to place an additional heater in the electrolyte circuit. In Figure 4.19 the response time is shown for the main output variables, including water management.
Initially the temperature increase results in a drop in output temperature for the electrolyte. This is possible due to the implementation of the model in Simulink and continuous and discontinuous calculation of the different heat transfers.
Besides this, the response time is similar to the load switch and about 500 to 600 seconds. The change in electrolyte inlet temperature will increase outlet temperature of the electrolyte, air temperature and voltage and decrease net water production.

4.4.2.3 Dynamic behaviour to a change of the air flow rate

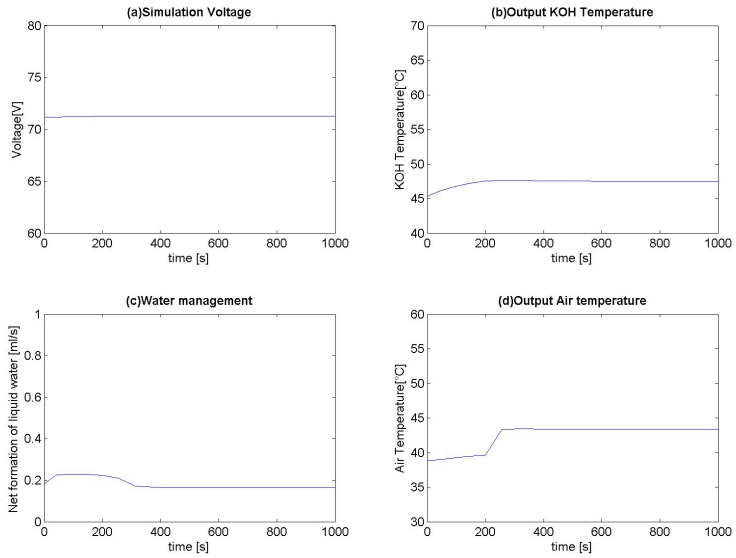

Figure 4.20: Overview of the dynamic response to a sudden increase in air rate switch (See Figure 4.17(c)), based on the main outlet variables.

Changing air flow rate is perhaps the most convenient way to control water management. However, since this has a cooling effect, this can even increase the problem. Figure 4.20 shows dynamic behaviour of the stack to changes in air rate. The air flow rate has a minor effect on voltage and electrolyte temperature. The initial rise in electrolyte is only due to the initialization of the stack, which is not yet completed in the simulation. After the step a negligible decrease in electrolyte temperature and even smaller decrease in voltage is observed.
The net water production reacts rather quickly to this new state and the transient behaviour fades out after 100s.
The air temperature increases, which is not expected at first. This is due to an increased heat and mass transfer, caused by a higher air velocity in the gas channels and higher amount of hot water vapour, which diffuses into the air flow.

4.4.2.4 Dynamic behaviour to a temperature switch in the air flow

Finally the possibility to place a heater in the external air circuit is discussed. Figure 4.21 shows dynamic behaviour of the stack to changes in air temperature.
As shown in the figures, only air temperature shows a significant reaction to this

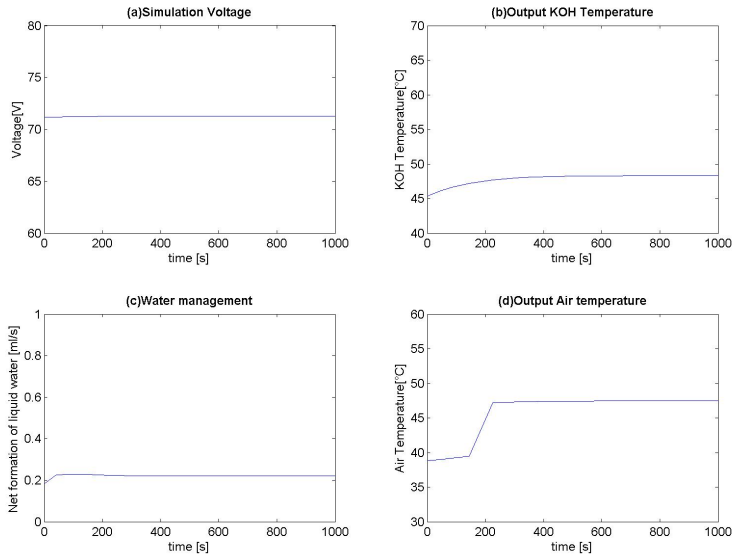

Figure 4.21: Overview of the dynamic response to an air temperature switch (See Figure 4.17(d)), based on the main outlet variables.

temperature switch, which is almost immediately.
However, it causes a slowly, almost negligibly rising electrolyte output temperature. The initial increase is due to initialization.
This rise is transposed to all other outlet variables, who all show a almost negligible increase or decrease. This effect is not ended yet after $1000s$, but despite this remark it can be accounted to be negligible.

4.4.3 Recommendations and considerations regarding control strategy

With respect to stack dynamics, transient behaviour shows to be limited to less than 10 minutes. It is expected this will influence system behaviour. This will be analysed in Chapter 6.
Based on the findings, following guidelines need to be taken into account with respect to an adequate control strategy.

- For changes in electrolyte inlet temperature or for load changes, the transient behaviour (about $500s$) has to be taken into account to avoid unstable behaviour.
- Increasing air flow rate to e.g. control the water management is less subordinate to transient behaviour. This makes air flow rate suitable to be used as a final tuning and control parameter for the water management in the stack.
- A changing air temperature has too little and too slow effect to be considered as a control parameter.

4.5 Closure

A thermal study is made on stack performance regarding micro-CHP-applications, based on steady state conditions. The summarized results in Section 4.3.3 are useful to take into account for an optimal design and improved control of a CHP-system based on alkaline fuel cell technology.
Next, also a brief dynamic analysis is elaborated, resulting in a number of additional guidelines to be considered within an adequate control strategy. These are summarized in Section 4.4.3.

The analyses in this chapter led to a number of recommendations and guidelines, which can be used to improve system design and control strategy. The translation of these recommendations to an effective integration of the AFC-stack within a micro-CHP system is discussed next, in Chapter 5.

5 Integration of an AFC-stack into a micro-CHP system

In Chapter 4 the behaviour of the stack is analysed regarding energy performance and water household. In Section 4.3.3 recommendations are formulated how to integrate a stack into a micro-CHP system.
In this chapter a description is given of a number of system configurations, in order to compare different set-ups and control strategies. The results of this comparison are presented in Chapter 6.

5.1 Multi-stack orientation and configurations

As multiple (sub)stacks can be integrated within a system, a first item which has to be considered is how the (sub)stacks are interconnected. The stack can be connected in parallel or serially for each fuel cell property:

- current
- electrolyte flow
- hydrogen flow
- air flow

Next to this variation the serial connections can be oriented in the same direction or counter wise. This means a large number of variations is possible.

5.1.1 Description of the inter stack connections

5.1.1.1 The circulating electrolyte and the electrical connection

An important problem with circulating electrolyte for alkaline fuel cell is the possibility of an internal or ionic short-circuit. Because the electrolyte flows through different cells within a stack, ionic conduction between cells within a stack can affect stack performance, enabling an internal short-circuit. [39] This problem can be addressed by connecting the cells electrically in series and in parallel to reduce internal voltages. To examine the effect of electrical alternative configurations, it is necessary to use a cell based model, with a prediction on ionic transport and internal current. This is not included in the stack model developed in Chapter 2, as it is beyond the scope of this work (See Section 1.6).
Therefore, the different ways to electrically connect the (sub)stacks to each other and its effect on performance is not evaluated nor taken into account to optimize stack configuration, within a CHP-system. The effect of the other properties, the different mass flows, is evaluated by a dimensional approach, discussed in the next section.

5.1.1.2 Orientation of the stack towards hydrogen, air and electrolyte flow

The stack orientation towards each mass flow can be different. This will have an effect on the thermal and water management of the stack.

Hydrogen flow

In the system used for validation (See Chapter 3), the different stacks are serially connected. This reduces piping and possible leaks and will facilitate purge and drain of condensate.
However, serially connecting stacks at the hydrogen side will cause a pressure drop. This pressure drop is not only due to dynamic pressure losses, but also due to the water vapour formed at the anode and diffused into the hydrogen flow. The decreased partial pressure of the hydrogen will only have a minor effect on performance, due to increased diffusion losses. The formation however of water droplets due to condensation of this water vapour can block hydrogen flow in one or more gas channels.
Especially at start-up or with a cool electrolyte this can be a problem and cause a voltage drop in the electrical output. A way to evaluate the possibility of this event is comparing the partial pressure of water vapour in the gas channels with the saturation pressure. As it is an end of pipe system, it is necessary to foresee a drain and/or to purge. A low chance on condensation will decrease purge frequency and improve overall efficiency.

Air flow

As the cold air passes through the stack, containing nitrogen next to an excess amount of oxygen, a serial connection of the stacks will cause lower thermal losses, compared to a parallel connection.
Nevertheless, the reaction kinetics and diffusion losses at the cathode, limit cell and stack capacity. For this reason the partial pressure drop of oxygen due to diffusion of oxygen into the previous stack and water vapour out of the previous stack also have to be considered in this evaluation.
Because of the pressure drop and the presence of water vapour in the (sub)stack outlet air flow, most systems have a parallel air flow, since thermal performance has never been a priority. However, for micro-CHP applications the expected advantage in thermal performance for a serial connection needs to be evaluated. Hereby, also its effect on water management is to taken into account, since in the present set-up water is ideally removed as vapour by the air flow.

Electrolyte flow

The stack(s) in the system used for validation are in parallel connected for the electrolyte flow. The main reason here is to deliver a sufficient pressure to ensure separation of both gas streams. Besides, it also reduces the possibility for an ionic short-circuit, which is discussed in Section 5.1.1.1.
Besides these reflections a serial connection of the stacks will increase electrolyte temperature, enabling higher electrical performances.

A comparison of performance between different configurations allows finding an optimal orientation and set-up of for the (sub)stacks.

5.1.2 Model adaptations to evaluate different stack orientation and configuration

With the model developed in Chapter 2, it is possible to evaluate general performance, thermal behaviour and water household of different stack orientations and connections.

5.1.2.1 Application domain of the results

However, not all aspects discussed in Section 5.1.1.2 can be simulated with the current model. The dynamic pressure losses, gravitational influence and the ionic short circuit cannot be evaluated with the model. Therefore, these limitations have to be taken into account, before conclusions are made based on the model results. These results will be summarized in Chapter 6. In this section the necessary

model adaptations are described. With these adaptations the model can be used to evaluate stack orientation and configuration.

5.1.2.2 Integration of the model within different inter stack orientations

In Figures 5.1, 5.2 and 5.3 it is shown how the stack model, presented in Figure 2.2, can be used to get differently orientated stack connections. In this way several stack configurations or stack-to-stack connections can be compared.
In Figure 5.1(a) it is shown how the anode gas chambers (AGC) of each stack model are all serially connected. This means the stacks are serially connected regarding the hydrogen flow. For the same figure also the fuel cell body (FCB) of each stack model and the cathode gas chamber (CGC) of each stack model is serially connected to the FCB, respectively CGC of the next stack model. This means also electrolyte flow, respectively air flow runs serially through the different (sub)stacks.
In Figure 5.1(b), the stacks are serially connected for all three flows. Compared to the stack configuration in Figure 5.1(a), the direction of air flow, represented by a serial connection of CGCs, is opposite to the hydrogen and electrolyte flow, which are represented by a serial connection of AGCs and FCBs. In Figure 5.2(a), the hydrogen flow is opposite to the other flows.
Figures 5.2(b) and 5.3 are different to the others, because in these configurations the electrolyte flow is in parallel connected to all stack models. For Figure 5.3 also the air flow is parallel connected, while in Figure 5.2(b) the gas flows are connected serially and oppositely to each other.
Figure 5.3 represents the present set-up, in which four stacks are connected in parallel regarding electrolyte and air flow. The hydrogen flow runs serially through the stacks. The direction how the hydrogen flows through these stack can be alternated in the present set-up. However this alternating direction has no influence on the steady state model, because at steady state these two configurations are completely similar. Its only goal is to remove water droplets during purge.
Next to the four discussed examples shown in Figures 5.1 and 5.2 a large number of configurations is possible. Table 5.1 gives an overview of all possible configurations.
Fuel cell body (FCB), anode (AGC) and cathode gas chamber (CGC) can be either parallel (P or ≡), serially upwards (u or ↑) or serially downwards (d or ↓) connected. In this way 13 different configurations are possible. It has to be taken into account that always one flow needs to be used as a reference to orientate the others, since a uuu-configuration is in fact the same as a ddd-configuration.

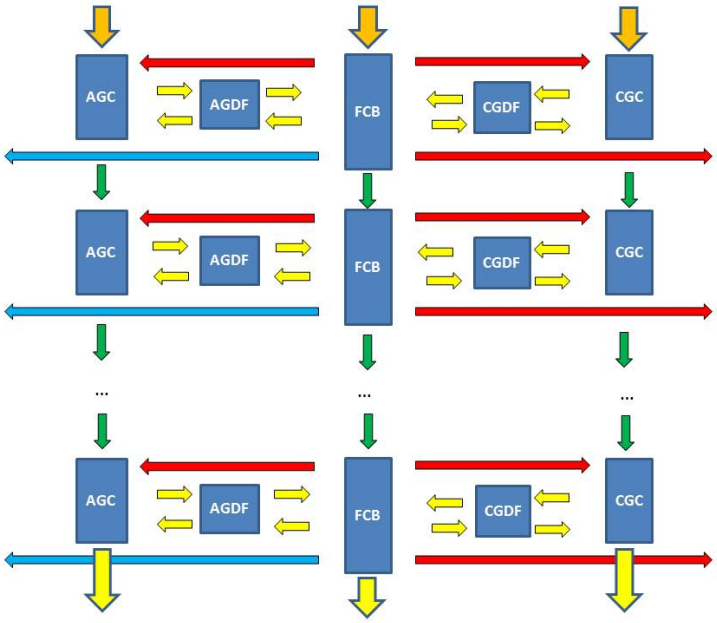

(a) ddd-configuration

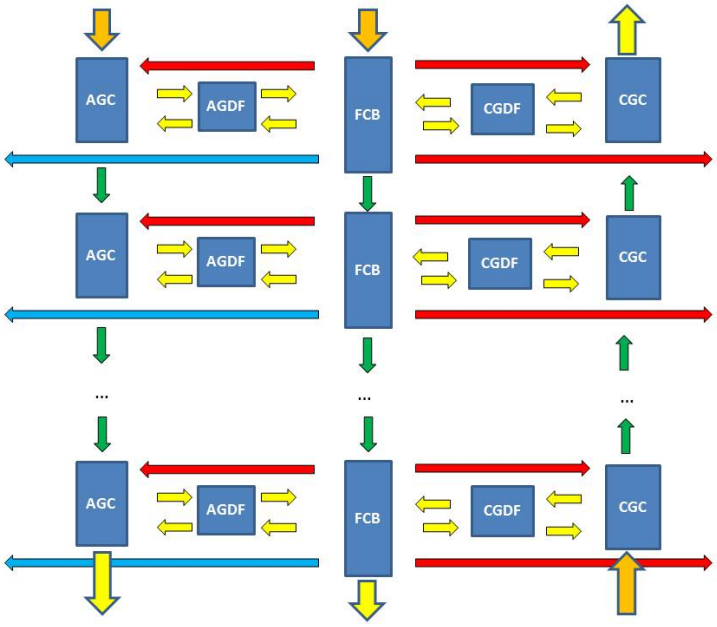

(b) ddu-configuration

Figure 5.1: Number of possible stack-to-stack - configurations with the presented model: a) hydrogen, air and electrolyte flow run in the same direction through (sub)stacks b) the air flow runs counter wise trough the (sub)stacks, compared to the electrolyte and hydrogen flow.

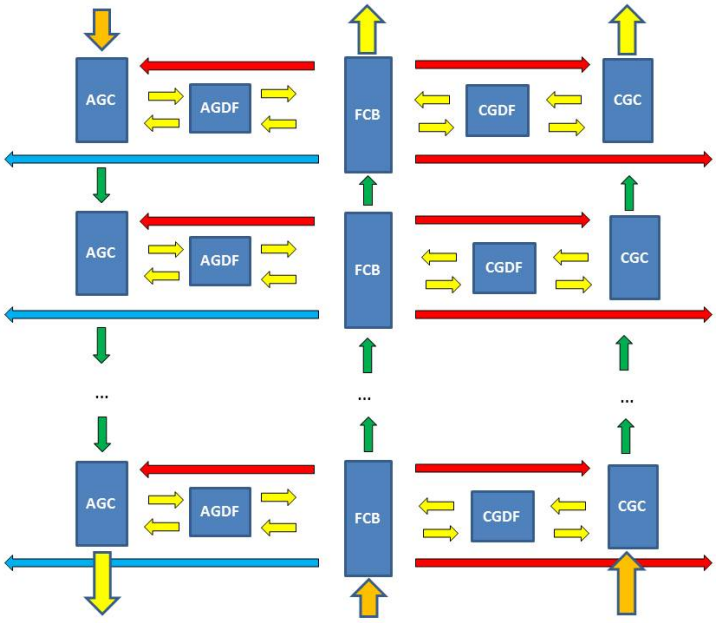

(a) duu-configuration

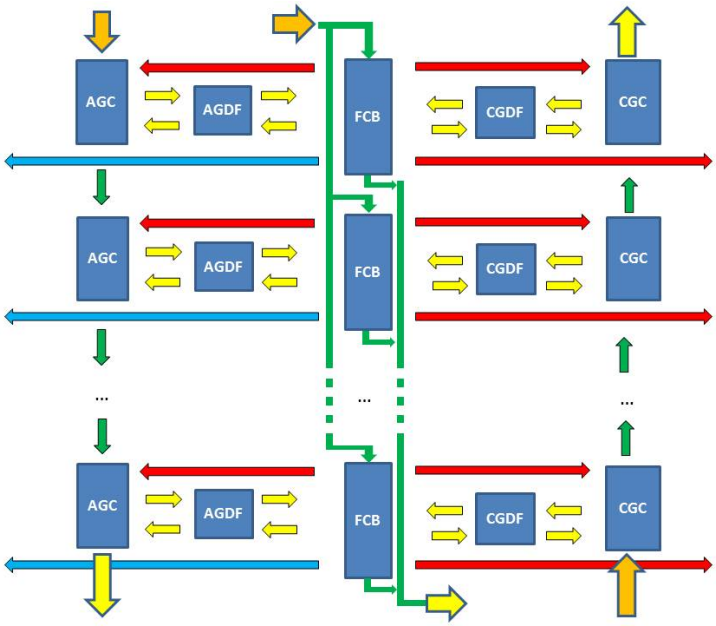

(b) dPu-configuration

Figure 5.2: Number of possible stack-to-stack - configurations with the presented model:a) the air flow flows counter wise trough the (sub)stacks, compared to the electrolyte and hydrogen flow b) the electrolyte flow runs parallel over all (sub)stacks, while hydrogen and air flow run counter wise.

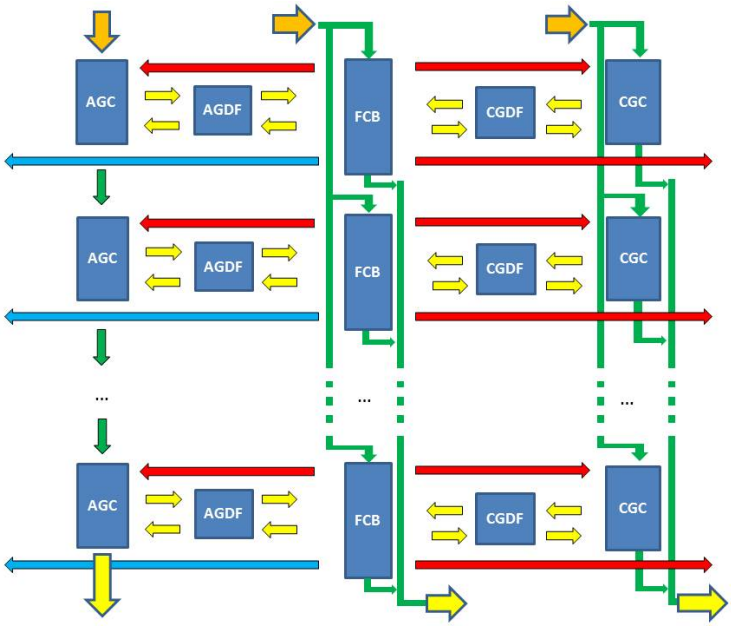

Figure 5.3: The original stack-to-stack - configuration for the present set-up (See Chapter 3). The present set-up has 4 stacks. These are parallel connected for both the air and electrolyte flow. The hydrogen passes serially through the stacks.

Configuration	AGC H_2-flow	FCB KOH-flow	CGC Air-flow	Reference
ddd	↓	↓	↓	Hydrogen flow (Figure 5.1(a))
ddu	↓	↓	↑	Hydrogen flow (Figure 5.1(b))
duu	↓	↑	↑	Hydrogen flow (Figure 5.2(a))
dud	↓	↑	↓	Hydrogen flow
dPd	↓	≡	↓	Hydrogen flow
dPu	↓	↓	↑	Hydrogen flow (Figure 5.2(b))
dPP	↓	≡	≡	Hydrogen flow (Figure 5.3)
ddP	↓	↓	≡	Hydrogen flow
duP	↓	↑	≡	Hydrogen flow
Pdd	≡	↓	↓	Electrolyte flow
Pdu	≡	↓	↑	Electrolyte flow
PdP	≡	↓	≡	Electrolyte flow
PPd	≡	≡	↓	Air flow
PPP	≡	≡	≡	similar to 1D approach

Table 5.1: Overview of different (sub)stack configurations, with reference flow always downwards. (≡ stands for a parallel connection of the sub models. ↑ represents a serially upwards connection and ↓ a serially downwards connection.)

5.1.2.3 Additional equations - boundary conditions

To make a comparison between the model application at (sub)stack level, with n sub models and the one dimensional use, and the model used at multi-stack level by a single model, following assumptions need to be used.

- For the serially connected sub models the output of one model will be used as an input for the next, which is defined by the downward or upward configuration. As mentioned in Section 2.3.3.2 a boundary condition is introduced, defining no hydrogen will leave the last gas chamber. This assumption has to be taken into account in the last AGC sub model.

- For a parallel connection of the sub models, the total flow rate, either hydrogen, air or electrolyte, needs to be divided by the number of sub models (n). In Eq.(5.1), this is illustrated for the input hydrogen flow in the i-th sub model within a parallel connected AGC - configuration. The result has to be summed to get the total output flow, as shown in Eq.(5.2)

$$F_{A,i} = \frac{F_A}{n} \tag{5.1}$$

$$F_B = \sum_{j=1}^{n} F_{B,j} \tag{5.2}$$

- The number of cells (electrically in serial or in parallel) will also be smaller since the number of cells in the (sub)stack should be used now. This will influence the voltage and current of the (sub)stack.

All these modifications are logical. They will not affect the basic assumptions and equations of the model developed in Chapter 2.

5.1.2.4 Influence on model (parameters)

Next to these influences on molar balance, also some model parameters will have to be adjusted to obtain the right results.

- Since parameter c_5, Eq.(2.7), depends on total contact area between the fuel cell body and the gas chamber. The equivalent parameter at single stack level, $c_{5,i}$, should be c_5 divided by the number of sub models (n).

$$c_{5,i} = \frac{c_5}{n} \tag{5.3}$$

- The heat loss to the surroundings is also parallel divided, which means that to calculate the total heat loss (See Eq.2.46) the sub losses should be summed (Eq.5.4).

$$Q_{FCB,surr} = \sum_{j=1}^{n} Q_{FCB,j} \tag{5.4}$$

$$hA_{FCB,surr} = \sum_{j=1}^{n} hA_{FCB,j} \tag{5.5}$$

  Next to this, similar to the remark on c_5 the surface responsible for the losses has to be distributed over the different sub models. This distribution, however, does not have to be proportional. This will depend on sub stack configuration, as neighbouring sub stacks will have a smaller contact surface with the surroundings than sub-stacks at the end or at the beginning of a stack. The general equation presented in Eq.(5.5) is always applicable.

With the model approach, discussed in this section it is possible to evaluate different stack connections, regarding performance and thermal and water management.
Since this chapter has the intention to describe the model set-up to evaluate stack integration in a system, the simulation results will be discussed in Chapter 6.

5.2 Complete system set-up for an AFC-based micro-CHP

In Section 5.1 the different ways to connect stacks to each other are discussed. A simulation approach is developed in order to evaluate the mutual interaction

between stacks, regarding general performance and stack integration. Next to this, also the impact of the stack to the other components and vice versa within a fuel cell based micro-CHP is to be investigated to improve system performance.
Therefore the stack-model developed in Chapter 2 is integrated in several CHP-system set-ups. This will enable a comparison with separated electricity and heat production and allows evaluation of possible improvements in system design and control strategy.

5.2.1 A general system approach

Before these set-ups are discussed, first a general system approach is discussed, including some general points of interest, based on the stack analysis in Chapter 4.

5.2.1.1 Description of an AFC based CHP-system

In Figure 5.4 an overview is presented of all necessary components for an AFC-based CHP-system.

- *Fuel cell,* represents the fuel cell stack, modelled and described in Chapter 2. The input of the model is characterized by the air flow, electrolyte flow, hydrogen flow and temperature of the surroundings. The output of the model is represented by the output air flow, electrolyte flow, the generated electric DC-power and by the heat losses to the surroundings.
- *Inverter,* translates the DC-power to AC-power, enabling the auxiliaries and the electric load. The inverter is only characterized by its efficiency, $\eta_{inverter}$.
- *Air circuit,* includes all components, handling the air flow which is necessary to deliver oxygen to the fuel cell. This includes heat exchanger(s), air treatment (e.g. CO_2-scrubber,...) and fan(s), depending on system configuration.
- *Electrolyte circuit,* represents the components, taking care of the electrolyte within the system. Depending on system configuration this includes electrolyte pump, electrolyte tank and heat exchanger(s).
- *Heat exchanger,* stands for the heat exchanger(s), in which the heat is transferred to the external heating circuit. These heat exchanger(s) can be part of the air or electrolyte circuit, depending on system set-up.
- *Water management,* represents in the first place the control strategy, used to maintain the electrolyte level. Furthermore, it also includes some additional components, like dehumidifiers or an electric resistance for heating if necessary.

- *Extra,* collects all other components, which aren't part of the other labels, e.g. the safety and monitoring equipment. These are modelled to consume only some fixed auxiliary power.
- *Overall system design.* Next to these components the general set-up, can be different.
  - A better overall insulation.
  - The specific implementation and connection details how it is integrated with the external load, including additional heat exchangers.

  Depending on system concept this will affect the performance of the system set-up.

The actual implementation of these components, depends on the system design. The energy and mass flows into and out of the system are the same for all set-ups and comparable for other micro-CHP-technologies. This will enable an objective evaluation of its energetic performance. Next to performance also water management for the different system designs will be discussed. The basis for this comparison is explained in following subsections.

5.2.1.2 Point of interest to optimize stack integration

In Section 5.2.1.1 the general lay-out of an AFC-based CHP-system is given. The heart of this system is the fuel cell stack, in which the energy conversion takes place. A model of an AFC-stack is developed and validated, predicting next to performance also thermal output and water management (See Chapters 2 and 3). The model is used to gain insight in the water management and to understand the heat management and influences on the CHP-potential of the fuel cell stack (See Chapter 4).
As a general conclusion towards system design, the performance can be improved by reducing heat losses or by applying hot and wet air instead of cold and dry air at high electrolyte temperatures. For an optimal control it is found that for every working point an optimal combination of current and electrolyte temperature exists. Next to that, suggestions and boundaries are set to alter air ratio for water management.

Overview of modelled system set-ups

These insights were translated into a number of improved system set-ups.

- The original set-up. This set-up is used as reference, since it is realised and presented in Refs. [58, 59].
- A set-up with heat recovery in the air flows to reduce heat losses.

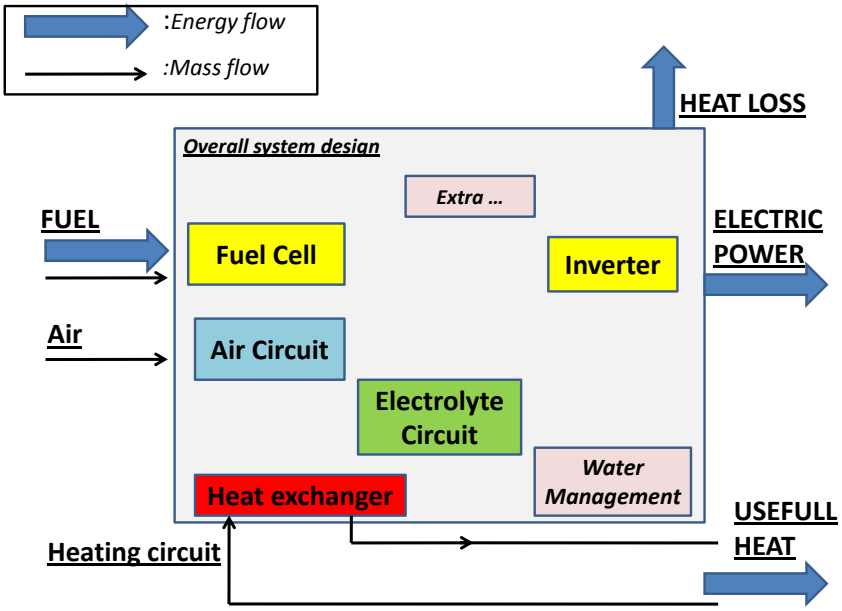

Figure 5.4: Overview of a general set-up for an AFC-based CHP-system.

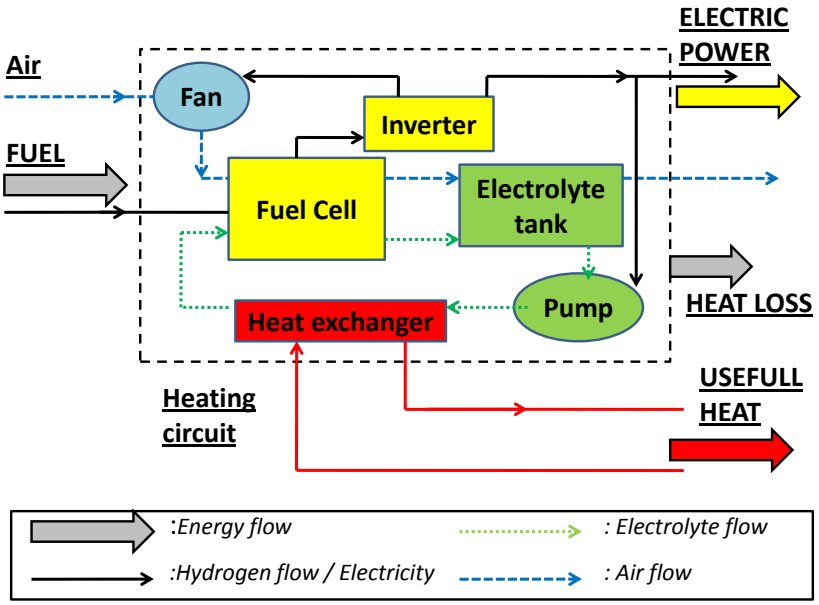

Figure 5.5: System set-up of original AFC-based CHP-system.

- A system set-up integrated in an insulated container to reduce heat losses and to humidify air input, allowing higher electrolyte temperatures.

These set-ups were modelled and simulated to evaluate performance and control strategy. The results of this evaluation are presented in Chapter 6. Here the different system models, used to perform this evaluation, are discussed.
This discussion includes a description of the components necessary to build up the model.

5.2.2 The original AFC-based CHP-system

5.2.2.1 Description of the original system

In [58] the first AFC-based system useful for CHP-applications was presented. In [59] a first system evaluation was performed based upon measurements. In Chapter 2 an alkaline fuel cell stack model was developed, which was validated with new measurements on the same system design (See Chapter 3). Therefore, this system design, shown in Figure 5.5, is taken as the present standard set-up.

The air flow is extracted by the fan out of the surroundings into the system, passing only an adsorptive CO_2-scrubber, and therefore has the same conditions

as the surroundings. The fan uses electric power to deliver sufficient air flow rate. The air flow and hydrogen flow (Fuel energy) enter the fuel cell stack, in which the oxygen out of the air flow reacts with the hydrogen to water, electric power and heat. An inverter converts the electric DC-power into AC-power.
Next to air and hydrogen, an electrolyte circuit is connected to the fuel cell stack, which ensures cooling and separation of the electrodes. The pressure and circulation of the electrolyte is delivered by an electric pump. The reaction heat results in a temperature rise of the electrolyte, in which part of the water is evacuated. The rest of the water is removed as water vapour in the overflow of the air stream. Both electrolyte and air flow are directed into the electrolyte tank, which has the purpose to evaporate the water out of the electrolyte into the air flow to ensure a constant electrolyte concentration. The air flow is ejected into the environment. The electrolyte is cooled to heat up an external heating circuit, after which it is redirected into the fuel cell stack.
Next to electricity ($P_{e,system}$) and heat to the heating circuit (Q_{useful}), there are still some energy losses to the environment by conversion losses (in the inverter ($\eta_{inverter}$), fuel handling (η_{purge}, ...), by energy use of the auxiliary components ($P_{e,aux}$), by radiation losses to the surroundings (Q_{loss}) and by waste heat in the air flow (Q_{air}).

5.2.2.2 Model of the components

Fuel cell stack
The complete stack model developed in Chapter 2 is used in this system model. As input both air, hydrogen and electrolyte flow and surrounding temperature are used to predict the thermodynamics and water management of the output air, hydrogen and electrolyte flow and the generated electric DC-power ($P_{e,FC}$) and heat loss to the surroundings (Q_{surr}).

Electrolyte tank
As described in Section 3.2.2.2 the electrolyte tank is modelled as a function of the following parameters:

- electrolyte temperature
- electrolyte flow
- air flow
- air temperature
- relative humidity of air
- percentage of evaporation: 0 means no evaporation - 100 means that the air is completely saturated

This last parameter is a fitting parameter, $c_{evaporation,tank}$, listed in Table 5.2. Since it is reasonable that the KOH tank has an influence, but complete saturation will not be reached, the parameter will be higher than 0 and lower than 100%. This depends on the lay-out of the electrolyte tank. For the present set-up, a best fit could be found at about 40%. If another lay-out will be used enabling more contact surface between air flow and electrolyte, this evaporation rate can be increased. This will be simulated in the system evaluation. The model predicts the thermodynamics and water management of the output flows. The model equations are based upon a heat balance, Eq. (5.6): the heat required for evaporation, Q_{vap}, Eq. (5.9), and the heat delivered by cooling of both mass flows, Q_{KOH} and Q_{air}, Eqs. (5.8) and (5.7). These mass and energy flows are illustrated in Figure 5.6.

$$Q_{vap} = Q_{air} + Q_{KOH} \tag{5.6}$$

$$Q_{air} = \dot{m_{air,in}} \cdot c_{air,in} \cdot (T_{air,in} - T_{air,out}) \tag{5.7}$$

$$Q_{KOH} = \dot{m_{KOH,out}} \cdot c_{KOH,out} \cdot (T_{KOH,in} - T_{KOH,out}) \tag{5.8}$$

$$Q_{vap} = \dot{m_{vap}} \cdot (h_s\,(T_{air,out}) - h_w\,(T_{KOH,in})) \tag{5.9}$$

If the electrolyte tank would be infinitely large, the electrolyte and air flow will come out at the same temperature ($T_{balance}$) as a result of the the zeroth law of thermodynamics. Next to this, the output air flow would be completely saturated, which means a maximum amount of water will be evaporated out of the electrolyte flow into the air flow. The heat required for this net evaporation will be delivered by cooling the air flow and/or electrolyte flow. This possibility corresponds to an evaporation rate of 100%. In the model, the evaporation rate is defined as

- the actual heat exchange for evaporation in relation to the heat exchange in an infinitely large electrolyte tank.
- the temperature change of the electrolyte flow in relation to the temperature change in an infinitely large electrolyte tank.

These assumptions allow a unique solution for all modelled output parameters (electrolyte temperature, electrolyte flow rate, air temperature, air flow rate and air humidity rate).

Heat exchanger

There are several ways to model a heat exchanger: based on temperature difference, on heat transfer coefficient or on effectiveness, ϵ_{HE} [91]. These last two methods are used to integrate the heat exchanger in our system:

- based on effectiveness, ϵ_{HE}
- based on heat transfer coefficient, hA_{HX}

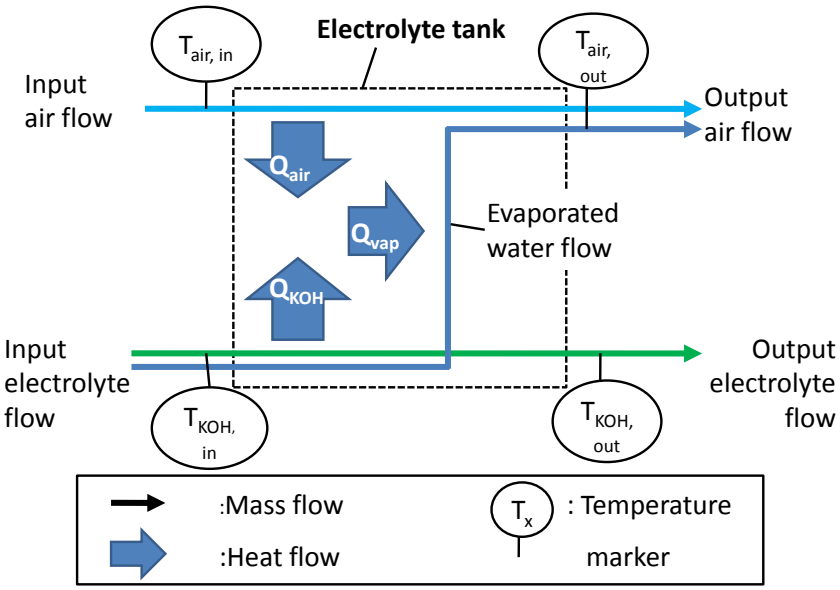

Figure 5.6: Heat balance within the electrolyte tank.

The method based on effectiveness has the advantage of being easily applied and allows straight forward computing. Besides, it is valid for every type of heat exchanger. For this reason this method is used to model the heat exchanger in our system model. It is based on following equations.

$$Q_{HE} = C_H \cdot (T_{H,in} - T_{H,out}) \tag{5.10}$$

$$Q_{HE} = C_C \cdot (T_{C,out} - T_{C,in}) \tag{5.11}$$

$$\Delta T_{max} = T_{H,in} - T_{C,in} \tag{5.12}$$

if $C_H < C_C$,

$$\epsilon_{HE} = \frac{T_{C,out} - T_{C,in}}{\Delta T_{max}} \tag{5.13}$$

else,

$$\epsilon_{HE} = \frac{T_{H,in} - T_{H,out}}{\Delta T_{max}} \tag{5.14}$$

In these equations,

- Q_{HE} represents the transferred heat
- C_i represents the total heat capacity of the flow i.
- subscripts i, j indicate flow (i), which can be cold (C) or hot (H), and flow direction (j).

For a water/water heat exchanger an effectiveness of 0.8 is a realistic average value. In the analysis other effectivenesses will be simulated. In these cases, it has to be taken into account that a higher effectiveness mostly results in higher pressure losses, resulting in more pump energy [91].

The drawback of using effectiveness to characterize a heat exchanger is that the actual size of the heat exchanger is not taken into account. Therefore, effectiveness cannot be used as characterization parameter for a heat exchanger, if the influence of different flow rates is to be investigated.
In a first approach fixed flow rates are assumed and effectiveness is used as a characterization parameter. However, if the flow rates of the electrolyte or from the external circuit are used as a control parameter, effectiveness is no longer used to model a heat exchanger. In that case the overall conductance of the heat exchanger, hA_{HX}, will be used to characterize the heat exchanger. To model heat transfer it is also necessary to define the heat exchanger typology. In our model the expression for a counter-flow heat exchanger is used to model the heat

exchanger. This behaviour in general is assumed to be representative for other types of heat exchanger.

$$T_{C,out} = \frac{T_{H,in} \cdot \left[C_H \cdot \left(1 - exp\left(\frac{hA_{HX}}{f}\right)\right)\right] + T_{C,in} \cdot [C_C - C_H]}{C_C - C_H \cdot exp\left(\frac{hA_{HX}}{f}\right)} \tag{5.15}$$

$$T_{H,out} = T_{H,in} - \frac{C_C \cdot [T_{C,out} - T_{C,in}]}{C_H} \tag{5.16}$$

$$f = \frac{C_C \cdot C_H}{C_H - C_C} \tag{5.17}$$

The value for the new model parameter, the heat transfer coefficient of the heat exchanger, is based on an effectiveness of 80% and the nominal flow rate of the external circuit, $1000\,l/h$.

(Electrolyte) pump

The pump model is only used to calculate the electric power, $P_{e,pump}$, needed to supply a sufficiently high electrolyte flow rate, $\dot{m}_{KOH}$. For the electrolyte pump an empiric equation is formulated to calculate mechanical pumping energy, P_{mech}, based on electrolyte flow rate, $\dot{m}$. This equation, Eq. (5.18), is based on flow and pressure measurements on the electrolyte pump in the system. An overall pump efficiency, η_{pump}, is introduced to complete the model. The average value for this efficiency is set at 50%, but can be altered in the model input to evaluate its effect on system performance.

$$P_{e,pump} = c_{pump,1} \cdot \dot{m}_{KOH}^3 + c_{pump,2} \cdot \dot{m}_{KOH} \tag{5.18}$$

$$P_{mech,pump} = \eta_{pump} \cdot P_{e,pump} \tag{5.19}$$

The parameters used in Eq.(5.18) are listed in Table 5.2.

CO_2-scrubber

In the scrubber the air is passed through a matrix of adsorption material resulting in a large pressure drop. This pressure drop will be balanced by the fan. In the scrubber CO_2 is removed form the inlet air. No temperature change is detected. Therefore, the scrubber is excluded from the system model. The pressure drop is taken into account in the fan model. The air is assumed to be free of CO_2.

(Air) fan

Similar to the pump model, the fan model calculates the consumed electric energy ,$P_{e,fan}$, based on the air flow rate, $\dot{m}_{air}$, and the overall efficiency, η_{fan}, according to an empirically determined equation, Eq. (5.20).

$$P_{e,fan} = c_{fan,1} \cdot \dot{m}_{air}^3 + c_{fan,2} \cdot \dot{m}_{air} \tag{5.20}$$

$$P_{mech,fan} = \eta_{fan} \cdot P_{e,fan} \tag{5.21}$$

For this fan the model parameters are based upon flow and pressure measurements on the fan integrated in the present system (See Table 5.2).

Model Parameters	Value	Unit
$c_{evaporation,tank}$	40	%
$c_{pump,1}$	0.014	$\frac{W \cdot min^3}{l^3}$
$c_{pump,2}$	4.886	$\frac{W \cdot min}{l}$
$c_{fan,1}$	4.1	$\frac{W \cdot s^3}{m^9}$
$c_{fan,2}$	678	$\frac{W \cdot s}{m^3}$

Table 5.2: List of model parameters for the original system

5.2.3 Improved system by integrating in a container

5.2.3.1 Description of container system

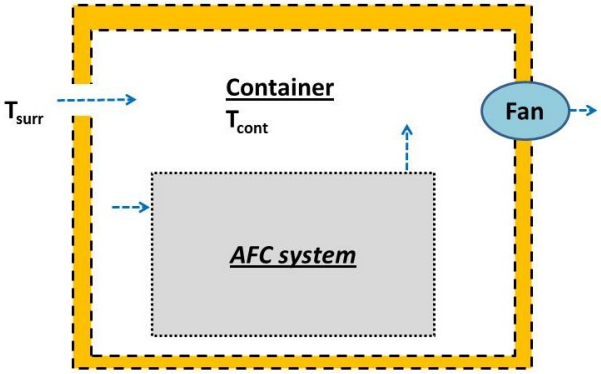

Figure 5.7: Container set-up: the integration of the AFC-system in a container, with indication of the air flows.

A first improvement on the system is made by integrating the system in a ventilated and insulated container (See Figure 5.7). In this way the surroundings of the original system will be set at a higher temperature and a higher humidity, due to the radiation losses and the air overflow, containing water vapour. This will result in better conditions of the input air flow and less heat loss of the system, because of the extra insulation layer. However, an extra fan will be necessary to supply enough fresh air, both for safety and for water management.

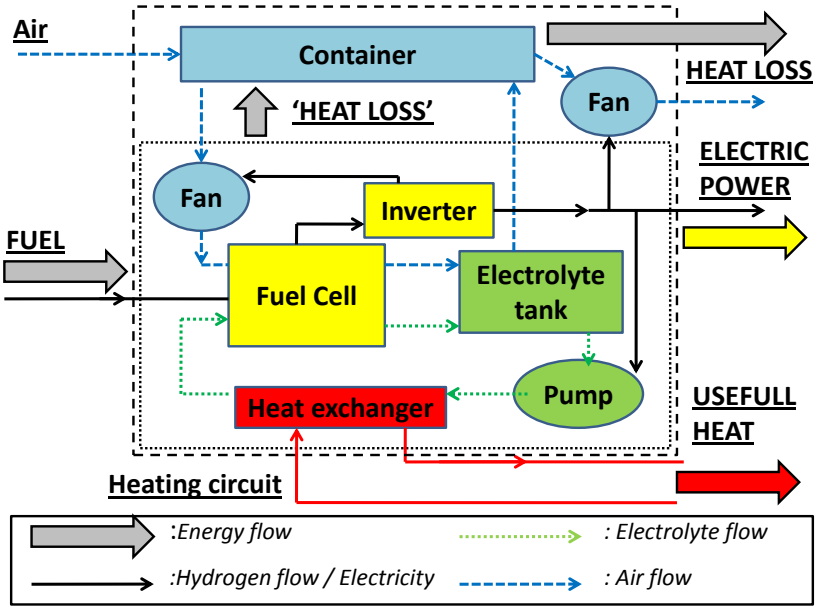

Figure 5.8: Model lay-out of the implementation of a container around the system.

5.2.3.2 Model of system

To model the integration of the system into the container, the lay-out of the original model is used, as can be seen in Figure 5.8. In comparison to the original model

- the air input and output flow passes through the container model.
- the heat losses from the fuel cell system, including radiation losses and internal parasitic load, are energy inputs for the container model.
- these radiation losses will be calculated based on air temperature within the container instead of the temperature of the surroundings.
- the heat loss to the surroundings is limited to the heat loss of the container to the surroundings.

A small description is given on the extra components of the new system:

- container
- extra fan

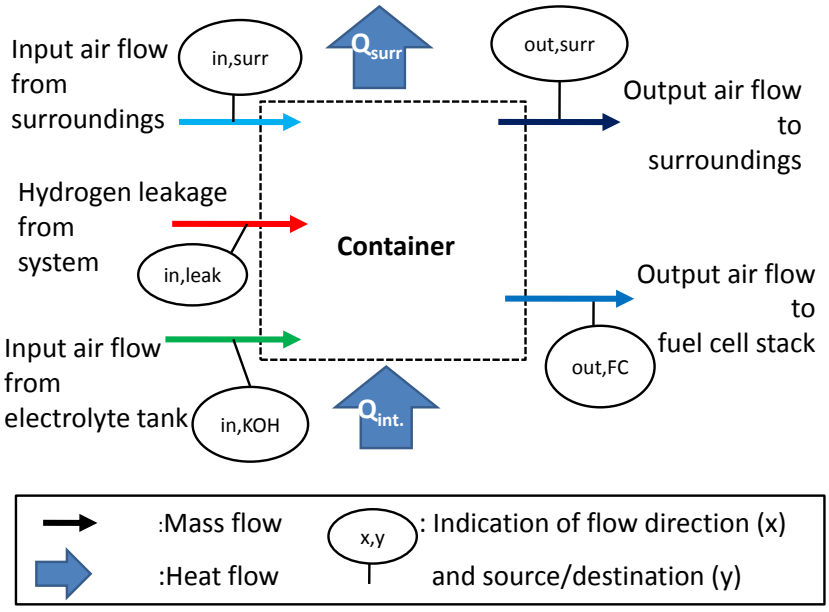

Figure 5.9: Overview of different air and energy flows in and out the container model.

Container

The container model is based on a mass and energy balance (See Figure 5.9). As input for the mass balance two air flows are fully given, namely the air leaving the electrolyte tank, $\left(\dot{M}, y_i\right)_{in,KOH}$, and the outdoor air entering the container, $\left(\dot{M}, y_i\right)_{in,surr}$. Next to these two mass flows, the air flow rate, $\dot{M}_{out,FC}$, which will be the input of the original system is given. To model safety also the possibility to include a hydrogen leak or hydrogen purge is included as input parameter, $\dot{M}_{in,Leak}$. Based on the input flows a typical composition of the air within the container can be modelled, $\left(\dot{M}, y_i\right)_{container}$. Both output air flows will have this composition, except for the hydrogen, which is modelled to leave the container only into the surroundings and not into the fuel cell system, Eqs.(5.25) and (5.26).

$$\dot{M}_{container} = \dot{M}_{in,surr} + \dot{M}_{in,KOH} + \dot{M}_{in,leak} \tag{5.22}$$

$$\dot{M}_{container} = \dot{M}_{out,surr} + \dot{M}_{out,FC} \tag{5.23}$$

$$\dot{M}_{container} \cdot y_{i,container} = \dot{M}_{in,surr} \cdot y_{i,in,surr} + \dot{M}_{in,KOH} \cdot y_{i,in,KOH} + \dot{M}_{in,leak} \cdot y_{i,in,leak} \tag{5.24}$$

$$y_{H_2,out,FC} = 0 \tag{5.25}$$

$$y_{j,out,FC} = \frac{y_{j,container}}{1 - y_{H_2,container}} \tag{5.26}$$

$$\dot{M}_{container} \cdot y_{i,container} = \dot{M}_{out,surr} \cdot y_{i,out,surr} + \dot{M}_{out,FC} \cdot y_{i,out,FC} \tag{5.27}$$

In this way the hydrogen is modelled to be mixed only in the exhaust air, which is realistic if the extra fan is built near the highest point within the container. This means the highest concentration is to be found in the exhaust air. Therefore, the hydrogen concentration of this air flow is to be taken into account to evaluate safety.

The energy balance is meant to calculate temperature of the air in the container. Next to the different input and output mass flows, mentioned above, the heat losses through the container walls and the internal heat load will be included. This internal heat load is based on the heat loss of the stack, Q_{system}, and parasitic load of the fuel cell based CHP-system, $P_{par.load}$.

$$Energy_{in} = \dot{M}_{in,surr} \cdot H_{in,surr} + \dot{M}_{in,KOH} \cdot H_{in,KOH} + Q_{int.} \tag{5.28}$$

$$Q_{int.} = Q_{system} + P_{par.load} \tag{5.29}$$

$$Q_{system} = hA_{FC}\left(T_{FC} - T_{container}\right) \tag{5.30}$$

$$Energy_{out} = \dot{M}_{out,surr} \cdot H_{out,surr} + \dot{M}_{out,FC} \cdot H_{out,FC} + Q_{loss,surr} \tag{5.31}$$

$$Q_{loss,surr} = hA_{cont} \cdot \left(T_{container} - T_{surr}\right) \tag{5.32}$$

$$Energy_{in} = Energy_{out} \tag{5.33}$$

Extra fan

Similar to the existing fan, discussed in Section 5.2.2.2, the fan model calculates

the consumed electric energy according to an empirically determined equation (Eq. (5.20)). However, for this fan the model parameters are different, because the pressure losses will be lower. The air flow now only passes the fan itself and a small opening in the container, while for the existing fan the air flow passes through the fuel cell stack, electrolyte tank and additional piping and measurement equipment. Measurements on the fan without connection to the system were used to determine the parameters for this extra fan (See Table 5.3).

Model Parameters	Value	Unit
$c_{fan,1}$	27.8	$\frac{W \cdot s^3}{m^9}$
$c_{fan,2}$	0	$\frac{W \cdot s}{m^3}$

Table 5.3: Model parameters for a fan with relatively small flow resistance.

5.2.4 Alternative system design with heat recovery on the output air flow

5.2.4.1 Description of the set-up

In Chapter 4 it is shown that the output air flow is responsible for a large amount of the thermal losses. Especially at higher currents and at higher electrolyte temperatures. Heat recovery from the output air flow is a possible solution to improve the energetic performance of the original set-up. As an increased input air temperature will have a positive effect on thermal and electrical performance, in this set-up an air/air heat exchanger is integrated in the system design to recover heat from the output air flow. This set-up can be compared to a heat recovery unit, often used in ventilation systems for buildings.

5.2.4.2 Description of the system model

Compared to the original model, described in Section 5.2.2.2, an additional fan is integrated in the system, next to the heat exchanger responsible for the heat recovery (See Figure 5.10).

Fan(s)
Compared to the original set-up, the fan(s) in this set-up has to conquer extra pressure losses in the air flow due to the passages in the air heat exchanger. Therefore, an extra fan is foreseen, resulting in a fan at the inlet and one at the outlet. The fan model, Eq. (5.20), discussed in Section 5.2.2.2, is used to calculate the consumed electric energy of both fans. However, different model parameters are used. The fan at the inlet, compensating for pressure losses in the first passage of the heat exchanger, the stack and tank inlet, is modelled with the same

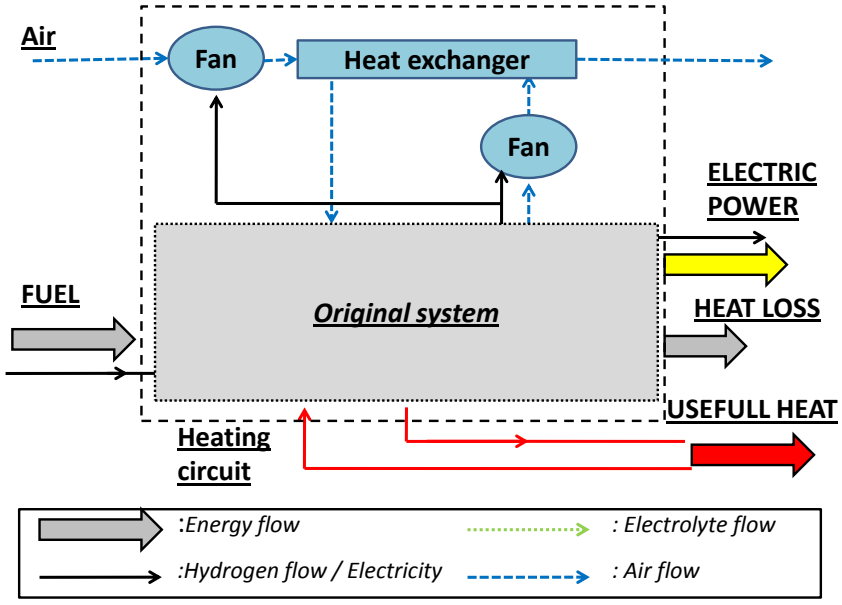

Figure 5.10: Model lay-out of the integration of an extra heat exchanger on the air flows.

parameters as in the original set-up (See Table 5.2). The extra fan, compensating for the pressure losses in the outlet of the tank and the second passage through the heat exchanger, is modelled similar to the outlet fan in the container set-up (See Table 5.3).

Heat exchanger
The same equations as for the heat exchanger in the electrolyte circuit, Eqs. (5.10), (5.11), (5.13) and (5.14), can be used to describe the air heat exchanger. Also for air heat exchangers, an effectiveness of 0.8 is a realistic value.

5.3 Different control strategies in AFC-based micro-CHPs

The implementation of control strategies also has to be evaluated with respect to system dynamics. Similar to the fuel cell model, the dynamics of the system are discussed separately. To evaluate dynamics, the dynamics of the original system, discussed in Section 5.2.2, are examined.

5.3.1 Description of system dynamics

Next to the dynamics of the stack, discussed in Chapters 2 and 4, the periphery of the stack has its own dynamics.

Electrolyte tank

In the steady state approach of the electrolyte tank only the evaporative effect of the air flowing over the water surface is taken into account in the model. Therefore, it is assumed the level of the electrolyte tank remains the same. However, an unstable water management will result in a rising or decreasing electrolyte level. As this will increase or decrease thermal inertia of the electrolyte, this will also affect the evaporation in the tank.

Heat exchanger

The heat exchanger in the system, discussed in Chapter 3, is a spiral in the tank. In a steady state approach the tank dynamics were neglected, which led to a direct integration of the heat exchanger in the electrolyte flow. As the dynamic evaluation of the tank takes into account tank dynamics, these tank dynamics cannot be ignored.
This will result in a different modelling approach, to be worked out in next section. The thermal inertia of the heat exchanger itself however is ignored, as its thermal mass is very low in relation to its heat exchanging surface.

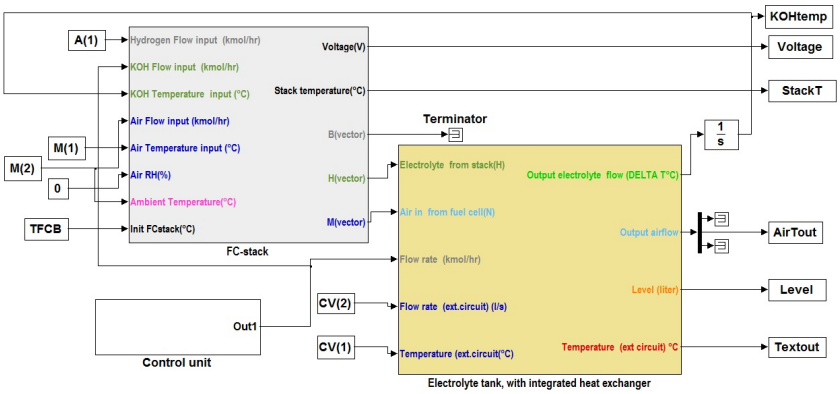

Figure 5.11: Implementation of the AFC-based micro-CHP system into the Simulink environment

Piping and other components

If flow rate changes at the end of the stack this effect occurs a little bit later at the inlet of the tank or heat exchanger and vice versa, due to piping length. These delays however are ignored as the pipe lengths and fluctuations in flow rate are limited.

5.3.2 Development of a dynamic system model

Figure 5.11 presents an overview of the complete system. The state of the stack model, developed in Chapter 2, is determined by the hydrogen, electrolyte and air flow. The hydrogen flow rate and air flow, which are characterized by temperature, humidity and flow rate are determined by a control unit. They depend on system set points and control strategy.
The electrolyte flow rate can be altered by the control unit, but its temperature is determined by the heat and mass transfer in the electrolyte tank.

Electrolyte tank model

The electrolyte tank model is an assembly of the evaporation effect in the steady state model (See Section 5.2.2.2), the heat exchanger model (See Section 5.2.2.2) and the dynamics of a buffer tank with different in- and outlets.
Figure 5.12 presents an overview of the different mass and temperature flows in the assembled tank model.
The electrolyte flows from the stack into the buffer tank at a flow rate, ϕ_{in}, and temperature, T_{in}, which is determined by the stack (model).

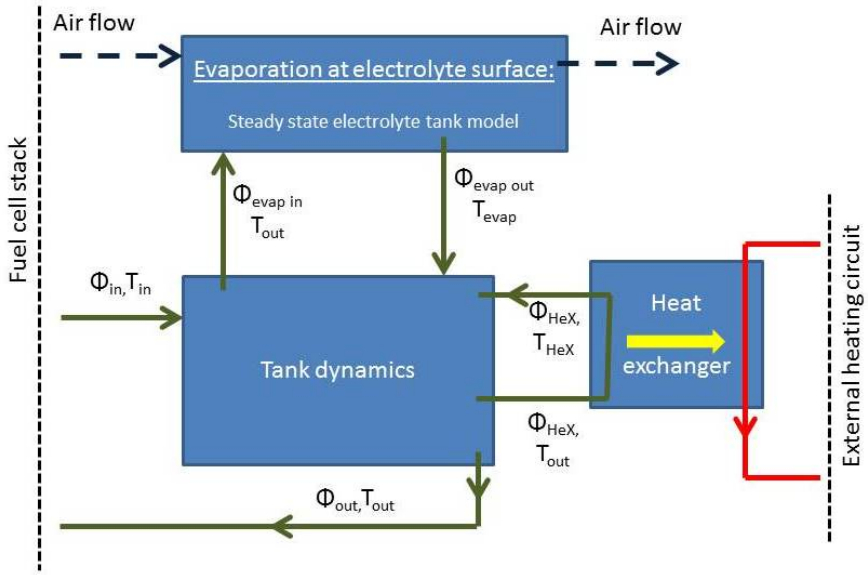

Figure 5.12: Indication of flow rates and temperature for the assembled tank model. The model exists out of three parts: a vessel, describing tank dynamics (evolution of content and temperature in the tank), the evaporation surface, describing the evaporative effect of the air flowing through the tank, and a heat exchanger, describing the heat transfer to an external circuit.

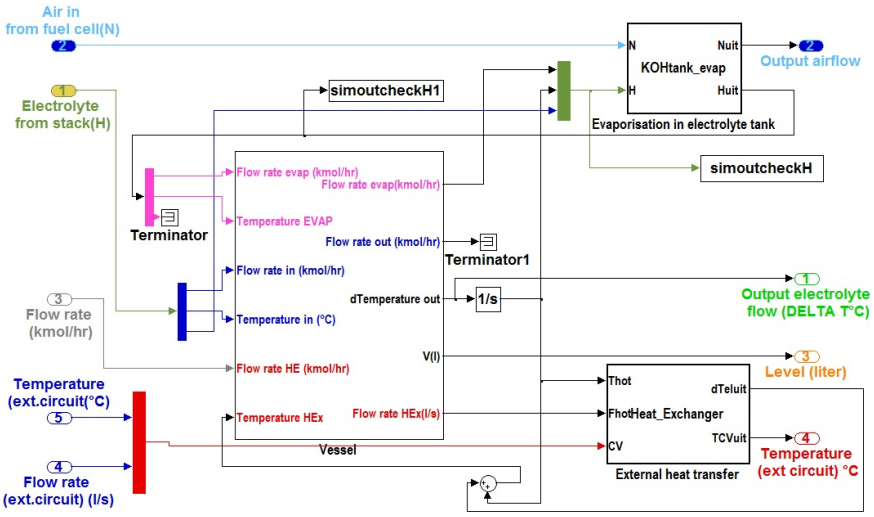

Figure 5.13: Implementation of the tank model into the Simulink environment.

The upper part of the model represents the tank evaporation and is discussed in Section 5.2.2.2 and shown in Figure 5.6. Important for the thermodynamics is that the evaporation will change both flow rate, from $\phi_{evap\,in}$ into $\phi_{evap\,out}$, and temperature from T_{out} into T_{evap}.
Similar to the evaporative effect, the heat exchanger has no (new) dynamic elements. The heat exchanger will only affect temperature, from T_{out} into T_{HeX}, and has no influence on flow rate, ϕ_{HeX} .
The only dynamic element is in fact the buffer tank shown in Figure 5.12, which has a changing amount of electrolyte, V_{level}. Within the model the output flows all have the tank temperature, T_{out}, based on the energy balance in the tank, Eq.(5.36). The tank level is determined by the mass balance, Eq.(5.34). To complete the description, flow rate, ϕ_{out}, represents the electrolyte flow which is fed to the stack.

$$\frac{d(V_{level})}{dt} = \phi_{in} + \phi_{evap\,out} - \phi_{evap\,in} + \phi_{out} \tag{5.34}$$

$$c_p \cdot V_{level} \cdot \frac{d(T_{out})}{dt} = c_p \cdot \sum \pm\phi_x \cdot T_x \tag{5.35}$$

$$\begin{aligned} V_{level} \cdot \frac{d(T_{out})}{dt} &= \phi_{in} \cdot T_{in} + \phi_{evap\,out} \cdot T_{evap} + \phi_{HeX} \cdot T_{Hex} \\ &\quad - \left(\phi_{evap\,in} + \phi_{HeX} + \phi_{out}\right) \cdot T_{out} \end{aligned} \tag{5.36}$$

This model is translated into the Simulink environment as shown in Figure 5.13.

5.3.3 Implementation of a control strategy

The control unit shown in Figure 5.11 is meant to set the input and control parameters based on values which can be measured and used as input for the control unit. In general the parameters, listed in Table 5.4, can be adjusted by the control unit. The measurements which can be used as input are shown in Table 5.5.
The goal of every control strategy is to maintain water management and deliver demanded electricity and heat. Different strategies can be thought of, which can be compared to find the best strategy.

Model Parameters	Range	Unit
Air flow rate	$0.2 - 1$	$kmol/h$
Flow rate ext.circuit	$0 - 1$	l/s
'Electric load'	$0 - 140$	A(DC)

Table 5.4: List of control parameters for the original system

Model Parameters	Unit
$T_{air,in}$	$^{\circ}C$
V_{level}	l
T_{out}	$^{\circ}C$
$T_{ext.,HeX,in}$	$^{\circ}C$

Table 5.5: List of possible input measurements for the control unit

Reference control strategy

In the present set-up, the AFC-system follows electric load. As a start-up strategy no heat is consumed until nominal electrolyte temperature, $60^{\circ}C$ is reached. During operation, the measurement on the tank level induces an increased air ratio if the level exceeds a certain limit.
As electrolyte temperature is getting too high and the level decreases, the external thermal load/cooling is increased manually if possible. Otherwise load is minimized with finally a shut-down.
Basically the present control strategy reacts to measurements. Because of the low precision on tank measurements, this offers sometimes problems, causing shut-down and blocking automatic operation.

Improved control strategy

In Chapter 6, it is found that the flow rate of the external circuit offers the widest range to control fuel cell operation.

Therefore this flow rate is used to anticipate to possible net water production or evaporation. To complete the control strategy, the air ratio is used to react on the measurements for fine tuning.

6 Analysis of system configurations

In Chapter 4 the behaviour of the stack is discussed. To compare different system set-ups with respect to performance the behaviour of the complete system, developed in Chapter 5, needs to be evaluated. Also for comparison with other micro-CHP technologies the evaluation needs to be done at system level.
In this chapter, the model developed in Chapter 5 is used to evaluate system behaviour at steady state. At the end of this chapter, system dynamics are discussed. A case study is elaborated in Chapters 7 and 8.

For this chapter, first a description is given on the indicators, which are useful to evaluate system performance. Next, the evaluation focuses on stack interconnectivity and sensitivity to system variations and variations in operation and control. Afterwards, the results are compared for different set-ups and control strategies. Finally a comparison is made with the behaviour of other micro-CHP technologies.

6.1 Evaluation criteria for an AFC-based micro-CHP

As can be expected, the energetic performance of a micro-CHP is an important evaluation criteria for the studied AFC-based system set-ups. Next to energetic performance also safety and water management will be important boundary conditions for an AFC-based micro-CHP system. In this section a brief discussion

is held on these topics in order to understand simulation results.

6.1.1 Water management

An important criterion for a fuel cell system is the effectiveness of the water management.

Net water production in the electrolyte flow

One of the requirements for the water management is to keep the electrolyte concentration constant. Therefore, an effective water management implies energy friendly solutions to remove excess water in the electrolyte flow or to prevent net evaporation of the water in the electrolyte solution.
Next to this, the robustness of the settings for nominal operation will be investigated. A robust or steady operation implies that small parameter changes results only in small net production or evaporation of water in the electrolyte flow. A low robustness will limit the range of safe operation of the fuel cell.
In correlation to the stack response, the thermal response of the system seems to be relatively slow. This is deduced from the measurements on the water level in Ref. [87], also discussed in Chapter 3. Another explanation could be that the noise and uncertainty on the measurements of the electrolyte level in the tank prevent a quicker response time.
Within the system measurements, a response time of 10 to 20 minutes of the water management on a new set-point is noticed. Therefore, a robust working point, regarding water management, is defined as a working point where the net water production or evaporation is kept lower than $0.2\,ml/s$, which corresponds to the contents of a glass of water every twenty minutes. The theoretical system response time is also simulated.

Water droplets

Next to the stability of the water level in the electrolyte tank within the system, an analysis of the water management also takes the possible occurrence of water droplets in the gas channels into account. At system level different stack-to-stack configurations can influence this occurrence, both at the anode and cathode side of the stack(s).
To examine the risk on the formation of water droplets, the vapour pressure is compared with the saturation pressure in the gas chambers. As the gas chambers can cool down to ambient temperature, relative humidity is calculated in the gas chamber at operating temperature and theoretically at ambient temperature.

6.1.2 Hydrogen concentration

Next to water management, safety can also be a limiting factor. To evaluate safety in this study only hydrogen concentration in indoor set-ups is taken into account. This concentration has to stay certainly below 4% to prevent ignition in presence of a heat source. Because local concentrations cannot be simulated, this limit has to be set at a much lower value for a safe operation. This will be discussed in the analysis.

6.1.3 Performance

To evaluate the performance of the different systems and the effect of different operating and system parameters on the CHP-potential, the methodology used in Chapter 4 is repeated: the primary energy savings are calculated. These savings are the result of a comparison with a separate production of heat and electricity. The reference situation for separate production is given in Section 4.1.4 in Chapter 4.

Definition of CHP-efficiencies at system level

The definition of the electrical and thermal efficiency is a little bit different from the one given in Section 4.1.3.2 as here the different system variables are taken into account separately.

- The electrical efficiency, α_e, is defined as the ratio of the net generated electric power, $P_{e,system}$, to the fuel input, $Q_{Fuel,system}$, Eq.(6.1). This efficiency, α_e, differs from the efficiency of the fuel cell stack itself, α_{FC}, which is discussed in Chapter 5 and defined by Eq.(6.2). This difference is found both in the definition of the fuel input as in the definition of the generated power. The fuel input of the system, $Q_{Fuel,system}$, includes the hydrogen, which is purged into the environment to remove water drops at the anode side and in the piping at the stack inlet. This is defined by a purge efficiency, η_{purge}, Eq.(6.3). The generated electric power (DC) by the fuel cell stack, $P_{e,FC}$, will be converted into AC power, $P_{e,AC}$, by the inverter at efficiency of the inverter, $\eta_{inverter}$, Eq.(6.4). The difference between the generated AC power, $P_{e,AC}$, and the net generated electric power, $P_{e,system}$, is found in the electric load of auxiliary equipment, $P_{e,aux}$, Eq.(6.5). This load is the result of the electric energy needed for the electrolyte pump, $P_{e,KOHpump}$, fan power, $P_{e,airfan}$, monitoring and

safety equipment,$P_{e,electronics}$, etc.,Eq.(6.6).

$$\alpha_e = \frac{P_{e,system}}{Q_{Fuel,system}} \tag{6.1}$$

$$\alpha_{FC} = \frac{P_{e,FC}}{Q_{Fuel,FC}} \tag{6.2}$$

$$\eta_{purge} = \frac{Q_{Fuel,FC}}{Q_{Fuel,system}} \tag{6.3}$$

$$P_{e,AC} = \eta_{inverter} \cdot P_{e,FC} \tag{6.4}$$

$$P_{e,system} = P_{e,AC} - P_{e,aux} \tag{6.5}$$

$$P_{e,aux} = P_{e,KOHpump} + P_{e,airfan} + P_{e,electronics} + ... \tag{6.6}$$

- The thermal efficiency, α_{th}, is defined as the ratio of the useful heat output, $Q_{TH,system}$, to the fuel input, $Q_{Fuel,system}$, Eq.(6.7). Depending on system set-up, this heat output will be the result of heat recovery in the electrolyte flow or in the air flow or in a combination. The useful heat output, $Q_{TH,system}$, is characterized by a temperature change of the water flow in the heating circuit, Eq.(6.8)

$$\alpha_{th} = \frac{Q_{TH,system}}{Q_{Fuel,system}} \tag{6.7}$$

$$Q_{TH,system} = \dot{m} \cdot c_w \cdot (T_{depart} - T_{return}) \tag{6.8}$$

6.2 Evaluation of stack to stack connectivity

As described in Section 5.1, the behaviour of 14 different multi-stack orientations and configurations can be modelled. These configurations are listed in Table 5.1. The model results are used to present an insight in the influence of the stack configuration on thermal and water management and overall performance.

6.2.1 Influence on thermal management

The thermal management is characterized by the output temperatures of the different mass flows of each (sub)stack, shown in Figure 6.1.

Electrolyte temperature

Figure 6.1(a) presents an overview of the impact of stack configuration on electrolyte temperature.
For a relatively high output electrolyte temperature the electrolyte is best connected in parallel over the stacks, if hydrogen and air flow are co-flow(dPd)

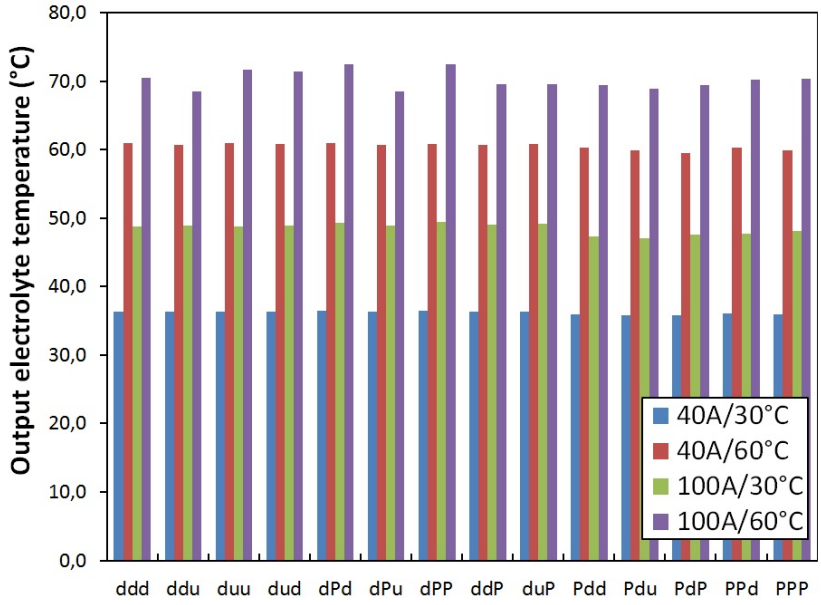

(a)

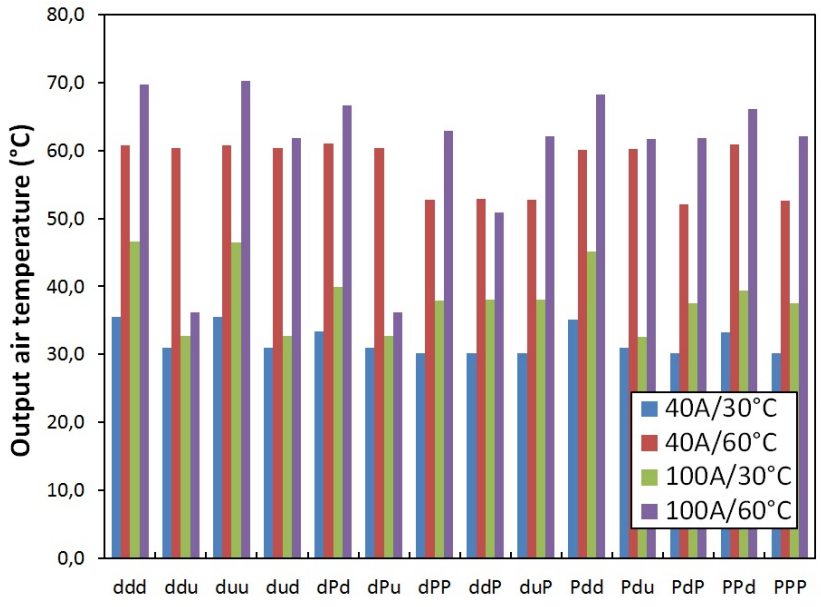

(b)

Figure 6.1: Comparison of modelled output temperatures for 14 different stack configurations, listed in Table 5.1; a) illustrates the output electrolyte temperature and b) the output air temperature. The comparison is made for four different working points, which are defined by electric load ($40A$ or $100A$ DC current) and inlet electrolyte temperature ($30°C$ or $60°C$).

or semi-parallel(dPP or PPd) oriented to each other. Only if hydrogen and air flow are in counter-flow oriented, the electrolyte is best serially connected at high temperatures: (duu)or(ddu) rather than (dPu). At low temperature the results are all similar, but negligible.
In general, no large differences in output electrolyte temperatures between stack configurations are shown. The highest temperature difference observed between two different stack configurations at the same operation point is $4°C$.
This means the influence of stack configuration on electric power due to a different electrolyte temperature is expected to be negligible. However, the influence on thermal power output can still be significant, since the absolute temperature rise in the electrolyte is relatively low, due to the high electrolyte flow rate. This will be discussed further in Section 6.2.3.

Air temperature

Figure 6.1(b) illustrates modelled output air temperatures for the different configurations.
For a similar set-up, it is noted that a counter-flow orientation from the air and electrolyte flow always results in a lower air temperature, compared to a co-flow orientation.
At high currents, a parallel connection can be situated between these two results. At lower current, a parallel connection has similar results to a counter-flow orientation.
To understand the influence of current here, it has to be noted that air flow rate is proportional to current. Therefore, high currents mean also high air flow rates and vice versa.
The difference in air temperature between configurations with a co- and counter flow orientation of the air and electrolyte flow, is because output air temperature is mainly influenced by the temperature of the last stack which the air flow passes. Stack temperature is defined by electrolyte temperature. As electrolyte temperature normally rises because of the heat output of the reaction, a counter-flow orientated air flow (compared to the electrolyte) will have the lowest output temperature.
This is illustrated in Figure 6.2. As can be seen in Figure 6.2(a) stack temperature rises parallel with the flow direction of the electrolyte.
Also air temperature (Figure 6.2(b)) follows this flow direction, which means that at opposite air flow direction the output temperature is lower.
To understand the figure it is important to note the global output temperature is measured at stack 1 for an upward air flow and at stack 4 for a downward air flow. A parallel connection is not illustrated in the graph but is based on an average stack output temperature.

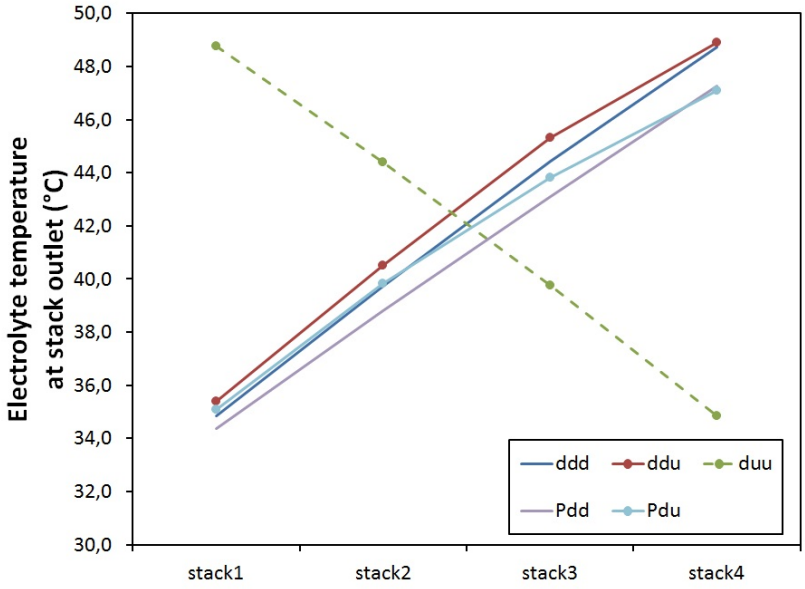

(a)

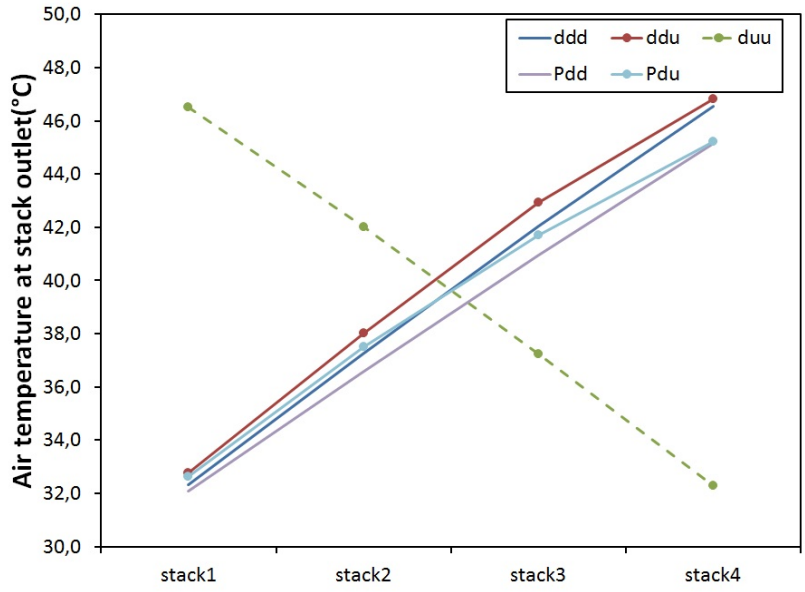

(b)

Figure 6.2: Temperature evolution for a number of stack configurations (See Table 5.1. a) illustrates the output electrolyte temperature at the end of each stack and b) the output air temperature. The comparison is illustrated for an input electrolyte temperature of $30°C$ *and a load of* $100A$.

6.2.2 Influence on the water management

Net water production

In general the water management can be evaluated by the net water production. In Figure 6.3 the total net water production (sum of all (sub)stacks) is shown. In

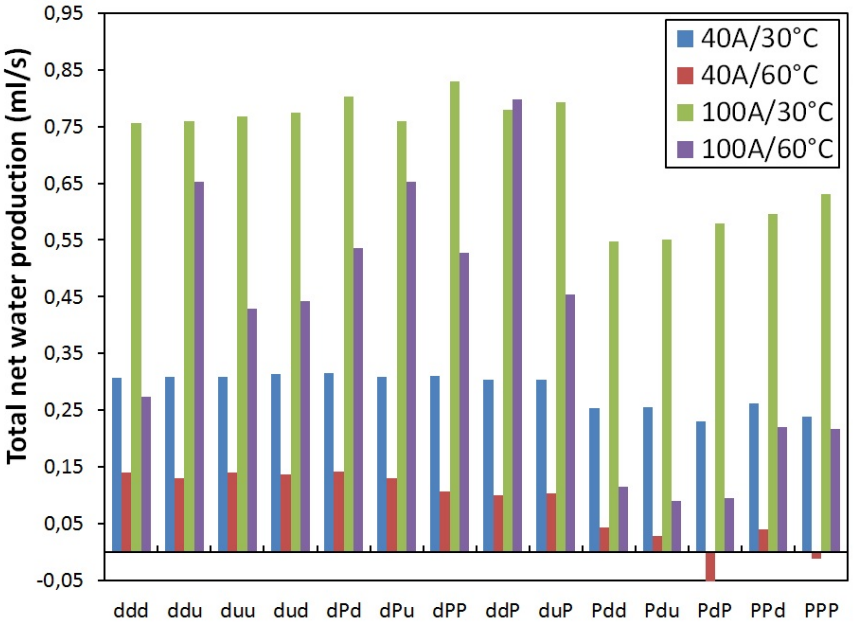

Figure 6.3: Comparison of the overall net water production for 14 different stack configurations, listed in Table 5.1. The comparison is made for four different working points, which are defined by electric load ($40A$ or $100A$ DC current) and inlet electrolyte temperature ($30°C$ or $60°C$).

practically all cases a net water production is found. Only at relatively low load and high temperature there is a net evaporation present for two configurations.
These configurations are characterized by parallel connected gas streams, both for hydrogen and for air. For this operation mode (low load and high temperature) it can be derived from the results shown in Figure 6.3, that parallel connected gas streams reduce net water production in the electrolyte. For hydrogen, this accounts for all operation modi.
With parallel connected gas flows, either hydrogen of air flow, the average partial pressure of water vapour in these gas flows is lower. This results normally in a higher partial pressure drop in the diffusion layers, stimulating the diffusion of water vapour into the gas flow. For this reason parallel connection of gas flows to the different stacks allows more removal of water as water vapour into these gas

flows. For the air flow, however, this is not true at every operation mode.
Some other annotations need to be considered here. Although the effect accounts for both gas flows, it is most pronounced for the parallel connection of the anode gas chambers and less pronounced for parallel connection of the air flow.
This is because of the high air ratio, compared to the end-of-pipe or stoichiometric hydrogen flow. At the cathode or air side there is an overflow of air, including nitrogen present. As nitrogen does not take part into the reaction and there is also oxygen left at the end of pipe, the difference between a parallel or non-parallel connection on water removal will have a small effect.
Besides, similar effects in other configurations are larger for the air flow, as with a connection in series, less heat will be lost here, resulting in higher electrolyte temperatures and saturation pressures. Since this will also increase diffusion from water vapour into the gas streams, the advantage of a parallel connection of air flow is less pronounced or even turns into a disadvantage.
This last is true for higher loads and higher air flow rates, as the cooling effect of the air flow is most pronounced here.

Water droplets in the hydrogen flow

Next to the net water production also the possible occurrence of water droplets in the hydrogen flow is of importance. A high probability of condensation of water vapour in the hydrogen gas flow has to be prevented to minimize purging and the corresponding efficiency loss. The relative humidity at the inlet of each stack can be representative for this probability (See Section 6.1.1).
In Figure 6.4 the relative humidity at the stack inlet is shown for different configurations. It is shown that for some configurations water vapour will condense between stacks as a relative humidity of more than 100% is calculated. This means condensation will take place in the anode gas chambers. The condensed water droplets will block the hydrogen channel and purging will be needed to remove and/or prevent the formation of these water droplets.
This occurs at higher electrolyte temperatures, $60°C$, with the electrolyte running serially through the different stacks. As both electrolyte and air flow are counter-flow oriented compared to the hydrogen flow (duu), the last stacks the hydrogen passes, are cooler than the first ones. Because of the high stack temperature at the first stack, a high amount of water vapour diffuses here in the hydrogen stream. This results in a relatively high vapour pressure at the inlet of the next stack. As the stack temperature drops in the next stacks the relative humidity rises to a critical level whereas condensation can take place. This occurs at higher load and higher temperature as a minimum temperature is required to initiate evaporation and diffusion.
Based on the risk of water droplets in the hydrogen channel, it can be stated that a counter-flow orientation of the hydrogen flow compared to the electrolyte flow is

to be avoided.

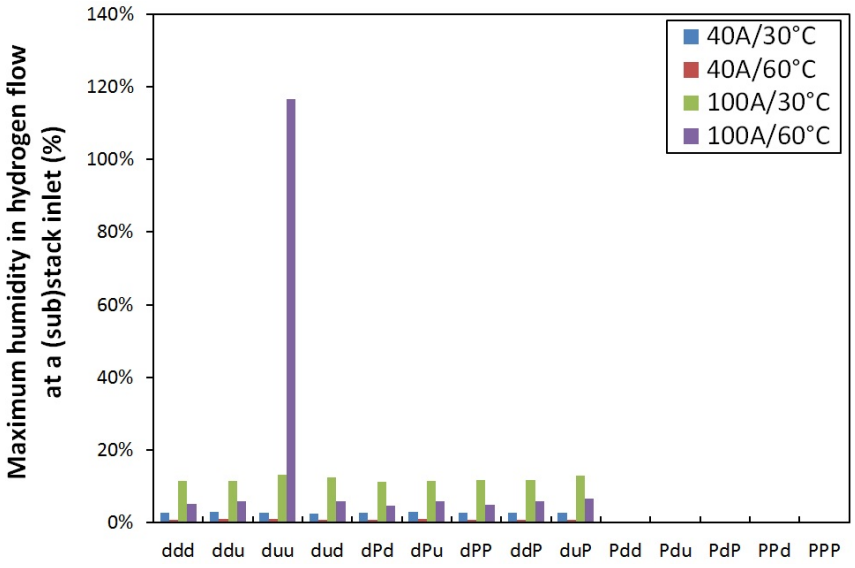

Figure 6.4: Comparison of the risk on water droplets in the hydrogen flow for 14 different stack configurations, listed in Table 5.1. The comparison is made for four different working points, which are defined by electric load ($40A$ or $100A$ DC current) and inlet electrolyte temperature ($30^{\circ}C$ or $60^{\circ}C$). The risk on the occurrence of water droplets in the hydrogen flow is represented by the maximum relative humidity, observed at the hydrogen inlet for the different (sub)stacks.

Water droplets in the air flow

Similar to the formation of water droplets in the hydrogen channel, water droplets can also be formed in the air channel. The same approach is used to evaluate the possibility of the formation of water droplets.
Figure 6.5 presents an overview of the relative humidity. A conclusion similar to the discussion on water droplets in the hydrogen flow is accountable for the air flow. A counter-flow orientation of the air flow to the electrolyte and hydrogen flow is to be avoided, since with some of these the simulation predicts the occurrence of water droplets (ddu) of (dPu). However, the problem is not that critical as for the hydrogen flow, because of the high air ratio and overflow with the possibility to increase this ratio, if necessary.

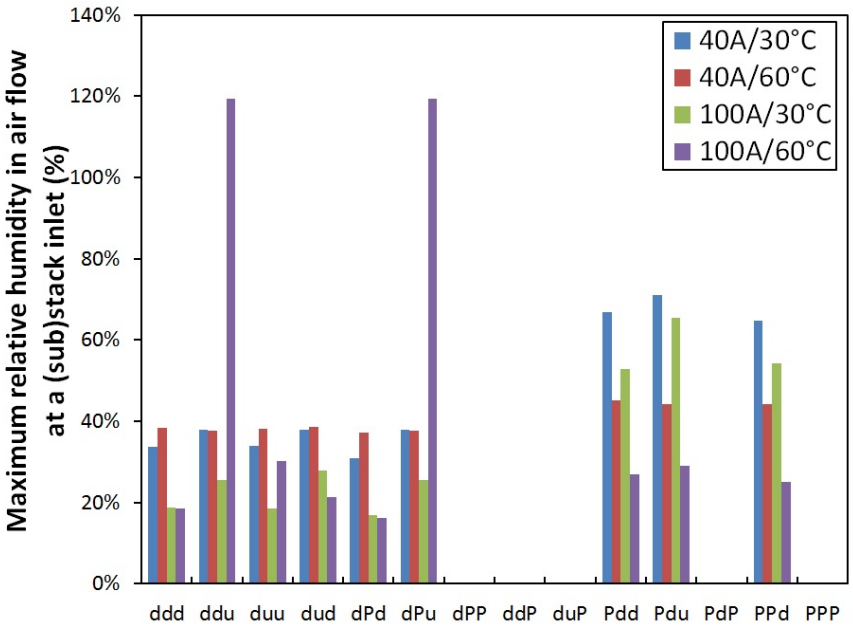

Figure 6.5: Comparison of the risk on water droplets in the air flow for 14 different stack configurations, listed in Table 5.1. The comparison is made for four different working points, which are defined by electric load ($40A$ or $100A$ DC current) and inlet electrolyte temperature ($30°C$ or $60°C$). The risk on the occurrence of water droplets in the air flow is represented by the maximum relative humidity, observed at the air inlet for the different (sub)stacks.

6.2.3 Influence on performance

As the configuration shows in most cases a relatively small influence on thermal and water management, it is investigated whether this will influence electric and thermal performance.

Electric performance

As shown in Figure 6.6(a) the influence on electric performance can be neglected as influence on average electrolyte temperature is very small.
There is however an influence on the individual stack performance. This is shown in Figure 6.7. The evolution is explained by the similar changes in electrolyte temperature through the stack, shown in Figure 6.2. As stated earlier electrolyte temperature has a positive effect on electric performance.

Thermal performance

Thermal performance is defined as basic heat output, meaning the temperature change in the electrolyte flow. Different from the discussion on electrolyte temperature output however is the importance of even relatively small temperature differences, since the temperature range itself is relatively small.
Figure 6.6(b) shows thermal output for the different stack-to-stack configurations. Thermal output is the highest with a parallel electrolyte connection.
Next to a higher heat output a parallel electrolyte connection offers also a safer operation. For a safe operation, it is necessary to induce a small overpressure in the electrolyte to ensure gas separation. With a parallel connection, this electrolyte pressure is in each stack the same, which facilitates control.
It is also shown that in most cases a parallel hydrogen connection for the stacks has a negative influence on thermal performance. Only for (ddu) and (dPu), compared with (Pdu) and (PPd), this depends on operation mode.

6.2.4 Summary of the results

Table 6.1 presents an overview of the analysis made in this section. The PPP configuration shows the best overall performance, as it is average or good in every aspect. The criterion the least critical for the multi-stack configuration is the net water production, as this can be solved with an additional control strategy. With this in mind the present set-up, dPP, and duP are considered the best possible solutions. Certainly if some practical remarks on hydrogen distribution are taken into account, since with a parallel hydrogen connection the occurrence of locally low hydrogen pressures are more likely. Next to that a serial connection offers the possibility to facilitate purging. Taking the remarks on the ionic short-circuit into

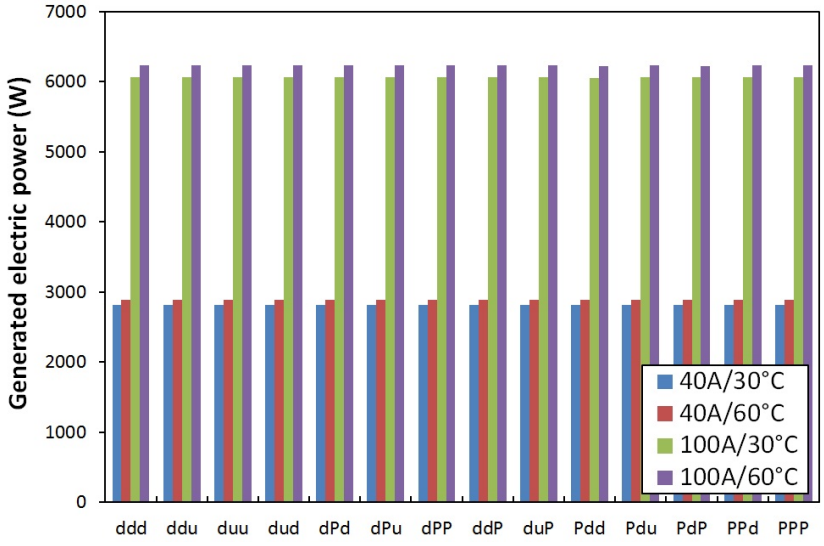

(a)

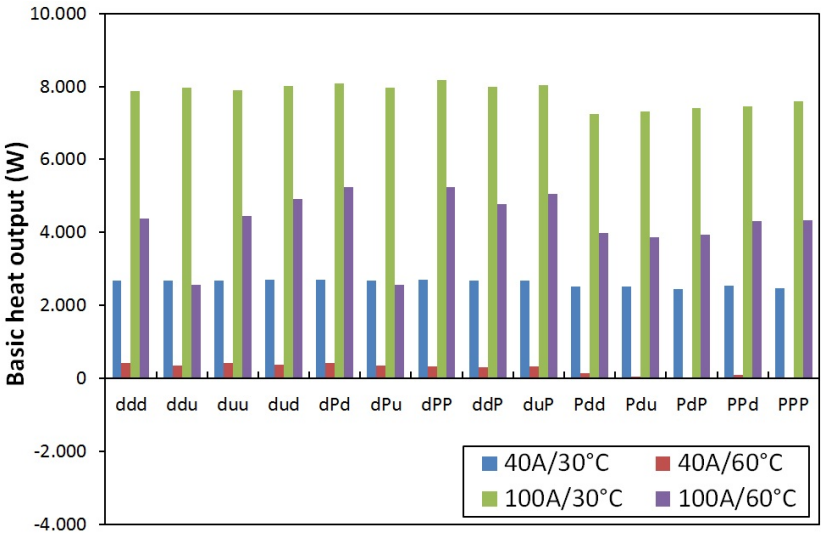

(b)

Figure 6.6: Comparison of modelled electric (a) and thermal (b) performance for the configurations, listed in Table 5.1. The comparison is made for four different working points, which are defined by electric load ($40A$ or $100A$ DC current) and inlet electrolyte temperature ($30^{\circ}C$ or $60^{\circ}C$).

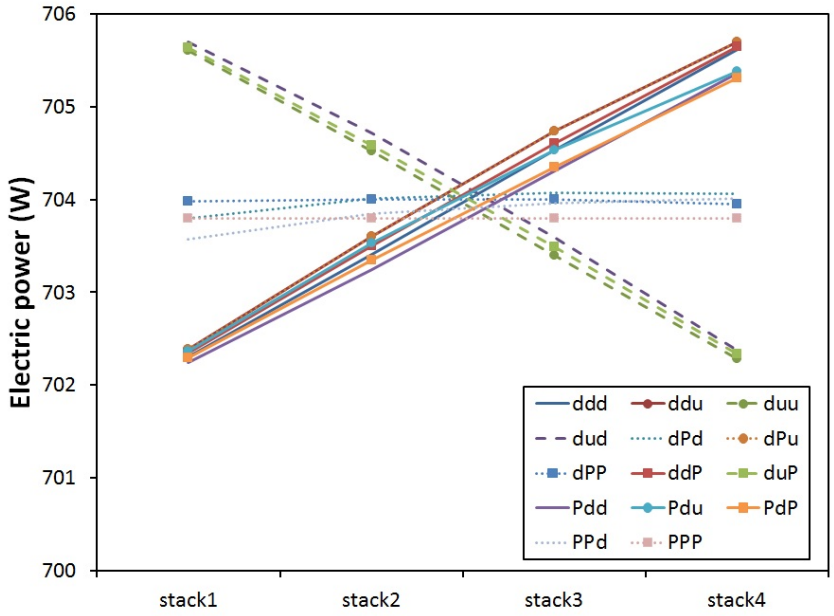

Figure 6.7: Evolution of electric performance of the different stacks in each configuration. The working point is defined by an electric load of $40A$ *and an electrolyte input temperature of* $30°C$.

Configuration	Electrical performance	Thermal performance	Risk on water droplets in the air channel	Net water production in the electrolyte	Risk on water droplets in the hydrogen channel
ddd	≤	≤	≤	−	+
ddu	≤	−	−−	−−	+
duu	≤	≤	≤	−	−−
dud	≤	+	≤	−	+
dPd	≤	++	−	−−	+
dPu	≤	−	−−	−−	+
dPP	≤	++	+	−−	+
ddP	≤	++	+	−−	+
duP	≤	++	+	−−	+
Pdd	≤	−	−	+	++
Pdu	≤	−	−	+	++
PdP	≤	−	+	+	++
PPd	≤	≤	−	≤	++
PPP	≤	≤	+	≤	++

Table 6.1: Overview of the results on the different performance criteria for all multi-stack configurations.

account, the present set-up (dPP) offers the best results compared to duP.

Nevertheless, comparing all results on different stack design, it is shown that the influence of different configurations is limited, for this reason and to simplify system modelling this is not taken into account any more in further analysis.
In the rest of this chapter the PPP-configuration is used to evaluate other system designs, to reduce model complexity, since it can be modelled as a single stack.

6.3 Evaluation of different system set-ups to integrate the AFC stack into a complete system

To evaluate system performance, system parameters, operation conditions and possible control parameters or strategies are examined. This investigation is performed for all three set-ups, described in Section 5.2: the original set-up, a set-up with heat recovery in the air flow and a set-up integrated in a container.

6.3.1 Evaluation of the system parameters

To evaluate the different system components a sensitivity study is performed on following parameters.

- η_{purge}, the purge efficiency, defined in Eq.(6.3).
- $\eta_{inverter}$, the efficiency of the inverter.
- η_{pump} and η_{fan}, the efficiencies of the electrolyte pump and air fan(s).
- $c_{evaporation,tank}$, percentage of evaporation in the electrolyte tank.
- ϵ_{HE}, the effectiveness of the heat exchanger(s).
- hA_{cont}, insulation thickness of the container (only for this set-up).

6.3.1.1 Purge efficiency

The purge efficiency, η_{purge} is altered from 90% to 100%. Because of its definition, Eq.(6.3) it affects all other efficiencies equally and proportionally. For the same output also the water management will remain constant. The hydrogen concentration can be an issue if the system is placed indoors. No problems are expected for the original set-up and the set-up including air heat exchanger, which are meant to be outdoors.
For the container set-up, these risks also depend on the air flow rate at the in- and outlet of the container. This effect is discussed in Section 6.3.2.2. In this analysis

a fixed air flow rate of $15\,m^3/h$ is chosen, allowing safe operation at nominal load and purge efficiency of the present system, about 98% (See Section 6.3.2.2).
Lowering purge efficiency to 90% becomes unacceptable at high load. In this case a hydrogen concentration of more than 3% is formed at nominal load (100 A). This is too close to the explosion boundaries.
Therefore in order to prevent unacceptable hydrogen concentrations, higher air flow rates have to be considered resulting in higher capital costs (bigger fans), extra parasitic load and additional thermal losses (See Section 6.3.2.2). A better solution will be additional piping, connecting the purge valve to the outdoors. Drawback of this solution are the extra hydrogen losses at every start-up, due to rinsing.

6.3.1.2 Efficiency of electric auxiliary equipment

Apart from the fuel cell, the efficiency of the electric components in the CHP-system influences the total electrical output for all three set-ups. Only for the container set-up, they also have an influence on thermal output.
In the original set-up and the one with the additional heat exchanger, the heat due to conversion losses is directly dissipated into the surroundings. In the container set-up this heat will result in a temperature rise in the container, influencing both thermal and electrical performance of the fuel cell stack (See Chapter 4).
In the outdoor set-ups the influence on electric efficiency can be easily understood. The inverter efficiency, $\eta_{inverter}$, altered from 82% to 100%, is equally proportional to the total electric efficiency of the CHP-system. The effect of the pump and fan efficiency, η_{pump} and η_{fan}, which are investigated together, on total electrical power output is negligible. For auxiliary equipment twice as efficient the gain in electrical output is limited to 0.3% (depending on system set-up), even at small loads. This is due to their relatively small electric load.
For the container set-up the conversion losses will result in a temperature rise in the container, depending on air refreshment ratio (See Section 6.3.2.2). This will result in a higher cell temperature and a higher electric performance (See Chapter 4). This effect however is limited to 0.15% compared to the outdoor set-ups for an inverter efficiency of 82% compared to one of 100%. However, the effect on thermal output can be up to more than 10%, strongly depending on outdoor conditions, load and return temperature.
Regarding pump and fan efficiency, the same reasoning can be made, but in accordance to their small load their influence is negligible.
Based on this discussion a cheap and standardized pump and fan selection is acceptable and will not affect efficiency in the three set-ups. The inverter, however, will always have a large influence on performance. Even at the container set-up an efficient inverter has a high priority, because a thermal efficiency improvement of 10% cannot erase an electric efficiency loss of 18%. Primary energy savings, compared to the average Belgian power plant, will be reduced with 22.5% for the

Index	DC-current A	Return temperature $°C$	Air condition T($°C$)	RH($\%$)
1	40	25	1	1
2			20	20
3			20	80
4		45	1	1
5			20	20
6			20	80
7	100	25	1	1
8			20	20
9			20	80
10		45	1	1
11			20	20
12			20	80

Table 6.2: Description of the enumerated working points, used in Tables 6.3 and 6.4.

outdoor solutions and with 14.5% for the container set-up for a drop in inverter efficiency from 100% to 82%.

6.3.1.3 The percentage of evaporation in the electrolyte tank

The percentage of evaporation in the electrolyte tank, $c_{evaporation,tank}$, will have an influence on both thermal power output as on net water production, depending on system configuration. Next to this also the electrolyte temperature is indirectly influenced which affects electrical efficiency, as discussed earlier. This effect however is limited to about 0.09%, which is negligible.

As can be seen in Tables 6.2 and 6.3, a higher evaporation rate implies a higher heat loss in the air flow, resulting in a lower useful heat output. The heat loss on the thermal power output due to a higher evaporation rate, $c_{evaporation.tank}$, will be compensated by an improved water management. This effect is more pronounced for the outdoor solutions. Within the container set-up, fresh input air is mixed with the wet air out of the electrolyte tank. The air mixture enters the fuel cell and electrolyte tank. The input air is more moist, compared with the other set-ups, which means less water will be evaporated.
Compared to the original set-up the influence on useful heat output, Q_{TH}, is relatively lower, since the thermal output with the heat recovery is larger and because the electrolyte temperature will rise instead of decline compared to the other set-ups. This increase is possible since more (latent) heat is available for preheating the input air. A higher air temperature has a positive effect on electrolyte temperature (See Chapter 4).

Index	Relative deviation for an increased evaporation rate from 10 to 70% [%]								
(See	Original system			Container system			System with heat recovery on air flow		
Table 6.2)	ΔQ_{TH} (%)	ΔP_e (%)	ΔH_2O (%)	ΔQ_{TH} (%)	ΔP_e (%)	ΔH_2O (%)	ΔQ_{TH} (%)	ΔP_e (%)	ΔH_2O (%)
1	−5.0%	−0.01%	−12.8%	−1.3%	0.01%	−8.6%	−7.7%	−0.01%	−14.7%
2	−4.2%	0.00%	−14.9%	−1.7%	0.00%	−9.2%	−4.2%	−0.01%	−15.8%
3	−4.4%	−0.01%	−14.2%	−2.0%	0.00%	−8.1%	−3.2%	−0.01%	−14.8%
4	−15.8%	−0.02%	−56.7%	−23.1%	−0.07%	−49.4%	−22.8%	−0.03%	−73.4%
5	−14.0%	−0.01%	−79.6%	−6.0%	0.02%	−35.1%	−11.5%	−0.01%	−83.7%
6	−12.0%	−0.01%	−62.4%	8.6%	0.06%	−28.1%	−12.1%	−0.02%	−68.2%
7	−9.6%	−0.05%	−48.2%	−3.1%	0.03%	−16.1%	−9.3%	−0.05%	−53.3%
8	−9.5%	−0.05%	−51.8%	−3.1%	0.03%	−17.5%	−9.4%	−0.05%	−55.3%
9	−8.8%	−0.05%	−45.5%	−3.1%	0.03%	−16.0%	−8.8%	−0.05%	−48.3%
10	−23.8%	−0.07%	−274.0%	−18.2%	−0.08%	−121.4%	−24.2%	−0.09%	−325.9%
11	−23.6%	−0.09%	−308.7%	−8.5%	0.02%	−72.0%	−22.2%	−0.09%	−374.1%
12	−22.8%	−0.10%	−248.5%	−21.5%	−0.13%	−90.9%	−21.2%	−0.09%	−279.1%

Table 6.3: Overview of the impact of the evaporation rate of the electrolyte tank on performance and water management for different system set-ups.

This means that for the container set-up a high evaporation rate has no significant influence. For the outdoor set-up a high evaporation rate will be a significant advantage.

6.3.1.4 Heat exchanger effectiveness

At a fixed return temperature of the external heating circuit. the effectiveness of the heat exchanger, ϵ_{HE}, determines the temperature of the electrolyte circuit. At a low effectiveness a higher electrolyte temperature is necessary to transfer heat at a fixed return temperature. This higher temperature combined with a low effectiveness. which is indirectly linked to the efficiency of the heat recuperation. results in a lower heat output. The electrical efficiency however increases at higher electrolyte temperature (See Chapters 3 and 4). Therefore, the effectiveness will have a negative impact on electrical performance. Since both thermal and electrical output experience opposite effect, primary energy savings are taken into account to evaluate the effect of the effectiveness of the heat exchanger.
Table 6.4 presents an overview of the influence of the effectiveness of the heat exchanger on primary energy savings, compared to an average Belgian power plant (See Section 4.2.4). This evaluation is done for all three set-ups. The influence is the highest for the original set-up and is the highest for high return temperatures of the external circuit. The influence is less pronounced at the set-up with the additional heat exchanger. In general for each set-up, a small but substantial increase in savings is found. Since a high effectiveness implies a large heat transfer coefficient, meaning a large or expensive heat exchanger, there is no critical need to maximize effectiveness but an average effectiveness of about 0.6 is acceptable.
Next to this, it is also shown that the water management is strongly influenced by the effectiveness, in particular at nominal load (100A DC). Since effectiveness depends on heat transfer coefficient and mass flows, this last one can be a possible control parameter for the water management (See Section 6.3.2).
Regarding the heat recovery in the air circuit, the impact of the effectiveness is shown in the comparison between the original set-up and the one with heat recovery.

6.3.1.5 Container insulation

For the container set-up, the insulation thickness will affect performance and water management. but will have no influence on safety. It has as positive influence on thermal output. The size of this influence is strongly dependent on operation modus and ambient conditions. In a cold environment and at high return temperatures the effect is the largest. since extra insulation will prevent more heat loss, due to this temperature difference. For a load of 40A DC, a return temperature of 40°C and at ambient temperature of 1°C an increase is noticed from $0.2\,kW$ or

Index	Original system					Container system					System with heat recovery on air flow				
(See	Net water prod.		RPES			Net water prod.		RPES			Net water prod.		RPES		
Table	Effectiveness HE		Effectiveness HE			Effectiveness HE		Effectiveness HE			Effectiveness HE		Effectiveness HE		
6.2)	30.0%	90.0%	30.0%	90.0%		30.0%	90.0%	30.0%	90.0%		30.0%	90.0%	30.0%	90.0%	
	ml/s	ml/s	%	%		ml/s	ml/s	%	%		ml/s	ml/s	%	%	
1	0.22	0.29	28.2%	30.7%		0.25	0.31	32.1%	34.2%		0.26	0.28	30.7%	32.1%	
2	0.22	0.29	30.8%	33.9%		0.25	0.31	33.4%	35.7%		0.26	0.29	33.2%	34.7%	
3	0.24	0.32	31.4%	34.5%		0.28	0.33	32.1%	36.2%		0.29	0.32	33.9%	35.4%	
4	0.09	0.15	19.0%	24.3%		0.11	0.21	27.9%	31.0%		0.11	0.14	21.9%	25.3%	
5	0.07	0.16	21.8%	27.9%		0.10	0.22	29.2%	30.8%		0.11	0.14	24.5%	28.4%	
6	0.10	0.18	22.5%	28.8%		0.12	0.24	29.6%	31.1%		0.14	0.18	26.0%	29.2%	
7	0.08	0.61	19.1%	27.4%		0.15	0.74	26.0%	30.7%		0.34	0.58	24.7%	27.9%	
8	0.02	0.62	20.3%	29.1%		0.12	0.75	26.5%	31.0%		0.31	0.58	26.2%	29.3%	
9	0.06	0.67	20.8%	29.6%		0.13	0.77	26.6%	32.5%		0.35	0.63	26.6%	29.8%	
10	−0.35	0.26	12.4%	22.4%		−0.33	0.51	20.8%	29.6%		−0.10	0.20	18.0%	22.4%	
11	−0.44	0.25	13.7%	24.2%		−0.37	0.52	21.2%	30.3%		−0.14	0.20	19.3%	23.7%	
12	−0.41	0.30	14.1%	24.8%		−0.36	0.54	21.2%	30.5%		−0.10	0.25	19.8%	24.2%	

Table 6.4: Overview of the impact of the heat exchanger effectiveness on performance and water management for different system set-ups.

10% for tripling the insulation thickness.
At higher loads the gain in thermal output is lower, also in absolute values, since at this load the air circulation of the container is higher. which partly neutralizes the effect of the container.
As electrolyte temperature rises with improved insulation also electrical performance will be higher, but this effect is negligible. Also for water management the effect is negligible.

6.3.2 Control strategy

Operating parameter		Value	
Description	unit	nominal	min-max
DC-current	(A)	100	20-140
Return Temperature(CV)	($^{\circ}C$)	40	20-65
Temperature surroundings	($^{\circ}C$)	20	1-35
Relative humidity	($\%$)	40	10-90
Air ratio	(-)	2.5	1-5.5
Electrolyte flow rate	(kmol/h)	20.5	-
Flow rate heating circuit	(l/s)	0.278	0-0.556

Table 6.5: List of operation parameters with nominal value and simulated range of variation.

With the system evaluation in Section 6.3.1, it is possible to choose an optimal design for each set-up. However, the performance of the system, not only energetically, but also regarding safety and water management, does not only depend on system configuration and system parameters. Also the operational conditions will influence this performance. We can divide these conditions into three sets of variables:

- operation mode, which is defined by the electric load and the return temperature of the heating circuit.
- environmental conditions or the weather conditions, since the system is placed outdoors: air temperature and humidity.
- control parameters, which can be adjusted to optimize performance or water management: air ratio, electrolyte flow rate and flow rate within the heating circuit.

Table 6.5 presents an overview of these variables and in which range their influence is analysed.

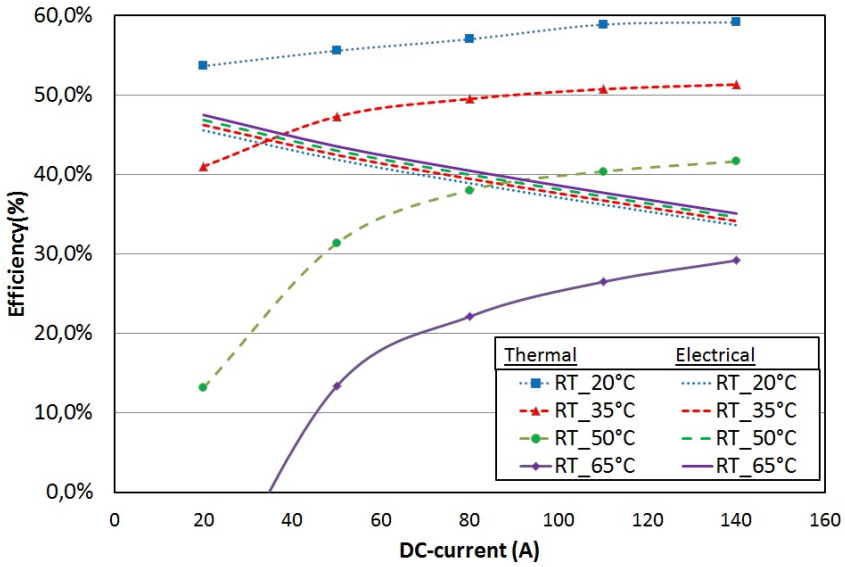

Figure 6.8: The thermal and electrical efficiency of the original system for different return temperatures as a function of DC-current.

Operation mode and environmental conditions

The first two sets of variables depend on the conditions in which the system is used. Without a proper control strategy the operation mode has a high impact on water management and overall performance. This is illustrated here for the original set-up.

The operation mode is defined by return temperature and electric load (DC-current). In Figure 6.8 is shown that electrical efficiency rises with increasing return temperature and drops with increasing current, while thermal efficiency reacts in an opposite way.

As discussed in Section 6.1.3, the (relative) primary energy savings are considered to define the overall performance. Similar conclusions as posed in Chapter 4 for the stack evaluation are valid. For every return temperature an optimal current can be found, which maximizes system performance based on primary energy savings. For a return temperature of $65°C$, this is about $60A$ (DC). For lower temperatures, the optimal current is lower.

Above the optimal current, the relative primary energy savings (RPES) are driven by the slightly decreasing electric performance. The RPES drop, but remain acceptable, similarly to the electric performance. At currents lower than optimal, the RPES drop rapidly, similarly to the thermal performance. Therefore, the

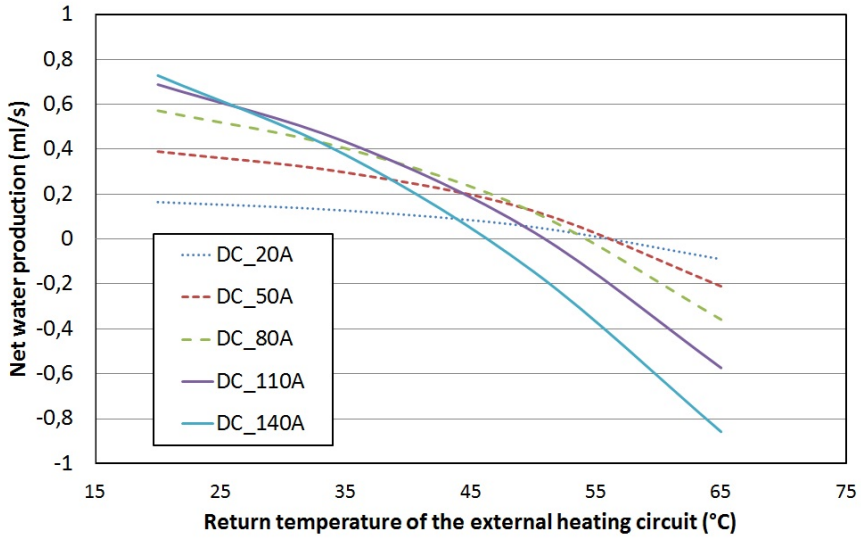

Figure 6.9: The net water production of the original system for different DC-currents as a function of return temperature.

optimal current can also be seen as a minimal electric load.
If we set water management as a boundary condition for the possible operation modes, Figure 6.9 illustrates in which range of the return temperature the water level can be kept under control (between -0.2 and $0.2\,ml/s$). Figure 6.9 shows that under the conditions listed in Table 6.5, a return temperature between $46°C$ and $53°C$ offers the widest range for different electric loads. It is also shown that for increasing electric load the upper limit shifts to lower temperatures, while the under limit shifts to higher temperatures.
Therefore, at high electric loads it is critical to work with the most appropriate return temperature. At high electric load not only a lot of water (vapour) is formed in the reaction, which has to be removed from the system, but also a lot of heat is generated which has to be cooled away to prevent dry heating.

Control parameters

The control parameters can make the system more flexible for these different operation modes. This last set of parameters depends on the control strategy used to operate the system. The scope of this strategy is to find a balance between maximizing energetic performance and ensuring safe and stable operation regarding water management. Without introducing extra components into the

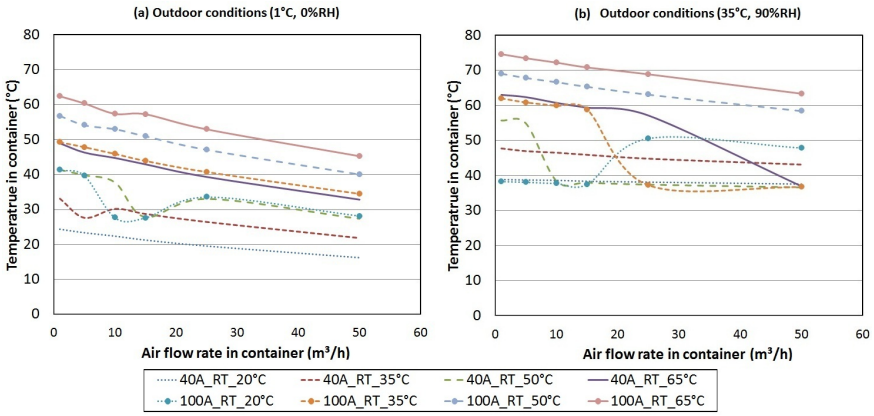

Figure 6.10: Influence of the air flow rate into the container on container temperature for (a) cold and (b) hot weather conditions.

system, three to four (only for container set-up) different parameters can be distinguished, which can be used in a control strategy:

- electrolyte flow rate
- air flow rate. into the container (only for this set-up)
- air ratio
- flow rate of the external heating/cooling circuit

6.3.2.1 Electrolyte flow rate

Although the electrolyte flow rate can be adjusted, this parameter is fixed, since in Chapter 4 the effect on water management was not noticed and a high flow rate is necessary to enable a stable working of the fuel cell. At lower flow rates the probability of a too low pressure in the electrolyte rises, which could result in a direct hydrogen flow through the electrolyte into the oxygen gas chamber or vice versa. This has to be prevented at all times. Therefore, a different set point for the electrolyte flow rate is not considered.

6.3.2.2 Container input air flow rate

In the container set-up an extra fan is installed. With a variable speed drive on the fan, the inlet air flow rate can be altered. Depending on outdoor conditions, this flow rate will have a weak or strong negative influence on the temperature within the container. Figure 6.10 shows the influence for cold and hot outdoor conditions.

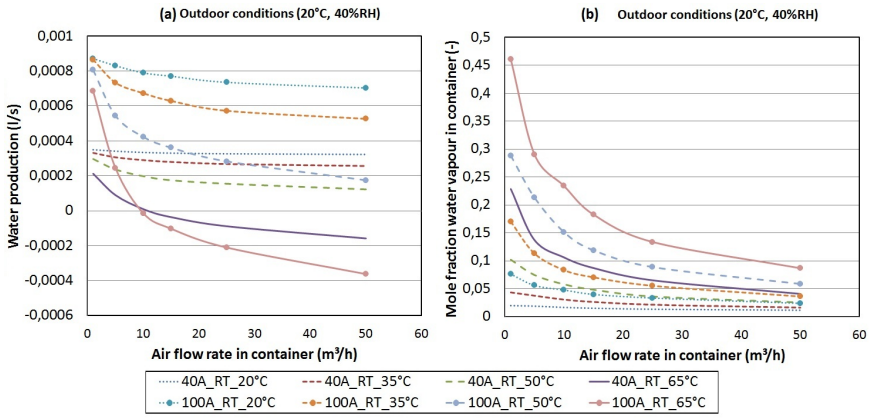

Figure 6.11: Influence of the air flow rate into the container on the water management based on (a) net water production and (b) humidity in the container.

As expected, this influence will be smaller for hot outdoor conditions and also the lower and upper limit will be higher.
Since the surrounding temperature has a serious influence on thermal performance of the stack, an increasing air flow rate will decrease thermal performance. The effect is the highest for low loads and high return temperatures, because here the heat losses are high due to a high temperature difference and relatively large compared to the produced heat (low load). Thermal performance drops to 40% of its initial value for an air flow rate of 50 instead of 1 m^3/h. The influence on electric performance is also negative but negligible.
Figure 6.11 shows the impact on water management. Regarding humidity in the container and water management in the stack it can be seen that at an air flow rate higher than 10 m^3/h the influence on the water management, both humidity and net water production drops. Therefore, an air flow rate higher than 10 m^3/h, with the additional thermal losses in mind, is not a good solution to optimize water management. This sets a higher boundary to this control parameter.
However safety issues can overrule this boundary condition, since the most important role of the input air flow rate is to prevent unacceptable hydrogen concentrations in the container (See Section 6.1.2). Therefore also the hydrogen concentration is simulated for the different air flow rates. For this a purge efficiency of 98%, measured on the present system, is taken into account. It is shown that for an air flow rate of 5 m^3/h the influence on the hydrogen concentration is still unacceptably high, over 2%, at high loads. At 10 m^3/h the maximum simulated concentration drops below 1%.
Because of these conflicting demands, the air inlet flow rate is not considered as

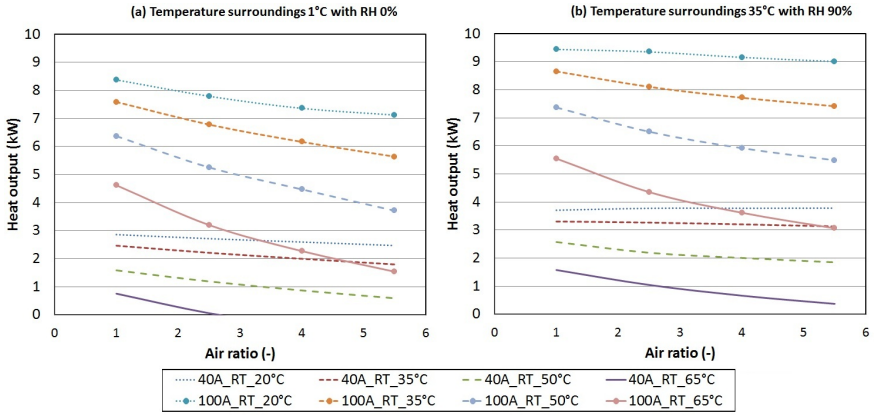

Figure 6.12: Influence of the air ratio on the thermal output (kW) in the original set-up for (a) cold weather conditions and (b) hot and wet environmental conditions.

a control parameter to optimize performance and water management, but set at a fixed value of 10 m^3/h.

6.3.2.3 Air ratio

Air ratio is an adjustable parameter which could be used to optimize performance and water management. Therefore, for different air conditions, temperature and humidity, the air ratio is altered for several working points, with DC currents from $40A$ to $100A$ and return temperatures from $20°C$ to $65°C$.

Regarding thermal power output a negative influence of increasing air ratio is found in almost all cases for the original set-up (See Figure 6.12). Only at very low return temperature and low currents this effect can be positive, if the electrolyte temperature is lower than the input air temperature and almost no water will be evaporated. For higher return temperatures ($65°C$) the negative effect is more pronounced: for high loads (100A DC) the thermal output can be reduced to 50% for an air ratio 5 times higher and for low loads the thermal output can become negative in a cold environment, because the extra heat losses are higher than the heat production. In a hot environment the air ratio has less effect on the thermal output, since less heat will be lost.

Because both alternative set-ups will have a higher input air temperature, due to heat recovery or mixture of air flows, it is expected that the negative effects of the air ratio will be smaller compared to the original set-up. This is most pronounced in cold weather conditions, in which case the advantage of the heat recovery has its largest impact (See Figure 6.13). As can be seen in the chart, it is shown that the set-up with the heat recovery behaves similar to changes in air ratio, only a little

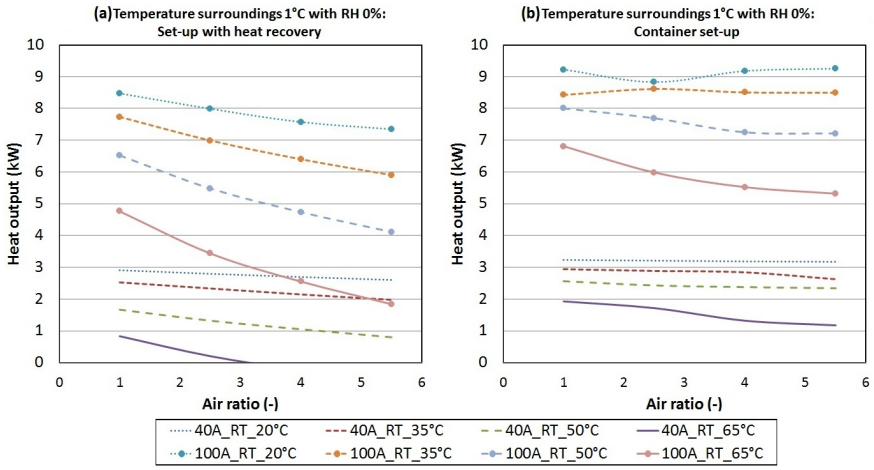

Figure 6.13: Influence of the air ratio on the thermal output (kW) in cold weather conditions (a) for the set-up with heat recovery on the air output and (b) for the container set-up.

bit less extremely. In the container set-up the influence on thermal performance is almost completely vanished, only for high return temperatures, the trend is still visible.

Since electrical performance is higher at higher electrolyte temperature, the influence of air ratio is also negative and more pronounced at higher return temperatures, but compared to thermal performance the effect is limited (up to 5.5% for an air ratio 5 times higher) for the original set-up and completely negligible for the alternative set-ups.

The impact of air ratio on water production is more significant, but its influence depends on air humidity. In Figure 6.14 is shown that for the original set-up in dry conditions for return temperatures higher than $35°C$ an air ratio can be found for which the water management is kept under control (See Section 6.1.1).

At high currents and high return temperature this air ratio is set to a minimum, 1, meaning that there is no air excess and a high chance on the formation of water droplets and pressure drops in the air channel. In moist conditions this is not a problem, but the lower limit for return temperatures rises up to $50°C$.

In the original set-up the use of air ratio as a control parameter for the water management is possible, but strongly limited and dependent on outdoor conditions, which cannot be controlled. In the set-up with the heat exchanger the same conclusions are applicable. For the container set-up the air ratio has little or no impact on the water management, due to higher moisture content of the air in the container. This is useful for high loads combined with a high return temperature,

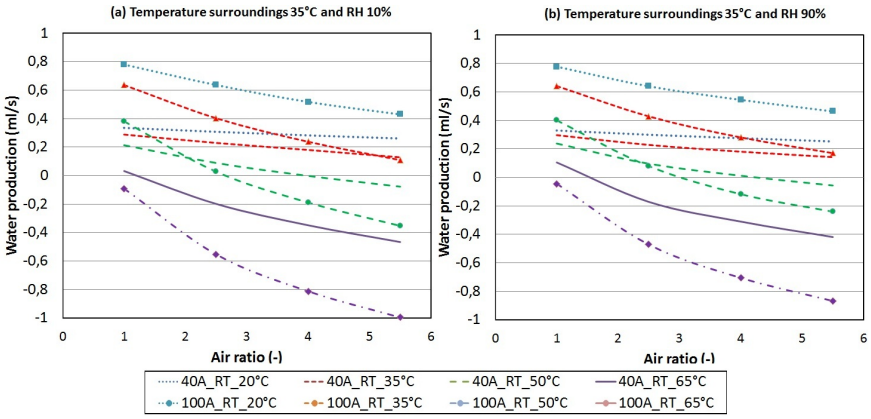

Figure 6.14: The net water production of the original system as a function of air ratio for different working points in dry and moist conditions.

as discussed in Chapter 4. These operation modi cannot be achieved with other set-ups, without exceeding the boundaries of a stable water management.
Based on these insights, the air ratio is not withheld as a prime control parameter to stabilize water management. However, the air ratio can still be useful in a more complex and advanced control strategy or as an additional or secondary control parameter for temporarily deviations.

6.3.2.4 Flow rate of the external heating circuit

A last control parameter is the flow rate of the external heating circuit. For the same heat exchanger with a certain overall conductance, hA_{HX}, the effectiveness, ϵ, changes with different flow rates. At higher flow rates, lower temperature changes and therefore lower effectiveness will be obtained, since effectiveness represents the temperature change in the flow, compared to the maximum possible temperature difference, Eqs.(6.9) or (6.11) and (6.13).
Therefore, using effectiveness as a model parameter for the heat exchanger does not allow an evaluation of the flow rate as a control parameter. To evaluate this control parameter the model of the heat exchanger is adapted, using following expressions, which are based on the expression for a counter-flow heat exchanger.

If $C_C = C_H$, following expression can be used to calculate $T_{C,out}$:

$$T_{C,out} = \frac{C_C \cdot T_{C,in} + hA_{HX} \cdot T_{H,in}}{C_C + hA_{HX}} \tag{6.9}$$

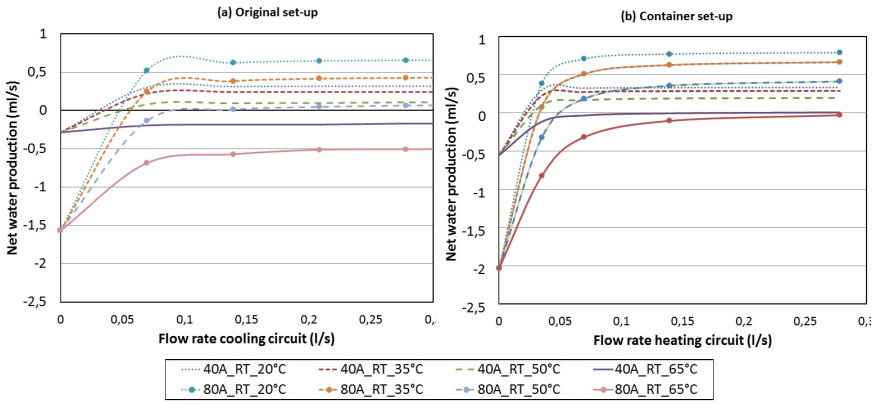

Figure 6.15: The net water production of the (a) original and (b) the container system as a function of the flow rate of the external cooling/heating circuit for different electric loads and return temperatures.

If C_C and C_H are not the same, following expression is to be used for $T_{C,out}$:

$$T_{C,out} = \frac{T_{H,in} \cdot \left[C_H \cdot \left(1 - exp\left(\frac{hA_{HX}}{f}\right)\right)\right] + T_{C.in} \cdot [C_C - C_H]}{C_C - C_H \cdot exp\left(\frac{hA_{HX}}{f}\right)} \tag{6.10}$$

(6.11)

with

$$f = \frac{C_C \cdot C_H}{C_H - C_C} \tag{6.12}$$

In both cases, $T_{H,out}$ is calculated afterwards with

$$T_{H,out} = T_{H,in} - \frac{C_C \cdot [T_{C,out} - T_{C,in}]}{C_H} \tag{6.13}$$

Instead of effectiveness, the heat exchanger is now characterized by the heat transfer coefficient of the heat exchanger, hA_{HX}. The value for this new model parameter is based on an effectiveness of 80% and the nominal flow rate of the external circuit, $1000\,l/h$.

In Figure 6.15 the net water production is evaluated at different flow rates. electric loads and return temperature for different set-ups. The conditions of the surroundings are set at $20°C$ with a relative humidity of 40%. It is shown that for every return temperature of the external circuit, lower than 55 – $65°C$ (depending on set-up), a flow rate can be found for which the net water production is zero. At

higher temperatures, there will always be evaporation at the used conditions of the surroundings. At flow rates lower than in the electrolyte circuit, the flow rate has a large impact on the heat transfer. At flow rates higher than the electrolyte flow rate, which is about $0.1025\,l/s$, the thermal power output and thereby also the net water production remain almost constant. Between $0\,l/s$ and this point the thermal output rises from zero to maximum.
The influence on both water management and thermal performance can be easily understood. At low flow rates, the electrolyte temperature will rise and the mean logarithmic temperature difference between the electrolyte and the cooling circuit will decline, resulting in a higher electrolyte temperature and lower heat output. Because of the higher electrolyte temperature, this effect will even be enforced due to more heat loss. This higher electrolyte temperature ensures stable operation regarding water management, as discussed in Chapter 4.
In all three set-ups, flow rate of the external circuit is a valuable control parameter. which can easily be applied.

6.3.2.5 Control strategy for water management

The previous discussion shows that a stable water management can be obtained using the flow rate of the external circuit as a prime control parameter. For this reason, a simplified control algorithm is implemented in the three set-ups. This will allow a fair comparison of their energetic performance, since both water management and safety (See Section 6.3.2.2) will be ensured.
Figure 6.15 shows which trends this algorithm has to contain.

- The flow rate increases with electric load. Because more heat is generated in the reaction, the electrolyte will rise in temperature. even without lowering the flow rate.
- The flow rate increases with higher return temperature, because the electrolyte temperature is already high.
- The outdoor conditions will also influence the flow rate, but this effect is less pronounced and stable, and harder to take into account in real time operation. Therefore, this last one is left out of the algorithm.

Based on simulation results for each set-up the control parameter is set as a function of return temperature and load (electric DC current).
For the original set-up and the set-up with the extra heat exchanger for every load ($40A$ - $100A$ DC) and every return temperature ($20°C - 50°C$) a flow rate could be found for which there is no net water production or evaporation. For the container set-up, the return temperature can be higher. At low loads (lower than $40A$ DC), a minimum return temperature of $40°C$ is required. For higher loads there are no limitations.

6.3.3 Overall comparison

With the control strategy, it is possible to make a fair comparison between all three set-ups. Figure 6.16 summarizes the differences in energetic performance between the three set-ups. This energetic performance is based on relative primary energy compared to the best possible alternative, taking also reforming efficiency into account (See Section 4.2.4).
In (a) the average value for different return temperatures is used for each load, showing that the original system becomes only interesting at higher nominal load. The alternatives distinguish themselves through high performances even at part load.
In (b) the average value for different electric loads is used for different values of the return temperature. This has no significant effect on performance, because the effect is compensated by the water management, which neutralizes this influence. The relation of the different efficiencies to each other is clearly shown.
The container set-up shows the best results, with about 13% relative primary energy savings. For the original set-up and the one with the air heat exchanger, this is respectively 4% and 8%.

6.4 Comparison with other technologies

With the results of the analysis in Section 6.3.1, the performance of the AFC-based micro-CHP-system is now discussed in comparison with other technologies.
For this comparison only the original set-up is used, as this set-up is already proven in a field test [58]. Next to a comparison of part load behaviour, also the influence of supply temperature will be discussed.

6.4.1 Description of the systems used in this comparison

6.4.1.1 Load factor and external heating circuit of the AFC

To compare the alkaline fuel cell system with other technologies a load factor and return temperature, should be defined. The nominal electric current of the present system is set at $100A$. This value is used to determine the nominal load. The electric load factor is defined as the ratio of the generated electric power to the electric power at nominal load.
Based on an optimized heat integration (discussed at the end of Section 6.3.2), the nominal return temperature is set at $40°C$. At nominal conditions this corresponds to a heating system working on a $60/40°C$-regime, which is acceptable for building heating systems. To complete the thermal integration, the flow rate of the external circuit will be used as a control parameter for the water management. In this way a realistic comparison can be made with other technologies.

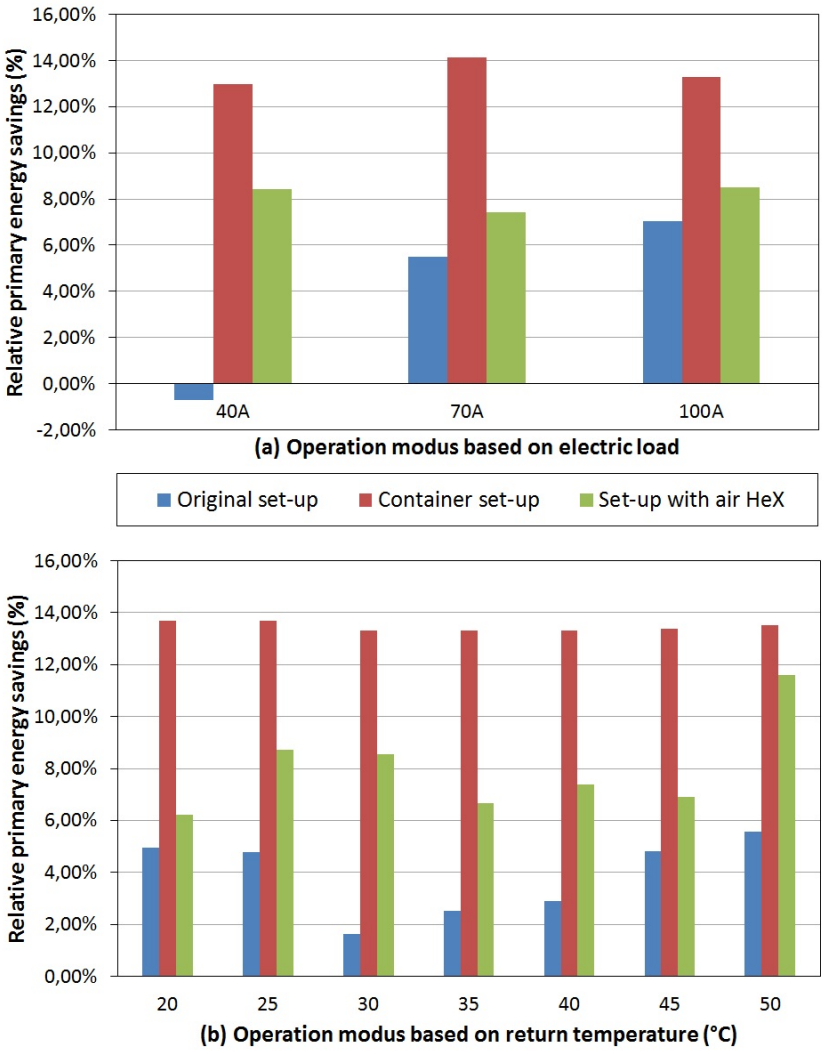

Figure 6.16: A comparison on energy performance of the three discussed set-ups, based on relative primary energy savings compared to a best possible alternative (See Section 4.2.4). The comparison is made for all operation modi.

6.4.1.2 Data for other technologies

The AFC-system is compared with other technologies suitable for micro-CHP. The used CHP technologies are listed in Table 6.6.

- Two gas engines running on natural gas: the Senertec Dachs [20, 27] and the Ecopower by PowerPlus. Their part load and temperature behaviour is discussed in [92] and combined with the total efficiencies in Refs. [20, 27]. In Ref. [27] also more data about the partial load performance of the Ecopower was presented.
- Two Stirling engines on natural gas: Solo and the Whispergen/Microtech. The part load behaviour is described in Ref. [27]. In [93] it is found Whispergen/Microtech is on/off regulated. Therefore, for the Whispergen/Microtech its part load behaviour is not considered, only its nominal working point is put at the different graphs, (See Figs. 6.17. 6.18. 6.19 and 6.20).
- A micro turbine on natural gas. The part load behaviour is discussed in ref. [94].
- A diesel engine. In ref. [95] the part load behaviour is simulated in Aspen for small CHP units. The part load behaviour is also presented in ref. [92], where similar results were presented.
- A hydrogen engine. In ref. [95] the hydrogen engine is compared with the diesel engine. These data were used to make a comparison.
- A PEM and a SOFC based fuel cell system. Next to a list of heat based micro-CHP-systems. the AFC-system is also compared to other fuel cell technology. Therefore. also a hydrogen fuelled PEM fuel cell and a gas filled SOFC are considered as alternative CHP-systems. The data used in this comparison are based on the PEMFC system evaluation made in Ref. [54] and on a techno-economic analysis of a SOFC-based micro-CHP in Ref. [52].

6.4.2 Part load behaviour

Figures 6.17, 6.18, 6.19 and 6.20 show a comparison of the part load behaviour of several micro-CHP-technologies. The data is based on a compilation of experimental and simulated work, described in the references listed in Table 6.6. In these references most efficiencies were based on lower heating values (See Table 6.6). In the figures these efficiencies were translated into efficiencies on higher heating value, allowing a more appropriate comparison, since the prime

CHP	P_e (kW)	η_e $(-)$	Q_{th} (kW)	η_{th} $(-)$	References
Gas engine (Senertec)	5.5	27.7%	12.5 – 15	63.6%	[20, 27, 92]
Gas engine (Ecopower)	4.7	24.7%	12.5	64.2%	[27]
Stirling (Solo)	2 – 9.5	26.8%	8 – 26	71.7%	[20, 27]
Stirling (Whispergen/ Microtech)	1.1	12 – 15%	6.6	80 – 90%	[20, 93]
Micro turbine	30	27%	54	49%	[94]
Diesel engine	6.53	31%	10.7	50%	[92, 95]
Hydrogen engine	6.50	30%	11.8	54%	[95]
PEMFC-system	4.8	48%	4.2	42%	[54]
SOFC-system	5.0	38%	6.8	52%	[52]

Table 6.6: Specifications (defined at LHV) and references of the micro-CHP technologies, used for comparison with the AFC.

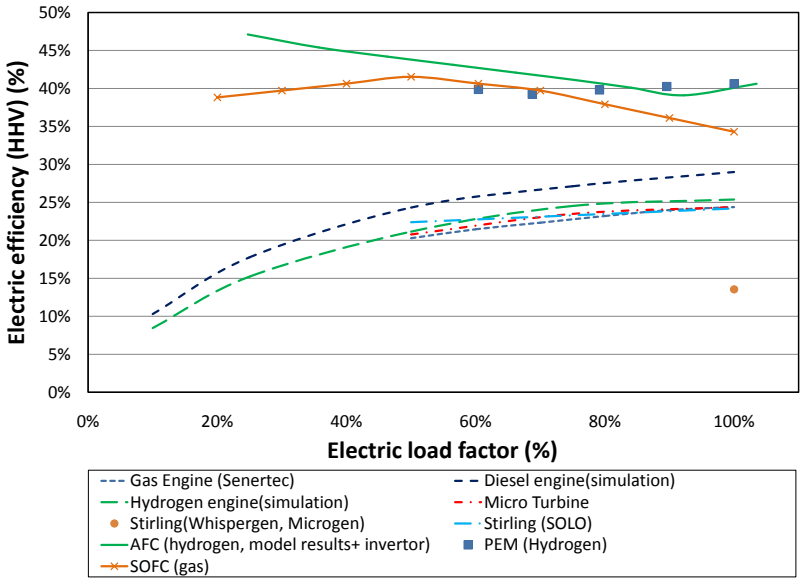

Figure 6.17: Comparison of electric efficiencies (defined at HHV) at partial load of several micro-CHP-technologies listed in Table 6.6.

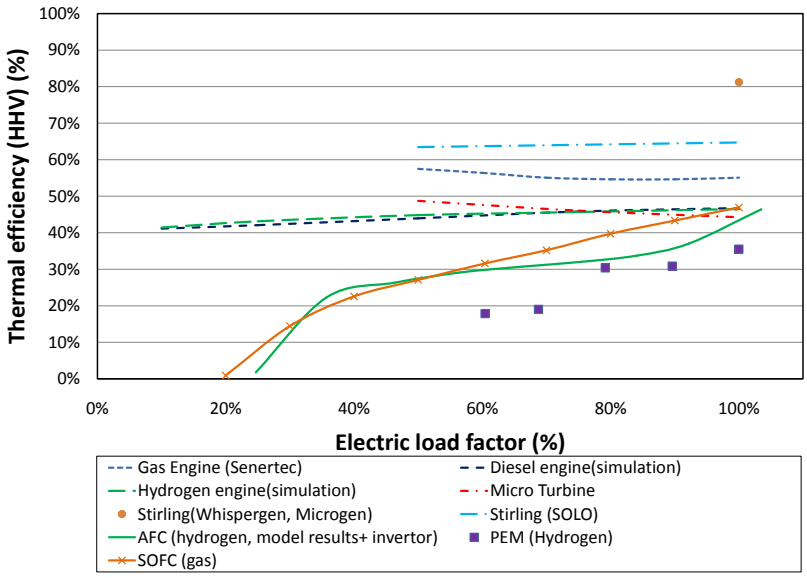

Figure 6.18: Comparison of thermal efficiencies (defined at HHV) at partial load of several micro-CHP-technologies listed in Table 6.6.

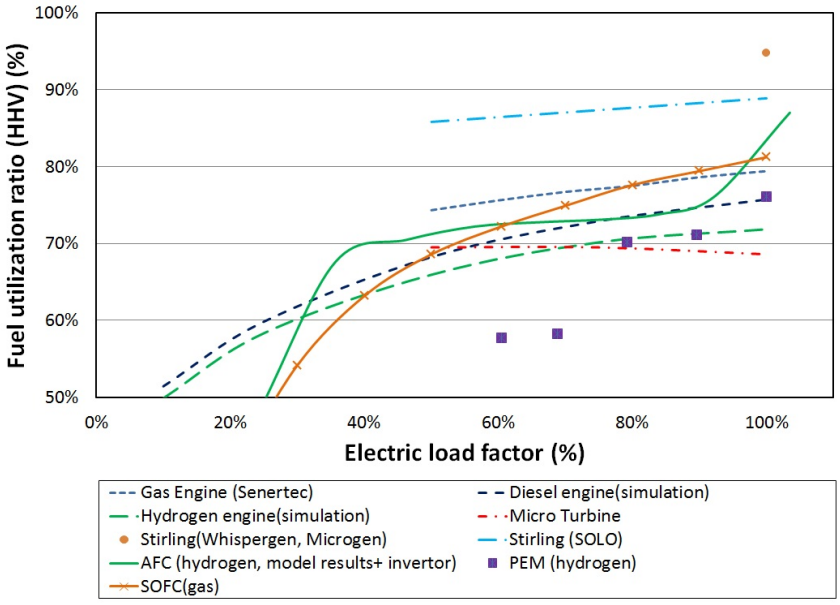

Figure 6.19: Comparison of fuel utilization ratio (defined at HHV) at partial load of several micro-CHP-technologies listed in Table 6.6.

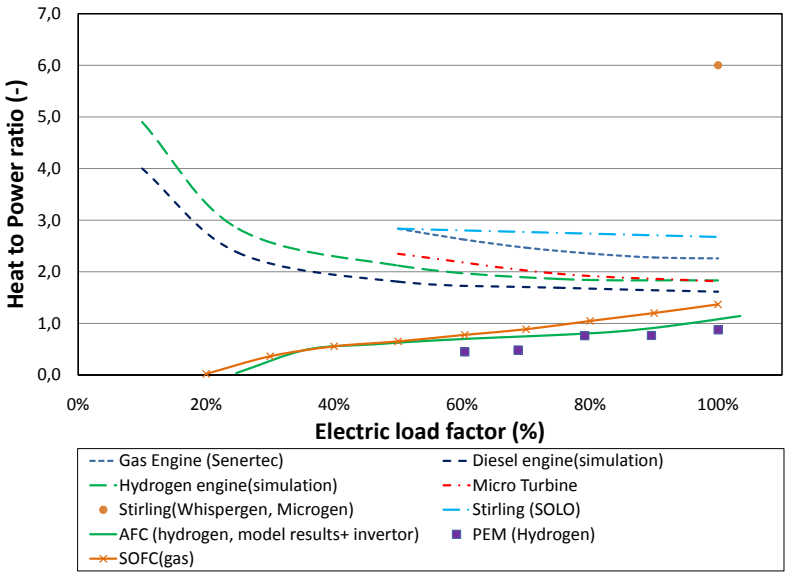

Figure 6.20: Comparison of heat to power ratio at partial load of several micro-CHP-technologies listed in Table 6.6.

energy source differs for the different options. Although a complete and honest comparison isn't possible for this reason, it is shown that the behaviour of fuel cell-based CHP-systems is completely different from the other technologies.
In Figure 6.17 is shown that the electric efficiency of the fuel cell-system rises at part load. This behaviour is completely different for all other technologies. Next to that the electric efficiency lies a lot higher than the others, which indicates the potential. It has to be taken into account however that hydrogen is used as primary energy source and that a reforming step could further reduce overall system efficiency, next to other system losses.
In Figure 6.18 is shown that the thermal efficiency is rather low, certainly at low load, due to a poor system design regarding heat losses.
The fuel utilization ratio reaches the same level of other technologies from a load factor of about 80%. This is shown in Figure 6.19. At smaller loads, the total fuel utilization is a lot smaller due to the poor thermal efficiency. This is compensated by a low heat to power ratio (See 6.20), which is interesting for applications with a low heating demand, like low energy buildings.
Comparing the fuel cell-based systems, it is shown that, in stationary conditions, the presented AFC-system is competitive with the PEMFC-based systems, regarding electrical performance. Besides this, AFC-systems have a higher thermal efficiency. This thermal performance is possible, because the circulating electrolyte facilitates the heat transfer from the reaction to the external circuit. SOFCs have to deal with higher operating temperatures, which results in a poor thermal efficiency at part load.

6.4.3 Influence of supply temperature

Within building applications, the supply temperature is highly dependent on the configuration of the heating system. Therefore, its influence is investigated.
The influence of supply temperature on system performance varies for different technologies. In Section 6.3.2 it is shown that supply temperature has a positive influence on electrical performance (about +3% for a temperature rise of 30^oC). A similar effect is to be expected for PEMFC, since the operating temperature of low-temperature fuel cells is strongly influenced by the supply temperature. For SOFC this effect is to be neglected. since operating temperature is hardly affected, due to the high fuel cell temperatures.
In [27] some heat based micro-CHPs were tested. It was shown that for a Stirling based micro-CHP, the electrical efficiency drops about 10% for an outlet temperature rise of 30^oC. For gas engines no influence is noticed in [27].
Regarding thermal efficiency, supply temperature has a negative influence for all systems. since less heat sources are available for useful applications and/or due to higher radiation losses.

Parameter	Value	Unit
Air Temperature	20	$^{\circ}C$
Air Humidity	0	$RH\%$
Ambient Temperature	20	$^{\circ}C$
Stack Temperature	50.76	$^{\circ}C$
Electrolyte flow rate	20	$\frac{kmol}{hr}$

Table 6.7: Overview of initial and ambient conditions during the dynamic simulations.

Parameter	Initial Value	Step Value	Unit
Air ratio	2.5	5	-
Electric Load	60	100	A(DC)
Flow rate sec.circuit	0.278	1	$\frac{l}{s}$
Supply temperature sec.circuit	41.25	60	$^{\circ}C$

Table 6.8: Overview of initial and new values for the different step response simulations.

6.5 Evaluation of system dynamics

As Section 6.4 shows, system efficiency depends on supply temperature and electric load. If a system is actually integrated for building applications, both load and supply temperature will change in time.
These changes are driven by the user characteristics. In this section the response (time) of the system to these changes is investigated. Also the response (time) to a change of setting for the different control parameters is evaluated. This evaluation is limited to the parameters. which were investigated and found useful in Section 6.3.1.
Therefore, the step response is evaluated for following parameters:

- Electric load; this depends on the user behaviour.
- Flow rate of the external heating circuit; this can be changed by a pump with a variable speed drive.
- Supply temperature; this can be changed by user behaviour and opening or closing of three-way valves at the side of the heat consumer.
- Air ratio; this can be changed by a fan with a variable speed drive.

The evaluation is based on the dynamic system model. described in Chapter 5.

Description of generic approach of each simulation

Every simulation is based on the same starting conditions, which are summarized in Table 6.7. The system is evaluated over 2000 seconds. in which the step takes place from second 1000 to 1001. The different step sizes for each variable are listed in Table 6.8.

6.5.1 Dynamic response to electric load switches

Figures 6.21 and 6.22 illustrate the step response to an electric load change from $60A$ to $100A$.
As shown in Figure 6.21(b), the output voltage will drop immediately, because the dynamics due to the capacitance in the Helmholtz double layer is not taken into account. This was already discussed in Section 4.4.2.
However, due to an increasing stack temperature the electrical efficiency will rise again, resulting in a slightly higher output voltage. This effect stabilizes after about 1000 seconds. The largest change is noticed in the first $750s$ (See Figure 6.21(a)). Initially, the load switch, will change the output electrolyte temperature. This change is stabilized after 500 seconds for the stack, but within the system it takes more time to stabilize, since the thermal inertia of the stack and of the electrolyte circuit enforce each other. This is best explained with Figure6.21(a).
Figure 6.21(a) shows that the stack temperature increases quickly at first. This is understandable, as the reaction takes place here and as more heat is produced at higher load (See Chapter 4). Due to a higher stack temperature also the electrolyte temperature will rise at the stack outlet. This will result in a higher overall electrolyte temperature.
Because of the thermal mass of the total amount of electrolyte, this temperature change is slower. As the electrolyte recirculates through the stack, this slowly increasing electrolyte temperature also has a positive effect again on the stack temperature, which increases further at the same rate as the electrolyte after the initial temperature jump.
As air temperature depends on stack and tank temperature, the air outlet temperature changes at the same rate.
Finally, Figure 6.22 shows the rising level in the electrolyte tank. As the production of reaction water is directly proportional to the electric load, the load increase initially results in a faster rising electrolyte level. However, the higher temperatures in the stack and the electrolyte tank. result in an increasing % of water vapour in the reaction water production. This effect is for this working point strong enough to result in a lower net water production. This can be deducted out of the ramp in Figure 6.22. In general the transient behaviour due to a changing load is gone after 2 minutes.

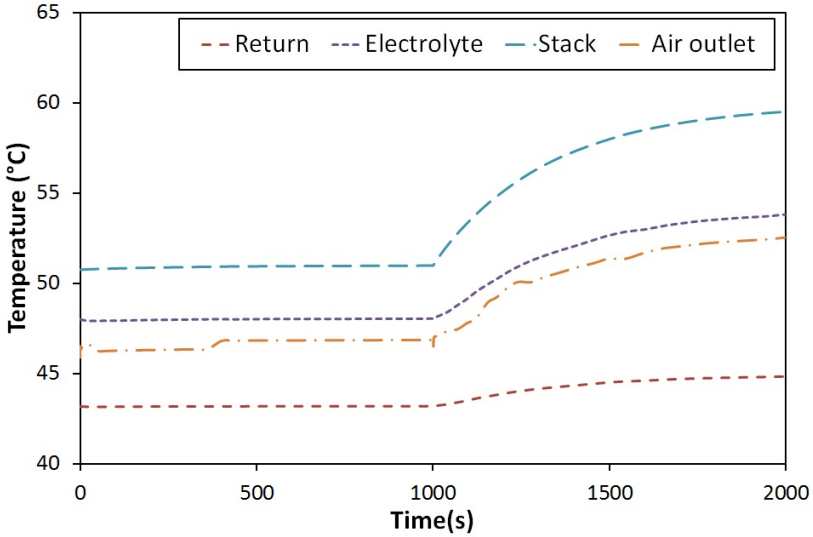

(a)

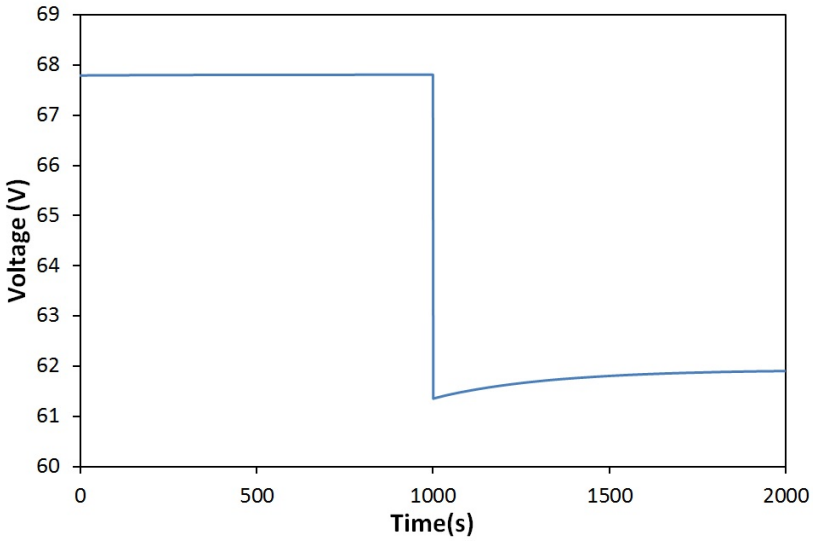

(b)

Figure 6.21: Step response to an electric load change for different parameters: a) Temperature changes for the external circuit (return). the electrolyte circuit. the stack and the air outlet: b) the output voltage.

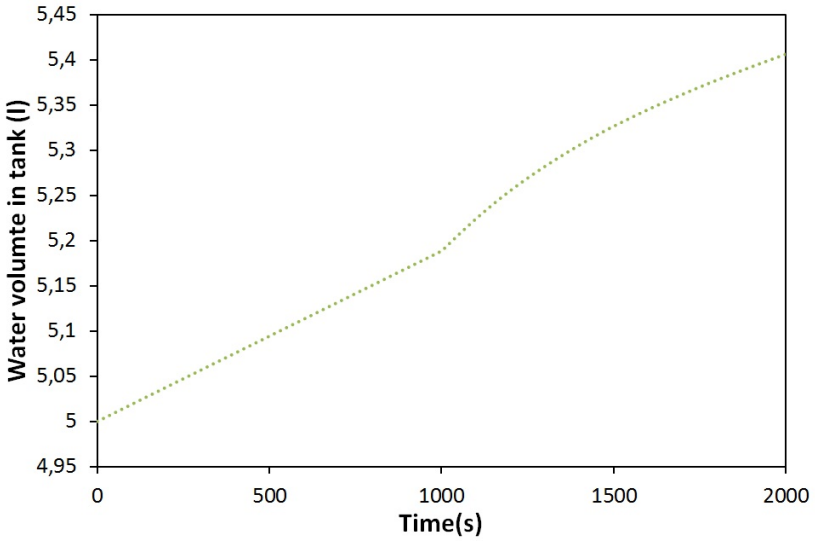

Figure 6.22: Step response to an electric load change for the water level in the electrolyte tank.

6.5.2 Dynamic response to changing flow rates of the external circuit

In Section 6.3.2 the usage of the flow rate of the external circuit as a control parameter is discussed. In this section possible transient behaviour due to this control strategy is discussed.
Figure 6.23 illustrates the step response to an increased flow rate from $0.278\,l/s$ to $1\,l/s$. The temperature of the external circuit is directly influenced, as the temperature change is almost 4 times lower now. The external circuit cools the electrolyte in the electrolyte tank. With higher flow rate this will lower temperatures in the electrolyte tank.
The effect is little due to the high thermal mass of the electrolyte and is more damped due to the heat exchange with the thermal mass of the stack. The air flow, which passes through this tank, has a low thermal mass. Therefore, the thermal response time of the air temperature is short.
This air outlet temperature is not only the result of a heat transfer from the electrolyte in the tank, but also of a mass transfer from this tank, due to evaporation. Together with its low thermal mass, this makes the air temperature more sensible for changes in the return temperature, compared to the electrolyte temperature.
Regarding water management and electric performance no influence is noticed.

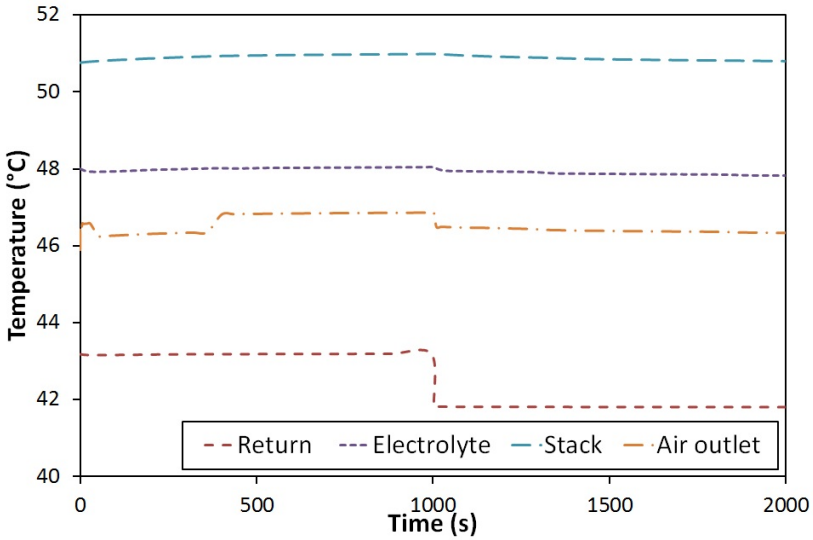

Figure 6.23: Step response to a changing flow rate of the external circuit for different temperatures: for the external circuit (return), the electrolyte circuit, the stack and for the air outlet.

This could be expected, since the temperature changes in the electrolyte flow and in the air flow are not substantial (less than $1°C$).

6.5.3 Dynamic response to a changing supply temperature

Similar to changes in flow rate of the external circuit, the temperature of the external circuit will influence the thermal and indirectly also the water management of the system.
In Figures 6.24 and 6.25 the step response of a temperature change from $41.25°C$ to $60°C$ is illustrated. Figure 6.24(a) shows a logical immediate response of the return temperature of the external circuit. It is clearly shown the temperature rise is first introduced in the electrolyte circuit and later affects stack temperature. Because of this the transient behaviour is not completely faded out yet after 1000 seconds. After about 15-20 minutes the transient behaviour is almost faded out and a new stationary regime sets in. As the air temperature depends on mass and heat transfer, the simulation of the air temperature is subordinate to some rounding errors, which explain the oscillations in the output air temperature.
Figure 6.24 shows that the voltage prediction changes similar with stack temperature.
The higher electrolyte temperature changes water management and results in a

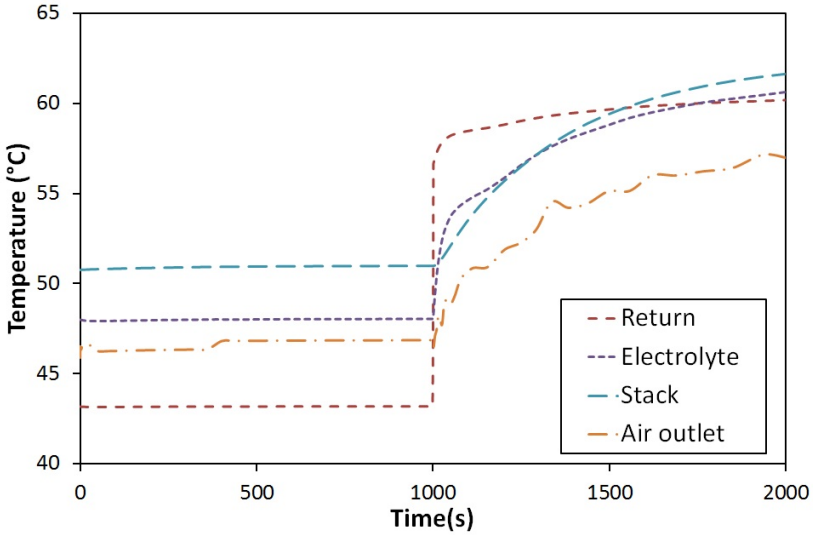

(a)

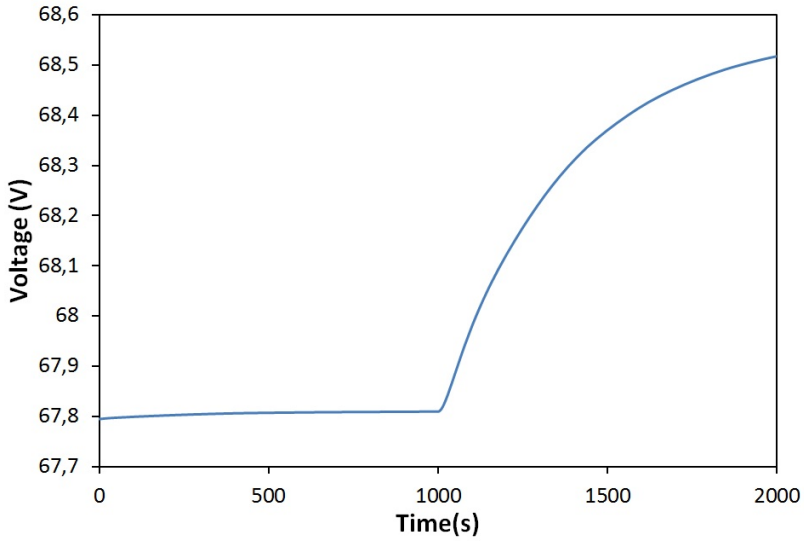

(b)

Figure 6.24: Step response to a temperature change in the external circuit for different parameters: a) Temperature changes for the external circuit (return). the electrolyte circuit. the stack and the air outlet: b) the output voltage.

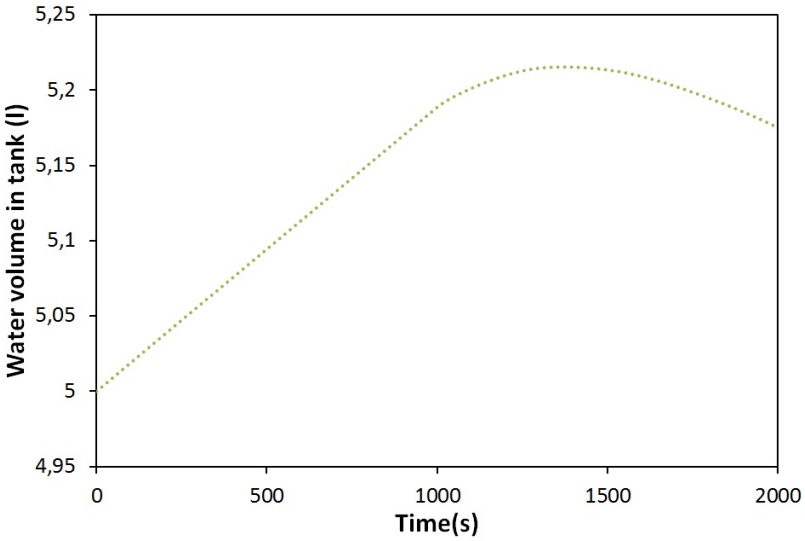

Figure 6.25: Step response to a temperature change in the external circuit for the water level in the electrolyte tank.

dropping water level. The response time of the water level is about 5 to 10 minutes.

6.5.4 Dynamic response to an increased air ratio

Next to a changing flow rate or return temperature from the external circuit. the air ratio is an important control parameter. This parameter was already used in the existing set-up, which was discussed in Chapter 3.
The size of the effect of a changing air ratio depends on outdoor conditions. In Figure 6.26 it is shown that a new equilibrium is found after 10 to 15 minutes. The largest changes, however, are fading out after 5 minutes. All parameters, both temperatures and voltage, show a similar behaviour.
Figure 6.27 shows the evolution of the water level at an increased, doubled air ratio. As expected a higher air ratio results in a decreasing net water production and thus slower rising electrolyte level in the tank. Almost no transient effects can be noticed here.

In general it can be said that after 15 minutes the system finds a new equilibrium. However, after 5 minutes the system is already near this new working point. A dynamic control strategy based on measurements has to take this response time into account in order to find a proper solution.

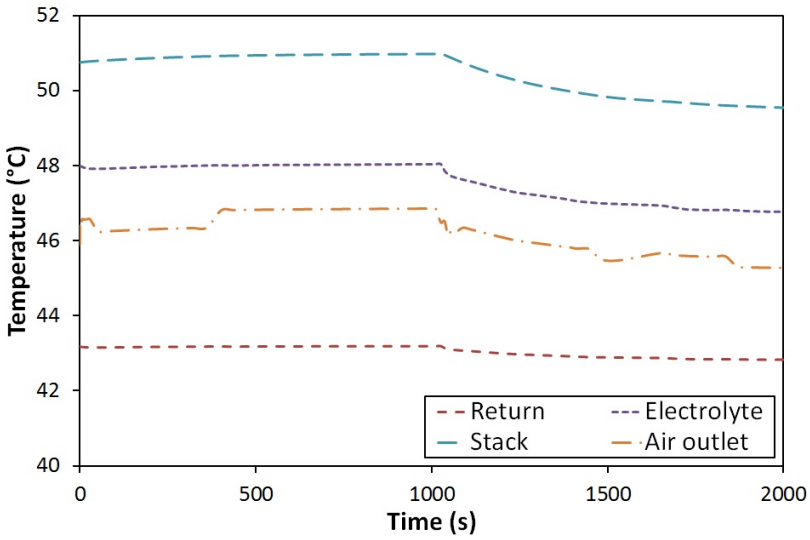

(a)

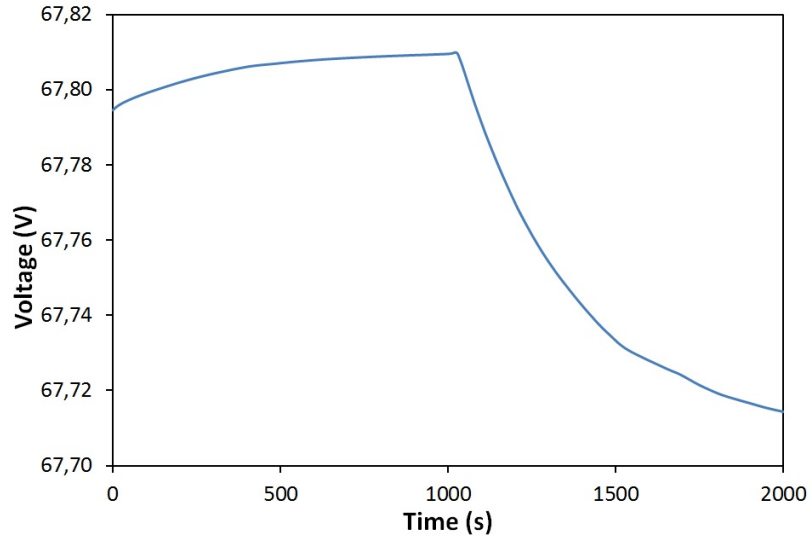

(b)

Figure 6.26: Step response to a changing air ratio for different parameters: a) Temperature changes for the external circuit (return). the electrolyte circuit. the stack and the air outlet: b) the output voltage.

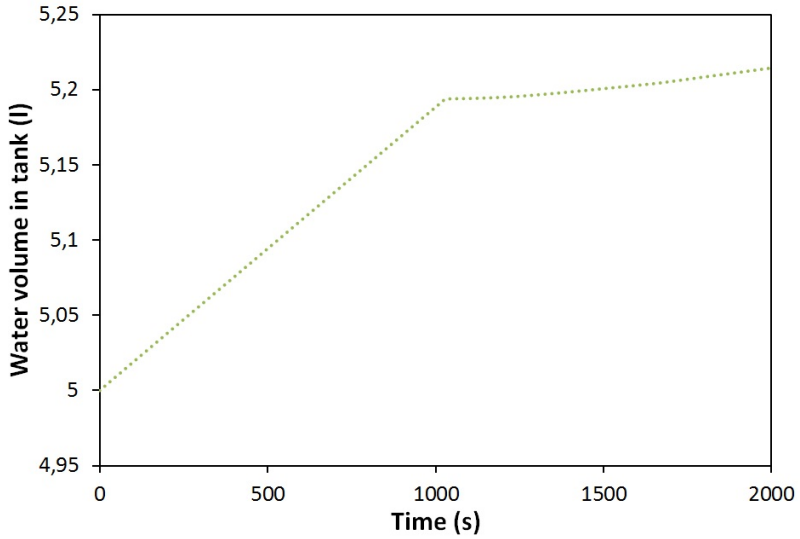

Figure 6.27: Step response to a changing air ratio for the water level in the electrolyte tank.

6.6 Closure

Stack-to-stack

Different stack to stack configurations are modelled and compared in order to optimize multi-stack systems. The differences are limited but a parallel air flow connection combined with a parallel electrolyte connection offers the best results, if the net water production is not considered in the evaluation. Overall, a complete parallel connection of all different flows (PPP) offers the best results based on the simulations, but since the net water production can be addressed with an appropriate water management, the present solution with a(dPP)-configuration is a good choice, since it has some advantages regarding gas management, which could not be evaluated in the simulations.

Set-up

Next, different set-ups for an AFC-based micro-CHP system are modelled and analysed in order to optimize each set-up:

- the original set-up, which is built as a proof of concept [58]
- an advanced concept with an additional heat exchanger to recover heat from the output, which is used to preheat the input air.

- an indoor solution, by placing the original set-up in an insulated and ventilated container

For all three set-ups, purge efficiency and inverter efficiency have a direct impact on performance. which is proportionally linked for the outdoor solutions. The container set-up offers a small heat recovery on the inverter losses. but this isn't sufficient to give a low priority to inverter efficiency.
The efficiencies of the pump and fans used in the set-up have little impact on performance. Cheap and standardized pumps are still acceptable and will not affect performance significantly. The effects of the evaporation rate on water management and on performance compensate each other. This statement is more applicable for the outdoor solutions.
For the container set-up the insulation thickness is analysed. It has no significant influence on the water management and its effect on performance is especially noticed at low outdoor temperatures. The insulation thickness can be used for further improvement of the container set-up.
A last system parameter was the effectiveness of the heat exchanger. This parameter has a significant impact on thermal performance and water management. Since effectiveness is also determined by the flow rate of the external circuit this last one will be used as a control parameter for water management. Other control parameters, such as air ratio or electrolyte flow rate are less appropriate for this. For the container set-up a minimum air flow rate is set to ensure a safe operation.
Based on this analysis all set-ups are energetically compared after implementation of a control strategy ensuring stable water management. It is shown that the container set-up offers the best results, 13% primary energy savings followed by the set-up with the heat exchanger, 8% and the original set-up, 4%.

CHP-characteristics in relation to other technologies.

A comparison is made with other micro-CHP-technologies. It is shown that for buildings with a decreasing heat demand and increasing electricity demand a fuel-cell based micro-CHP has better results (See also Chapter 1). These results are also influenced by the temperature of the heat distribution system. Compared to a PEMFC based system the AFC system has a better thermal performance and similar electrical performance in stationary conditions.

System dynamics

Looking at the dynamic behaviour a response time of 5 minutes has to be taken into account for quick changes in settings, before its effect starts fading out. This dynamic behaviour is similar to other micro-CHP technologies like engines.

7 Integration in buildings

In Chapter 2 a model of an AFC stack is developed. In Chapter 5 the stack model was integrated in a complete system set-up. In previous chapter this system set-up is used to evaluate general system behaviour of an AFC-based CHP-system.
These insights are used to integrate the system within a building environment. This chapter presents a general lay-out, how the system is integrated within the energy management in a building. An overview is given of the used control strategy in order to obtain a stable and energy efficient CHP-system.
Next to this integration strategy itself, it is also discussed how the model is manipulated to deal with this increased complexity.
With the results of this chapter, it will be possible to perform a case study, which will be discussed in Chapter 8.

7.1 Integration of CHP-system in a heating system of a building

Due to system complexity, discussed in previous chapters, the integration of the AFC-system for CHP-applications is expected to require a complex control strategy. However, this also depends on the purpose of the application and the integration strategy:

- How is the CHP-system integrated within the energy installation of the building ?

- Which goals towards autonomy are set for the CHP-system, since both electricity, E_{demand} and heat demand, Q_{demand} fluctuate and depend on user behaviour.

Therefore, first the boundary conditions towards energy autonomy are discussed, after which the physical integration and organization of control are discussed.

7.1.1 Boundary conditions towards energy autonomy

Electrical autonomy

With the electricity-to-heat ratio on the demand side varying in time, it is necessary to provide electrical storage to allow a shift between production and consumption of electricity, as a CHP-unit is not able to fluctuate its ratio quickly. Compared to other CHP-systems, fuel cells are able to shift their heat to power ratio very rapidly within a range from by changing position (load) on the polarization curve [96]. For the investigated system, this ratio can be changed in a range from 0% (or even negative) to about 100%, as illustrated in Figure 6.20.
Nevertheless, electrical storage is also necessary for fuel cell based systems, as this ratio defines electrical and thermal power output and a strong alternation of electric load shortens fuel cell lifetime.
For most CHP-systems this 'storage' is found in the grid. If the CHP produces more electricity than is instantly consumed, this electricity is put on the grid. If the electricity production is too low, electricity is bought from the grid. Another way to store electrical energy is in batteries and/or ultracaps. These can be complementary to CHP-units regarding energy autonomy [97]. Besides this, they are complementary to fuel cells in a number of applications [96, 98–100] and they even enlarge fuel cell lifetime as they stabilize the load drawn from the fuel cell [101].

Within the present Belgian context, for small electricity production units below $10kVA$ no costs are charged based on the actual use of the own produced electricity. Recently, is announced that in 2013 there will be a charge fee requested for these small production units. However, this fee will be based on yearly production and not on the actual grid utilization. In the future with smart energy meters installed, it is possible this will be charged instantly. However, how this will be organised is not clear, since from a general approach CHPs are often seen complementary to other distributed energy production units like photovoltaic solar panels at district level [60].
In this perspective Baeten et al. [102] developed a tool to evaluate electrical and heating systems. So it is also possible that a bonus can be earned with a temporary over production. These concepts are now tested in large-scale demonstration tests [103]. Next to that, the translation of these concepts into technically feasible

economic models, is topic of a large amount of conceptual studies [104].
It is clear that this time dependency can become a drive for future economic optimization of CHP-operation, but because of the wide variety of economic models and different opinions, it is chosen to consider only the present economic model. In future research the optimization in the context of these new economic models can be explored.
Nevertheless, for production units larger than $10\,kVA$ this time dependency is already taken into account. For these cases, a production fee can sometimes be obtained for the electricity put on the grid. However, this fee is about 4 times lower than the costs charged for electricity taken from the grid.
For larger CHP-units an optimized control regarding dynamics of the own electricity consumption becomes profitable, but for smaller CHP-units it is often chosen to install a capacity lower than $10\,kVA$ or a capacity lower than the own base load consumption. In this way no attention needs to be paid to the own electricity consumption.
Therefore, in a first approach the micro-CHP is coupled with the grid and no attention is paid to the own electric profile. The yearly consumption however is still taken into account to calculate financial feedback.

Thermal autonomy

In normal operation mode and from a primary energy point of view, CHPs are heat driven as electricity can be easily transported by the grid, but heat has to be used on site.
In Chapter 6, the complexity and sensibility of the system regarding a stable water management was discussed. It is shown that air ratio, electric load, temperature and flow rate of the cooling circuit all influence water management. As user behaviour fluctuates significantly, it is best that the production and consumption side are not directly linked, but that a storage capacity damps changes in user behaviour and gives the AFC-based CHP-unit some time to react and to provide the requested heat demand.
Especially for the heat demand some time has to be taken into account to achieve nominal operation. For this reason, a buffer is provided, which can be foreseen with an auxiliary burner to compensate for peak demand.

The complete set-up and building integration is presented in Figure 7.1.

7.1.2 Description of the building integration of the CHP-system

As shown in Figure 7.1, hydrogen fuel, Q_{Fuel}, enters the CHP-system, $Q_{Fuel,system}$, and the auxiliary burner, $Q_{Fuel,aux}$. Part of the hydrogen entering the CHP-system will be lost, due to purging. In Chapter 6, the purge efficiency,

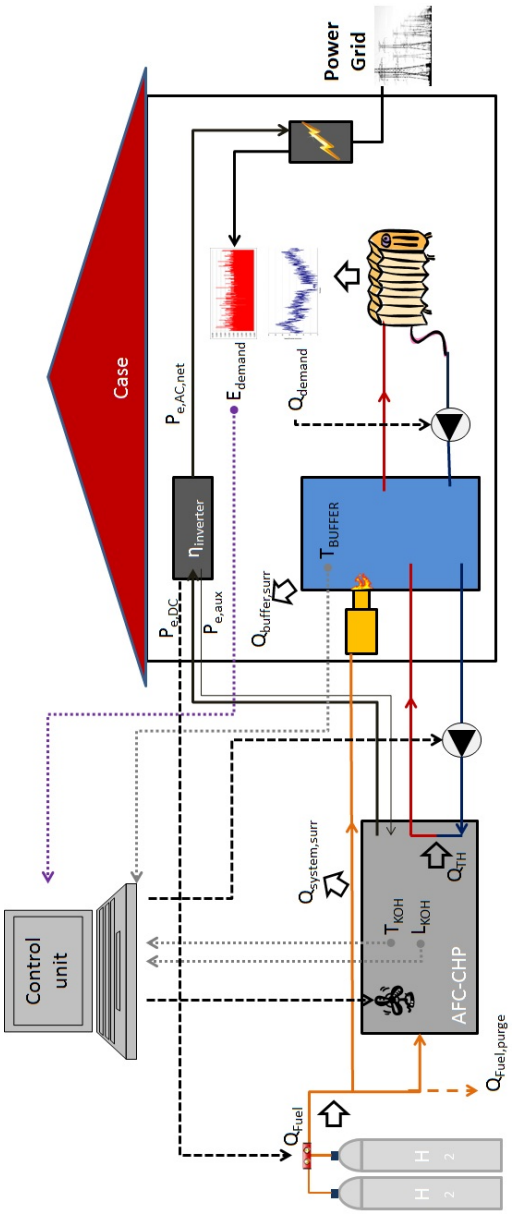

Figure 7.1: General set-up for integration of an AFC-based micro CHP-system in a building, with indication of different mass flows, energy flows, control input and output parameters.

η_{purge}, was defined to take these losses into account, Eq.(6.3).

The hydrogen used in the CHP-system is, as discussed earlier, directly linked to the DC-current drawn from the system. Together with the stack voltage, this results in the generated DC-Power, $P_{e,DC}$, which enters the inverter. This inverter converts the DC-electricity in useful AC-electricity, $P_{e,AC}$, which can be used in the building or be put on the grid. Not all DC-power will be converted into useful AC-power due to conversion losses in the inverter, $\eta_{inverter}$, and power needed for auxiliary equipment, $P_{e,aux}$, in the CHP-system.
The heat generated in the CHP-system in the electrolyte flow, which is stored in the electrolyte tank, is cooled away into a secondary circuit which is connected to the buffer tank. The flow rate in the secondary circuit is controlled by a pump, which is commanded by the general control unit. Next to this flow rate also the fan which ensures the necessary air flow in the system is directed from this control unit.
As a result from the analysis in Chapter 6, both control parameters are regulated in order to keep the water management in the AFC-based CHP-system under control. For this, the temperature, T_{KOH} and level, L_{KOH} of the electrolyte in KOH-tank are monitored by the control unit. An overview of all control parameters which are monitored or regulated by the control unit are listed in Table 7.1.

As can be deducted out of this Table, not only the water management is controlled by this unit, but also the heat demand of the building. The heat demand is kept under control by monitoring the temperature in the buffer tank. The buffer tank is characterized by its size or volume, $V_{buffertank}$ and its heat loss coefficient, $hA_{buffertank}$, which depends on size of the buffer tank. Table 7.2 presents a list of some used buffer sizes in the simulation and their corresponding heat loss coefficient.

When the temperature is too low in the buffer tank, the CHP-system will be activated to heat up the tank by the secondary circuit. The heat demand of the building will drive the pump in the tertiary circuit to enable a flow rate drawing hot water out of the tank and putting water into the tank, which is cooled by the heat load. If the temperature in the buffer drops below a certain set point, it is possible to generate additional heat by the auxiliary burner. How this is implemented in the control unit is discussed in the following section.

7.1.3 Control strategy

Although every control strategy is bound to the limitations discussed in Section 7.1.2, a numerous amount of variations is possible within these boundaries.
In general, two strategies are most know within CHP-control:

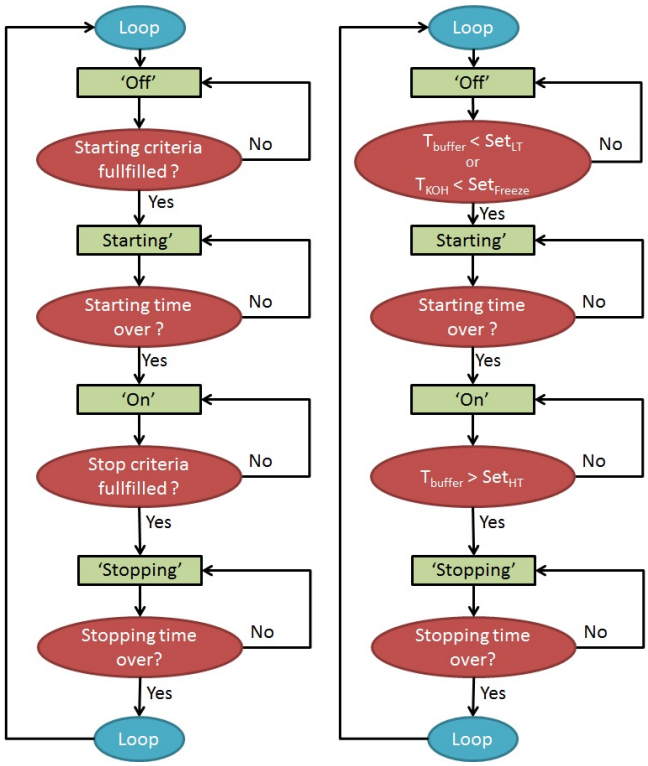

(a) a (b) b

Figure 7.2: a) General flow chart, representative for all control strategies:change of operation modus is presented within a loop. The decision criteria depend on specific strategy. In b) the decision criteria are specified for the heat based control strategy.

Variable	Symbol	Link with control unit (C.U.)
Temperature electrolyte	T_{KOH}	monitored by control unit
Electrolyte level in tank	L_{KOH}	monitored by control unit
Temperature in buffer tank	$T_{buffertank}$	monitored by control unit
Flow rate sec.circuit	$\dot{m}_{sec.circuit}$	regulated by control unit through adaptable pump speed
Electric Load	I_{DC}	regulated by control unit with inverter
Air ratio	n_{air}	regulated by control unit by fan speed
Flow rate tert.circuit	$\dot{m}_{tert.circuit}$	based on heat demand
Electricity demand	$P_{e,demand}$	monitored by control unit

Table 7.1: Overview of control parameters, which are used to organize a stable operation of the AFC-based micro-CHP within a building applications.

Buffer size $V_{buffertank}(Liter)$	Heat loss coefficient $hA_{buffertank}(W/K)$
300	1.4
500	1.9
100	0.9

Table 7.2: List of buffer sizes and their corresponding heat loss coefficient.

- The first strategy is based on an optimization of primary energy savings. For this the results of the evaluation made in Chapter 6 can be used. In this chapter the influence of different control parameters on primary energy savings was investigated. The results of this evaluation are translated into a simple but transparent **heat based control strategy**.
- As the self-consumption or electrical autonomy will become important for economical optimization, as discussed earlier, also an **electricity based control strategy** can be proposed. However, this strategy is not discussed any further in this book, which is limited to a discussion on primary energy savings at building level. Nevertheless, in future research, also this strategy could be implemented to get an idea of the possibilities and limitations of the AFC-based CHP-system in actual cases.

The actual optimization is case dependent and is probably situated between these two strategies, combining the best of these different approaches. For this, future research is necessary, whereas the model can be used to evaluate these more complex control strategies within a more complex environment.

However, the methodology to implement such a control strategy is in general

Set point specification	Symbol	Typical value
Lower temperature bound in the buffer tank	Set_{LT}	$40°C$
Higher temperature bound in the buffer tank	Set_{HT}	$55°C$
Bound for return temperature in tert.circuit	Set_{RT}	$25°C$
Safety temperature to prevent freezing	Set_{Freeze}	$7.5°C$
Lower electrolyte temperature bound for the heating mode	Set_{TK}	$30°C$
Extra temperature set point in buffer tank	Set_{B+}	$50°C$
Lower bound electrolyte level	Set_{NivL+}	$4.9l$
Upper bound electrolyte level	Set_{NivH}	$5.1l$

Table 7.3: List of used set points within the heat based control strategy and their most common values.

similar for all possible strategies. Therefore, first a brief description is given of the general lay-out of such a strategy in order to introduce some terms and definitions. Later, as an illustration, the heat based control strategy is elaborated and specified, since this strategy will be used in the elaborated case studies, presented in Chapter 8.

General lay-out for control

Every control strategy can be defined based on the flow chart shown in Figure 7.2(a). First, a new term is introduced, which is the modus of operation. The modus of operation determines the state of the system. This state can be either on, off, starting or stopping. Based on the monitored values by the control unit and the used control strategy, this state of operation is changed into a new one, as shown in Figure 7.2(a). As start-up and stopping procedure take about one minute, this state or modus of operation is re evaluated every 60 seconds.
As an illustration this will be specified for the first of the two most known strategies within CHP-control:

Heat based control

The decision criteria to change the modus of operation depend on control strategy are based on the value of the control parameters, monitored by the control unit. These are shown in Figure 7.2(b). Next to that, the translation of this state into the settings for the different regulated control parameters can vary. Therefore, a description is given how each modus is implemented and which decision criteria are used to switch to another one.

Modus = on
First modus which is discussed is the modus 'on'. The system will remain in this

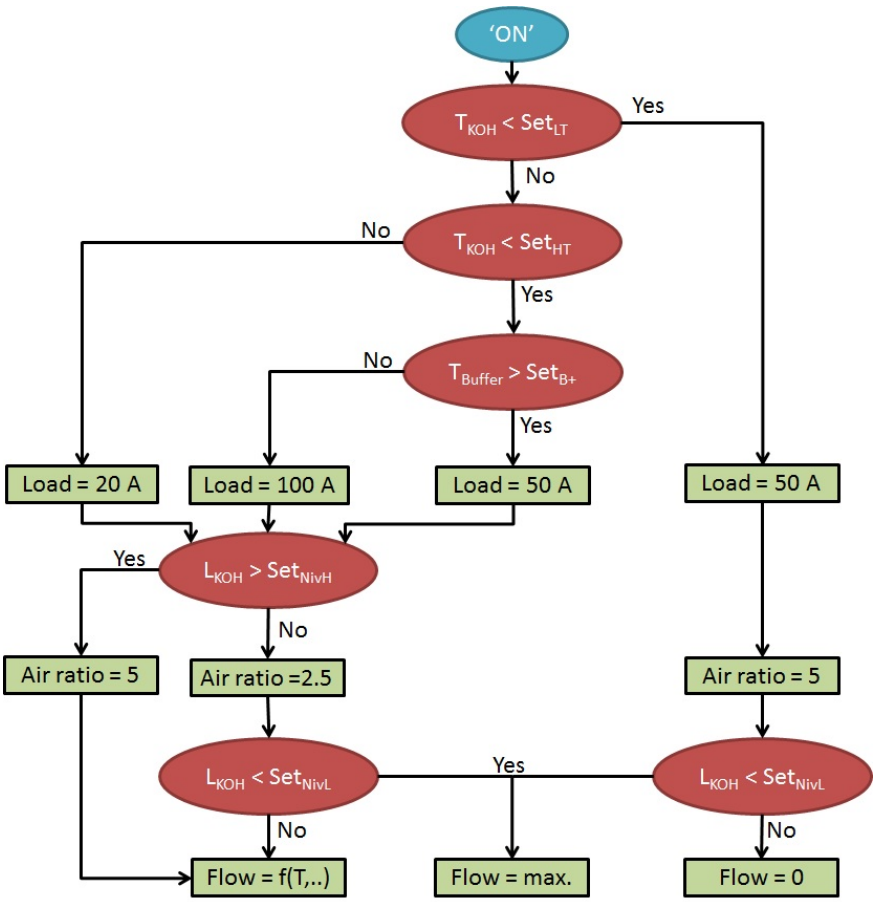

Figure 7.3: Flowchart to define load, flow rate of the secondary circuit and air ratio for the 'ON' modus by the control unit.

modus as long as the temperature within the buffertank, $T_{buffertank}$ is below a first set point value, Set_{HT} (See Table 7.3). If the temperature exceeds this value, the modus is changed to 'stopping'.
If the modus is 'ON', load, defined by DC-current, flow rate in the secondary circuit and air ratio (or air flow rate) are set by the control unit. Figure 7.3 represents the decision criteria to manage these control parameters.
A first point of attention is the electrolyte level. To maintain the water management a function is developed based on the analysis in Chapter 6 to determine a flow rate of the secondary circuit at which the water management is stable. This flow rate is based on temperature in the buffer tank and on electric load and is valid within the nominal range of operation. To avoid negative flow rates also a minimum is set. If the electrolyte level exceeds the upper boundaries, despite this measure, the air ratio will be doubled to increase evaporation.
At high electrolyte temperatures, it is possible that the lower boundary electrolyte level will be reached within a certain time. In this case the load is set to a minimum to generate less heat. However, if the lower limit for the electrolyte level actually is trespassed, the secondary flow rate is maximized to increase cooling of the electrolyte. This strategy is translated into a flowchart (See Figure 7.3).

Modus = off, starting or stopping
A similar approach is used to define load, flow rate of the secondary circuit and air ratio (or flow rate) for the modi 'Off', 'Starting' and 'Stopping'. This is illustrated in Figure 7.4.
In these modi, load is always set to zero. For air ratio the system shifts to a minimum air flow rate at starting modus, to prepare actual start-up. At stopping modus the air ratio drops to zero, at this point the system shifts to Off modus.
Depending on the temperature difference in the buffer tank and the electrolyte tank, in 'off' and 'stopping' modus the electrolyte tank is cooled to heat up the buffer tank, which is directly connected to the heat load. At starting mode it is possible to preheat the electrolyte tank with heat from the buffer tank. In this way the heat loss is limited at stopping or off modus as the buffer is better insulated and always placed indoors. At start-up, the system is able to get faster to its nominal working point.
The different set points for temperature and electrolyte level at which the control unit takes action are listed in Table 7.3.

7.2 Integration in model environment

In Section 7.1 the integration of the AFC-based micro-CHP-system is discussed. This discussion included the boundary conditions, physical integration and implementation of a control strategy.

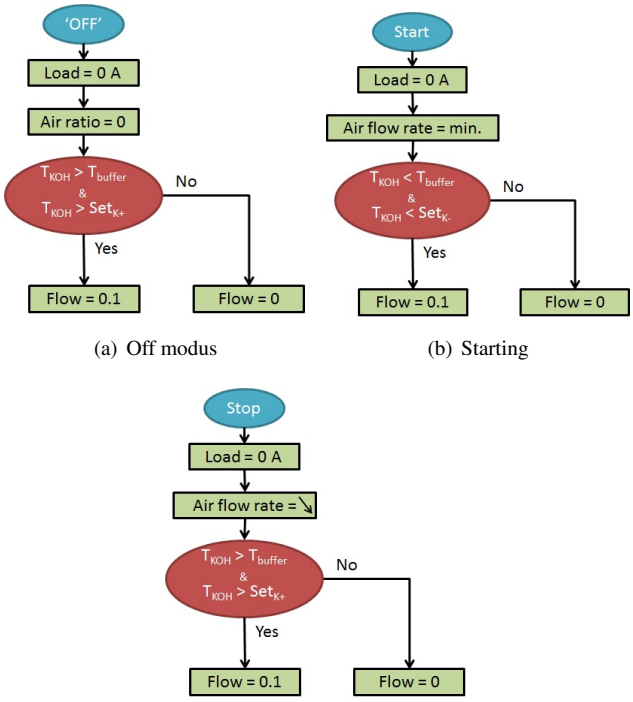

(a) Off modus (b) Starting

(c) Stopping

Figure 7.4: Flowcharts to define load, flow rate of the secondary circuit and air ratio (flow rate) for a) Off modus b) Starting modus and c) Stopping modus.

The model built in Chapter 5 can be used to evaluate the performance of the AFC-based CHP-system within a case study. However, some practical issues about this model integration need to be solved:

- Due to the model complexity, the integration of different components and the large number of variables, simulation time exceeds reasonable limits to evaluate a year performance.
- Next, it is also necessary to implement the building aspects and control strategy of the model.
- Without a proper control strategy the model exceeds not only the physical limits of the system. In some cases also the limits of operation are exceeded in which the model is valid. Nevertheless, these states exist in practice. Therefore, a model extension needs to be included to calculate and predict the behaviour in these points.

Consequently, to reduce complexity a model simplification is executed based on regression analysis and model selection. Next to that the missing components and control strategy are implemented in the Matlab environment in order to obtain results for a whole year simulation of a case study.

7.2.1 Model adjustments and simplifications based on regression analysis and black box modelling

In this section it is discussed how the model is adapted to integrate the complex model of the AFC-based CHP-system into a whole-year simulation.
First, a general approach is discussed, after which the necessary regression analysis is discussed and translated into a simplified model.

7.2.1.1 Determination of the general lay-out of a simplified model for the AFC-based micro-CHP-system

Most of the complexity is found in the fuel cell model. It is chosen to strongly simplify this part of the system. The electrolyte tank with the integrated heat exchanger is not simplified as this part directly interacts with the heating system.
Looking at the fuel cell stack model all relevant in- and output variables are listed in Table 7.4. These variables are only relevant if they can change during system operation. Table 7.4 shows that some variables can be excluded from the regression analysis. This is acceptable because either they are kept fixed during system operation, or they can be assumed to change little and therefore have a minor influence on operation or because their value is of no importance within the system.
Analysing the model developed in Chapter 2, in general it is built upon a mass and

Description	Type	Importance
Air flow rate	In- and output	Both relevant
Air temperature	In- and output	Both relevant
Air humidity	Input	Only little variations at inlet, due to lower temperature assumed to be zero
Air humidity	Output	Outlet relevant for evaporation in tank
Electrolyte flow rate	Input	Fixed within system set-up
Electrolyte flow rate	Output	Relevant for water management
Electrolyte temperature	In- and output	Both relevant
Hydrogen flow rate	In- and output	Both relevant
Heat loss to surroundings	Output	Relevant
Stack temperature	Input	Only relevant in relation to heat to stack, because of the dynamic effect.
Heat to mass of the stack	Output	See previous remark
Electricity production	Output	Relevant

Table 7.4: List of in- and output variables of the fuel cell stack and their relative importance within the system model.

energy balance. Next to this, the model predicts water and thermal management. The model complexity is mainly due to this prediction of output temperatures and water (vapour) content. For this the different layers, each with mass and energy balance, and the gas diffusion equations are introduced, increasing the number of variables and equations.
Therefore, the simplified model will be built upon:

- an overall mass balance for the stack, not for every layer separately.
- regression based functions to predict water management, directly based on input variables
- a function (based on regression) to determine a linear relation between the different output temperatures.
- an overall energy balance for the stack, not for every layer separately.

In this way the model equations are linearised. Moreover, if this order is respected in the simulation, no iteration is necessary to obtain model results.

Summary of equations

Mass balance

$$F_{O_2,consumed} = \frac{1}{2} \cdot F_{H_2} \tag{7.1}$$

$$F_{H_2O,production,total} = F_{H_2} \tag{7.2}$$

$$F_{H_2O,production,total} = \left(F_{KOH,out} - F_{KOH,in}\right) + F_{vap.,cat} + F_{vap.,an} \tag{7.3}$$

$$F_{anode,out} = F_{vap.,an} \tag{7.4}$$

$$F_{Air,out} = F_{Air,in} - F_{O_2,consumed} + F_{vap.,cat} \tag{7.5}$$

Next to these molar flows, current is calculated with the law of Faraday, Eq.(2.45).

Water management: function based on regression analysis
Out of the mass balance the total water production can be calculated, Eq.(7.2). However, for a complete prediction on the water management there are still two degrees of freedom, Eq.(7.3). For this, two functions based on regression analysis, Eqs.(7.7) and (7.6) are posed as an alternative and simplification for the equations in the model presented in Chapter 2.

$$F_{KOH,out} - F_{KOH,in} = f_1\left(x_{input,i}, \Theta_2\right) \tag{7.6}$$

$$F_{vap.,cat} = f_2\left(x_{input,i}, \Theta_1\right) \tag{7.7}$$

A function will be determined for the prediction of water content in the output air flow, Eq.(7.7), and for the prediction of the net (liquid) water production, Eq.7.6. To specify the parameters, Θ_i, and shape of these functions a regression analysis is discussed in Section 7.2.1.2.

Thermal management: assumptions and regression based function
With the equations from the mass balance and the water management all flow rates are specified and characterized. The last variables which need to be solved are the temperatures of these mass flows. At stack level three output mass flows can be specified. Taking into account one of these temperatures can be calculated out of the energy balance, two degrees of freedom need to be solved.
The molar flow out of the anode gas chamber, $F_{anode,out}$, is negligible, as it only represents the water vapour in the anode gas chamber, which is removed by purging. Its temperature is assumed to be at the same value as the output air flow, $F_{Air,out}$, Eq.(7.8).

$$T_{anode,out} = T_{Air,out} \tag{7.8}$$

$$T_{Air,out} = f_3\left(x_{input,i}, T_{KOH,out}, \Theta_3\right) \tag{7.9}$$

For this output temperature, $T_{Air,out}$, a function (Eq.7.9) is developed, specifying a linear correlation with the output electrolyte temperature, $T_{KOH,out}$. This linear correlation was already noticed in Figure 3.7 in Chapter 3. In Section 7.2.1.2 this correlation will be further specified.

Energy balance
Finally, with the determination of the output electrolyte temperature, $T_{KOH,out}$, all remaining output flows can be calculated. Next to the three output mass flows, there are also a number of energy flows present: the electric power generated by the stack,$P_{e,DC}$, the heat loss to the surroundings, Q_{surr}, and the heat dissipated in the thermal mass of the stack, Q_{stack}.
The electric power output can be calculated out of the voltage and current drawn from the stack. The voltage prediction is still based on the same empiric formula, developed in Section 2.3.3.7. Also for the calculation of the heat flows, both Q_{surr} and Q_{stack}, no changes are made.
As can be seen in Chapter 2 all these energy flows only depend on the same remaining variable, $T_{KOH,out}$.
Finally, this temperature can be determined by the energy balance of all mass and energy flows into and out of the stack. However, because the balance is sensitive to small distortions, which may appear due to the approach based on regression, it is chosen to determine electrolyte temperature also based on a regression function.

$$T_{KOH,out} = f_4\left(x_{input,i}, \Theta_4\right) \tag{7.10}$$

7.2.1.2 Regression analysis to predict thermal and water management

As discussed in the previous section, it is necessary to find a linear correlation between the input variables and some of the output variables. The original model is used to examine the influence of the relevant input variables (See Table 7.4).
These input variables can be calculated from the parameter set listed in Table 7.5. Therefore, the original model is used to examine the influence of these variables and combinations of variables on the different output variables.
The output variables, for which it is useful to define these new functions, f_1, f_2, f_3 and f_4, are examined in following discussion.

The net water production, f_1
As can be seen in Figure 7.5(a) a clear positive linear correlation between load and net water production can be observed. However, at higher loads the difference between the upper value and lower value grows a little, which is an indication that this linearity also depends on other variables.
Figure 7.5(b) shows a similar pattern for the negative influence of the air ratio on net water production and Figure 7.5(c) illustrates a negative linear correlation,

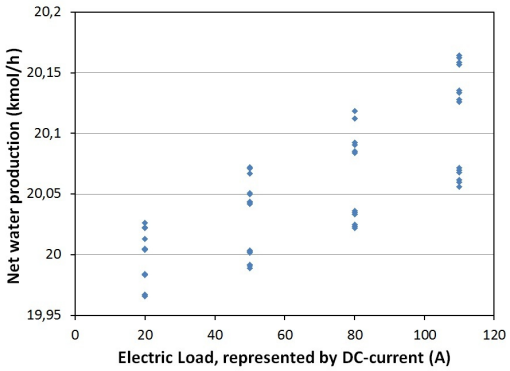

(a) $f_1(x)$

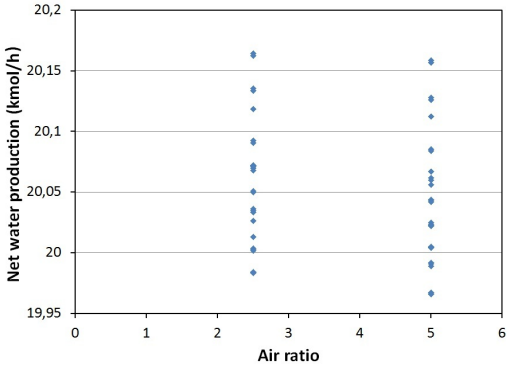

(b) $f_1(y)$

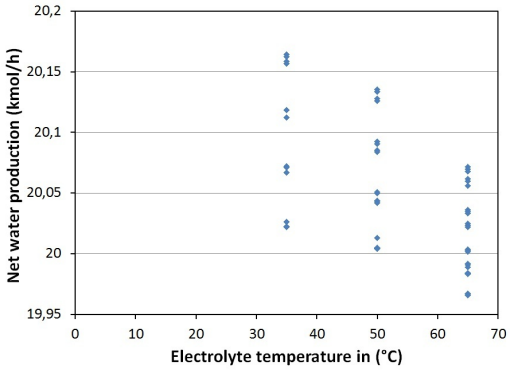

(c) $f_1(z)$

Figure 7.5: Evaluation of the influence on the net water production of a) the electric load, b) the air ratio and c) the electrolyte input temperature at different working points and based on simulation.

Parameter	Minimum	Maximum	Step size
DC,current	$20A$	$110A$	$30A$
Air ratio	2.5	5	2.5
Temperature electrolyte input	$35°C$	$65°C$	$15°C$
Temperature difference stack and electrolyte	$-5°C$	$5°C$	$5°C$
Ambient temperature	$5°C$	$35°C$	$15°C$

Table 7.5: Overview of the variation of the input variables to examine its influence on output variables.

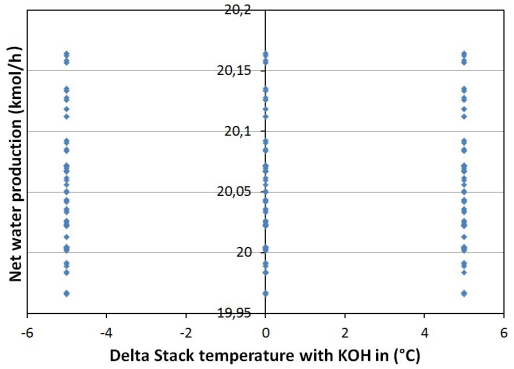

(a) $f_1(w)$

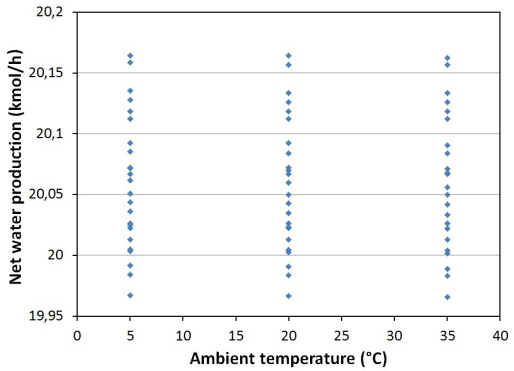

(b) $f_1(v)$

Figure 7.6: Evaluation of the influence on the net water production of a) the temperature difference between stack and electrolyte and b) the ambient temperature at different working points and based on simulation.

	Net water production	Flow rate of water vapour in the air flow	Output air temperature	Output electrolyte temperature
Unit	$\frac{kmol}{h}$	$\frac{kmol}{h}$	$°C$	$°C$
Input parameter	f_1	f_2	f_3	f_4
Electric load (A,DC)	x	x	x	x
Air ratio (-)	y	y	y	y
Electrolyte input temperature ($°C$)	z	z	-	z
Stack temperature ($°C$)	-	-	z	-
Temperature difference between electrolyte and stack ($°C$)	w	w	-	w
Electrolyte output temperature ($°C$)	-	-	w	-
Ambient temperature ($°C$)	v	v	v	v

Table 7.6: Description of the variables used in the regressive functions (Eq.(7.11)*) to calculate water and thermal management.*

which can also be interpreted as a quadratic correlation between electrolyte input temperature and net water production in the electrolyte.
In Figure 7.6 it is shown that the difference between the electrolyte input temperature and the stack temperature on the one hand, or the ambient temperature, which is also the input air temperature, on the other hand, has no strong influence on the net water production.
Based on these analyses a general correlation can be posed, Eq.(7.11).

$$\begin{aligned} f_1 = {} & \Theta_{1,1} \cdot x^2 + \Theta_{1,2} \cdot x \cdot y + \Theta_{1,3} \cdot \Theta_{1,1} \cdot x \cdot z + \Theta_{1,4} \cdot y^2 \\ & + \Theta_{1,5} \cdot y \cdot z + \Theta_{1,6} \cdot z^2 + \Theta_{1,7} \cdot x + \Theta_{1,8} \cdot y \\ & + \Theta_{1,9} \cdot z + \Theta_{1,10} \cdot w + \Theta_{1,11} \cdot v + \Theta_{1,12} \end{aligned} \tag{7.11}$$

The description of x,y,z,w and v to calculate the net water production is given in the first column of Table 7.6. To calculate the parameters ($\Theta_{1,i}$) in this equation a regression is made. It is possible that some trends in the data are captured in more terms, which makes the regression less stable. Therefore, this regression is

Parameter	Value in f_1	Value in f_2	Value in f_3	Value in f_4
$\Theta_{i,1}$	$-6.40 \cdot 10^{-5}$	$3.73 \cdot 10^{-5}$	-	-
$\Theta_{i,2}$	$-6.88 \cdot 10^{-5}$	$6.86 \cdot 10^{-5}$	-	-
$\Theta_{i,3}$	$-1.68 \cdot 10^{-5}$	$2.06 \cdot 10^{-6}$	-	-
$\Theta_{i,4}$	-	-	-	-
$\Theta_{i,5}$	-	-	-	-
$\Theta_{i,6}$	$1.58 \cdot 10^{-6}$	$-1.57 \cdot 10^{-5}$	-	-
$\Theta_{i,7}$	$1.93 \cdot 10^{-3}$	$2.86 \cdot 10^{-4}$	$6.13 \cdot 10^{-2}$	$2.28 \cdot 10^{-2}$
$\Theta_{i,8}$	-	-	$8.70 \cdot 10^{-1}$	$-3.22 \cdot 10^{-2}$
$\Theta_{i,9}$	$5.21 \cdot 10^{-3}$	$-2.59 \cdot 10^{-3}$	$9.11 \cdot 10^{-1}$	$9.75 \cdot 10^{-1}$
$\Theta_{i,10}$	-	-	$-7.98 \cdot 10^{-3}$	1.75
$\Theta_{i,11}$	-	$5.45 \cdot 10^{-5}$	$1.52 \cdot 10^{-1}$	$1.12 \cdot 10^{-2}$
$\Theta_{i,12}$	$-9.83 \cdot 10^{-2}$	$3.69 \cdot 10^{-2}$	-9.19	$4.05 \cdot 10^{-1}$

Table 7.7: List of parameter values,$\Theta_{i,j}$ for the different regressive functions, f_i based on the expression in Eq.(7.11)

repeated 4095 times taking one or more terms out of the expression. A best fit is chosen based on the BICs criterion for model selection, described in Ref. [105] by De Brauwere et al. This criterion selects a model based on a cost function based on the least square method, Err_{LSQM}, and a penalty factor based on the number of simulated points, N, and the number of parameters, $n\Theta$ in the model expression. The model is chosen by minimizing following expression:

$$p = Err_{LSQM} \cdot \frac{2 \cdot (n\Theta + 1)}{N - n\Theta - 2} \tag{7.12}$$

As can be understood from this expression a best fit is chosen based on minimizing the deviation, considered in the cost function, within the boundaries of a limited number of terms. The result of this model selection is summarized in the first column of Table 7.7.

The water content in the air flow, f_2

A similar approach can be used to predict the flow rate of water vapour in the air flow. It is to be expected the same parameters will have a similar importance, although some correlations are opposite, like for the ambient and electrolyte temperature. In Figure 7.7 it is shown that load, air ratio and electrolyte temperature all have a positive effect on the vapour flow rate. Similar but opposite to the net water production the electrolyte temperature now has a strong positive influence on the vapour flow rate in the air flow. As for the ambient temperature and temperature difference of the electrolyte with the stack the correlations found are less strong (See Figure 7.8).

As can be expected the same parameters can be used to calculate a regressive function, similar to the one in Eq.(7.2.1.2). The results are listed in Table 7.7.

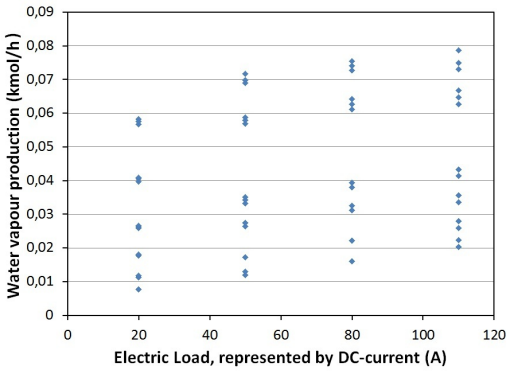

(a) $f_2(x)$

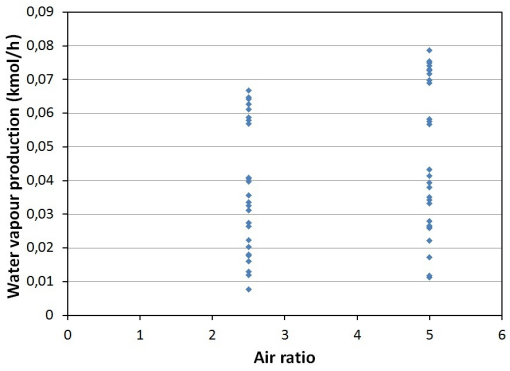

(b) $f_2(y)$

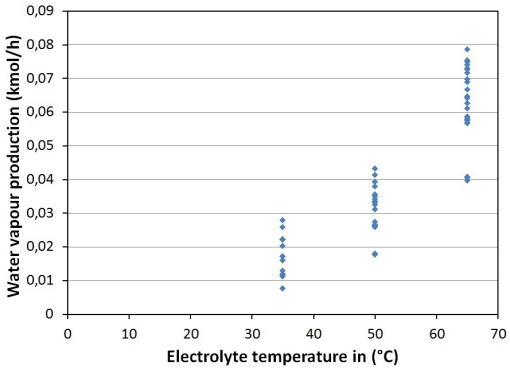

(c) $f_2(z)$

Figure 7.7: Evaluation of the influence on the vapour production in the air flow of a) the electric load, b) the air ratio and c) the electrolyte input temperature at different working points and based on simulation.

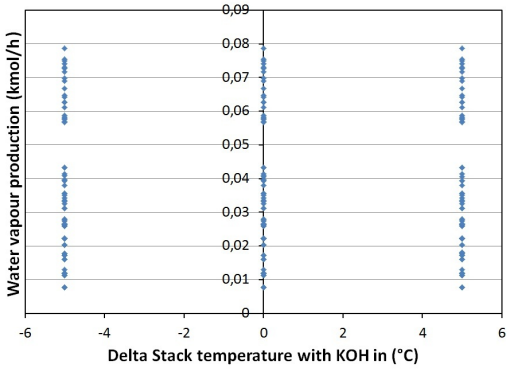

(a) $f_2(w)$

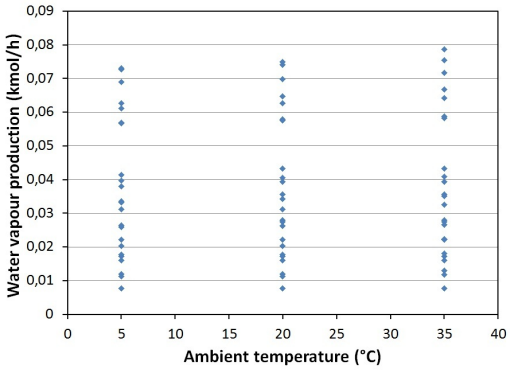

(b) $f_2(v)$

Figure 7.8: Evaluation of the influence on the vapour production in the air flow of a) the temperature difference between stack and electrolyte and b) the ambient temperature at different working points and based on simulation.

The air temperature at the outlet, f_3

To define a regression function for the air temperature, it is noticed in Figure 7.9(a) the load will have only a minor positive linear or quadratic effect on air temperature. Other than first expected, Figure 7.9(b) shows that air ratio has also a small positive effect on air output temperature, due to an increased heat and mass transfer from the electrolyte.

Figures 7.9(c) and 7.10(a) show that electrolyte input temperature and the temperature difference from the electrolyte and stack have a strong linear influence on the air output temperature. The ambient temperature (See Figure 7.10(b)) only shows to have an influence at low output air temperatures. Because of the very pronounced linear correlation between output electrolyte and output air temperature in the experimental results in Chapter 3, also a correspondance between these two output temperatures is shown for different working points in Figure 7.10(c).

Based on this analysis, stack temperature and electrolyte output temperature are taken into account instead of the input electrolyte temperature and the temperature difference (See Table 7.6). The parameter values found after regression and model selection are listed in the third column of Table 7.7.

The output electrolyte temperature, f_4

For the simulated output electrolyte temperature, Figure 7.11(a) shows a weak linear correlation. The linear correlation was expected, since, as discussed earlier, at higher loads more reaction heat is available to increase electrolyte temperature. As expected, it is shown in Figs. 7.11(c) and 7.12(a) that both electrolyte input temperature and the temperature difference with the stack show a strong linear correlation with output electrolyte temperature. The direct influence of the input electrolyte temperature is obvious, while the temperature difference also has a direct influence on electrolyte temperature based on the energy balance within the stack.

Figures 7.11(b) and 7.12(b) show that the influence of the air flow and surroundings is almost negligible.

With these analysis the regression based functions, f_1, f_2, f_3 and f_4 are determined. Their relevance and accordance to the original model is illustrated in Table 7.8, which gives an overview of the largest differences found between the values generated by the simplified model and the original model. As can be seen some deviation is present, but for most variables within acceptable limits. The largest difference is found to quantify the heat transfer between stack and electrolyte flow. However, this only affects the dynamics and transient thermal behaviour of the stack. As the time step is 15 minutes in the whole-year simulation

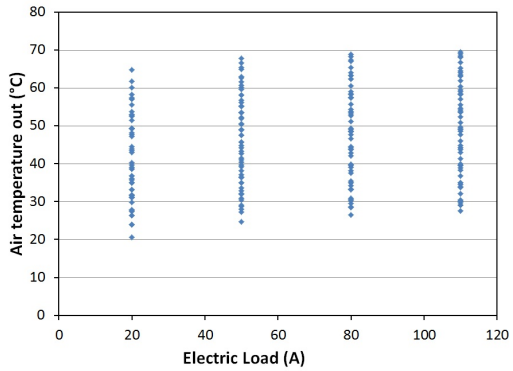

(a) $f_3(x)$

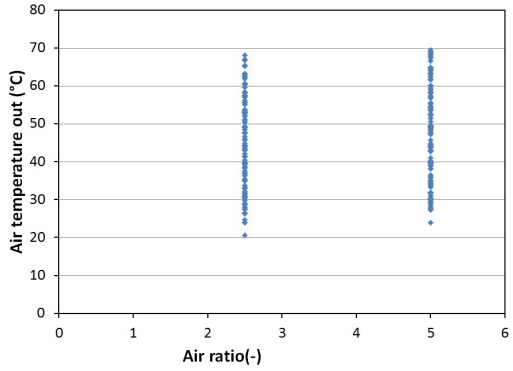

(b) $f_3(y)$

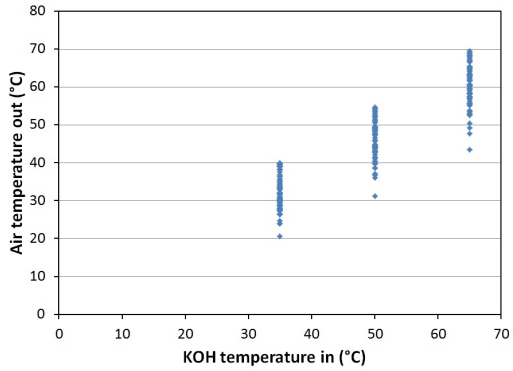

(c) $f_3(-)$

Figure 7.9: Evaluation of the influence on the output air temperature of a) the electric load, b) the air ratio and c) the electrolyte input temperature at different working points and based on simulation.

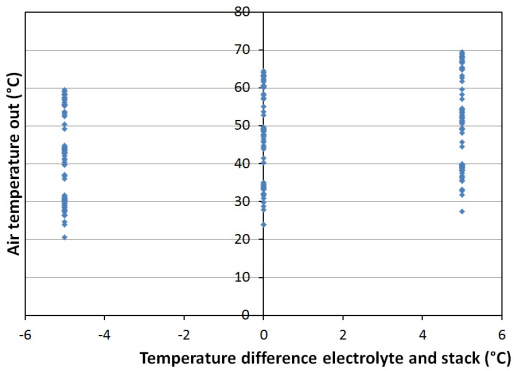

(a) $f_3(-)$

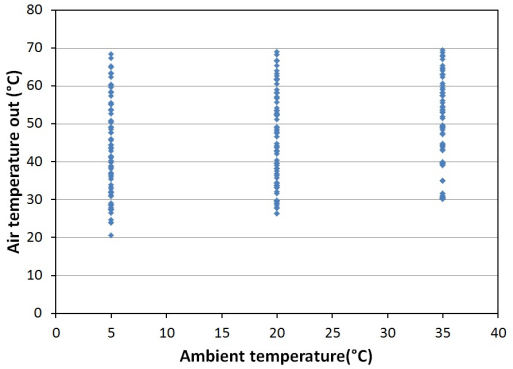

(b) $f_3(v)$

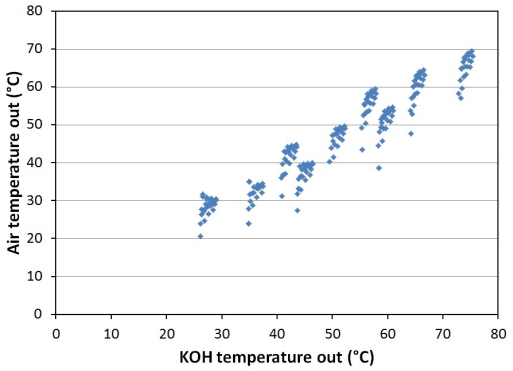

(c) $f_3(w)$

Figure 7.10: Evaluation of the influence on the output air temperature of a) the temperature difference between stack and electrolyte, b) the ambient temperature and c) the electrolyte output temperature at different working points and based on simulation.

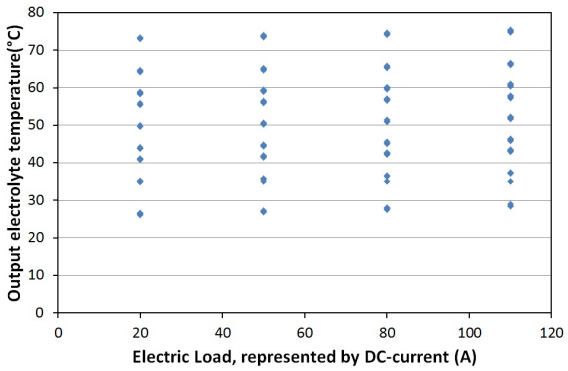

(a) $f_4(x)$

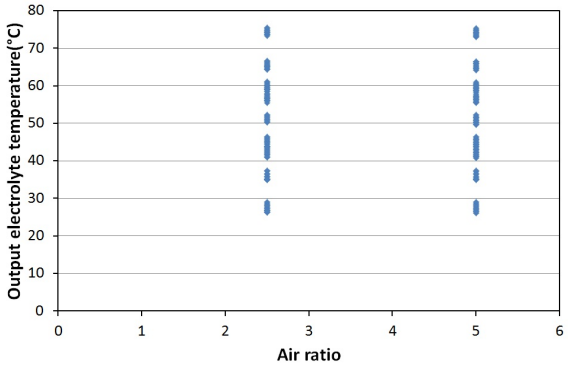

(b) $f_4(y)$

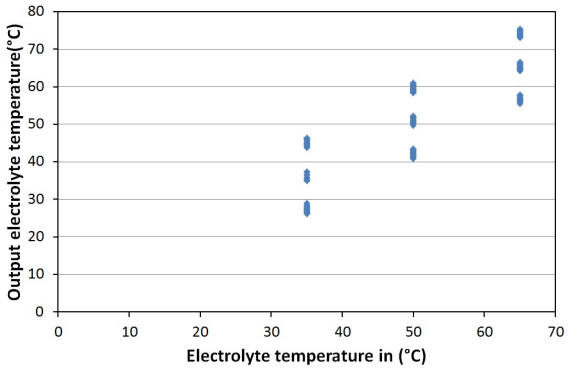

(c) $f_4(z)$

Figure 7.11: Evaluation of the influence on the output electrolyte temperature of a) the electric load, b) the air ratio and c) the electrolyte input temperature at different working points and based on simulation.

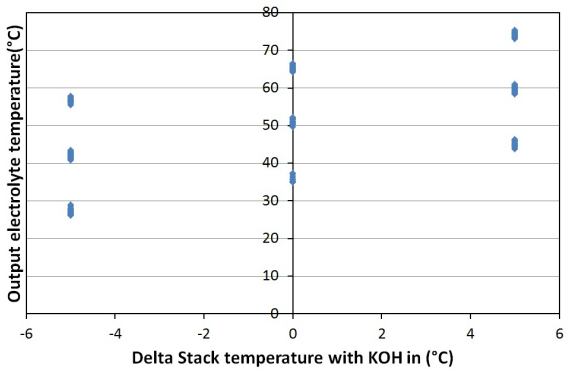

(a) $f_4(w)$

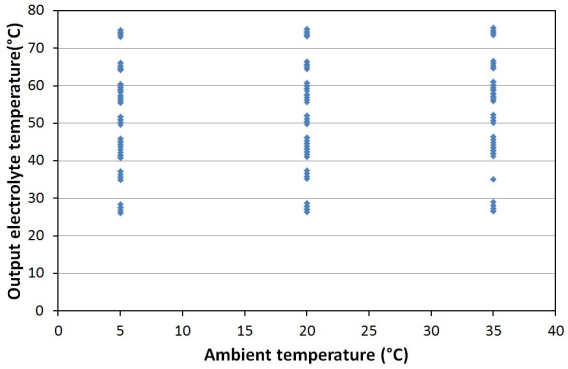

(b) $f_4(v)$

Figure 7.12: Evaluation of the influence on the output electrolyte temperature of a) the temperature difference between stack and electrolyte and b) the ambient temperature at different working points and based on simulation.

Parameter	Maximum difference	Unit
Output electrolyte flow rate	$8.3 \cdot 10^{-3}$	$kmol/hr$
Output electrolyte temperature	0.5	$°C$
Output air flow rate	$4.0 \cdot 10^{-3}$	$kmol/h$
Output air temperature	4.9	$°C$
Output air vapour fraction	$1.3 \cdot 10^{-2}$	–
Generated stack voltage	$9.0 \cdot 10^{-7}$	$Volt$
Heat to the stack	1362	W

Table 7.8: An overview of the differences between the simplified and original model

this transient behaviour fades out and looses its importance.
Therefore, the regression model is acceptable to use in a whole year simulation. However, to study dynamics on a time basis lower than 15 minutes the model is not accurate enough.

7.2.2 Implementation of the building dependent aspects into the model

7.2.2.1 Additional equations for the building and case dependent model components

To implement the building aspects in the simulation, a model of the heat demand, Q_{demand}, is translated into a temperature difference in the tertiary circuit, Eq.(7.13). This heat demand is in fact the thermal load profile from the studied case. The interference with building dynamics is not considered here, since the focus here is to evaluate the CHP-system.
Both the tertiary circuit and secondary circuit are linked to the buffer. The temperature in this buffer is the result of our dynamic energy balance, Eq.7.14. To model the buffer a simple one point model, with a perfect mixture is assumed. The buffer constants applied in these equations are already listed in Table 7.2.

$$Q_{demand} = \dot{m_{tert}} \cdot c_{p,w} \cdot (T_{buffer} - T_{return}) \tag{7.13}$$

$$\begin{aligned} V_{buffer} \cdot c_{p,w} \cdot T_{buffer} = {} & \dot{m_{sec}} \cdot c_{p,w} \cdot (T_{supply} - T_{buffer}) \\ & - \dot{m_{tert}} \cdot c_{p,w} \cdot (T_{buffer} - T_{return}) \\ & - Q_{loss,buffer} \end{aligned} \tag{7.14}$$

$$Q_{loss,buffer} = hA_{buffertank} \cdot (T_{buffer} - T_{surr}) \tag{7.15}$$

In future research it is possible to include the interference with building dynamics to optimize control strategy, as illustrated in [106] for a weather compensated control.
A more complex model of the buffer, including stratification, could also lead to further improvement of the control strategy, especially to increase flexibility to manage the electrolyte level in the tank.
Despite these remarks, which could initiate future research, the present model is capable to give a clear view on the potential of an AFC-based micro-CHP.

7.2.2.2 Translation of the control strategy into the model

Next to these additional equations to simulate the heat demand and how it is experienced by the system, it is also necessary to implement the used control strategy into the simulation.
For this, every time step the modus of operation will be calculated on the last

conditions. The modus of operation is directly implemented into the model. At the 'ON' modus, no adaptation of the model was needed, as the modus of operation determined the working point for the simplified stack model. However, the stack model is only valid if there is a minimal load. Therefore, the stack model is also extended to simulate its behaviour in 'Off' modus. In 'Off' modus, the stack model is modelled as a heat exchanger of the electrolyte and air flow, with additional heat losses to the surroundings.

Finally, a simple Euler based solving method is used applying a fixed time step approach to calculate a case study.

7.3 Closure

With the discussion in this chapter, the aspects regarding building integration are discussed, which are general to all cases. A methodology to implement a control strategy is discussed and specified for a heat driven control strategy, since this most representative for (micro-)CHP-applications.
These aspects are translated into a model, consisting of a building heating system, thermal load profile and system model, developed in Chapter 5. To reduce calculation time the original stack model in the system model is simplified with regressive functions for the water management, f_1 and f_2, and predictions of output temperatures the air and the electrolyte flow, f_3 and f_4. Besides this, also the stack behaviour when no current is drawn from the stack is implemented in the model.
With this building model different case studies, specified by their load profile, and different control strategies can be evaluated in Chapter 8.

8

Case study

In the introduction the evolution of energy demand in buildings was discussed (See Chapter 1). With an increasing power-to-heat ratio, fuel cell based micro-CHPs promise to become an interesting alternative for combustion based micro-CHP-systems. To understand the boundary conditions for this presumption, two different case studies are investigated with the model built and validated in previous chapters:

- a micro-CHP application for residential purposes; for this study, two alternative settings for the applied control strategy are presented.

- a micro-CHP application within an office building; for this study, the best of these different settings is applied.

Each case study is an illustration that the model can be used to perform these analyses, although the outcome can differ depending on energy demand and applied control strategy.
The results of each simulation are analysed regarding control, primary energy savings and possible (future) economical savings. Within this perspective, the complementarity of the fuel cell based micro-CHP with other energy systems is briefly illustrated and discussed.

8.1 CASE 1A: Low-energy building for residential purposes: original heat based control strategy

A first application to be evaluated is the implementation of the micro-CHP within a residential building.

8.1.1 Description of case: energy demand

To evaluate the feasibility of a micro-CHP system within a single household dwelling a realistic load profile is generated in order to implement these load profiles in the building integrated model developed in Chapter 7.

8.1.1.1 Specification of the energy demand

The energy demand in this case study is based on the demand of a recently built detached house with an insulation rate above average.
This building is characterized by following properties:

- a net heat demand of $45 - 50 \frac{kWh}{m^2 \cdot year}$ for space heating
- a floor area of $200\, m^2$
- an A-label, regarding electric appliances
- a family with two working parents and two children going to school or daycare

The total annual heat demand of this building is $12\,000\, kWh$ and its annual electricity consumption is $5\,000\, kWh$.
However, yearly consumption data are not sufficient to perform this case study; a dynamic load profile for both heat and electricity demand is required. Figure 8.1 shows a representative energy profile for the specified building.
This dynamic load profile is generated with a tool developed at KCE [1], which is explained further in Section 8.1.1.2.

8.1.1.2 A generic load profile: description of the tool

At KCE[1], a tool is developed generating dynamic load profiles for heat and electricity demand based on building characteristics. In order to evaluate the usefulness of the generated dynamic load profile, a brief description is given on the tool, used for this purpose.

[1] www.kenniscentrumenergie.be

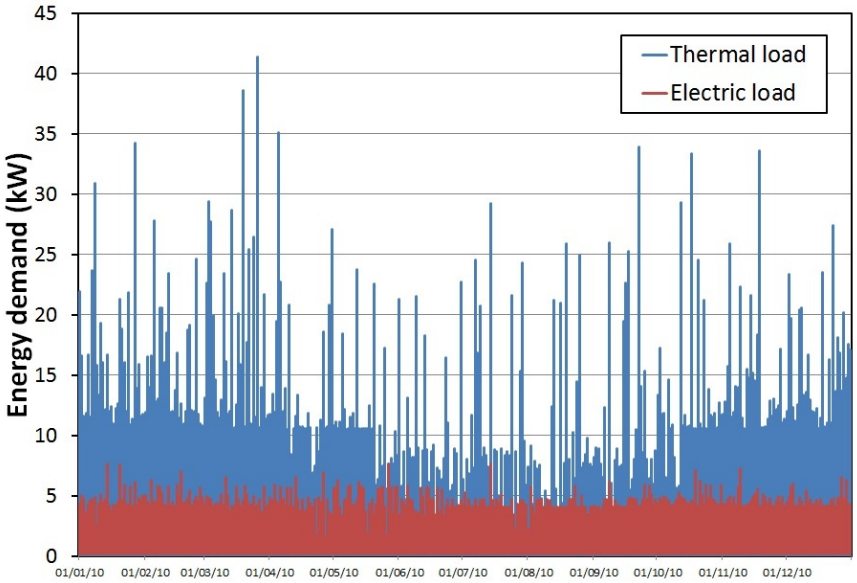

Figure 8.1: An overview of the yearly heat and electricity demand within the simulated residential building based on 15 minute data.

The energy demand and its corresponding thermal and electric load profiles within residential buildings depend on building insulation, user behaviour, comfort demand and heating system. Therefore, the tool generates thermal and electric 15-minute load profiles for a single household dwelling, based on the insulation rate, number of inhabitants, rate of occupancy and the energy label corresponding to their electrical appliances.

In Ref. [107] Govaerts implemented the general concept of the tool in a worksheet and used it to evaluate the feasibility of micro-CHP in residential dwellings for units which are already available on the market. The tool combines the results of the electric profile generator developed by Baeten and Put [102], the generated load profiles for space heating generated by validated and adjustable building models in a TRNSYS environment [11, 108] and thermal load profiles for domestic hot water, developed in the IEA ECBCS programme annex 41 [109].

The electric load profile

Based on a classification of the inhabitants an electric profile is developed. The classification is based on the number of inhabitants, and working or non-working. For every class a realistic pattern of day and week is suggested with a number of

activities like eating, washing, ... Within these fixed patterns random factors are introduced to allow shifting in time of these activities within certain boundaries, different for each activity. These activities are linked with the use of electric appliances. For each of these appliances, for which electricity consumption also depends on their energy label, realistic dynamic load profiles based on measurements are used to translate the behaviour pattern in realistic electricity profiles. More details and the validation of this methodology can be found in Ref. [102].

The thermal load profile for space heating

In [11] Van der Veken et al. presented a methodology to determine efficiency of the heating system at building level based on TRNSYS simulation. Later, this methodology is applied to a specific building in Ref. [108]. By determining comfort level and occupancy an actual heat demand is specified. The occupancy is linked to the same day and week patterns, which were used to generate the electric profile. In this way a realistic thermal load profile for space heating can be generated, based on input on inhabitant behaviour, size of the building and insulation rate. Only the central heating system is not varied and considered to be based on radiators.

The model, which is used to generate thermal load profiles for space heating is originally developed to evaluate the influence of inhabitant behaviour [108] and insulation rate on energy performance of the heating system.
This model is validated with experimental data obtained by Ruts in Ref. [110]. In Ref. [110] measurements were executed in the building simulated in Ref. [108] and in similar buildings but with a different occupancy and number of inhabitants. All these dwellings are almost similar, because they are the property of a social housing company.
The model showed a good accordance between measurement and simulation for different inhabitant behaviour.

To generate a number of generic heating profiles based on this model, next to variation in occupancy also building insulation rate and used energy systems are varied.
As for the weather dependency, the weather data for Uccle available in the TRNSYS libraries are considered.

The thermal load profile for domestic hot water

In order to evaluate micro-CHP-systems in buildings, load profiles of domestic hot water consumption were already developed in the IEA ECBCS programme annex 41 [109]. These data were used and scaled to the number of inhabitants.

All these profiles, for electricity, space heating and domestic hot water, are made scalable to be representative for other larger or smaller buildings. To scale these load profiles, it is necessary to define a yearly energy use for the specified building.

Based on the characteristics of the building and its inhabitants, which are specified in Section 8.1.1.1, the tool generates the dynamic energy profile of the case study to which the feasibility of the AFC-based micro-CHP is evaluated here. The result is shown in Figure 8.1.

8.1.2 Sizing of components and control strategy

Figure 8.1 clearly shows some temporary peaks of about $40kW$ on heat demand. However, since the profile is based on 15 minute data and considering thermal inertia of the building and heating system, hourly data are more representative for the heat demand. Rescaling the data to hourly time steps, the peak, mainly due to the hot water demand, drops to about 10 – $15kW$. This is to be taken into account to size the auxiliary system, which is sized on peak load.
To optimize CHP-utilization, it is best to use a buffer. Ideally, the daily consumption is covered with this buffer tank. In this way, the CHP is able to achieve a lot of running hours and to heat the buffer tank in steady state. From this buffer tank the heat is distributed into the building whenever necessary.
In Figure 8.2 the daily heat demand is shown. It is shown that in summer a buffer of about $10\,kWh$ is sufficient to supply heat demand for a complete day, while in winter this would require a buffer of about 70 – $80\,kWh$. With a daily load of maximum $80\,kWh$, thermal base load can be limited to about $4\,kW$. As can be seen in Chapter 6, the AFC based CHP-system has a thermal output of about $4\,kW$, depending on operating conditions. In the simulation a buffer is chosen from $300\,l$, which is realistic for households. Taking a temperature difference of about $20°C$ into account, this represents a buffer from about $7\,kWh$.
A heat based control strategy is implemented with the standard thresholds listed in Table 7.3. Next to that, both system and buffer are placed indoor.

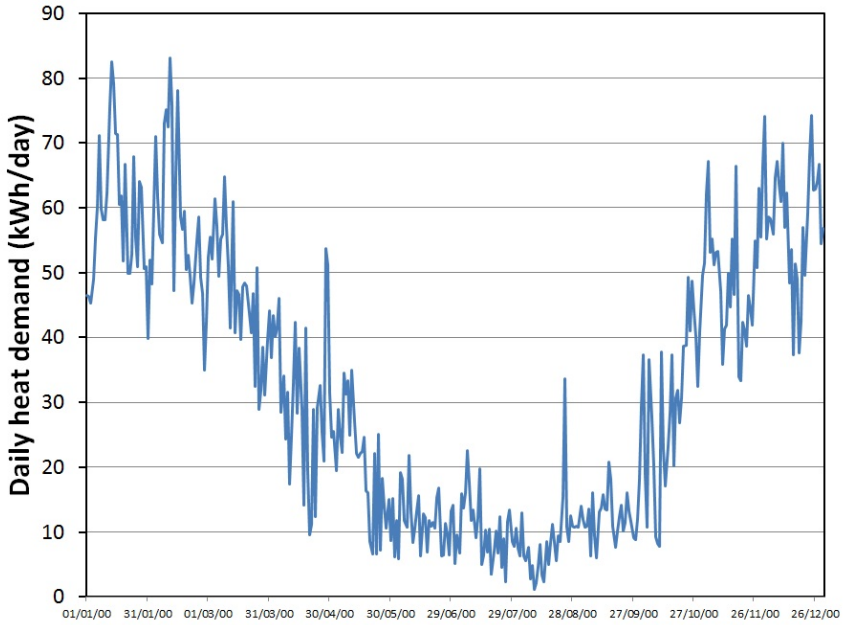

Figure 8.2: An overview of the yearly heat demand within the simulated residential building on a daily basis.

Period	8-14 JAN	8-14 APR	29JUL-4AUG	28OCT-3NOV
Pe, CHP	471	426	363	462
$P_{e,demand}$	129	120	93	127
Q_{demand}	475	201	60	344
Q_{aux}	128	4	0	36
$H_{2,aux.}$	150	4	0	43
$H_{2,CHP}$	1198	1069	886	1173
$H_{2,tot}$	1348	1073	886	1215

Table 8.1: Overview of the results for a week in every season for CASE 1A. All values are expressed in kWh.

8.1.3 Results

8.1.3.1 Evaluation of system behaviour based on a week of operation

To interpret the results of the simulation, first the behaviour is discussed for a number of weeks, spread over the year. In Figure 8.3 an overview is given of the system behaviour and its heat and electricity production in comparison to demand. As can be seen in Figure 8.3(b), in winter the system is (almost) always 'ON' as the base heat load of the building is a bit higher than the nominal heat output of the system. If the system is not able any more to deliver the heat, requested by the building, the auxiliary burner delivers additional heat output. In Figure 8.3(a) this is represented by the purple bars.
As for the stability of the system it is clear the temperatures are kept under control. However, during heating mode, the temperature fluctuations in the electrolyte rise. This is partly due to the chosen time step in the simulation, but also due to the chosen control strategy. As can be seen in Figure 8.3(b) the load permanently switches between minimum and maximum values. This is because the electrolyte level is unstable, leading to suboptimal operation.
The results of this period are summarized in Table 8.1 and compared to other seasons. As can be seen in winter time the power-to-heat ratio of the AFC-based CHP-system is 5-6 times higher than the power-to-heat demand ratio of the building. For this reason the auxiliary burner will have to be used and a lot of net electricity is put on the grid.

Next to a week in winter the same graphs are made for a week in the summer. Figure 8.4(b) illustrates that with the present control strategy the system is kept 'on', but only the electric load is set to a minimum. This has some advantages to systems stability, but will result in suboptimal operation, since at low load no primary energy savings are obtained. In Chapter 6 it was shown that at this load, there was no net heat output. From a primary energy point of view this can be optimized.

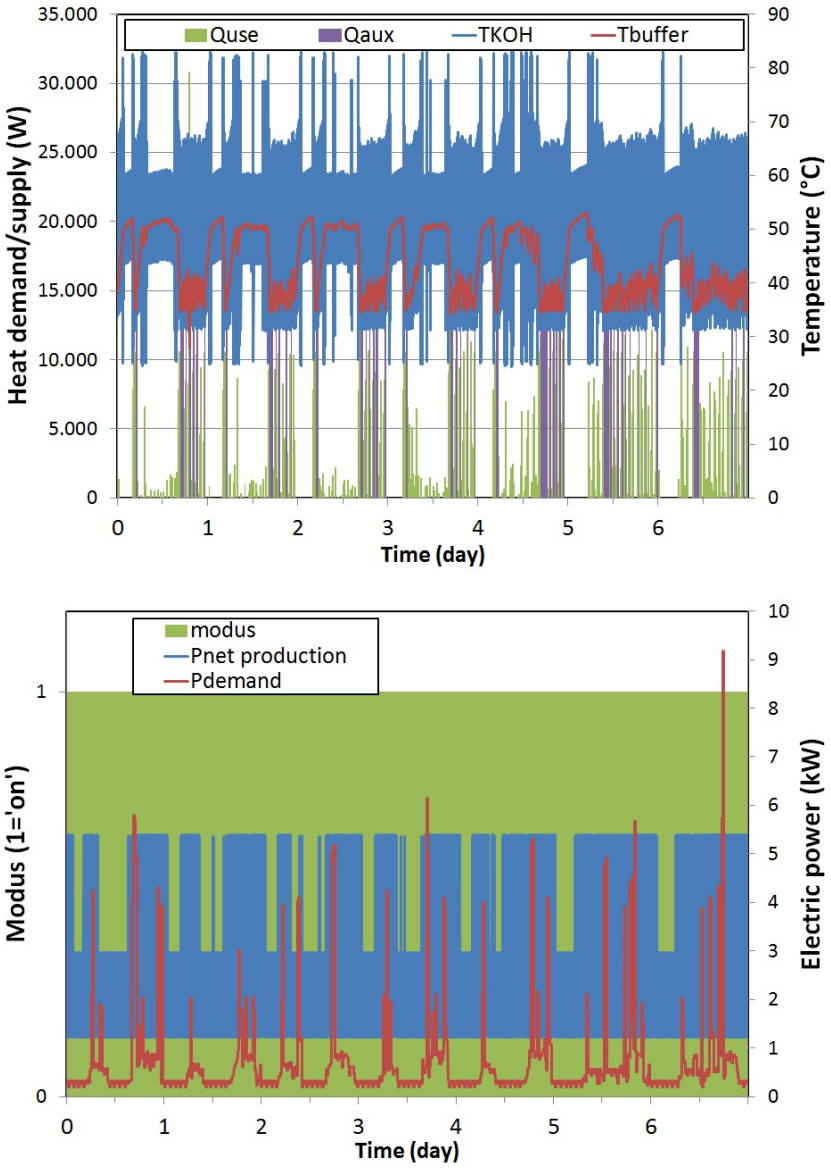

Figure 8.3: Simulation result of CASE 1A for the second week of January. In a) the temperatures of the electrolyte, T_{KOH}, and in the buffer tank, T_{buffer}, are shown together with the actual heat demand. In b) the electricity production and consumption are shown together with the modus of operation.

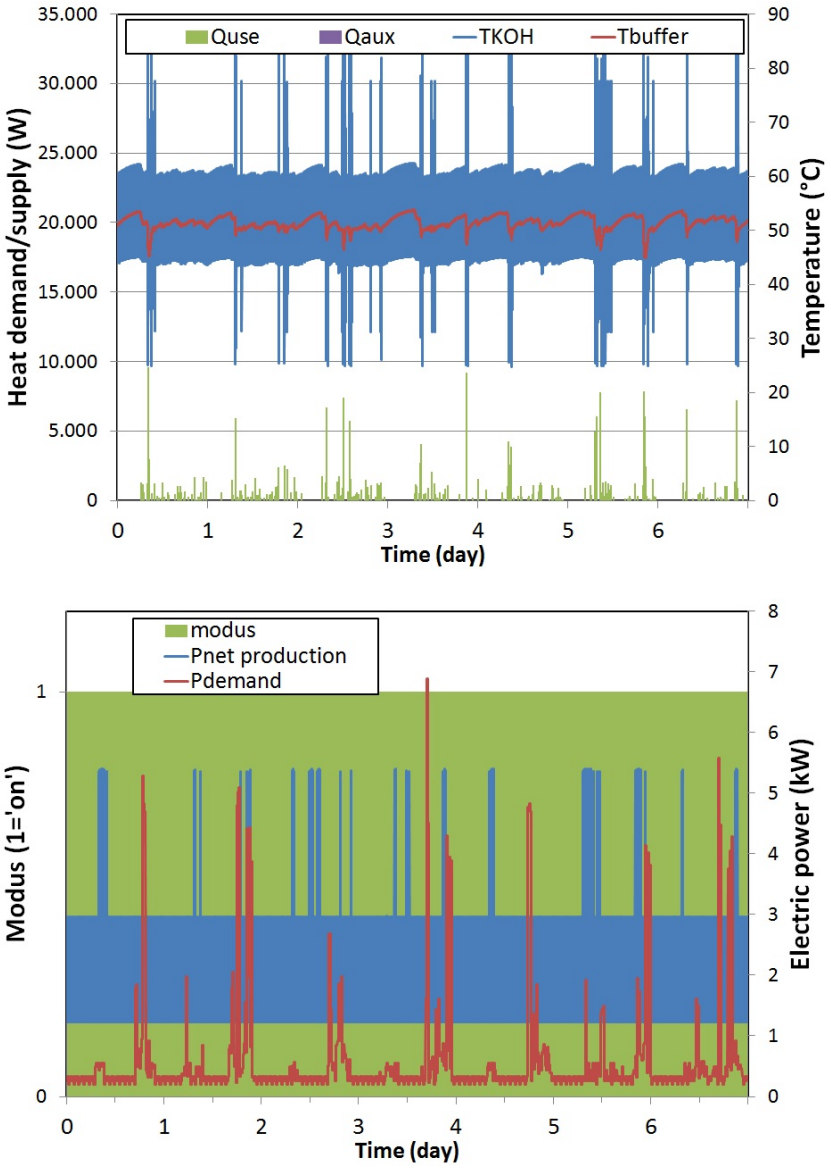

Figure 8.4: Simulation result of CASE 1A for the last week of July. In a) the temperatures of the electrolyte, T_{KOH}, and in the buffer tank, T_{buffer}, are shown together with the actual heat demand. In b) the electricity production and consumption are shown together with the modus of operation.

Energy carrier	Cost (EUR/kWh)	Remarks
Electricity (buy)	0.20	Based on average electricity price, including distribution tariff and taxes
Electricity (sold)	0	Based on common practice for households
Natural gas	0.07	Based on average gas price, including distribution tariff and taxes
Hydrogen	0.13	Market price for hydrogen, including taxes

Table 8.2: Overview of used price settings for financial analysis

The ratio power-to-heat demand becomes here more beneficial to the AFC-based CHP-unit, but the heat demand is too low.
The heat based control strategy with the present thresholds for safe operation forces the system to work in suboptimal conditions. Instead of turning 'OFF' the system works at low load, when there is no heat demand.

8.1.3.2 Evaluation based on primary energy and operation costs

To evaluate the use of an AFC-based CHP-unit within residential buildings, a comparison is made with the best possible separate production of electricity and heat, while for the AFC-based CHP-unit, all efficiency losses due to purging or inverter or auxiliary equipment are incorporated.
For primary energy savings, the same approach is used, as explained in Section 4.1.4 in Chapter 4, considering the best positive alternative and taking also a conversion (reforming) efficiency into account for hydrogen production.
As discussed earlier in Chapter 4, this conversion efficiency, however, remains disputable, because it is difficult to compare the primary energy savings with hydrogen as a fuel. The remarks made on this in Section 4.2.4 remain valid.

For the financial evaluation, Table 8.2 summarizes the used assumptions.
Due to these for the fuel cell based CHP severe conversion factors, no primary energy savings are obtained with this control strategy and used thresholds. Without taking the conversion factor for hydrogen into account (a conversion factor of 1) fuel savings of about 24% are reached.
From a financial point of view, the use of hydrogen is even less interesting, due to the relatively high costs for hydrogen fuel. However, with higher electricity costs (e.g. at peak hours) and lower hydrogen costs (e.g. by electrolysis out of renewable over production of electricity.) this can change in other techno-economic models.

Description Unit	Demand or Production kWh	Primary Energy (HHV) kWh	Cost EUR
Heat Demand	12 000	14 666	1 026
Electric Demand	5 000	11 000	1 000
Reference Demand		25 666	2 026
CHP Electric production	21 912		
CHP Heat production	10 472		
CHP Hydrogen consumption	54 804	64 475	7 124
Heat aux.burner	1 528	1 867	131
Hydrogen consumption (aux)	1 910	2 247	233
Electricity from the grid	−16 912	−37 206	0
CHP+aux on natural gas		29 136	7 255
CHP+aux (all hydrogen based)		29 516	7 357
Savings with CHP		−3 470	−5 229
Savings relative to reference demand		−13%	−259%
Savings relative to CHP Hydrogen consumption		−5.4%	−73%

Table 8.3: Overview of the results for CASE 1A, compared to separate production.

8.2 CASE 1B: Low-energy building for residential purposes: heat based control strategy with different thresholds

8.2.1 Description

The first case study showed that the original operation strategy resulted in a permanent 'ON' modus, which had a negative effect on performance in summer time. This was due to the fact that at low heat demand, the system switched to minimal load. In this case study the same control strategy is used, however with different threshold values. In this strategy the minimal load is increased.
The principle of the new flowchart is shown in Figure 8.5. As shown in Figure 8.5 the system operates at either nominal load or at high part load (70A). In this way there is always a heat production at 'ON' modus allowing to reach the upper temperature boundary to switch 'OFF'. In CASE 1 the load was decreased when the system almost reached this set point. Long periods of inefficient operation are now avoided.

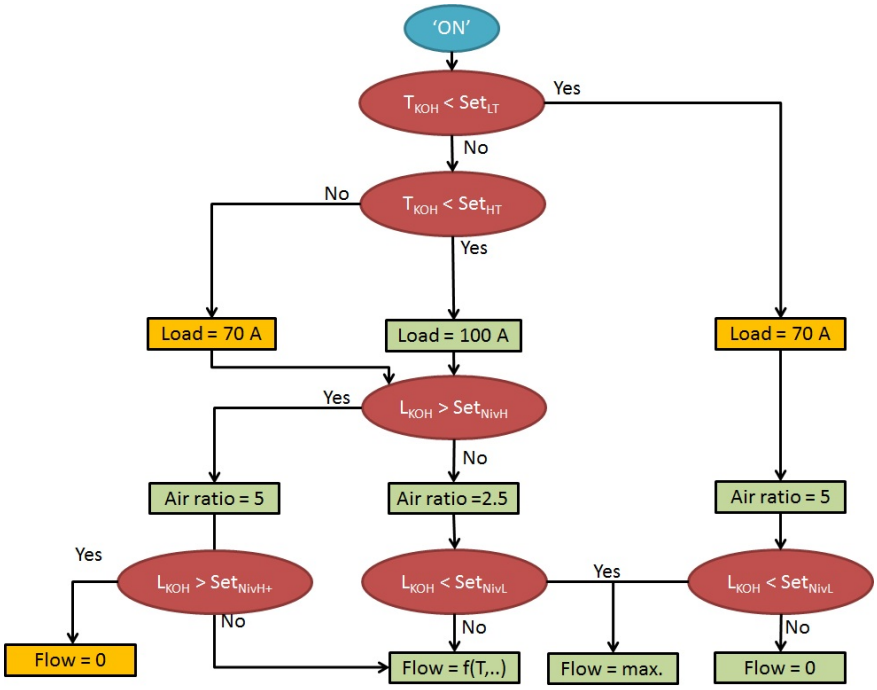

Figure 8.5: Implementation of the control strategy with new thresholds to minimize part load operation.

Period	8-14 JAN	8-14 APR	29JUL-4AUG	28OCT-3NOV
Pe, CHP	580	367	124	513
$P_{e,demand}$	129	120	93	127
Q_{demand}	475	201	60	344
Q_{aux}	110	6	0	38
$H_{2,aux.}$	129	7	0	44
$H_{2,CHP}$	1513	938	321	1327
$H_{2,tot}$	1642	945	321	1372

Table 8.4: Overview of the results for a week in every season for CASE 1B. All values are expressed in kWh.

8.2.2 Results

8.2.2.1 Evaluation of system behaviour based on a week of operation

Similar to CASE 1A, first the behaviour is discussed for a number of weeks, spread over the year. In Figure 8.6 an overview is given of the system behaviour and its heat and electricity production in comparison to demand. As can be seen in Figure 8.6(b), in winter the system is not always 'ON' anymore, although it is still 'ON' most of the time as the base heat load of the building is a bit higher than the nominal heat output from the system. At peak load, the auxiliary burner delivers additional heat output. This is more or less similar to the results in case 1. The results of this period are summarized in Table 8.4 and compared to other seasons. As can be seen in winter time the power-to-heat ratio of the AFC-based CHP-system is 5-6 times higher than the power-to-heat demand ratio of the building. For this reason, the auxiliary burner will have to be used and a lot of net electricity is put on the grid.

Next to a week in winter the same Figures are shown for a week in the summer. Figure 8.7(b) illustrates that with this new control strategy the system is almost all the time 'off' in summer. This is a big difference with CASE 1A, but more than expected with a heat based control strategy.

8.2.2.2 Evaluation based on primary energy and operation costs

For the evaluation of primary energy and energy costs, the same assumptions were used. The results for the same weeks, each representing another season, are summarized in Table 8.4

Because of the extra heat losses in the buffer and the additional conversion factors for primary energy based on hydrogen consumption, no primary energy savings are realised compared to the best possible alternative with separate heat and electricity generation.

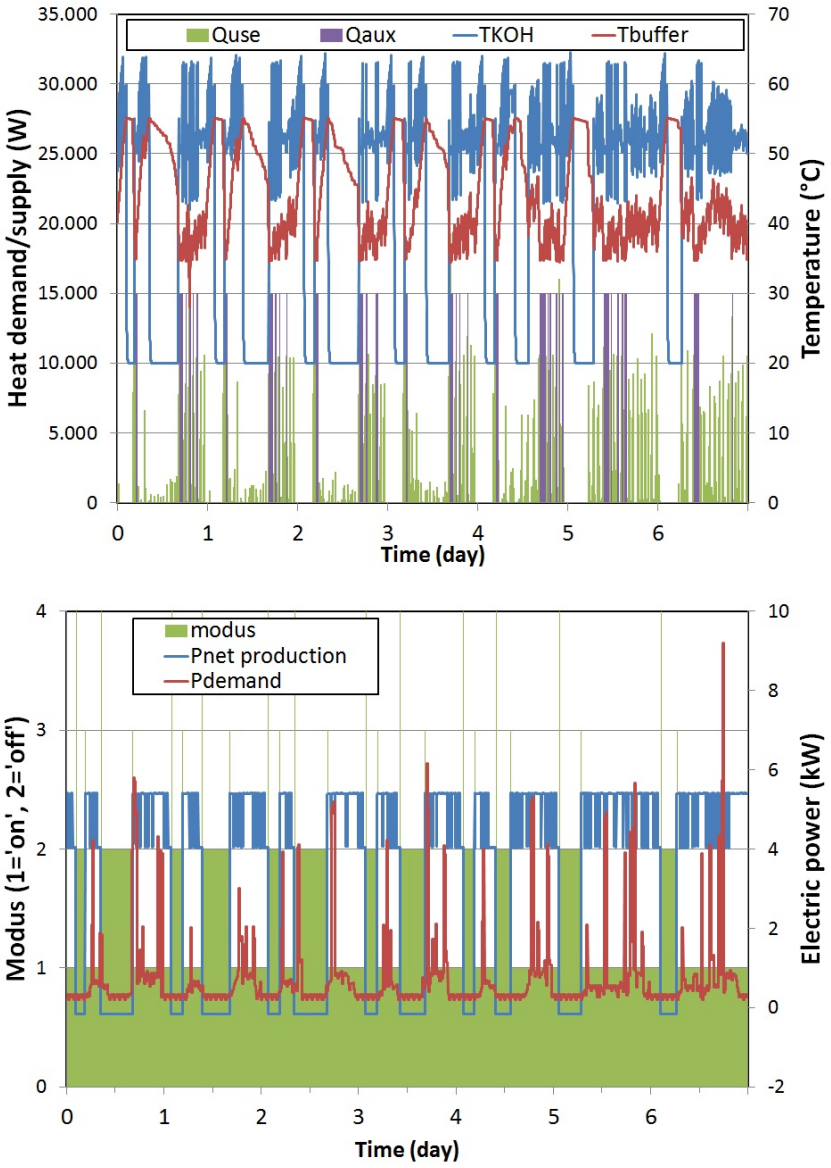

Figure 8.6: Simulation results of CASE 1B for the second week of January. In a) the temperatures of the electrolyte, T_{KOH}, and in the buffer tank, T_{buffer}, are shown together with the actual heat demand. In b) the electricity production and consumption are shown together with the modus of operation.

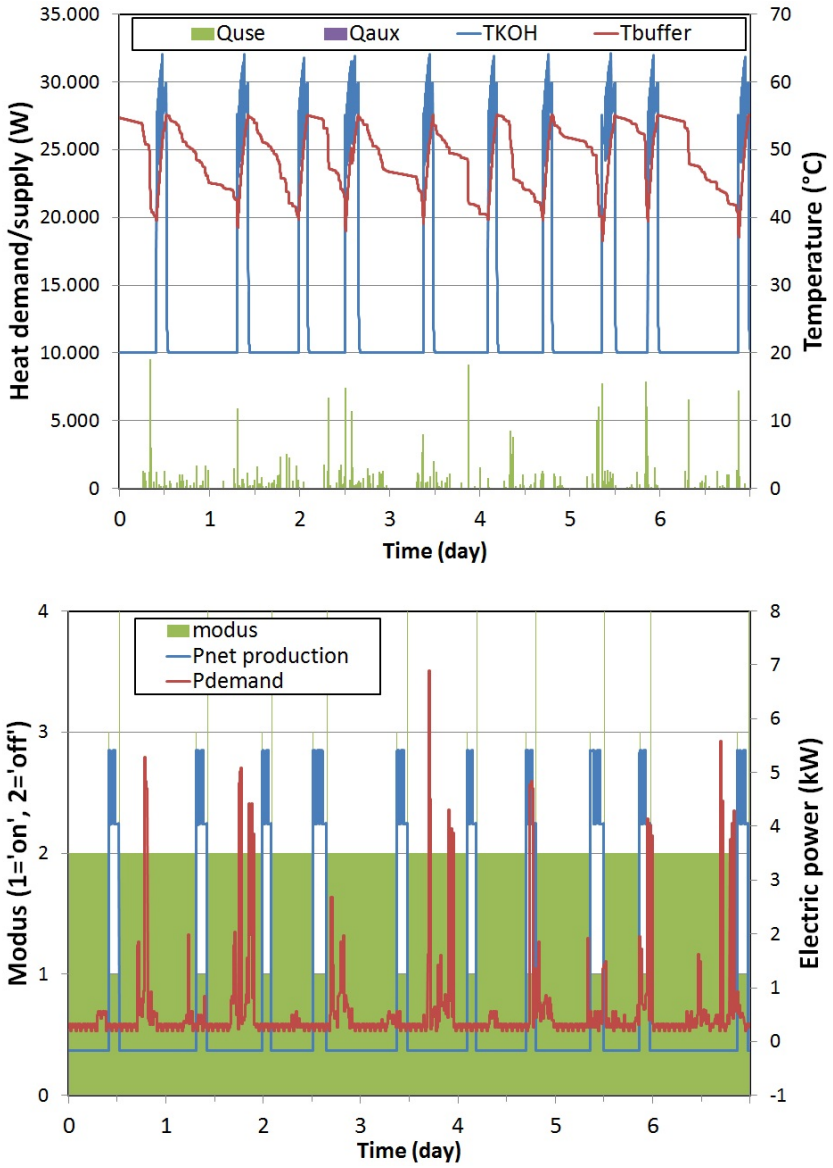

Figure 8.7: Simulation results of CASE 1B for the last week of July. In a) the temperatures of the electrolyte, T_{KOH}, and in the buffer tank, T_{buffer}, are shown together with the actual heat demand. In b) the electricity production and consumption are shown together with the modus of operation.

Description Unit	Demand or Production kWh	Primary Energy (HHV) kWh	Cost EUR
Heat Demand	12 000	14 666	1 026
Electric Demand	5 000	11 000	1 000
Reference Demand		25 666	2 026
CHP Electric production	18 277		
CHP Heat production	10 458		
CHP Hydrogen consumption	47 229	55 563	6 140
Heat aux.burner	1 542	1 884	132
Hydrogen consumption (aux)	1 927	2 268	250
Electricity from the grid	−13 277	−29 209	0
CHP+aux on natural gas		28 238	6272
CHP+aux (all hydrogen)		28 622	6 380
Savings		−2 566	4 246
Savings relative to reference demand (%)		−10%	−210%
Savings relative to CHP Hydrogen consumption (%)		−4.6%	−69%

Table 8.5: Overview of the annual results for CASE 1B, compared to separate production.

However, compared to an average power plant or with an alternative system, the result will be positive, although no spectacular savings are to be expected. Also here the conversion factor for hydrogen has a too big influence on overall performance.
From a financial point of view as the electricity cannot be sold to the grid, the over production and higher fuel price result in a negative scenario.

8.3 CASE 2: Low-energy/ passive office building: heat based control strategy with same thresholds as used in CASE 1B

As mentioned earlier in Chapter 1, offices, and more particularly low energy or passive offices, show an interesting potential for implementation of a fuel cell based micro-CHP system (See also Figure 1.5).
Therefore, also for this purpose a case study is elaborated.

8.3.1 Description of case: energy demand

Available energy profile

To obtain a representative dynamic energy demand for an office building, the measured data of a public administration office are considered to be representative to generate a dynamic load profile. For this public building, electricity and gas consumption within every 15 minutes was measured and logged during a whole year (2011).
However, before using these data, some remarks have to be made on the measured building.

Building characteristics

The measured public building has a floor area of about $1000m^2$. Besides, its annual gas consumption amounts to $194\,MWh$ and its yearly electricity consumption amounts to $53.4\,MWh$.
Compared to the average office buildings presented in Figure 1.5, the electricity consumption, $53.4\,kWh/m^2$, is rather low and the gas consumption rather high, $194\,kWh/m^2$.

Scaling of the energy profile

Especially the gas demand is too high to be representative for a low energy building. This is due to a poor insulation rate. Therefore, the data of the gas consumption are scaled to a yearly heat consumption of $30\,kWh/m^2$. In Belgium, this number is the maximum value for the sum of the net heat and cooling demand in order to define a building officially to be low energy.

These adaptations to the measurements resulted in following energy profile, shown in Figure 8.8.

8.3.2 Sizing of components and control strategy

Figure 8.8 shows a maximum heat demand of about 25 – $30\,kW$. Compared to the residential building, the heat demand is spread more in time. This is due to the higher thermal inertia of the building and its less user-driven behaviour, as the office is controlled at comfort temperature during office hours.

Since the maximum heat output of the AFC-based micro-CHP is about $4\,kW$, the auxiliary heater has to be about 20 – $25\,kW$. Because the hourly peak is even lower, which could be further lowered with the use of a buffer tank, it is chosen to work with a boiler similar to the case in a residential building.
This is justified by the daily energy use, shown in Figure 8.9. It is shown there

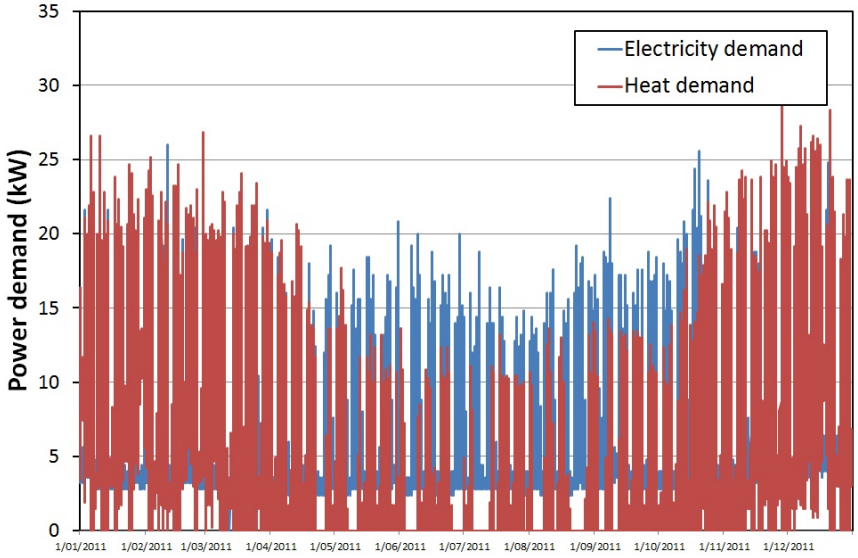

Figure 8.8: An overview of the scaled heat and electricity demand for an office building, based on the actual energy measurements of a public administration office in 2011. The time step for these measurements was 15 minutes. The scaling sized the heat demand to be representative for a low energy building.

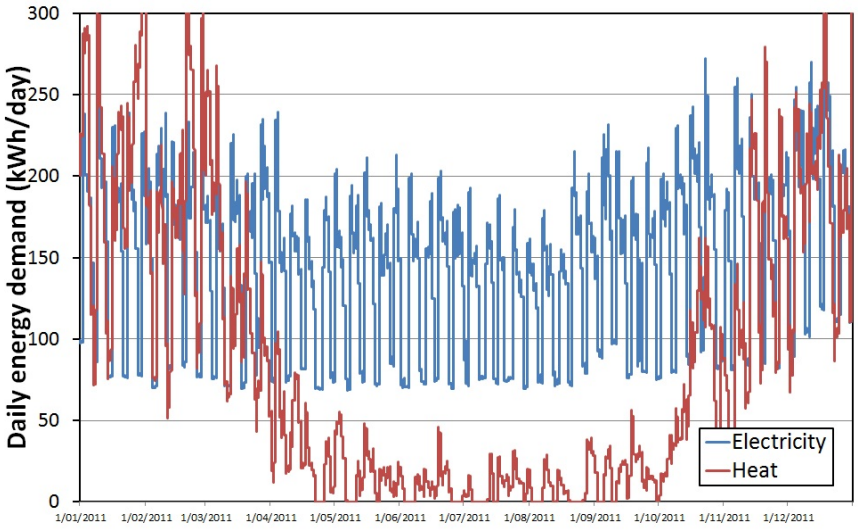

Figure 8.9: The daily energy use for both electricity and heat for the building case.

is a base load of 200 – $300\,kWh/day$ in winter or 10 – $13\,kW$. Taking this into account and to facilitate comparison it is chosen to work with an auxiliary heater $20\,kW$ and a buffer of $500\,l$, representing about $20\,kWh$ of storage with a maximum temperature difference of $20°C$.
Regarding control strategy, the same strategy is used as in CASE 1B, in this way a comparison of the results of these case studies will be a good illustration of their influence on the final results.

8.3.3 Results

8.3.3.1 Evaluation of system behaviour based on a week of operation

Similar to CASE 1, first the behaviour is discussed for a number of weeks, spread over the year. In Figure 8.10 an overview is given of the system behaviour and its heat and electricity production in comparison to demand in the office building. As can be seen in Figure 8.10(b), in winter the system is always 'ON' and almost all the time at nominal power, which is about $5\,kW$. Different from CASE 1A, this is due to the constant heat load of the building. As can be seen in Figure 8.6(a), the useful heat from the CHP is constantly about 3 to $4\,kW$. Besides, electrolyte temperature is about $50°C$, which is near optimum. Next, temperature in the buffer is relatively low, which minimises heat losses from the buffer tank. This results in a very efficient behaviour in winter.
The results of this period are summarized in Table 8.6 and compared to other seasons. As can be seen, during winter the heat demand is higher than nominal load of the CHP-unit. Similar to CASE 1B, which uses the same control strategy, in summer when there is no heat load the system is shut downs.
In spring and autumn the base load is almost sufficient to deliver the requested heat. These seasons are least efficient, as can be seen in Figure 8.11 the modus is running less time in optimal conditions. If this inefficiency could be addressed with more advanced control strategies, this could bring the system on a level where it is saving primary energy, compared to the best possible alternative separate production.

8.3.3.2 Evaluation based on primary energy and operation costs

For the evaluation of primary energy and energy costs the same assumptions were used. The results for the weeks, each representing another season and discussed in the previous section, are summarized in Table 8.4.
Because of the extra heat losses in the buffer and the low conversion factors for primary energy based on hydrogen consumption, no primary energy is saved compared to the best possible alternative with separate heat and electricity generation.
However, as can be seen from the results presented in Table 8.7, for an office case the system becomes competitive. As discussed earlier, system improvements can

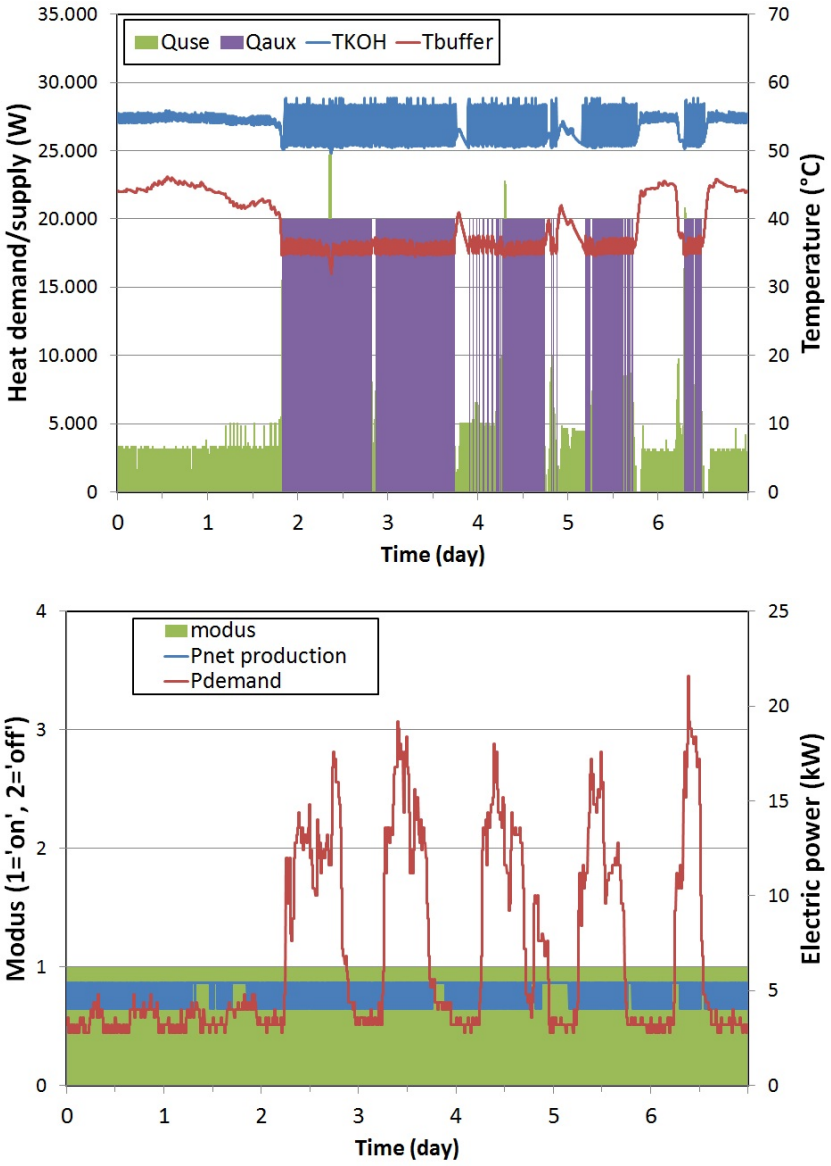

Figure 8.10: Simulation results of CASE 2 for the second week of January. In a) the temperatures of the electrolyte, T_{KOH}, and in the buffer tank, T_{buffer}, are shown together with the actual heat demand. In b) the electricity production and consumption are shown together with the modus of operation.

Period	8-14 JAN	8-14 APR	29JUL-4AUG	28OCT-3NOV
Pe, CHP	902	569	80	520
$P_{e,demand}$	1146	954	841	854
Q_{demand}	1211	349	29	420
Q_{aux}	630	40	0	105
$H_{2,aux.}$	741	47	0	124
$H_{2,CHP}$	2332	1438	201	1391
$H_{2,tot}$	3073	1485	201	1514

Table 8.6: Overview of the results for a week in every season for CASE 2. All values are expressed in kWh.

Description Unit	Demand or Production kWh	Primary Energy (HHV) kWh	Cost EUR
Heat Demand	30 000	33 333	2 333
Electric Demand	53 361	118 500	10 672
Reference Demand		151 833	13 005
CHP Electric production	26 989		
Consumed on site	83%		
CHP Heat production	16 322		
CHP Hydrogen consumption	69 296	81 493	9 008
Heat aux.burner	13 678	15 198	1 064
Hydrogen consumption (aux)	17 097	20 114	2 223
Electricity from the grid	26 372	58 604	5 274
CHP+aux on natural gas		155 295	15 346
CHP+aux (all hydrogen)		160 211	16 505
Savings with CHP		−3 462	−2 341
Savings relative to reference demand (%)		−2%	−18%
Savings relative to CHP Hydrogen consumption (%)		−4.2%	−26%

Table 8.7: Overview of the annual results for CASE 2, compared to separate production.

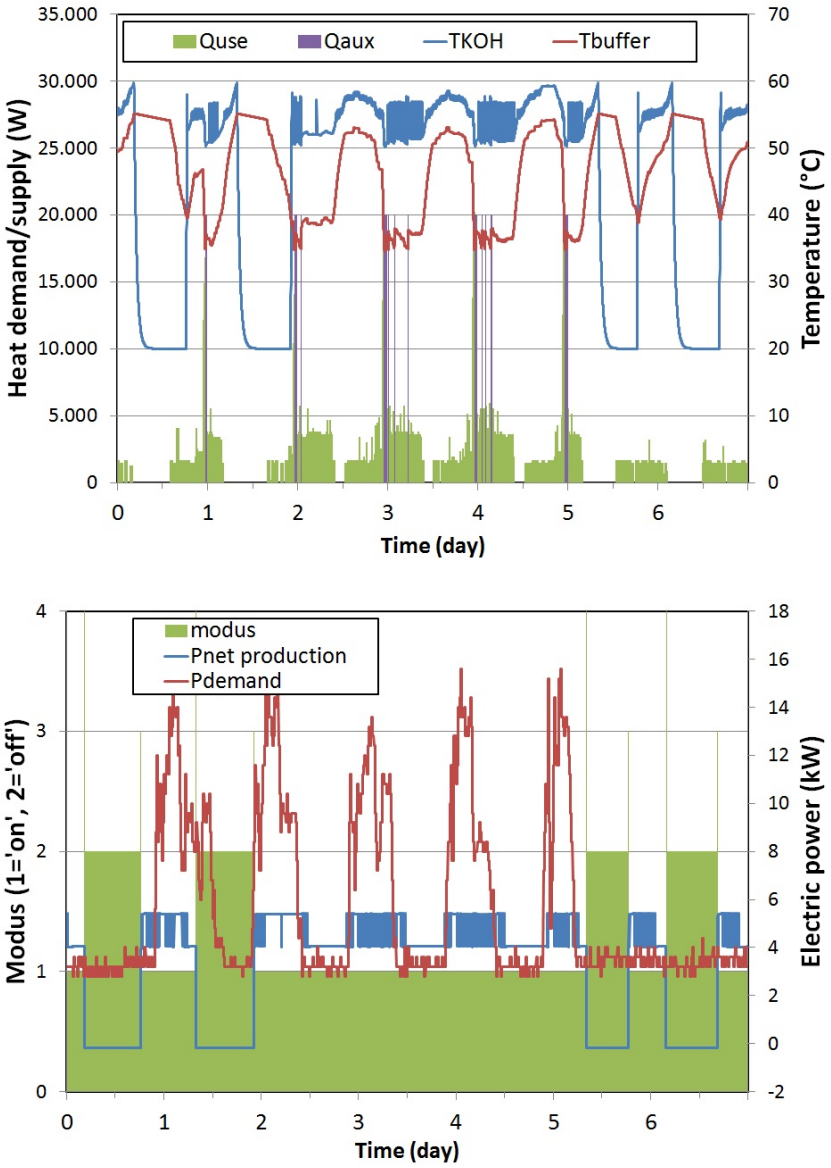

Figure 8.11: Simulation results of CASE 2 for the second week of April. In a) the temperatures of the electrolyte, T_{KOH}, and in the buffer tank, T_{buffer}, are shown together with the actual heat demand. In b) the electricity production and consumption are shown together with the modus of operation.

be achieved by heat recovery.

Besides, it has to be stated out that these results are strongly dependent on the chosen reference efficiencies. Figure 8.12 shows the influence of the chosen reformer efficiency and the reference efficiencies for heat and electricity.
In the center of the figure the used efficiencies are shown, resulting in a relative primary energy saving of -4%. By comparing the system with the present average Belgian power plant ($40\%(LHV)$ or $36\%(HHV)$), it is shown that for an office case savings are achieved up to 15%.
Also here the conversion factor for hydrogen has a big influence on overall performance. As can be seen in Figure 8.12, increasing reformer efficiency increases saving potential substantially.
From a financial point of view, also in offices hydrogen cost has to drop before the system becomes profitable. Since here electricity can be consumed on site, the cost benefit analysis still shows a negative result but less pronounced.
A sustainable hydrogen production, e.g. by electrolysis from renewable electricity, which cannot be consumed instantaneously, can be represented by high 'reformer' efficiencies in Figure 8.12. Sustainable hydrogen production will enable the system to become profitable both from an energy point of view as financially.

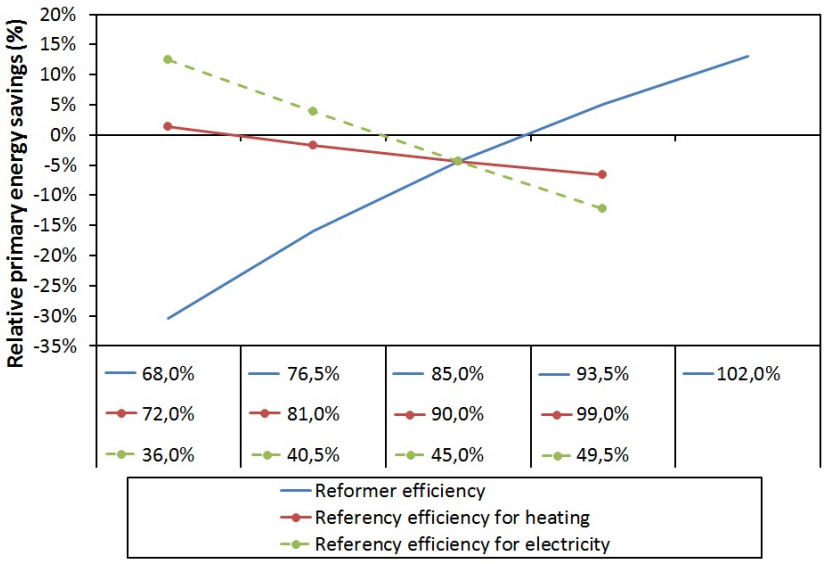

Figure 8.12: Sensitivity of the relative primary energy savings to the reformer efficiency (efficiency for hydrogen production) and the reference efficiencies for separate heat and electricity production.

Efficiency	Fuel	CASE 1A	CASE 1B
Thermal	Hydrogen	19%	22%
Electrical	Hydrogen 40%	39%	
Thermal	Natural Gas (85%)	16%	19%
Electrical	Natural Gas (85%)	34%	33%

Table 8.8: Overview of net CHP efficiencies over a whole year operation for the studied cases.

8.4 Closure

As illustrated in the case studies an AFC-based CHP-system does not result in primary energy savings within a low energy building, although it is necessary to put these results in perspective.

The main reason the case study turned out to be negative is due to the low thermal efficiency (See Table 8.8). With the conversion factor for hydrogen the AFC-based fuel cell system is still competitive regarding electrical performance, but thermal efficiency is too low.

Other system set-ups or control strategies can solve this disadvantage by reducing this heat loss and can make the system competitive, but savings will not be spectacular. With fossil energy and reforming as a source for hydrogen fuel, AFC-based CHP-systems show a limited (or even negative) saving potential.

However, this saving potential can be increased substantially with an integrated reformer. In this case, the heat losses due to reformer can be recovered as a useful heat output. For alkaline fuel cells, this set-up would also require additional fuel treatment, because of the CO_2-sensitivity of the electrolyte.

Nevertheless, for hydrogen fed systems with hydrogen out of fossil fuels the saving potential is limited.

With hydrogen as a storage medium or alternative energy carrier from waste or renewable energy, these conclusions change, because the conversion factor will change. As stated at the World Hydrogen Energy Conference 2012 in Toronto, hydrogen from renewables is the future for all hydrogen applications.

9 Conclusions

9.1 Conclusions

In this study an alkaline fuel cell stack model is presented, which is able to predict electric performance, thermal and water household. The model is based on a control volume approach, applying general thermodynamic laws to understand stack behaviour.
Compared to existing studies, which focus mainly on the electric performance, the present model includes two important extra aspects:

- all outlet temperatures are predicted
- no preliminary assumptions are made as to the removal of water (vapour)

For the water balance, all possible pathways removing water are considered, including dilution of the electrolyte.
These extra degrees of freedom in the model are solved assuming a saturated condition of the reaction water in the reaction layer and applying the gas diffusion equations. With this model, the experienced dilution of the electrolyte at low temperatures can be explained.

This new model is validated with experimental work on a prototype of an AFC-based micro-CHP.

Within the scope of this book to develop a more efficient control strategy

and/or to design an improved system set-up, **the developed stack model is proven to be useful for a thorough analysis on stack behaviour with respect to thermal system integration**.

With respect to this, several multi-stack configurations are modelled and analysed.
The results of these analyses show that a parallel electrolyte flow through the different stacks offers good results regarding performance and water management. Considering also air and hydrogen flow, the present multi-stack configuration is an acceptable choice.

Next, the influence on thermal and electrical performance by system dependent parameters like air flow rate, load, electrolyte flow,... but also by insulation rate of the stack are analysed. This analysis is first made on the level of the stack.
Here, it is shown that

- for every current an ideal electrolyte temperature exists and vice versa.
- system improvement is to be found in increasing input air temperature and/or reducing heat loss to the surroundings.

However, these improvements have to be achieved within the boundaries of a stable water management. This fact limits the range of the electrolyte temperature, which has an influence on both electrical and thermal performance.
Stack analysis showed that the upper boundary can be increased by applying hot humidified air. This will allow higher electrolyte temperatures, resulting mainly in an increased electrical performance of the stack.

Based on these insights several system set-ups are modelled, next to the reference system, used for validation.
For each of these set-ups, the guidelines for an effective control strategy and the sensitivity to different component efficiencies are elaborated. It is shown that for most components, like pumps and fans, cost effective solutions are acceptable, since they have little influence on performance. The inverter and purge efficiency however are more critical to the overall performance of the system.
Regarding the general system configuration, the suggested improvements promise to have a substantially better performance.

With these system models the initial theorem about micro-CHP characteristics is illustrated. It is shown that the fuel cell based system has a more interesting **part load behaviour** than conventional micro-CHPs; their power-to-heat ratio is significantly higher, which is interesting regarding future expectations on energy demand in building, as discussed in Chapter 1.

However, before the system can be implemented in these buildings, some **practical aspects regarding building integration, model complexity and control strategy** needed to be implemented.
First, to simplify the models' complexity a regression analysis is applied to preserve the main characteristics, but without the details about its complex non-linear behaviour.
Secondly, to deal with the system complexity and to stabilize water management, an external buffer tank is implemented. The buffer tank allows control to focus on system stability and efficiency.

Finally, the potential and application of an AFC-based micro-CHP for building applications is simulated with two case studies, as an illustration of the relevance of the model.
For these two case studies, buildings with a relatively low heat demand are chosen, in accordance with modern building design. These are elaborated for a residential building and for an office building. Based on these case studies, it is possible to pose some general remarks, although results will be different for every case study. Compared to the best possible alternative with a separate production of heat and electricity, no primary energy savings are only obtained. However, competitive results are achieved in the office case, which has a higher number of operating hours and a more stable heat demand. These conditions are not different from those for other CHP-systems. In general, primary energy savings are expected to be small or even negative, due to the incorporated efficiency for hydrogen production.
Regarding economics within the present financial model for energy, it is necessary that the produced electricity is consumed on site. As for now this means on a yearly basis. Next to that the price for hydrogen has to reach the same level as alternative fuels to achieve payback.
In residential buildings with a normal consumption pattern, the electricity demand is never high enough compared to the heat load to consume all produced electricity on site. Even in passive houses a heat load, for domestic hot water, exists, resulting in too high electricity production, compared to the own consumption.
In low energy offices or passive offices, this ratio in electricity demand compared to heat demand is more interesting from a financial point of view.
Regarding both costs and energy savings, offices show the largest potential for future applications, based on these two case studies. With respect to feasibility, the issue of hydrogen conversion is still a decisive parameter. In general, also reducing investment costs and enhancing lifetime remain key factors for successful commercialisation of fuel cell based systems.
Some interesting evolutions are present though, offering perspective for future research and developments.

9.2 Perspectives

As the energy market is changing and as the electricity production is linked with heat demand, which is the highest in winter time, the technology shows to be compatible with solar electricity production. This offers new opportunities for the use of micro-CHP.

Recommendations for future research

The combination of these technologies on a building scale can be topic of further research, challenging technical, economical and optimization problems.
As the system is hydrogen based, the cycle could be completed with on site hydrogen production at high solar gains. At the World Hydrogen Energy Conference in Toronto 2012, this point of view is growing in interest. It is stated, hydrogen research has to focus on sustainable hydrogen application facing all technical, conceptual and economical challenges with this respect. This can change the primary energy ratio for hydrogen, which will have a serious impact on the results as shown in the case studies.

Regarding control optimization, recommendations and guidelines for control strategy are proposed. In the presented work this is implemented in a rule based control strategy. Regarding dynamics and set point identification, improvements are still possible. Complex control strategies, based on fuzzy logic combined with more generic self-learning algorithms, can be developed to improve control. The model can be used to evaluate these more advanced control strategies.

Next to generalization and translation of the results to different circumstances, also improvements are possible regarding model development itself.
As mentioned earlier, the model can be improved by implementing degradation and CO_2 contamination or electrolyte dilution.
Integrating a reformer can change the thermal household completely. However, in this case the CO_2-sensibility of alkaline fuel cells, has to be taken into account.
The insight out of the AFC model can be combined with those from existing PEMFC models in order to develop a model for alkaline membrane fuel cells as this shows to be a promising new type of fuel cell, combining the best of both fuel cell technologies.
These model improvements or adjustments will allow to evaluate the feasibility of AFC-based micro-CHP implementation in an broader context.

A Publications

A.1 Publications in peer reviewed international journals

- I. Verhaert, G. Mulder and M. De Paepe. *Thermodynamic model for an alkaline fuel cell*. Journal of Power Sources, 193(1):233–240, August 2009.

- I. Verhaert, S. Verhelst, G. Janssen, G. Mulder, and M. De Paepe. *Water management in an alkaline fuel cell*. International Journal of Hydrogen Energy, 36 (17): 11011-11024, August 2011.

- I. Verhaert, S. Verhelst, G. Janssen, G. Mulder and M. De Paepe. *Electrical and Thermal Performance of an Alkaline Fuel Cell*, Applied Thermal Engineering, 40: 227-235, 2012.

- I. Verhaert, G. Mulder and M. De Paepe. *Evaluation of an AFC as a micro-CHP*, Energy Conversion and Management, (submitted August 2012, under revision)

- I. Verhaert, G. Mulder and M. De Paepe. *Optimization of control strategy and system integration of an AFC-stack within a micro-CHP*, Applied Thermal Engineering, (to be submitted in 2013)

A.2 Related publications in proceedings of international conferences

- I. Verhaert, G. Mulder and M. De Paepe.*Thermodynamic model for an alkaline fuel cell*. Fuel Cells Science and Technology 2008, Scientific Advances in Fuel Cell Systems(FUCE2008), 2008, Kopenhagen, Denmark.
- I. Verhaert, G. Mulder and M. De Paepe.*HEAT AND WATER MANAGEMENT IN AN ALKALINE FUEL CELL*. 8th International Conference on Heat Transfer, Fluid Mechanics and Thermodynamics(HEFAT2011), 2011, Pointe Aux Piments, Mauritius. Awarded as best session paper.
- I. Verhaert, G. Mulder and M. De Paepe.*Model based evaluation of an AFC-system as a micro CHP in comparison with other technologies*. World Hydrogen Energy Conference (WHEC2012), 2012, Toronto, Canada.

A.3 Other publications and presentations

- I. Verhaert, *Thermodynamic model for an alkaline fuel cell*. PhD symposium in Ghent, 2008, Ghent, Belgium.
- I. Verhaert, G. Mulder and M. De Paepe.*Thermodynamic Model and Water Management for an Alkaline Fuel Cell*. Fuel Cells Science and Technology 2010, Scientific Advances in Fuel Cell Systems(FUCE2010), 2010, Zaragoza, Spain.
- I. Verhaert, G. Mulder and M. De Paepe.*Thermodynamic Model and Water Management for an Alkaline Fuel Cell*. Fuel Cells Science and Technology 2010, Scientific Advances in Fuel Cell Systems(FUCE2010), 2010, Zaragoza, Spain.
- I. Verhaert, G. Mulder and M. De Paepe.*Performance evaluation of an AFC-stack as a possible micro-CHP*. Fuel Cells Science and Technology 2010, Scientific Advances in Fuel Cell Systems(FUCE2012), 2012, Berlin, Germany.

B
Diagnosis tool

Within fuel cell development, it is important to characterize fuel cell performance. A certain 'measurement tool' could be used to evaluate the effect of degradation and/or contamination of a fuel cell. It could also be used for on-site management of the cells and stack [59].
In this appendix a brief overview is given of the existing techniques to characterize the mostly electric behaviour of the fuel cell. Afterwards some work is presented regarding model estimation to characterize a fuel cell based on polarization curves. This technique can be used to characterize the electrochemical model for new stacks or to characterize the electrochemical model for degenerated stacks.

B.1 The electrochemical model

B.1.1 Fuel cell characterization techniques

In Refs. [36, 39] a more elaborated overview is given on the different characterization techniques. Two types of characterization are possible.

- electrochemical characterization techniques (in situ): These techniques use the variables of voltage, current and time to characterize performance under operating conditions
- Ex situ characterization techniques: here structure details are analysed, specific components. The fuel cell is not evaluated under operating conditions.

Within in situ characterization four methods are used.

- current-voltage measurement or interpretation of the polarization curve. To interpret these measurements some model estimation techniques are also required.
- current interrupt method. This technique allows to separate ohmic losses from the other losses.
- Electrochemical Impedance Spectroscopy (EIS). This technique can distinguish ohmic, activation and diffusion losses, although is sometimes difficult to interpret.
- Last method is cyclic Voltametry (CV). It can require some modification to the fuel cell, to operate with additional test gases, like argon or nitrogen.

Although CV and EIS can distinguish more influences, the polarization curve is still very important to follow up on stack performance during operation.

B.1.2 Polarization curve

This is in fact the electrochemical model used in Chapter 2.

$$P_e = U \cdot I \tag{B.1}$$

$$U = E_{Nernst} - \eta_{act} - \eta_{res} - \eta_{diff} \tag{B.2}$$

$$E_{Nernst} = -\frac{\Delta G_0}{2Far} + \frac{RT_{cell}}{2Far}\left[ln\left(p_{H_2}\right) + \frac{1}{2}ln\left(p_{O_2}\right)\right] \tag{B.3}$$

$$\eta_{act} = \frac{R \cdot T}{\alpha \cdot n \cdot Far} ln\left(\frac{\frac{I_{cell}}{A}}{j_0}\right) \tag{B.4}$$

$$\eta_{res} = R_e \cdot I_{cell} \tag{B.5}$$

$$\eta_{diff} = \frac{R \cdot T}{\alpha \cdot n \cdot Far} ln\left(\frac{j_L}{j_L - \frac{I_{cell}}{A}}\right) \tag{B.6}$$

$$j_0 = c_1 \cdot exp\left(\frac{-c_2}{T_{cell}}\right) \tag{B.7}$$

$$R_e = c_3 - c_4 \cdot T_{cell} \tag{B.8}$$

This model has different versions. In Refs. [39] another approach of the diffusion losses is used.

$$\eta_{diff} = m.exp(n \cdot i) \tag{B.9}$$

In Eq.B.9 m and n are model parameters. A general expression and simplified expression lead to following expressions.

$$V = E - i \cdot r - A \cdot ln(i) + m.exp(n \cdot i) \tag{B.10}$$

or with the other model

$$V = E - i \cdot r - A \cdot ln(i) + B \cdot ln\left(\frac{i_L}{i_L - i}\right) \tag{B.11}$$

$$= C_1 - i \cdot C_2 + C_3 \cdot ln(i) + C_4 \cdot ln\left(1 + C_5 \cdot i\right) \tag{B.12}$$

The last expression makes a more general approach with 5 model parameters, C_i.

B.2 Model estimation

In this section the current - voltage approach is used to define the electrochemical model. However first the robustness of the model is tested.

B.2.1 Model validation

This kind of model validation differs from the one executed in Chapter 3. Several models were generated based on Eq.B.12.

$$V = C_1 \tag{B.13}$$

$$V = C_1 - i \cdot C_2 \tag{B.14}$$

$$V = C_1 - i \cdot C_2 + C_3 \cdot ln(i) \tag{B.15}$$

$$V = C_1 - i \cdot C_2 + C_4 \cdot ln\left(1 + C_5 \cdot i\right) \tag{B.16}$$

$$V = C_1 - i \cdot C_2 + C_3 \cdot ln(i) + C_4 \cdot ln\left(1 + C_5 \cdot i\right) \tag{B.17}$$

$$V = C_1 + C_3 \cdot ln(i) + C_4 \cdot ln\left(1 + C_5 \cdot i\right) \tag{B.18}$$

To validate the robustness of the model, data were elaborated with the model and based on the routine of a Levenberg-Marquardt solver, model estimation is performed. First this was performed with perfect model data, later with distortion on the model results.
It is shown that the complete model is not very robust because the ohmic losses can't well be separated from the diffusion losses. Using model estimation based on BIC-criterion the polarization curve can be evaluated.

C

Results: measurement and simulation

In Chapter 3 is referred to a large set of data points with which the model is validated. In this Appendix the complete set of measurement and simulation data are listed, allowing the reader to evaluate the validation.
In Chapter 3 this complete list is reduced to a few data points, in order to allow a brief discussion. The complete set is not used in Chapter 3, because this would hamper a smooth reading.

C.1 Model validation in 50 data points

First the measurements are shown which are used as input data for the validation. Secondly each modelled and measured output parameter is shown, allowing validation and comparison. Finally the modelled water management is shown for the 50 data points, although it has not been validated for these points. All these data points are represented by their mean value and their standard deviation (s.d).

C.1.1 Input data

Working point	Current		Electrolyte input flow		Electrolyte input temperature		Air input flow	
	A		kmol/h		$^{\circ}C$		kmol/h	
	mean	s.d.	mean	s.d.	mean	s.d.	mean	s.d.
1	18.5	0.9	22.1	0.0	29.4	1.8	0.3	0.2
2	18.4	0.1	21.7	0.0	33.9	3.1	0.3	0.2
3	18.4	0.1	22.2	0.0	38.0	0.9	0.3	0.1
4	23.5	0.9	21.4	0.5	29.2	1.7	0.4	0.0
5	23.5	0.1	21.7	0.0	33.7	3.1	0.3	0.1
6	23.4	0.3	21.8	0.0	38.8	2.5	0.3	0.1
7	30.5	2.8	20.9	0.8	29.0	1.9	0.4	0.1
8	28.3	0.2	21.6	0.0	33.4	2.4	0.3	0.2
9	28.4	0.2	21.6	0.0	39.3	3.0	0.3	0.1
10	34.6	2.2	20.4	1.0	31.1	1.3	0.5	0.2
11	33.5	2.0	20.1	0.6	33.2	2.1	0.3	0.1
12	33.3	0.2	21.6	0.0	37.9	2.1	0.3	0.1
13	33.3	0.2	21.8	0.0	44.4	1.9	0.3	0.0
14	34.9	1.8	19.2	1.5	64.6	2.6	0.8	0.3
15	34.6	3.2	20.2	0.0	68.0	3.5	0.6	0.3
16	39.1	2.9	21.2	1.6	33.6	1.9	0.4	0.3
17	38.3	0.6	20.5	0.0	38.4	1.7	0.3	0.1
18	38.2	0.2	22.2	0.6	43.7	1.8	0.3	0.0
19	39.8	2.3	22.4	0.0	49.1	2.7	0.6	0.3
20	39.7	2.6	21.8	0.0	54.0	2.3	0.5	0.3
21	38.5	0.8	21.9	0.0	64.3	3.3	0.6	0.3
22	38.4	0.4	20.2	0.0	69.1	2.6	0.8	0.2
23	43.4	1.9	21.3	0.0	34.0	1.9	0.4	0.3
24	43.4	1.6	20.4	0.0	38.6	1.7	0.5	0.4
25	43.4	0.8	21.8	0.0	52.5	3.4	0.4	0.3

Working point	Current		Electrolyte input flow		Electrolyte input temperature		Air input flow	
	A		kmol/h		$^{\circ}C$		kmol/h	
	mean	s.d.	s.d.	s.d.	mean	s.d.	mean	s.d.
26	43.5	1.4	20.4	0.0	59.7	3.7	0.4	0.3
27	43.4	1.1	21.5	0.0	63.7	2.9	0.6	0.3
28	44.0	2.5	20.8	0.0	69.2	2.7	0.8	0.2
29	48.3	1.3	21.6	0.0	34.9	1.9	0.5	0.4
30	48.1	0.3	19.7	0.0	49.6	3.8	0.3	0.2
31	48.2	0.4	21.8	0.0	53.2	2.8	0.4	0.3
32	48.2	0.6	20.9	3.9	58.1	5.2	0.3	0.2
33	49.1	2.4	19.2	1.0	70.7	3.6	0.8	0.3
34	53.4	1.5	21.2	0.0	39.4	2.7	0.6	0.3
35	55.9	2.2	20.0	0.0	42.9	2.2	0.4	0.4
36	54.7	2.4	20.8	0.0	49.4	1.1	0.6	0.4
37	54.1	2.6	21.7	0.6	53.8	2.9	0.6	0.3
38	54.3	2.5	20.4	0.7	58.8	3.4	0.6	0.3
39	54.5	3.0	20.9	0.7	64.5	3.6	0.7	0.1
40	53.8	1.9	19.2	0.0	68.8	2.7	0.8	0.3
41	59.9	2.8	19.5	0.9	44.3	1.6	0.5	0.3
42	58.5	1.7	20.6	0.0	49.5	1.4	0.5	0.4
43	59.6	2.2	19.1	0.0	70.2	2.9	0.8	0.2
44	63.3	2.3	18.8	0.0	49.3	1.9	0.5	0.3
45	65.0	2.9	19.3	1.3	63.7	2.0	0.7	0.3
46	63.3	0.8	18.6	1.1	68.4	1.3	0.8	0.1
47	68.4	1.5	19.4	0.9	63.3	3.4	0.8	0.2
48	68.1	1.0	18.9	2.2	68.4	1.5	0.8	0.1
49	74.2	3.6	18.6	1.0	62.9	3.9	0.8	0.2
50	73.3	1.8	19.8	0.0	68.3	1.9	0.9	0.1

C.1.2 Model and measurements: voltage

Working point	Voltage V				
	Measurement		Model output		
	mean	s.d.	mean	lower	upper
1	75.2	0.7	75.5	75.1	75.9
2	75.8	0.5	75.8	75.6	76.1
3	75.9	0.3	76.1	76.0	76.2
4	74.2	0.5	74.0	73.7	74.4
5	74.8	0.5	74.4	74.1	74.6
6	74.9	0.3	74.7	74.5	75.0
7	72.8	1.1	72.3	71.6	73.1
8	72.8	0.4	73.1	72.9	73.3
9	73.7	0.6	73.5	73.3	73.8
10	71.9	1.0	71.6	71.0	72.1
11	71.9	0.6	71.9	71.4	72.5
12	72.4	0.5	72.3	72.1	72.5
13	73.3	0.2	72.7	72.5	72.9
14	73.6	0.4	73.6	73.0	74.2
15	73.2	1.2	73.9	73.0	74.9
16	70.9	1.0	70.8	70.1	71.5
17	71.5	0.6	71.3	71.0	71.5
18	72.5	0.2	71.6	71.4	71.7
19	71.5	1.6	71.6	71.0	72.3
20	71.5	1.2	71.9	71.3	72.7
21	72.8	0.3	72.8	72.4	73.2
22	72.8	0.4	73.1	72.8	73.4
23	69.8	0.6	69.9	69.5	70.5
24	70.6	1.1	70.3	69.8	70.7
25	71.4	0.6	71.1	70.7	71.5

Working point	Voltage V				
	Measurement		Model output		
	mean	s.d.	mean	lower	upper
26	71.8	0.8	71.5	71.0	72.1
27	72.0	0.4	71.8	71.4	72.2
28	71.7	2.0	72.0	71.3	72.7
29	69.2	1.1	69.1	68.7	69.4
30	70.2	0.3	70.0	69.7	70.3
31	70.6	0.4	70.2	70.0	70.5
32	70.9	0.4	70.5	70.1	71.0
33	70.4	2.3	71.1	70.4	71.8
34	68.9	1.3	68.4	68.0	68.9
35	67.9	0.9	68.2	67.7	68.8
36	69.3	0.9	68.8	68.3	69.3
37	69.3	0.7	69.2	68.5	69.8
38	70.1	1.3	69.4	68.8	70.1
39	70.1	0.7	69.7	69.0	70.5
40	69.7	1.7	70.1	69.6	70.6
41	67.3	0.9	67.6	67.0	68.2
42	68.3	0.6	68.2	67.8	68.6
43	68.9	1.5	69.2	68.6	69.7
44	67.4	0.8	67.4	66.9	67.9
45	68.4	0.8	67.9	67.3	68.5
46	68.6	0.6	68.4	68.2	68.6
47	67.9	0.4	67.3	66.9	67.8
48	67.7	0.5	67.6	67.4	67.9
49	66.7	1.1	66.4	65.6	67.2
50	67.0	0.6	66.8	66.4	67.2

C.1.3 Model and measurements: Electrolyte output temperature

Working point	Electrolyte output temperature $^{\circ}C$				
	Measurement		Model output		
	mean	s.d.	mean	lower	upper
1	31.4	2.0	30.9	29.2	32.8
2	35.6	2.6	34.9	32.1	37.7
3	39.3	1.0	38.3	37.4	39.3
4	31.3	1.9	31.7	30.0	33.4
5	35.4	2.6	35.5	32.8	38.3
6	40.2	2.7	39.9	37.7	42.2
7	29.4	1.6	32.8	30.5	35.2
8	36.2	2.2	36.2	34.0	38.6
9	41.3	2.4	41.3	38.6	43.9
10	31.7	1.3	35.5	33.7	37.4
11	36.0	2.6	37.3	34.9	39.7
12	40.7	2.2	40.9	39.1	42.8
13	44.8	1.8	46.4	44.7	48.0
14	64.6	2.5	61.6	58.8	64.5
15	68.8	2.6	64.4	60.8	68.3
16	36.3	2.5	38.4	35.8	41.3
17	41.3	1.9	42.4	40.8	44.1
18	44.2	1.6	46.6	45.0	48.2
19	51.8	4.2	51.0	48.1	54.0
20	56.8	3.5	55.2	52.5	58.3
21	65.2	2.9	62.6	59.6	65.8
22	69.4	2.9	65.5	63.3	67.8
23	37.2	1.0	39.5	37.4	41.9
24	41.8	2.2	43.5	41.5	45.7
25	55.1	2.8	54.7	51.4	59.3

Working point	Electrolyte output temperature $^{\circ}C$				
	Measurement		Model output		
	mean	s.d.	mean	lower	upper
26	60.4	3.4	60.6	57.1	64.8
27	64.8	2.8	63.0	60.2	66.2
28	69.5	2.8	66.7	64.1	69.4
29	39.4	0.7	41.0	38.9	43.3
30	52.8	3.2	53.7	50.4	57.1
31	55.9	2.8	56.2	53.5	59.3
32	60.8	4.1	60.2	55.2	65.5
33	71.1	3.1	68.5	65.2	71.9
34	42.2	0.9	45.8	43.1	48.7
35	44.5	2.0	49.7	47.1	52.7
36	52.4	3.1	54.3	52.5	56.3
37	56.4	3.2	57.5	54.2	60.9
38	60.1	1.2	61.5	57.9	65.2
39	66.6	5.2	65.4	62.0	68.7
40	70.1	1.4	68.2	65.6	70.9
41	46.0	1.8	51.8	49.2	54.8
42	53.5	2.7	55.3	53.4	57.6
43	70.9	1.5	70.1	67.5	72.7
44	53.0	3.7	56.7	54.3	59.5
45	66.1	5.5	67.2	64.5	70.2
46	69.5	1.1	69.8	68.7	71.0
47	65.6	2.6	67.5	64.4	70.5
48	69.6	1.2	70.7	69.1	72.3
49	65.7	2.8	68.6	64.5	72.6
50	69.5	1.9	71.5	69.8	73.2

C.1.4 Model and measurements: Air output temperature

Working point	Air output temperature $^{\circ}C$				
	Measurement		Model		
	mean	s.d.	mean	lower	upper
1	27.7	1.5	27.3	24.6	29.5
2	31.0	2.3	30.2	26.5	33.5
3	34.6	1.1	32.6	29.9	34.5
4	27.7	1.3	27.6	26.3	29.0
5	30.8	2.1	30.6	27.9	33.3
6	35.3	2.4	33.4	30.8	36.0
7	25.9	1.6	28.3	26.3	30.4
8	32.4	1.8	30.4	25.7	33.5
9	36.3	1.8	34.2	31.1	37.2
10	27.2	1.3	30.4	28.0	32.4
11	32.0	2.6	30.8	27.6	33.5
12	35.9	1.8	33.6	31.1	36.0
13	36.4	1.7	38.0	36.7	39.4
14	60.8	1.4	58.4	53.9	62.0
15	62.4	1.1	59.9	52.6	64.8
16	30.9	2.5	31.8	26.3	35.0
17	35.9	2.3	34.5	31.4	37.0
18	35.8	1.5	37.9	36.6	39.2
19	43.9	3.4	45.3	39.8	49.2
20	47.3	2.3	47.8	38.2	52.3
21	60.3	2.5	57.4	51.4	61.9
22	63.5	1.6	62.2	58.4	65.3
23	31.4	1.1	32.3	26.8	35.5
24	35.6	3.0	36.6	29.6	39.8
25	48.0	2.8	45.9	4.5	51.7

Working point	Air output temperature $^{\circ}C$				
	Measurement		Model		
	mean	s.d.	mean	lower	upper
26	52.8	3.3	51.0	39.1	57.0
27	59.3	3.6	57.4	50.5	61.8
28	63.5	1.5	62.6	58.5	66.0
29	32.2	2.1	34.2	27.9	37.3
30	46.0	3.9	43.3	37.2	48.2
31	49.2	2.5	46.7	35.3	51.8
32	52.5	2.2	49.7	40.3	56.5
33	64.2	2.4	64.1	58.6	68.5
34	34.7	3.0	38.7	33.5	42.3
35	37.8	3.3	40.5	29.0	44.7
36	44.1	3.4	46.3	39.5	49.5
37	47.4	2.5	49.9	42.9	54.5
38	52.8	3.7	54.3	47.6	59.1
39	60.3	2.2	59.5	55.4	63.3
40	62.3	2.3	63.1	58.5	66.7
41	38.7	2.7	42.1	32.9	46.1
42	44.9	2.1	45.7	33.2	49.6
43	63.8	2.9	64.9	61.1	68.3
44	44.4	3.3	46.2	35.2	50.5
45	59.0	3.0	59.6	54.2	63.3
46	62.2	1.1	63.6	62.1	65.0
47	58.4	2.0	60.2	56.0	63.9
48	61.7	1.8	64.5	62.5	66.4
49	58.0	2.2	60.7	55.6	65.3
50	61.6	2.5	65.1	62.9	67.2

C.1.5 Modelled output of the water management

Working point	Electrolyte output flow rate kmol/hr			Net water production mol/hr		
	mean	lower	upper	mean	lower	upper
1	22.14	22.13	22.14	25.0	20.0	30.0
2	21.75	21.75	21.76	22.0	18.0	28.0
3	22.22	22.22	22.22	20.0	16.0	24.0
4	21.42	20.88	21.97	33.0	29.9	36.1
5	21.76	21.76	21.76	31.0	27.0	34.0
6	21.85	21.84	21.85	29.0	24.0	33.0
7	20.95	20.11	21.78	45.0	37.7	52.3
8	21.68	21.68	21.69	39.0	34.0	46.0
9	21.63	21.63	21.64	36.0	31.0	40.0
10	20.46	19.47	21.44	50.0	43.0	57.0
11	20.15	19.51	20.79	49.0	42.1	55.9
12	21.64	21.64	21.65	45.0	41.0	49.0
13	21.88	21.88	21.88	39.0	36.0	42.0
14	19.20	17.63	20.77	-18.0	-36.8	0.8
15	20.16	20.13	20.19	-29.0	-58.0	6.0
16	21.22	19.66	22.79	57.0	47.7	68.3
17	20.58	20.57	20.58	53.0	48.0	59.0
18	22.23	21.67	22.79	48.0	45.4	50.6
19	22.44	22.42	22.45	35.0	23.0	51.0
20	21.87	21.86	21.90	29.0	13.0	54.0
21	21.88	21.86	21.90	-9.0	-30.0	14.0
22	20.15	20.13	20.17	-33.0	-53.0	-14.0
23	21.39	21.38	21.40	65.0	56.0	74.0
24	20.47	20.46	20.48	58.0	50.0	72.0
25	21.88	21.87	21.93	40.0	23.0	84.0

Working point	Electrolyte output flow rate kmol/hr			Net water production mol/hr		
	mean	lower	upper	mean	lower	upper
26	20.46	20.44	20.49	25.0	2.0	55.0
27	21.48	21.46	21.51	0.0	-20.0	26.0
28	20.76	20.74	20.79	-27.0	-50.0	-4.0
29	21.69	21.68	21.70	70.0	62.0	82.0
30	19.73	19.72	19.74	56.0	42.0	67.0
31	21.89	21.87	21.91	46.0	31.0	68.0
32	20.98	17.02	24.95	36.0	11.5	60.5
33	19.14	18.12	20.15	-29.0	-63.1	2.0
34	21.29	21.28	21.30	72.0	63.0	83.0
35	20.08	20.07	20.10	74.0	62.0	93.0
36	20.87	20.86	20.89	61.0	49.0	78.0
37	21.72	21.09	22.36	49.0	31.5	70.5
38	20.41	19.67	21.16	34.0	13.5	58.5
39	20.93	20.24	21.62	11.0	-13.5	31.5
40	19.15	19.12	19.17	-12.0	-37.0	12.0
41	19.57	18.61	20.54	79.0	66.5	97.5
42	20.64	20.62	20.66	67.0	56.0	90.0
43	19.10	19.07	19.13	-14.0	-40.0	11.0
44	18.90	18.89	18.92	76.0	61.0	98.0
45	19.30	17.95	20.65	30.0	9.9	52.1
46	18.64	17.57	19.72	2.0	-7.7	10.7
47	19.45	18.51	20.39	34.0	12.9	54.1
48	18.88	16.65	21.12	7.0	-5.6	18.6
49	18.63	17.57	19.69	44.0	15.6	69.4
50	19.80	19.78	19.81	13.0	-3.0	29.0

References

[1] IEA. *World Energy Outlook 2010*. 2010.

[2] H. Khatib. *IEA World Energy Outlook 2011A comment*. Energy Policy, pages 1–7, June 2012.

[3] EC. *European 2020 targets*, 2011.

[4] S. de Ia Rue du Can and L. Price. *Sectoral trends in global energy use and greenhouse gas emissions*. Energy Policy, 36(4):1386–1403, April 2008.

[5] ECBCS. *Annex 49, Low Exergy Systems for High-Performance Buildings and Communities*. Technical report, 2011.

[6] G. Dall O, A. Galante, and G. Pasetti. *A methodology for evaluating the potential energy savings of retrofitting residential building stocks*. Sustainable Cities and Society, 4:12–21, February 2012.

[7] European Parlement. *Energy Efficiency Plan 2011*.

[8] EU(European Parlement). *European Building Directive 2002/91/CE on the energy performance of buildings*, 2002.

[9] European Environment Agency (EEA). *http://www.eea.europa.eu/data-and-maps/figures/households-energy-consumption-by-end-uses-1*, 2011.

[10] L. Pérez-Lombard, J. Ortiz, and C. Pout. *A review on buildings energy consumption information*. Energy and Buildings, 40(3):394–398, January 2008.

[11] J. Van der Veken and H. Hens. *Determination of the heating efficiency at building level*. In Proceedings of Clima2010 conference, 2010, Antalya, Turkey, pages 67–72, 2010.

[12] E.G. Hertwich and C. Roux. *Greenhouse Gas Emission from the Consumption of Electric and Electronic Equipment by Norwegian Households*. Environmental Science Technology, 45(19):8190–8196, 2011.

[13] M.C. Sanchez, J.G. Koomey, M.M. Moezzi, A. Meier, and W. Huber. *Miscellaneous electricity in US homes: Historical decomposition and future trends*. Energy Policy, 26(8):585–593, July 1998.

[14] R.A. Zogg and D.L. Alberino. *Electricity Consumption by Small End User in Residential Buildings, Final Report*. Technical report, Building Department of Energy (DOE), 1998.

[15] J. Cockroft and N. Kelly. *A comparative assessment of future heat and power sources for the UK domestic sector*. Energy Conversion and Management, 47(15-16):2349–2360, September 2006.

[16] U.S departement of Energy. *Buildings Energy Data Book*, 2011.

[17] M. Pehnt. *Environmental impacts of distributed energy systemsThe case of micro cogeneration*. Environmental Science & Policy, 11(1):25–37, February 2008.

[18] H.I. Onovwiona and V.I. Ugursal. *Residential cogeneration systems: review of the current technology*. Renewable and Sustainable Energy Reviews, 10(5):389–431, October 2006.

[19] V. Dorer and A. Weber. *Energy and CO2 emissions performance assessment of residential micro-cogeneration systems with dynamic whole-building simulation programs*. Energy Conversion and Management, 50(3):648–657, 2009.

[20] M. De Paepe, P. D' Herdt, and D. Mertens. *Micro-CHP systems for residential applications*. Energy Conversion and Management, 47(18-19):3435–3446, November 2006.

[21] H. Lund and E. Münster. *Modelling of energy systems with a high percentage of CHP and wind power*. Renewable Energy, 28(14):2179–2193, November 2003.

[22] *Directive 2004/8/EC of 11 February 2004 on the promotion of cogeneration based on a useful heat demand in the internal energy market and amending Directive 92/42/EEC*. Technical report.

[23] M. De Paepe and D. Mertens. *Combined heat and power in a liberalised energy market*. Energy Conversion and Management, 48(9):2542–2555, 2007.

[24] A. Fragaki and A.N. Andersen. *Conditions for aggregation of CHP plants in the UK electricity market and exploration of plant size*. Applied Energy, 88(11):3930–3940, November 2011.

[25] H. Ren, W. Gao, and Y. Ruan. *Optimal sizing for residential CHP system*. Applied Thermal Engineering, 28(5-6):514–523, April 2008.

[26] VREG. *Energiebesluit*, artikel 1.1.1, 2, 66.

[27] B. Thomas. *Benchmark testing of Micro-CHP units*. Applied Thermal Engineering, 28(16):2049–2054, November 2008.

[28] K. Alanne, N.s Söderholm, K. Sirén, and I. Beausoleil-Morrison. *Techno-economic assessment and optimization of Stirling engine micro-cogeneration systems in residential buildings*. Energy Conversion and Management, 51(12):2635–2646, 2010.

[29] Capstone. *Product sheet - C15 MicroTurbine*. pages found online August 19th 2012,.

[30] *Honda Ecowill*, http://www.ambientediritto.it/dottrina/Politiche energetiche ambientali/politiche e.a/img_micro-cogenerazione/img8.jpg found online 24 october 2011.

[31] J. Harrison. *Micro Combined Heat & Power (CHP) for housing no. June, pp. 28-30, 2004.* pages 28–30, 2004.

[32] V. Dorer, R. Weber, and A. Weber. *Performance assessment of fuel cell micro-cogeneration systems for residential buildings*. Energy and Buildings, 37(11):1132–1146, November 2005.

[33] I. Beausoleil-Morrison. *An Experimental and Simulation-Based Investigation of the Performance of Small-Scale Fuel Cell and Combustion-Based Cogeneration Devices Serving Residential Buildings Energy Conservation in Buildings and*. Number April. 2008.

[34] A.D. Hawkes, D.J.L. Brett, and N.P. Brandon. *Fuel cell micro-CHP techno-economics: Part 1 model concept and formulation*. International Journal of Hydrogen Energy, 34(23):9545–9557, December 2009.

[35] Jülich_Forschungszentrum. *Basic terms and operating principle of a fuel cell electricity generation system.*

[36] R. O'Hayre, S.-W. Cha, W. Colella, and F.B. Prinz. *Fuel Cell Fundamentals*. John Wiley en Sons Inc, 2006.

[37] DOE (U.S. Department of Energy). *http://srnl.doe.gov/hilights01.htm*.

[38] Roads2HY. *Illustration of a polarization curve*, http://www.ika.rwth-aachen.de/r2h/index.php/File:Polarization_curve_neu2.jpg found online 6th Ocotober 2012.

[39] J. Larminie and A. Dicks. *Fuel Cell Systems Explained*. John Wiley en Sons Inc, Chichester, 2nd edition, 2003.

[40] R. Onanena, L. Oukhellou, D. Candusso, F. Harel, D. Hissel, and P. Aknin. *Fuel cells static and dynamic characterizations as tools for the estimation of their ageing time*. International Journal of Hydrogen Energy, 36(2):1730–1739, January 2011.

[41] W. G. Colella. *Modelling results for the thermal management sub-system of a combined heat and power (CHP) fuel cell system (FCS)*. Journal of Power Sources, 118(1-2):129–149, May 2003.

[42] I. Staffell and A. Ingram. *Life cycle assessment of an alkaline fuel cell CHP system*. International Journal of Hydrogen Energy, 35(6):2491–2505, March 2010.

[43] A. Hawkes and M. Leach. *Solid oxide fuel cell systems for residential micro-combined heat and power in the UK: Key economic drivers*. Journal of Power Sources, 149:72–83, September 2005.

[44] I. Staffell and R.J. Green. *Estimating future prices for stationary fuel cells with empirically derived experience curves*. International Journal of Hydrogen Energy, 34(14):5617–5628, July 2009.

[45] Waterstofnet. *www.waterstofnet.eu* ,found online in September 2012.

[46] I. Staffell. http://wogone.com/iq/review_of_fuel_cell_performance.pdf (2009) [cited December 2010].

[47] A. Musa. *Fuel Cell Power Cycles for Future Power Supply*. Phd, Ghent University, 2008.

[48] J. A. Schuler, Z. Wuillemin, A. Hessler-Wyser, C. Comminges, N. Y. Steiner, and J. Van Herle. *Cr-poisoning in (La,Sr)(Co,Fe)O3 cathodes after 10,000h SOFC stack testing*. Journal of Power Sources, 211:177–183, August 2012.

[49] A.D. Hawkes, D.J.L. Brett, and N.P. Brandon. *Fuel cell micro-CHP techno-economics: Part 2 Model application to consider the economic and environmental impact of stack degradation*. International Journal of Hydrogen Energy, 34(23):9558–9569, December 2009.

[50] R. Barrera, S. Debiase, S. Ginocchio, S. Bedogni, and L. Montelatici. *Performance and life time test on a 5kW SOFC system for distributed cogeneration*. International Journal of Hydrogen Energy, 33(12):3193–3196, June 2008.

[51] O.A. Shaneb, G. Coates, and P.C. Taylor. *Sizing of residential μCHP systems*. Energy and Buildings, 43(8):1991–2001, August 2011.

[52] K. Alanne, A. Saari, V. Ismet Ugursal, and J. Good. *The financial viability of an SOFC cogeneration system in single-family dwellings*. Journal of Power Sources, 158(1):403–416, July 2006.

[53] Y. Wang, K.S. Chen, J. Mishler, S. Chan Cho, and X.C. Adroher. *A review of polymer electrolyte membrane fuel cells: Technology, applications, and needs on fundamental research*. Applied Energy, 88(4):981–1007, 2011.

[54] N. Briguglio, M. Ferraro, G. Brunaccini, and V. Antonucci. *Evaluation of a low temperature fuel cell system for residential CHP*. International Journal of Hydrogen Energy, 36(13):8023–8029, July 2011.

[55] P.E. Santangelo and P. Tartarini. *Fuel cell systems and traditional technologies. Part I: Experimental CHP approach*. Applied Thermal Engineering, 27(8-9):1278–1284, June 2007.

[56] J. Wu, X. Z. Yuan, J. J. Martin, H. Wang, J. Zhang, J. Shen, and W. Wu, S.and Merida. *A review of PEM fuel cell durability: Degradation mechanisms and mitigation strategies*. Journal of Power Sources, 184(1):104–119, September 2008.

[57] L. Barelli, G. Bidini, F. Gallorini, and A. Ottaviano. *An energeticexergetic comparison between PEMFC and SOFC-based micro-CHP systems*. International Journal of Hydrogen Energy, 36(4):3206–3214, February 2011.

[58] G. Mulder, P. Coenen, A. Martens, and J. Spaepen. *The development of a 6kW fuel cell generator based on alkaline fuel cell technology*. International Journal of Hydrogen Energy, 33(12):3220–3224, June 2008.

[59] G. Mulder. *FUEL CELLS ALKALINE FUEL CELLS — Overview*. In Encyclopedia of Electrochemical Power, pages 321–328. 2009.

[60] G.F. Mclean, T. Niet, and N. Djilali. *An assessment of alkaline fuel cell technology*. International Journal of Hydrogen Energy, 27:507–526, 2002.

[61] M. Cifrain and K.V. Kordesch. *Advances, aging mechanism and lifetime in AFCs with circulating electrolytes*. Journal of Power Sources, 127(1-2):234–242, March 2004.

[62] E. Gülzow and M. Schulze. *Long-term operation of AFC electrodes with CO2 containing gases*. Journal of Power Sources, 127(1-2):243–251, March 2004.

[63] A. Kucernak, F. Bidault, and G. Smith. *Membrane electrode assemblies based on porous silver electrodes for alkaline anion exchange membrane fuel cells*. Electrochimica Acta, 82:284–290, 2012.

[64] C. Coutanceau, L. Demarconnay, C. Lamy, and J.-M. Léger. *Development of electrocatalysts for solid alkaline fuel cell (SAFC)*. Journal of Power Sources, 156(1):14–19, May 2006.

[65] P. Gouérec, L. Poletto, J. Denizot, E. Sanchez-Cortezon, and J.H. Miners. *The evolution of the performance of alkaline fuel cells with circulating electrolyte*. Journal of Power Sources, 129(2):193–204, April 2004.

[66] R. Cozzolino, S.P. Cicconardi, E. Galloni, M. Minutillo, and A. Perna. *Theoretical and experimental investigations on thermal management of a PEMFC stack*. International Journal of Hydrogen Energy, 36(13):8030–8037, July 2011.

[67] F. Bidault and A. Kucernak. *Cathode development for alkaline fuel cells based on a porous silver membrane*. Journal of Power Sources, 196(11):4950–4956, June 2011.

[68] E. Guelzow, J.K. Nor, P.K. Nor, and M. Schulze. *A renaissance for alkaline fuel cells*. The Fuel Cell Review, pages 19–25, 2006.

[69] F. Bidault and A. Kucernak. *A novel cathode for alkaline fuel cells based on a porous silver membrane*. Journal of Power Sources, 195(9):2549–2556, May 2010.

[70] M. Schulze and E. Gülzow. *Degradation of nickel anodes in alkaline fuel cells*. Journal of Power Sources, 127(1-2):252–263, March 2004.

[71] E. Gülzow, M. Schulze, and U. Gerke. *Bipolar concept for alkaline fuel cells*. Journal of Power Sources, 156(1):1–7, May 2006.

[72] M.C. Kimble and R.E. White. *A Mathematical Model of a Hydrogen / Oxygen Alkaline Fuel Cell*. 138(11):3370–3382, 1991.

[73] J.-H. Jo and S.-C. Yi. *A computational simulation of an alkaline fuel cell*. Journal of Power Sources, 84(1):87–106, November 1999.

[74] M. Duerr, S. Gair, A. Cruden, and J. McDonald. *Dynamic electrochemical model of an alkaline fuel cell stack*. Journal of Power Sources, 171(2):1023–1032, September 2007.

[75] P. De Schepper, V. Danilov, and J.F.M. Denayer. *A tank in series model for alkaline fuel cell in cogeneration of hydrogen peroxide and electricity*. International Journal of Hydrogen Energy, pages 1–10, September 2012.

[76] S. Rowshanzamir, M. Kazemeini, and M. Kabiri Isfahani. *Mass balance and water management for hydrogen-air fuel cells of the alkaline matrix type*. International Journal of Hydrogen Energy, 23(6):499–506, 1998.

[77] I. Verhaert, M. De Paepe, and G. Mulder. *Thermodynamic model for an alkaline fuel cell*. Journal of Power Sources, 193(1):233–240, August 2009.

[78] H. Zhang, G. Lin, and J. Chen. *The performance analysis and multi-objective optimization of a typical alkaline fuel cell*. Energy, 36(7):4327–4332, July 2011.

[79] H. Huisseune, A. Willockx, and M De Paepe. *Semi-empirical along-the-channel model for a proton exchange membrane fuel cell*. International Journal of Hydrogen Energy, 33(21):6270–6280, November 2008.

[80] B.Y.S. Lin, D.W. Kirk, and S.J. Thorpe. *Performance of alkaline fuel cells: A possible future energy system?* Journal of Power Sources, 161(1):474–483, October 2006.

[81] J.C. Amphlett, R.F. Mann, B.A. Peppley, P.R Roberge, and A. Rodrigues. *A model predicting transient responses of proton exchange membrane fuel cells*. Journal of Power Sources, 61:183–188, 1996.

[82] I. Verhaert, S. Verhelst, G. Janssen, G. Mulder, and M. De Paepe. *Heat and water management in an alkaline fuel cell*. (July), 2011.

[83] J. Jo, S. Moon, and S. Yi. *Simulation of influences of layer thicknesses in an alkaline fuel cell*. Applied Electrochemistry, 30:1023–1031, 2000.

[84] M. Holmgren. *Matlab function: X STEAM*, www.x-eng.com, 2006.

[85] G. Mulder, F. Deridder, P. Coenen, D. Weyen, and A. Martens. *Evaluation of an on-site cell voltage monitor for fuel cell systems*. International Journal of Hydrogen Energy, 33(20):5728–5737, October 2008.

[86] C. Depcik and D. Assanis. *A universal heat transfer correlation for intake and exhaust flows in an spark-ignition internal combustion engine*.

[87] I. Verhaert, S. Verhelst, G. Janssen, G. Mulder, and M. De Paepe. *Water management in an alkaline fuel cell*. International Journal of Hydrogen Energy, 36(17):11011–11024, August 2011.

[88] L. Venturelli, P.E. Santangelo, and P. Tartarini. *Fuel cell systems and traditional technologies. Part II: Experimental study on dynamic behavior of PEMFC in stationary power generation*. Applied Thermal Engineering, 29(17-18):3469–3475, December 2009.

[89] S.G. Kandlikar and Z. Lu. *Thermal management issues in a PEMFC stack A brief review of current status*. Applied Thermal Engineering, 29(7):1276–1280, May 2009.

[90] Y. Zhang, M. Ouyang, Q. Lu, J. Luo, and X. Li. *A model predicting performance of proton exchange membrane fuel cell stack thermal systems*. Applied Thermal Engineering, 24(4):501–513, March 2004.

[91] R. K. Shak and D. P. Sekulic. *Chapter 3: Basis thermal design theory for recuperation*. In Fundamentals of Heat Exchanger Design, pages 114–118+132. 2003.

[92] Energik. *Handboek Warmtekrachtkoppeling*, http://www.energik.be/belcogen/index.html, 2004.

[93] M. Houwing, R.R. Negenborn, P.W. Heijnen, B. De Schutter, and H. Hellendoorn. *Least-cost model predictive control of residential energy resources when applying microCHP.* In Proceedings of Power Tech Lausanne, Switzerland, page 291, 2007.

[94] P. Mancarella and G. Chicco. *Global and local emission impact assessment of distributed cogeneration systems with partial-load models*. Applied Energy, 86(10):2096–2106, October 2009.

[95] Y. Wang, Y. Huang, E. Chiremba, A. P. Roskilly, N. Hewitt, Y. Ding, D. Wu, H. Yu, X. Chen, Y. Li, J. Huang, R. Wang, J. Wu, Z. Xia, and C. Tan. *An investigation of a household size trigeneration running with hydrogen*. Applied Energy, 88(6):2176–2182, June 2011.

[96] W. Colella. *Design options for achieving a rapidly variable heat-to-power ratio in a combined heat and power (CHP) fuel cell system (FCS)*. Journal of Power Sources, 106(1-2):388–396, April 2002.

[97] X.P. Chen, Y.D. Wang, H.D. Yu, D.W. Wu, Yapeng Li, and a.P. Roskilly. *A domestic CHP system with hybrid electrical energy storage*. Energy and Buildings, (2010), August 2012.

[98] F. Barreras, M. Maza, A. Lozano, S. Báscones, V. Roda, J. E. Barranco, M. Cerqueira, and A. Vergés. *Design and development of a multipurpose utility AWD electric vehicle with a hybrid powertrain based on PEM fuel cells and batteries*. International Journal of Hydrogen Energy, 37(20):15367–15379, October 2012.

[99] P. Bubna, Suresh G. Advani, and Ajay K. Prasad. *Integration of batteries with ultracapacitors for a fuel cell hybrid transit bus*. Journal of Power Sources, 199:360–366, February 2012.

[100] S.G. Tesfahunegn, Ø. Ulleberg, P.J.S. Vie, and T.M. Undeland. *Optimal shifting of Photovoltaic and load fluctuations from fuel cell and electrolyzer to lead acid battery in a Photovoltaic/hydrogen standalone power system for improved performance and life time*. Journal of Power Sources, 196(23):10401–10414, December 2011.

[101] B. Pregelj, D. Vrečko, and V. Jovan. *Improving the operation of a fuel-cell power unit with supervision control A simulation study*. Journal of Power Sources, 196(22):9419–9428, November 2011.

[102] T. Baeten and D. Put. *Evaluatie van WKK met buffervat voor collectieve verwarming*. Master thesis, 2012.

[103] Linear. *Local Intelligent Networks and Energy Active Regions*, http://www.linear-smartgrid.be found online June 2012.

[104] E. Peeters, R. Belhomme, C. Batlle, F. Bouffard, S. Karkkainen, D. Six, and M. Hommelberg. *ADDRESS: Scenarios and architecture for Active Demand development in the smart grids of the future*. In CIRED 2009, 20th International Conference and Exhibition on Electricity Distribution - Part 1, pages 1–4, 2009.

[105] A. de Brauwere, F. De Ridder, R. Pintelon, M. Elskens, J. Schoukens, and W. Baeyens. *Model selection through a statistical analysis of the minimum of a weighted least squares cost function*. Chemometrics and Intelligent Laboratory Systems, 76(2):163–173, April 2005.

[106] J. Verhelst, J. Van der Veken, G. Van Ham, D. Saelens, and L. Helsen. *Tuning of Control Parameters by Combining Building Simulations and a Multi-Magnitude Wireless Sensor Network : A Case Study*. In Cobee: The second international conference on building energy and environment 2012, pages 1273–1282, 2012.

[107] T. Govaerts. *Micro-WKK voor residentiële gebouwen: een dimensioneringstool*. Master thesis, 2012.

[108] Y. Van Gestel. *Simulatie van de invloed van het gebruikersgedrag op de thermische prestatie van een woning*. Master thesis, KULeuven/KHKempen, 2012.

[109] I. Knight, N. Kreutzer, M. Manning, M. Swinton, and H. Ribberink. *European and Canadian non-HVAC Electric and DHW load profiles for use in simulating the performance of residential cogeneration systems (subtask of Annex 42)*. Technical report, 2007.

[110] S. Ruts. *Meetmethodiek voor de energieprestatie van een woning: Analyse van de installatiefouten en gebruikersgedrag.* Master thesis, 2012.